関西学院大学審査 博士学位論文

# The Structures of the Aggregate Forms of Bacteriochlorophyll c as Determined by NMR and Electronic-Absorption Spectroscopies

—Their Dependence on the Stereoisomeric Configurations and on the Bulkiness of the C8 Sidechain—

溝口 正

(1)

# The Structures of the Aggregate Forms of Bacteriochlorophyll *c* as Determined by NMR and Electronic-Absorption Spectroscopies: Their Dependence on the Stereoisomeric Configurations and on the Bulkiness of the C8 Sidechain

*A Thesis Submitted to*
*Faculty of Science, Kwansei Gakuin University,*
*in Fulfillment of the Requirements*
*for the Degree*
*of*
*Doctor of Science*

**Tadashi Mizoguchi**

**January, 2000**

## CONTENTS

## ABBREVIATIONS

1D, one dimensional

2D, two dimensional

3D, three dimensional

BChl *c*, Bacteriochlorophyll *c*

Chl, chlorophyll

COSY, correlation spectroscopy

CP, cross poralization

DEPT, distortionless enhancement by poralization transfer

E, ethyl

EDTA, ethylenediaminetetraacetic acid

eq, equation

exp, exponential

hfs, high field shift

FT, Fourier transform

HMBC, heteronuclear multiple-bond correlation

HMQC, heteronuclear multiple quantum correlation

HPLC, high performance liquid chromatography

HSQC-NOESY, heteronuclear single-quantum correlation - nuclear Overhauser effect spectroscopy

I, isobutyl

lfs, low field shift

MAS, magic angle spinning

Me, methyl

NOE, nuclear Overhauser effect

obs, observed

OD, optical density

ODS, octadecylsilane

P, propyl

ppm, part per million

ROESY, rotating frame Overhauser effect spectroscopy

R[E,E], ($3^1$R)-8-ethyl-12-ethyl bacteriochlorophyll **c**

R[I,E], ($3^1$R)-8-isobutyl-12-ethyl bacteriochlorophyll **c**

R[P,E], ($3^1$R)-8-propyl-12-ethyl bacteriochlorophyll **c**

S[I,E], ($3^1$S)-8-isobutyl-12-ethyl bacteriochlorophyll **c**

S[P,E], ($3^1$S)-8-propyl-12-ethyl bacteriochlorophyll **c**

TMS, tetramethylsilane

Tris-HCl, tris(hydroxymethyl)aminomethane-hydrochloric acid

# INTRODUCTION

Recently, the three-dimensional structures of light-harvesting antenna complexes (LH2) from purple photosynthetic bacteria have been determined by X-ray crystallography with high resolution [1, 2]. The function of those antenna complexes is to absorb the light energy and transfer it to the photo-reaction center. On the basis of those structures, numerous experimental and theoretical studies have been done to elucidate the mechanisms of the antenna function [3, 4]. The structure of the LH2 complex from *Rhodopseudomonas acidophila* 10050 has 9-fold symmetry, and the bacteriochlorophyll (BChl) **a** macrocycles are stacked together just like the blades of a turbine. Here, each repeating subunit consisting of a pair of BChl **a** molecules and $\alpha$ and $\beta$ peptides is aligned perpendicular to the membrane plane, and the coordination bonds are formed between each BChl **a** molecule and the histidine residue of peptide $\alpha$ or $\beta$ [1]. On the other hand, the antenna complexes from green photosynthetic bacteria, called 'chlorosomes', have never been crystallized. Therefore, the structure of chlorosomes, i.e., the stacking of the BChl **c** macrocycles, has not been determined, and therefore, their antenna function has never been studied in detail.

Figure 1a depicts the schematic cross-sectional view of a chlorosome. Each chlorosome is covered with a 2-3 nm thick envelope made of a lipid monolayer (mostly galactolipid), and has approximate dimensions of 70 - 180 nm long, 30 - 60 nm wide, and ~ 25 nm high [5, 6]. It is supposed to contain 10-30 'rod-elements' having BChl **c** as the major component: each rod-element is 10 nm in diameter and may have a central hole of about 3 nm [6]. These rod-elements are made of a higher aggregate of BChl **c**, and expected to play important roles of absorbing the light energy and transferring it to the photochemical reaction center [7-9]. In the rod-elements, no proteins are involved in the formation of the aggregate of BChl **c** [10, 11], in contrast to the case of the purple bacteria mentioned above. Here, direct pigment-pigment interactions in the aggregate is supposed to play a key role in forming the aggregate structure. Therefore, we can mimic the structure of chlorosomes by forming an *in vitro* BChl **c** aggregate (hereafter, I simply call it 'the BChl **c** aggregate'), because both *in vivo* and *in vitro* aggregates are characterized by their $Q_y$ absorption strongly red-shifted to above 740 nm [7, 8, 12]. Concerning the basic structural motif of the stacking of the macrocycles in chlorosomes, numerous spectroscopic studies have been done on both intact chlorosomes and various BChl **c** aggregates. As a result, two different models have been proposed as

shown in Fig. 1(b): One consisting of stacked monomers, proposed by Holzwarth, de Groot and co-workers [10, 13, 14], is often referred to as 'the parallel-chain stacking'. The other consisting of stacked piggy-back dimers, proposed by Nozawa and co-workers [11, 15], is referred to as 'the antiparallel-chain stacking'. Both models were based on the solid-state $^{13}$C-NMR spectroscopy of basically the same *intact* chlorosomes and artificial aggregate of extracted BChl **c** from *chlorobium* (*Cb.*) *tepidum*; nevertheless, two different models have been proposed. No definitive conclusion has been obtained so far for the chlorosome structure.

The BChl **c** aggregates have been classified, as follows, in terms of the wavelength of the $Q_y$ absorption; a dimer absorbing around 675 nm, a lower aggregate absorbing around 705 nm, a medium aggregate absorbing around 720 nm, and a higher aggregate absorbing around 745 nm [16, 17]. Hereafter, I will call them 'the (B675) dimer', 'B705 aggregate', 'B720 aggregate' and 'B745 aggregate', respectively, according to their apparent $Q_y$ absorption. It is to be noted that no definitive information has been available concerning the size of each aggregate form except for the dimer, although numerous spectroscopic studies have been performed in order to elucidate their structures.

Green photosynthetic bacteria having chlorosomes as antenna complexes are characterized by a unique structure of BChl **c** molecules they contain. The uniqueness of BChl **c**, in comparison with BChl **a** and **b** in the purple bacteria, resides in the presence of the hydroxylethyl group at the C3$^1$ position and the carbonyl group at the C13$^1$ position. Figure 2 compares the chemical structures of (a) BChl **a** and (b) BChl **c**. Because of its unique structure, the BChl **c** molecules can readily form the aggregate showing the strongly red-shifted $Q_y$ absorption, without adding water molecules often used by other chlorophylls to form such a higher aggregate [18, 19]. BChl **c** derivatives lacking the hydroxylethyl group at the C3$^1$ position (called pyrochlorophylls) do not form an aggregate showing such red-shifted $Q_y$ absorption under the same conditions where the intact BChl **c** readily does [20].

The green photosynthetic bacteria can be divided into two categories; one, the green filamentous bacteria *chloroflexaceae* (e.g. *chloroflexace aurantiacus*), and the other, the green sulfur bacteria *chlorobiaceae* (e.g. *chlorobium (Cb.) tepidum* and *Cb. limicola*). First, let us focus our attention on the stereoisomeric configurations of the hydroxylethyl group at the C3$^1$ position as shown by asterisk in Fig. 2(b). Concerning this stereoisomeric configuration, chlorosomes from *chloroflexaceae* contain a 2 : 1 mixture of the (3$^1$R)- and (3$^1$S)-isomers [21], whereas those from *chlorobiaceae* contains a 9 : 1 mixture of them [16, 22]; both strains have the (3$^1$R)-isomers as the major

component. Second, let us consider the bulkiness of the sidechains attached to the C8 and C12 positions. The BChl **c** component of *chloroflexaceae* consists of only the 8-ethyl-12-methyl homologue, and no variety is found in the sidechains [21]. On the other hand, a variety of the C8 and C12 sidechains is found in *chlorobiaceae*. In this strain, the BChl **c** component consists of a mixture of homologues having the 8-ethyl-12-ethyl, 8-propyl-12-ethyl, and 8-isobutyl-12-ethyl sidechains as the major component [16, 23-25]. Figure 2b shows the chemical structure of the BChl **c** homologues isolated from *Cb. limicola* (note that the sidechain varies only at the C8 position in this set, which I am going to examine). It has not been systematically examined how the bulkiness of the sidechain at the C8 position as well as the stereoisomeric configurations at the $C3^1$ position affect the structures of chlorosomes and artificial aggregates, although Holzwarth, Tamiaki and co-workers suggested that the stereoisomeric configurations can affect the amount of aggregate showing the strongly red-shifted $Q_y$ absorption [17, 26, 27]. Further, Olson, Nozawa, Uehara and co-workers suggested that the bulkiness of the C8 sidechain can also affect the amount of such aggregate formed [16, 23-25, 28]. Interestingly, Huster and Smith [29] suggested that the mixing of such homologues should enhance the hydrophobic interaction between the individual BChl **c** molecules in forming larger aggregates, and as a result, should increase the light-harvesting efficiency of chlorosomes [29]. Thus, it has been suggested that the composition of the BChl **c** homologues in chlorosomes may play an important role in building the chlorosomal structure.

Although no definitive structures have been proposed for either chlorosomes or artificial BChl **c** aggregates, the following conclusions have been drawn based on previous investigations: (1) On the basis of solid-state $^{13}C$ NMR studies mentioned above, each chlorosome contains a higher aggregate of BChl **c**, whose formation is governed by direct pigment-pigment interactions [10, 11, 14]. Hexanol treatment of chlorosomes, i.e. reversible conversion from the higher aggregate to the monomeric form of BChl **c** by addition of 1-hexanol to their suspension, also supports this idea [30, 31]. (2) On the basis of linear and circular dichroism studies, BChl **c** molecules in the aggregates must have a long-range ordering which aligns their $Q_y$ transition moments parallel to the long axis of the rod element [31-33]. (3) Resonance-Raman and FT-IR spectroscopies showed that the central Mg atom of each BChl **c** molecule in both chlorosomes and in the artificial BChl **c** aggregates is pentacoordinated [34, 35]. The hydroxylethyl group at the $C3^1$ position of one BChl **c** molecule is most likely directly coordinated to the Mg atom of the neighboring BChl **c** molecule, and hydrogen

bonded to the keto-carbonyl group at the C13[1] position of a third BChl **c** molecule [17, 26, 36].

In addition to the above information concerning the partial structures, it is necessary to determine the stacking of the macrocycles in chlorosomes in order to obtain complete pictures of the chlorosomes and the artificial aggregates. In this investigation, I have addressed the following three questions: (1) What kinds of structural motifs do the B675 dimer, the B705 aggregate and the B745 aggregate have? (2) What kind of entire aggregate structure can be formed out of such structural motifs? (3) What kind of pathways of transformation are present starting from the monomer eventually to the higher B745 aggregate? How do the stereoisomeric configuration and the bulkiness of the C8 sidechain affect the above transformation pathways?

In order to answer to those questions, the following series of investigations have been performed: First, the stackings of the macrocycles in the BChl **c** aggregates including the B675 dimer, the B705 aggregate and the B745 aggregate were determined by means of high-resolution NMR spectroscopy (Section I). Concerning the solution-state NMR studies of the BChl **c** aggregates, only a dimeric form of BChl molecules had been determined when I started this series of investigation [37, 38]. The solution-state NMR approaches to elucidate the stacking of the macrocycles in the lower to higher aggregates were hampered by substantial broadening of the NMR signals. This can be ascribed to the high ordering of the BChl **c** molecules during the process of the aggregate formation. From this viewpoint, I have attempted, for the first time, stepwise titration of alcohol into the aggregate suspension in order to suppress the broadening of the NMR signals. Here, the alcohol titration decomposes the higher aggregates into small fragments, which I call 'the structural motif', by breaking down the coordination bonds between the central Mg atom and the hydroxylethyl group as well as the hydrogen bond between the hydroxylethyl and the carbonyl groups. Thus, I have attempted to determine those structural motifs in the aggregate suspension by means of high-resolution NMR spectroscopy; here, I took advantage of the fact that the chemical shift of the $^{1}H$ and $^{13}C$ nuclei of BChl **c** can be varied due to the ring-current effect originating from the neighboring macrocycles in the aggregates [39]. First, changes in the chemical shift upon stepwise titration of alcohol were continuously traced to determine 'the aggregation shifts', which are defined as the chemical-shift differences between the aggregate forms (without or with smaller amount of alcohol) and the monomeric form (with an excess amount of alcohol). Second, the ring-current effect on both the $^{1}H$ and $^{13}C$ nuclei were calculated by using the magnetic-dipole and the loop-current

approximations: (a) The magnetic-dipole approximation was first developed by Abraham et al. [40], and applied to the porphyrin and chlorin rings. Here, the conjugated macrocycle of BChl **c** is split into three pyrrole rings and four hexagonal rings, and the ring-current effect due to the ring was approximated by a pair of magnetic-dipoles above and below the ring. (b) The loop-current approximation was first developed by Johnson and Bovey [41], and applied to the benzene ring. Here, I newly derived an equation to calculate the z-component of the magnetic flux generated by a current loop, which is assumed to cover the conjugated macrocycle of BChl **c**. Then, a structural motif was proposed by comparison between the experimentally-determined aggregation shifts and the calculated ring-current effects. Independently, a technique using $^{1}H$-$^{1}H$ intermolecular Nuclear Overhauser Effect (NOE) correlations was applied to the BChl **c** aggregates. This is potentially a powerful technique to determine the mutual orientation of the relevant molecules, but it was not straightforward to distinguish 'intermolecular' and 'intramolecular' NOE correlations for the BChl **c** molecules in the aggregate suspension. Here, I have first applied three-dimensional F1 $^{13}C$-edited F3 $^{13}C$-filtered HSQC-NOESY spectroscopy to a suspension consisting of a 1 : 1 mixture of $^{13}C$-labeled and unlabeled BChl **c** molecules [42], and succeeded in the selective detection of the intermolecular $^{1}H$-$^{1}H$ NOE correlation between the $^{13}C$-labeled and unlabeled BChl **c** molecules. On the basis of the ring-current effects and the intermolecular NOE correlations, I could determine the stacking of the macrocycles in the structural motifs of the fragmented BChl **c** aggregates.

In Section II, changes in the electronic absorption spectra during the formation of aggregates were traced for a complete set of BChl **c** isomers and homologues from *Cb. limicola*, including R[E,E], R[P,E], R[I,E], S[P,E] and S[I,E]BChl **c**. In order to elucidate the entire aggregate structures and transformations among the various aggregate forms, I used a mixture of dichloromethane and *n*-hexane as the solvent, and reduced the amount of $CH_2Cl_2$ to reversibly form the higher BChl **c** aggregates. Here, the BChl **c** aggregates were kept 'intact', during their aggregate formation or decomposition, under completely hydrophobic environment without affecting the coordination and hydrogen bonds, in contrast to the case of stepwise titration of alcohol mentioned above. Each electronic absorption spectrum in the set of transformations of the various BChl **c** isomers and homologues could be systematically analyzed by spectral deconvolution, assuming five Gaussian components, including the monomer, the B675 dimer, and the B705, B720 and B745 aggregates. Further, the shifts of the $Q_y$ absorption in each aggregates was theoretically predicted for

the models consisting of the structural motifs, which have been determined by solution-state, high-resolution NMR spectroscopy (Section I). Here, transition dipole - transition dipole interactions among the BChl molecules were calculated by the point-monopole approximation to explain the shifts of the $Q_y$ absorption, which was first developed by Sauer et al [43]. The dipole moment of the entire BChl molecule was treated as a sum of the transition monopole on each atom. I have tried to determine the entire structures of various BChl **c** aggregates which were obtained by extending their structural motifs to the y- and/or z-direction(s), as a function of the number of stacked molecules, and by comparing the observed and calculated shifts of the $Q_y$ absorption after scaling. Figure 3 summarizes the structures of the BChl **c** aggregates thus proposed. In this figure, the structural motifs which were determined by means of high-resolution NMR spectroscopy were also shown by the dotted lines.

In order to understand the mechanism of the formation of the higher aggregate in chlorosomes, the transformations of both *in vitro* and *in vivo* aggregates were investigated. Concerning the intact chlorosomes, hexanol treatment was applied to characterize the transformation to the higher aggregate. Further, the changes in electronic absorption spectra caused by addition of the ($3^1$S)-isomer to the ($3^1$R)-isomers were continuously traced. Independently, the steric energies due to the interlayer and the intercolumn van der Waals interaction were calculated to theoretically investigate the transformation from the dimer eventually to the higher aggregate.

Two different forms of stacking of the macrocycles have been identified in the present investigation depending on the stereoisomeric configurations: one is the monomer-based, stepwise stacking for the ($3^1$S)-isomers (parallel-chain stacking) and the other is the piggy back dimer-based stacking for the ($3^1$R)-isomers (antiparallel-chain stacking). I have identified two different kinds of the B745 aggregates, and confirmed that both the parallel-chain and the antiparallel-chain stackings can be formed depending on the stereoisomers or the isomeric composition. I am going to conclude that the stereoisomeric configurations of the hydroxylethyl group at $C3^1$ govern the form of stacking of the macrocycles in the aggregates, and the bulkiness of the sidechain at C8 enhanced the formation of the B745 aggregates, and that 'the parallel-chain stacking' is most likely as the chlorosomal aggregate.

## REFERENCES


(1) G. McDermott, S. M. Prince, A. A. Freer, A. M. Hawthornthwaite-Lawless, M. Z. Papiz, R. J. Cogdell and N. W. Isaacs, *Nature*, **374** (1995) 517-521.

(2) J. Koepke, X. Hu, C. Muenka, K. Schulten and H. Michel, *Structure*, **4** (1996) 581-597.

(3) O. Kühn and V. Sundström, *J. Phys. Chem. B*, **101** (1997) 3432-3440.

(4) O. Kühn, T. Renger, V. May, J. Voigt, T. Pullerits and V. Sundström, *Trend in Photochem. Photobiol.*, **4** (1997) 213-256.

(5) J. Oelze and J. R. Golecki, In *Anoxygenic Photosynthetic Bacteria* eds by R. E. Blankenship, M. T. Madigan and C. E. Bauer (1995), pp. 259-278, Kluwer Academic Publishers, The Netherlands.

(6) L. A. Staehelin, J. R. Golecki and G. Drews, *Biochim. Biophys. Acta*, **589** (1980) 30-45.

(7) J. M. Olson, *Photochem. Photobiol.*, **67** (1998) 61-75.

(8) R. E. Blankenship, J. M. Olson and M. Miller, In *Anoxygenic Photosynthetic Bacteria* eds by R. E. Blankenship, M. T. Madigan and C. E. Bauer (1995), pp. 399-435, Kluwer Academic Publishers, The Netherlands.

(9) A. R. Holzwarth, K. Griebenow and K. Schaffner, *J. Photochem. Photobiol. A*, **65** (1992) 61-71.

(10) T. S. Balaban, A. R. Holzwarth, K. Schaffner, G.-J. Boender and H. J. M. de Groot, *Biochemistry*, **34** (1995) 15259-15266.

(11) T. Nozawa, K. Ohtomo, M. Suzuki, H. Nakagawa, Y. Shikama, H. Konami and Z.-Y. Wang, *Photosynth. Res.*, **41** (1994) 211-223.

(12) K. M. Smith, L. A. Kehers and J. Fajer, *J. Am. Chem. Soc.*, **105** (1983) 1387-1389.

(13) A. R. Holzwarth and K. Schaffner, *Photosynth. Res.*, **41** (1994) 225-233.

(14) B.-J. van Rossum, G. J. Boender, F. M. Mulder, J. Raap, T. S. Balaban, A. R. Holzwarth and K. Schaffner, S. Prytulla, H. Oschkinat and H. J. M. de Groot, *Spectrochim. Acta Part A*, **54** (1998) 1167-1176.

(15) T. Nozawa, K. Ohtomo, M. Suzuki, Y. Morishita and M. T. Madigan, *Bull. Chem. Soc. Jpn.*, **66** (1993) 231-237.

(16) J. M. Olson and J. P. Pedersen, *Photosynth. Res.*, **25** (1990) 25-37.

(17) J. Chiefari, K. Griebenow, N. Griebenow, T. S. Balaban, A. R. Holzwarth and K. Schaffner, *J. Phys. Chem.*, **99** (1995) 1357-1365.

(18) G. J. Boender, J. Raap, S. Prytulla, H. Oschkinat and H. J. M. de Groot, *Chem. Phys. Lett.*, **237** (1995) 502-508.

(19) H.-C. Chow, R. Serlin and C. E. Strouse, *J. Am. Chem. Soc.*, **97** (1975) 7230-7237.

(20) D. C. Brune, G. H. King and R. E. Blankenship, *in Photosynthetic Light-Harvesting Systems* ed. by H. Scheer (1988), pp. 141-151, Walter de Gruyter, Berlin, New York.

(21) F. Fages, N. Griebenow, K. Griebenow, A. R. Holzwarth and K. Schaffner, *J. Chem. Soc. Perkin Trans I*, (1990) 2791-2797.

(22) K. Ishii, Y. Nagano, M. Kimura and K. Uehara, In *Photosynthesis: Mechanisms and Effects* (Edited by G. Garab) Vol. I, pp. 169-172, Kluwer Academic Publishers, The Netherlands.

(23) J. M. Olson, *Photosynth. Res.*, **30** (1991) 45-48.

(24) J. M. Olson and R. P. Cox, *Photosynth. Res.*, **30** (1991) 35-43.

(25) K. Uehara, M. Mimuro, Y. Ozaki and J. M. Olson, *Photosynth. Res.*, **41** (1994) 235-243.

(26) T. S. Balaban, H. Tamiaki, Holzwarth and K. Schaffner, *J. Phys. Chem. B*, **101** (1997) 3424-3431.

(27) H. Tamiaki, S. Takeuchi, R. Tanikaga, T. S. Balaban, A. R. Holzwarth and K. Schaffner, *Chem. Lett.*, (1994) 401-402

(28) T. Nozawa, K. Ohtomo, N. Takeshita, Y. Morishita and M. Madigan, *Bull. Chem. Soc. Jpn.*, **65** (1992) 3493-3494.

(29) M. S. Huster and K. M. Smith, *Biochemistry*, **29** (1990) 4348-4355.

(30) K. Matsuura and J. M. Olson, *Biochim. Biophys. Acta*, **1019** (1990) 233-238.

(31) K. Matsuura, M. Hirota, K. Shimada and M. Mimuro, *Photochem. Photobiol.*, **57** (1993) 92-97.

(32) H. van Amerongen, H. Vasmel and R. van Grondelle, *Biophys. J.*, **54** (1988) 65-76.

(33) K. Griebenow, A. R. Holzwarth, F. van Mourik and van Grondelle, *Biochim. Biophys. Acta*, **1058** (1991) 194-202.

(34) M. Lutz and G. van Brakel, in *Green Photosynthetic Bacteria* eds. by J. M. Olson, J. G. Ormerod, J. Amesz, E. Stackebrandt and H. G. Trüper (1988), pp. 23-34, Plenum Press,

New York.

(35) T. Nozawa, T. Noguchi and M. Tasumi, *J. Biochem.*, **108** (1990) 737-740.

(36) P. Hildebrandt, H. Tamiaki, A. R. Holzwarth and K. Schaffner, *J. Phys. Chem.*, **98** (1994) 2192-2197.

(37) K. M. Smith, F. W. Bobe, D. A. Goff and R. J. Abraham, *J. Am. Chem. Soc.*, **108** (1986) 1111-1120.

(38) Z.-Y. Wang, M. Umetsu, M. Kobayashi and T. Nozawa, *J. Phys. Chem. B*, **103** (1999) 3742-3753.

(39) R. J. Abraham, K. M. Smith, D. A. Goff and J.-J. Lai, *J. Am. Chem. Soc.*, **104** (1982) 4332-4337.

(40) R. J. Abraham, C. M. Stephen and K. M. Smith, *Org. Magn. Reson.*, **9** (1977) 367-373.

(41) C. E. Johnson and F. A. Bovey, *J. Chem. Phys.*, **29** (1958) 1012-1014.

(42) K. Ogura, H. Terasawa and F. Inagaki, *J. Biomol. NMR*, **8** (1996) 492-498.

(43) K. Sauer, R. J. Cogdell, S. M. Prince, A. Freer, N. W. Isaacs and H. Scheer, *Photochem. Photobiol.*, **64** (1996) 564-576.

## FIGURE CAPTIONS

**Figure 1.** (a) Schematic presentation of the cross-sectional view of a chlorosome model. This model is based on the electron microscopy of Staeheline et al. [6]. (b) Schematic presentation of the parallel-chain stacking model and the antiparallel-chain stacking model. The open and shaded sides indicate the left-hand-side and the right-hand-side of BChl **c** plane in Figure 2.

**Figure 2.** Chemical structures of (a) BChl **a** and (b) BChl **c**. The typification of carbon atoms in the macrocycle is given by numbering. Concerning the BChl **c**, optically-active carbon atom is indicated by asterisk; the R and S stereoisomers are defined at the $C3^1$ position. The R isomers having the ethyl group at the C12 position, and the ethyl, propyl and isobutyl group at the C8 position are named R[E,E], R[P,E] and R[I,E], respectively; the S isomers are named similarly.

**Figure 3.** Schematic presentation of the aggregate forms consisting of the piggy-back dimers (labeled 'd') and the monomers (labeled 'm'): The former include B675d, i.e., the piggy-back dimer; B705d (B705d') a linear array of straight (inclined) columns consisting of a pair of the piggy-back dimers; B720d and B745d, an assembly of two and five shifted-inclined columns of more than six piggy-back dimers. The latter include B720m and B745m, an assembly of one and two parallel, stepwise stacking of ~ 30 monomers (only 20 monomers are shown in the figure). The open and shaded sides indicate the left-hand-side and the right-hand-side of the BChl *c* plane shown in Figure 2.

Fig.1

(a)

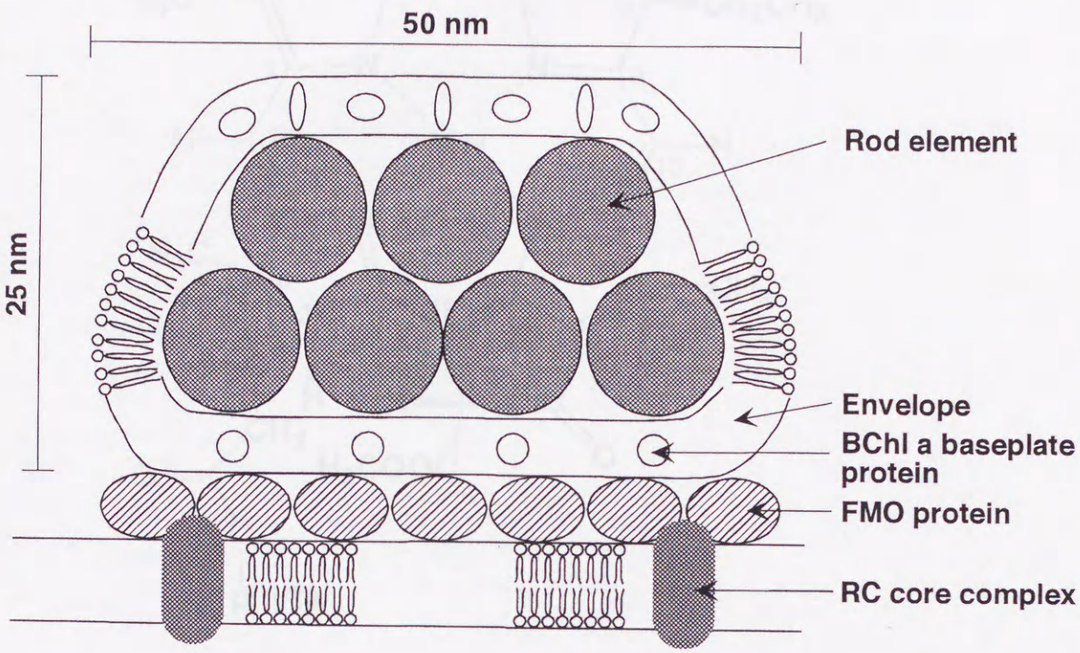


(b)

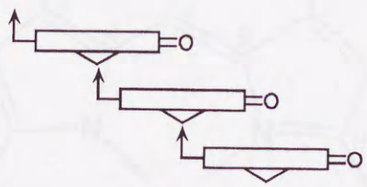

Parallel-chain stacking

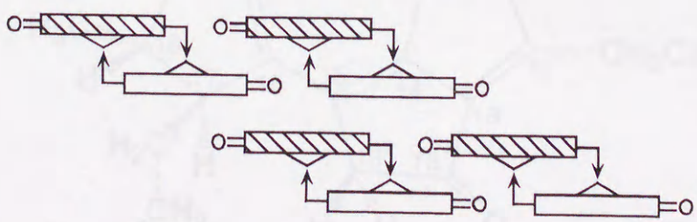

Antiparallel-chain stacking

Fig. 2

(a)

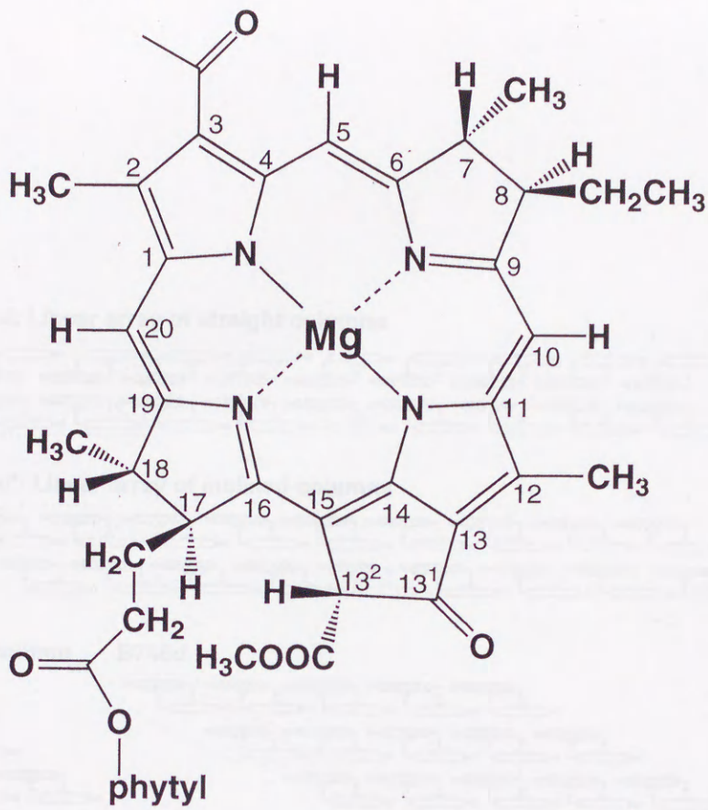


(b)

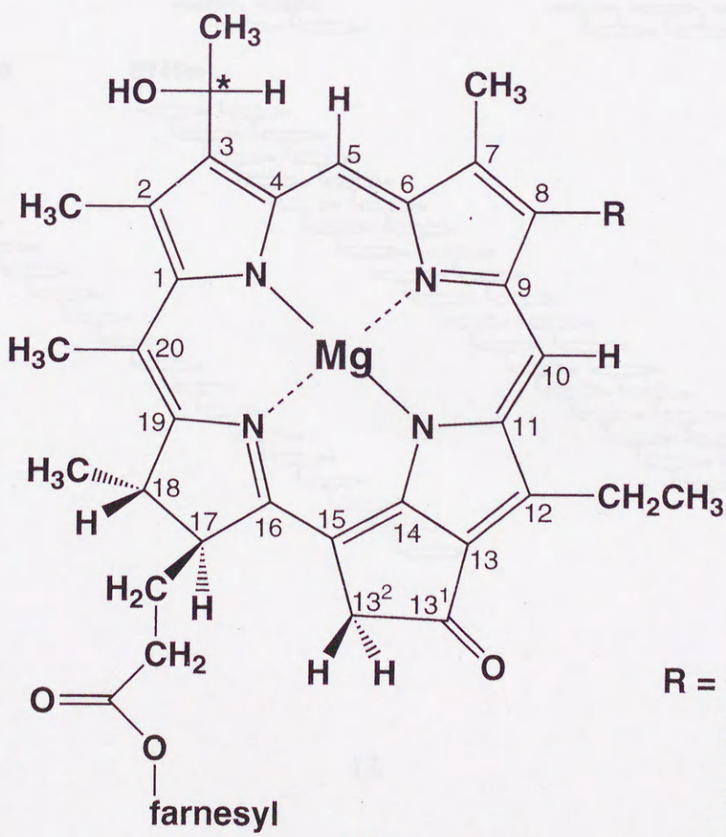


R = $CH_2CH_3$,
$CH_2CH_2CH_3$,
$CH_2CH(CH_3)_2$

Fig. 3

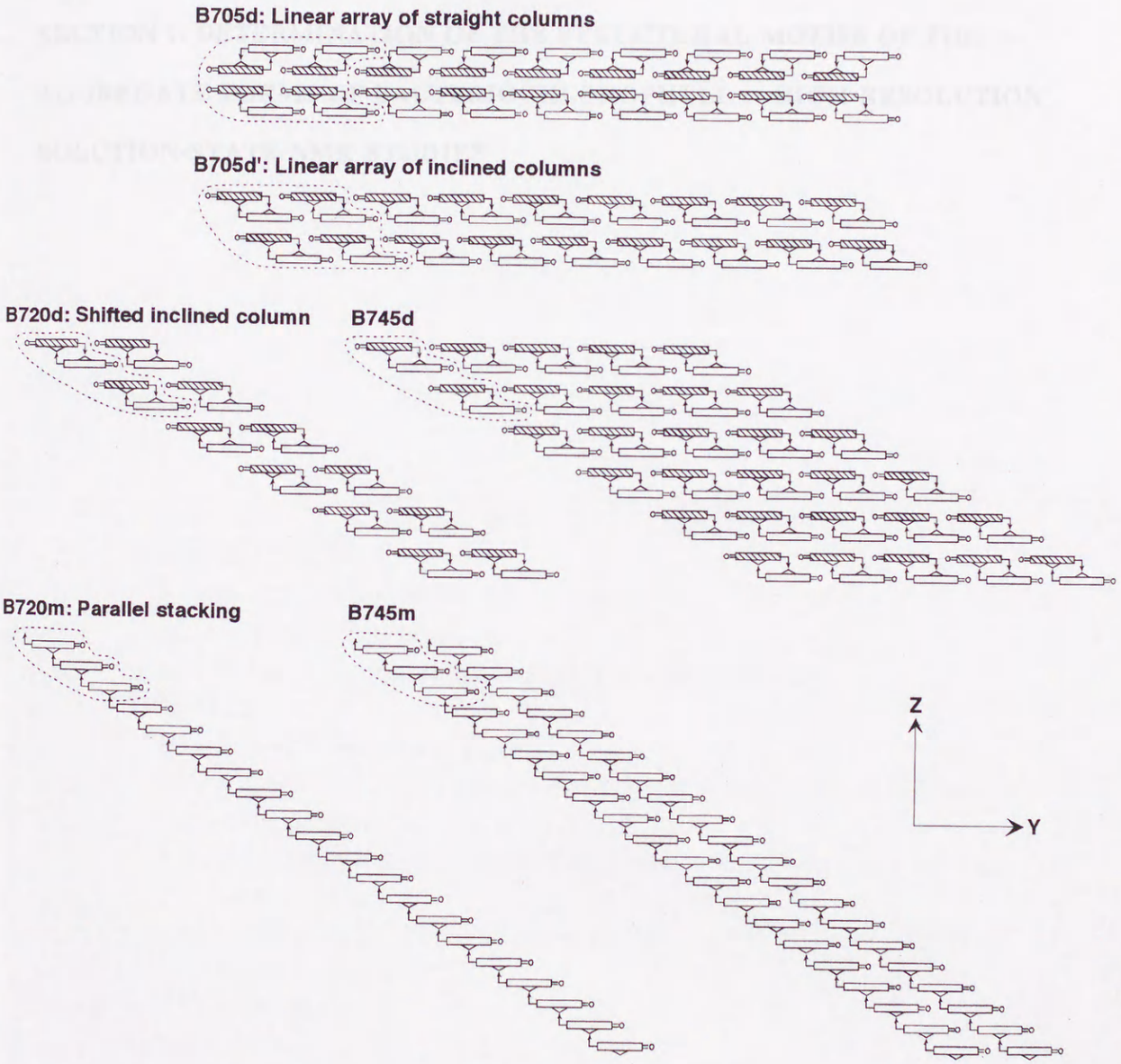
B705d: Linear array of straight columns
B705d': Linear array of inclined columns
B720d: Shifted inclined column
B745d
B720m: Parallel stacking
B745m
Z
Y

# SECTION I: DETERMINATION OF THE STRUCTURAL MOTIFS OF THE AGGREGATE FORMS OF BACTERIOCHLOROPHYLL *c*: HIGH RESOLUTION SOLUTION-STATE NMR STUDIES

Chapter 1

# The Structure of the Aggregate Forms of ($3^1$R), 8-Ethyl-12-Ethyl Farnesyl Bacteriochlorophyll c Showing the $Q_y$ Absorption at 675 and 705 nm as Determined by $^1$H-NMR Spectroscopy

## 1. ABSTRACT

8-Ethyl-12-ethyl farnesyl bacteriochlorophyll **c** was dissolved into chloroform and changes in the $^1$H-NMR spectrum due to the titration of methanol were traced. Based on the changes in chemical shift and in peak intensity, the structures of two aggregate forms have been proposed. Form I showing the $Q_y$ electronic absorption at 675 nm was ascribed to a dimer which has a "piggy-back" stacking of the macrocycles and a pair of Mg···OH coordination bonds. This structure was confirmed by an intermolecular $^1$H-$^1$H NOE correlation. On the other hand, Form II showing the $Q_y$ absorption at 705 nm was ascribed to an oligomer in which the dimer units are stacked to form an inclined column.

## 2. INTRODUCTION

The structures of bacteriochlorophyll **c** (BChl **c**) aggregates in solutions are expected to provide basic information concerning both the real chlorosome structure [1, 2] and the mechanisms of its formation. Various forms of aggregate have been classified in terms of the $Q_y$ electronic absorption: Smith et al. [3] dissolved BChl **c** (the detailed chemical structures were not identified) in a hexane-methylene chloride (200:1) mixture, and identified an aggregate form which absorbs at 748 nm as do the chlorosomes. Olson and Pedersen [4] found that the forms of aggregate depend on the stereoisomeric configuration of the hydroxyethyl group: (3$^1$R) BChl **c** [n-Pr, Et, farnesyl] in $CCl_4$ forms the monomer (666 nm), the dimer (685 nm), "a trimer or a tetramer" (705 nm), while (3$^1$S) BChl **c** [iBu, Me/Et, farnesyl] in $CCl_4$ forms the monomer (667 nm), the dimer (685 nm), and "a polymer" (747 nm). Very recently, Chiefari et al. [5] made a similar classification for BChl **c** [Et, Me, St]: The R stereoisomer forms the monomer (667 nm), the dimer (682 nm), "an aggregate of the dimers" (703 nm), while the S isomer forms the monomer (667 nm), and "a direct aggregate of the monomers" (750 nm). Based on the above classifications, hereafter I will call the 666-667 nm component "the monomer", the 682-685 component "Form I", the 703-705 component "Form II", and the 747-750 nm component "Form III".

NMR spectroscopy has been used to determine the stacking of the BChl molecules by relating the changes in the chemical shifts of the H signals (in reference to those of the monomer) to the ring-

current effect due to the neighboring macrocycle [6]: Smith et al. [7] examined by $^1$H-NMR spectroscopy the aggregate of methyl bacteriochlorophyllide **d** [Et, Et] in chloroform. Based on the ring-current effect, they proposed two different models for a dimer consisting of spectroscopically nonequivalent components. One had a face-to-face stacking and the other had a "piggy-back" stacking of a pair of macrocycles, the latter of which seemed to be more favored. Both models had a pair of coordination bonds between the hydroxyl group of one BChl molecule and the magnesium atom of the other. Nozawa et al. [8] found a similar dimer for BChl **c** [Et or n-Pr,Et, farnesyl] in chloroform. They proposed the piggy-back model on the basis of the ring-current effect. Further, Nozawa et al. [9] examined the aggregate forms of the same BChl **c** in hexane/methylene chloride and hexane /methanol mixtures. They ascribed Form II to a linear aggregate of the dimers formed through the -C=O···H-O- hydrogen bondings, and Form III to a two-dimensional aggregate consisting of the linear aggregates stacked in "a direct ring overlap" configuration. Very recently, Chiefari et al. [5] proposed models for Forms I - III by using additional data of infrared absorption. In the models, they assumed the face-to-face stacking of the macrocycles in both Form I (the dimer) and Form II (a linear aggregate of the dimers similar to the above), while they assumed the piggy-back stacking in Form III (a two dimensional aggregate of the monomers formed through the -C=O···H-O- hydrogen bonding as well as by the Mg···OH coordination). Therefore, the way of stacking in the dimer is still not established.

In this Chapter, I have addressed the following two questions: (1) What is the structure of the dimer (Form I) of BChl **c**? Does it have the face-to-face stacking or the piggy-back stacking? Since the structure of the dimer must be stabilized by a pair of coordination bonds, and since the overlap of the peripheral groups of one molecule with the macrocycle of the other will depend on the way of stacking, the structure may be determined by chemical-shift changes caused by dimerization. Further, intermolecular $^1$H-$^1$H NOE correlation will provide us with conclusive evidence for one particular dimeric structure. (2) What is the structure of Form II (the 705 nm component)? More specifically, what kind of stacking configuration does it have? The idea underlying the present investigation is to trace continuously the changes in the NMR spectrum when the polarity of the solvent was decreased, and to obtain structural information on the aggregate form(s) being created in the solution. I have titrated methanol by many steps into the chloroform solution of BChl **c** [Et, Et, farnesyl], carefully analyzed the changes in chemical shift and in peak intensity of each H signal in terms of both the ring-

current effect and the broadening due to steric interactions, and tried to obtain structural information on Forms I and II showing the $Q_y$ absorption at 675 and 705 nm, respectively.

## 3. MATERIALS AND METHODS

### 3.1. Sample preparation

*Chlorobium limicola* f. sp. *thiosulfatophilum* was grown at 28°C for seven days in the medium of Wahlund et al. [10], to which casamino acids (1.0 g/l) and vitamin $B_1$ (50 mg/l) were added. The pigment components were extracted from packed wet cells with methanol, transferred to a mixer of petroleum ether and diethyl ether (1:2 v/v), and then concentrated to dryness. The residue was washed with n-hexane (three times) to remove carotenoids and BChl **a**. 8-Ethyl-12-ethyl farnesyl BChl **c** (hereafter I will call this simply "BChl **c**") was isolated and purified by high-pressure liquid chromatography (HPLC) from the crude BChl **c** mixtures thus obtained. The HPLC conditions were as follows: column, 4.6 mm $\phi \times 250$ mm (for analyses) or 7.6 mm $\phi \times 250$ mm (for collection) columns packed with ODS hypersil 5 $\mu$m (SHANDON, batch 3347); eluent, 6.0 - 7.5 % $H_2O$ in methanol; flow rate 1.0 ml/min; and detection, 440 nm (for analyses) or 455 nm (for collection).

### 3.2. Electronic absorption and $^1$H-NMR measurements

BChl **c** was dissolved into 550 $\mu$l chloroform-$d_1$ (99.8 % Nacalai tesque) which was dried over 3 Å molecular sieve (Kishida Chemicals) at the concentration of $2.5 \times 10^{-3}$ M, and then the following amounts of methanol-$d_4$ (99.8 %, Nacalai tesque) were added: (1) 0.5, (2) 1.0, (3) 1.5, (4) 2.0, (5) 2.5, (6) 3.0, (7) 3.5, (8) 4.0, (9) 4.5, (10) 5.0, (11) 6.0, (12) 7.0, (13) 8.0, (14) 9.0, (15) 10, (16) 11, (17) 12, (18) 14, (19) 16, (20) 18, (21) 20, (22) 25, (23) 30, (24) 40, and (25) 50 $\mu$l.

The electronic absorption spectra of the sample solutions, i.e., (1), (2), (4), (6), (8), (11), (13), (16), (18), (20), (22) and (25), were recorded at room temperature by the use of a 50 $\mu$m cell and a Hitachi U-2000 spectrophotometer.

The $^1$H-NMR spectra of all the sample solutions were recorded at 0°C by the use of a JEOL JNM-A400 FT NMR spectrometer and a JEOL NM-VT 1A temperature controller; TMS was used as an internal standard. A set of 1D spectrum (digital resolution, 0.24 Hz) and 2D $^1$H-$^1$H COSY and $^1$H-$^1$H ROESY spectra (digital resolution 8.59 Hz) were recorded for each sample solution; pulse

sequences were $90°$-$t_1$-$90°$-$t_2$ for $^1$H-$^1$H COSY and $90°$-$t_1$-$\tau_m$ (spin-lock)-$t_2$, $\tau_m$ = 250 ms, for $^1$H-$^1$H ROESY measurements.

## 4. RESULTS

### 4.1. A molecular model of BChl c

Figure 1 shows a molecular model of BChl **c** (8-ethyl-12-ethyl farnesyl bacteriochlorophyll **c**). Larger and smaller open circles indicate the carbon and hydrogen atoms, respectively, and the dotted, shaded and closed circles indicate the atoms of oxygen, nitrogen and magnesium. The closed bar indicates two coordination bonds along the x axis; it is used to visualize the orientation of the macrocycles in complicated stacked structures.

The molecular structure in the figure is based on the results of X-ray crystallography of ethyl chlorophyllide **a** [11] and ethyl chlorophyllide **b** [12] dihydrates. The following modifications have been made to construct a model of BChl **c** used here: (1) The vinyl group attached to C3 is replaced by the hydroxylethyl group in the R stereoisomeric configuration, and the rotational angle around the C3 - $C3^1$ bond can be adjusted whenever necessary in modelling aggregates to form the Mg···OH coordination bond. (2) The formyl group attached to C7 is replaced by a methyl group. (3) The methyl group attached to C12 is replaced by an ethyl group, whose conformation is assumed to be similar to that of the ethyl group attached to C8. (4) The ethyl group attached to the ester group is replaced by a methyl group in place of the farnesyl group (this is for simplicity but also because the conformation of the farnesyl group is not known.) (5) The central magnesium atom is assumed to be in the penta-coordinated state according to the resonance Raman results [13, 14]; the direction of its deviation out of the macrocycle plane can be adjusted whenever necessary to form a Mg···OH coordination bond.

### 4.2. Dependence of the electronic absorption spectrum on the solvent composition

Figure 2 shows the electronic absorption spectra of BChl **c** in mixed solvents of (a) 50, (b) 18, (c) 14, (d) 11, (e) 8, (f) 6, (g) 4, (h) 2 and (i) 1 $\mu$l methanol added to 550 $\mu$l chloroform. Spectrum (a) is essentially the same as that of BChl **c** dissolved in pure methanol [$\lambda_{max}$ for the Soret and $Q_y$ absorptions were 434 and 668 nm, respectively], and therefore the spectrum can be ascribed to the

BChl **c** monomer. However, when the amount of methanol is decreased, it is expected that the dimer as well as lower and higher oligomers of BChl **c** may be formed in this order. Spectrum (b) shows a weak shoulder on the longer wavelength of the $Q_y$ absorption, which can be ascribed to the formation of a dimer. The maximum of the $Q_y$ absorption starts to shift to longer wavelengths in spectrum (e) and shifts continuously to 674 nm in spectrum (i). In contrast, a new shoulder becomes visible in spectrum (d) around 705 nm, finally forming a clear shoulder in spectrum (i). This absorption grows at the expense of the 675 nm absorption as is clearly shown in the spectral change from (f) to (i).

In general, the spectral changes described above should be ascribed to a continuous shift of the equilibrium among the monomer, the dimer, and oligomers of different sizes. As a result, each spectrum must be ascribed to a mixture of these. However, as described in the Introduction, the monomeric and aggregated forms of ($3^1$R) BChl **c** have been classified spectroscopically into three forms, i.e., the monomer (666 - 667 nm), Form I (682 - 685 nm) and Form II (703 - 705 nm). Therefore, the above spectral changes, when the amount of methanol added to chloroform was decreased, can be safely ascribed to the creation of Form I (a dimer) followed by that of Form II (an oligomer or a mixture of them).

### 4.3. Dependence of the $^1$H-NMR spectrum of BChl c on the solvent composition

Figure 3 shows the $^1$H-NMR spectra of BChl **c** in the mixed solvents of (a) 50, (b) 18, (c) 14, (d) 11, (e) 8, (f) 6, (g) 4, (h) 2 and (i) 1 $\mu$l methanol added to 550 $\mu$l chloroform. The signals due to the solvents, i.e., methanol and chloroform, are indicated as M and C; the signals due to the farnesyl group are indicated as F. The factors of ordinate expansion are indicated in the figure except for the value 1.0. Systematic high-field-shift and decrease in peak intensity (broadening) are seen for the 5-H, $3^1$-H and 2Me-H, for example. (Hereafter, high-field-shift and low-field-shift will be abbreviated as hfs and lfs, respectively.) Such changes in chemical shift and in intensity have been examined for each $^1$H signal by the use of 25 different solvents (see the Experimental section for details). Assignment of the $^1$H signals was based on the $^1$H-$^1$H COSY and $^1$H-$^1$H ROESY spectra for each solution. [Hereafter, I abbreviate $^1$H as "H" when referring to the protons (hydrogen atoms) in BChl **c**.]

*Solvent dependence of chemical shifts*. Table 1 lists the values of the H chemical shifts for the 25 solvent mixtures; Figure 4 depicts each chemical shift as a function of the solvent composition.

Changes in chemical shift when the amount of methanol added to chloroform is decreased can be classified into four phases, i.e., the primary phase (P) and phases A, B and C. This classification is based on the patterns of the chemical-shift changes shown in the figure; the characteristics of these in each phase will be described below. Phase P: No clear changes are found except for some indication of changes in the subsequent phase A. Phase A: Gradual hfs of the 5-H, $3^1$-H, 2Me-H and $3^1$Me-H signals are found. For the remaining H signals, no clear changes in chemical shift are seen except for some indication of changes in phase B. Phase B: Progressive hfs starts for the above signals except for the $3^1$Me-H signal, which is not clear because of overlap with one of the farnesyl signals (see spectrum 3e). In contrast, gradual and progressive lfs take place for the 10-H and 17-H signals; some indication of lfs can also be observed for the 18-H, $8^1$-H and $8^1$Me-H signals. Phase C: Progressive hfs of the $12^1$-H signal takes place. High-field-shift of the $12^1$Me-H signal to be accompanied is unclear, because this signal overlaps with the solvent (methanol) signal and then disappears (see Figure 3e and 3g). In contrast, progressive lfs takes place for the 10-H, 18-H, 17-H, $8^1$-H and $8^1$Me-H signals. The above characteristics are summarized in Table 2.

The above classification of the four phases is somewhat arbitrary, but the following conclusions can be safely drawn: (1) Changes in chemical shift in phase A (and possibly in phase P) are the result of the formation of the dimer as the smallest aggregate. (2) The subsequent changes in phase B are progressive (of the same direction, additive and cooperative), and, therefore, they are ascribable to continuous formation of the dimers. (Possible formation of *lower* oligomers consisting of the above dimers stacked in a straight column will be mentioned in the Discussion.) (3) Some chemical-shift changes in phase C are similar to, but some of them are definitely different from, those in phase B. More specifically, the direction of changes is the same, but the magnitude increases progressively for the 10-H, 18-H, 17-H, $8^1$-H and $8^1$Me-H signals; the chemical shift continues to be constant for the $13^2$-H and 7Me-H signals; the chemical shifts start to change abruptly for the 18-H and $8^1$-H signals. The results suggest that the dimers are stacked not in a straight column but in an inclined column; if a straight column is being formed, the changes in the chemical shifts of all the H signals should be continuous between phase B and phase C.

*Solvent dependence of peak intensities.* Figure 5 shows the peak intensity of each H-signal as a function of the solvent composition: (a) a curve fitting to the observed points of each H signal, and (b) a comparison of the curves among all the H signals (except for $8^1$-H). The intensity of each H

signal is scaled to 1.0 for the solution containing 50 $\mu$l methanol in 550 $\mu$l chloroform. The intensity changes can be characterized as follows in terms of the four phases which have been defined above. Phase P: A quasi-linear decrease in intensity takes place for the 2Me-H, $3^1$Me-H, 5-H and $3^1$-H signals, while a gradual decrease in intensity takes place for the rest of signals. Phase A: The quasi-linear decrease in intensity continues to take place for all the above signals throughout this phase. The signal of $3^1$Me-H is an exception; it continuously decreases in intensity, overlaps the methanol signal (spectrum 3e), and then disappears. A progressive decrease in intensity commences for both the $12^1$-H and $12^1$Me-H signals, but the other signals continue to decrease gradually. Phase B: The quasi-linear decrease in intensity for the 2Me-H, 5-H and $3^1$-H signals continues with a slope similar to the above. Another quasi-linear decrease with a steeper slope takes place for the $12^1$-H and $12^1$Me-H signals, while a progressive decrease in intensity commences for the remaining signals, i.e., the 10-H, 18-H, 7Me-H, 17-H, $13^2$-H, $8^1$Me-H and 20Me-H signals (the latter two become unclear within this phase). Phase C: A progressive or continuous decrease in intensity takes place for the 18-H, 10-H, 17-H, $13^2$-H and 7Me-H signals, which alone remain in the NMR spectra. The above characteristics are summarized in Table 2.

The nature of the decrease in intensity for the H signals can be classified into three groups: (1) The 5-H, $3^1$-H, 2Me-H and $3^1$Me-H signals decrease in intensity linearly with a constant slope throughout the three phases, P, A and B; when extrapolated, the decrease is expected to persist even in phase C. It is interesting that the decrease in intensity of these signals starts in phase P before the clear changes in chemical shift, which have been described in the previous section, take place in phase A. (2) The $12^1$-H and $12^1$Me-H signals decrease in intensity gradually in phase P, progressively in phase A, and sharply in phase B (the slope gets steeper in the later phases); when extrapolated, the lines are expected to reach phase C. If it is a general rule that the broadening (decrease in peak intensity) of a signal precedes a change in its chemical shift, the extensive broadening of the $12^1$-H and $12^1$Me-H signals in phase B corresponds well with their changes in chemical shift in phase C. (3) The rest of signals, i.e., those of 10-H, $13^2$-H, 18-H, 17-H and 7Me-H, decrease gradually in phases P and A, progressively in phase B, and then sharply in phase C. These three groups of signals are expected to reflect different types of intermolecular interactions.

*NOE correlations.* Table 3 lists a set of intramolecular (○) and intermolecular (◎) NOE correlations found for BChl **c** dissolved into 11 $\mu$l methanol and 550 $\mu$l chloroform (phase B). $8^1$-H

correlates with the neighboring 7Me-H, $8^1$Me-H and 10-H (see Figure 1), and $8^1$Me-H correlates with both 7Me-H and 10-H. On the other hand, $12^1$-H correlates with neighboring 10-H and $12^1$Me-H, but $12^1$Me-H does not correlate with 10-H. Further, 17-H correlates with both $13^2$-H and 18Me-H; 18-H correlates with both 18Me-H and 20Me-H; and 18Me-H correlates with 20Me-H. These are all intramolecular correlations among the neighboring peripheral groups. Correlations among 2Me-H, $3^1$-H, $3^1$Me-H and 5-H were not clear in this solution due to the decrease of the intensity of these signals.

Figure 6 shows a ROESY spectrum obtained for the particular solution. A clear NOE peak is seen between the 7Me-H and 20Me-H signals. Since these Hs are located spatially apart within a single BChl **c** molecule, the peak can only be ascribed to an *intermolecular* correlation. This NOE peak is weaker than the intramolecular NOE peak between the 18-H and 20Me-H signals, but it is stronger than another intramolecular peak between the 20Me-H and 2Me-H signals. This intermolecular NOE peak was clear neither for solutions containing a larger amount of methanol probably due to the presence of a smaller amount of the dimers nor for solutions containing a smaller amount of methanol due to the overlap of the 20Me-H and $8^1$-H signals. A careful choice of the solvent composition enabled the observation of this particular signal.

### 4.4. Models for the BChl c aggregate forms in methanol-chloroform solvent mixtures

In modelling the aggregate forms in the methanol-chloroform mixtures I have made the following assumptions: (1) High-field-shift (low-field-shift) should take place for a signal of H which is located inside (outside) the contour of the macrocycle of the neighboring BChl **c** molecule [6], when the particular H is projected along the direction perpendicular to the macrocycle plane. No shifts should take place for a signal of H which is located on the edge of the macrocycle contour. (2) The environment of each BChl **c** molecule in the dimer should be approximately equivalent. (The BChl **c** molecules can never be equivalent in a strict sense, because only one stereoisomer is present in the dimer.) It must be a rule of nature that the environment of each molecule should become as equivalent as possible in an isotropic medium. The exchange rate is so large that the pair of molecules produce only one signal for each H, even though they are not equivalent. (3) The keto carbonyl and the hydroxyl groups should be hydrogen bonded with the solvent, methanol. The methanol/BChl **c**

mole ratio is nine even in the solvent mixture containing the minimum amount of methanol, i.e., 0.5 $\mu$l methanol in 550 $\mu$l chloroform. Therefore, those groups in one BChl molecule *should not* facilitate hydrogen bonding with the neighboring BChl molecule. (4) The structure of dimer should be stabilized by van der Waals interaction due to stacking and by a pair of Mg···OH coordination bonds. Actually, all the observables, i.e., changes in chemical shift and in peak intensity when the amount of methanol is decreased, lead us to models which satisfy the above assumptions. Therefore, some of these conditions were not necessarily prerequisite in building our models.

*Form I (the 675 nm component).* When the amount of methanol in the methanol-chloroform mixture is decreased, the dimer of BChl **c** is the first to be formed. Its formation seems to start in phase P and to complete in phase B. The dimer must satisfy the following conditions: (1) The $Q_y$ absorption should be shifted to approximately 675 nm (Figure 2). (2) Its formation should cause the hfs of the 5-H, $3^1$-H, 2Me-H and $3^1$Me-H signals, which becomes obvious in phase A and progressive in phase B (Figure 4). The shift is ascribable to the ring-current effect, and therefore, the hfs indicates that those Hs are located inside the contour of the neighboring macrocycle (Table 2). (3) The formation of the dimer should also cause a linear decrease in peak intensity (broadening) of the above signals (Figure 5). This must be due to the steric interaction of these Hs with the neighboring macrocycle (Table 2). (4) The formation of the dimer should cause simultaneously the lfs of the 10-H and 17-H signals (and possibly of the 18-H, $8^1$-H and $8^1$Me-H signals as well). This must be ascribed to the other type of the ring-current effect indicating that these Hs are located outside the contour of the neighboring macrocycle (Table 2). The progressive decrease in peak intensity for these H signals found in phase B must be due to the steric interaction among Hs in the peripheral groups. (5) The dimer should give rise to the intermolecular NOE correlation between 7Me-H and 20Me-H.

Figure 7a shows a model which substantiates all the above conditions: The changes in chemical shift and in peak intensity as well as the intermolecular NOE correlation of the relevant H signals can be easily traced in the front view and the top view of the dimer (use the labels of carbons to which the relevant Hs are attached). This structure enables the formation of a pair of Mg···OH coordination bonds. The pair of BChl **c** molecules constitute a $C_2$ rotation-translation symmetry, the geometry of which is usually referred to as "piggy-back" stacking [3, 5, 8, 9]. It is to be noted that this arrangement of the molecules causes close contact between 20Me-H and 7Me-H.

*Form II (the 705 nm component).* The second aggregate form to be created in the mixed

solvents, when the amount of methanol in chloroform is further decreased, is an oligomer (or a mixture of oligomers with different sizes). The formation of the oligomer(s) may start in phase B and becomes apparent in phase C. The oligomer should satisfy the following conditions: (1) Its $Q_y$ absorption should be further shifted to approximately 705 nm (Figure 2). This red shift suggests an inclined stacking of the macrocycles in the aggregate. (2) The formation of the oligomer should cause a completely different pattern in chemical-shift changes due to the ring-current effect: (a) Progressive hfs of the $12^1$-H signal shows that the particular H is located inside the contour of another macrocycle. (b) Progressive lfs of the 10-H, 18-H, 17-H, $8^1$-H and $8^1$Me-H signals indicates that a pair of macrocycles are almost completely overlapped. (c) No changes in chemical shift are seen for the $13^2$-H and the 7Me-H signals, and therefore, these Hs are located on the edge of the contour of the macrocycle. (3) The intensity of the $12^1$-H and $12^1$Me-H signals should decrease sharply in phase B prior to the hfs in phase C. The formation of the oligomer should cause a severe steric interaction around the 12-ethyl group.

Figure 7b shows a model for an oligomer which substantiates all the above conditions (I leave the size of the oligomer as an open question). A close examination of each condition by the use of the front and top views as well as the labels of the carbon atoms to which the relevant Hs are attached will reveal that this is the case. In particular, the hfs and the intensity decrease of Hs which are related to the 12-ethyl group have played a crucial role in building a model having this inclined packing of the dimers.

## 5. DISCUSSION

The "piggy-back" stacking of a pair of macrocycles in the dimer was first proposed by Smith et al. [7] for methyl bacteriochlorophyllide **d** in chloroform solution as one of two possible models, and it was subsequently proposed by Nozawa et al. [8] as a most probable model for bacteriochlorophyll **c** from *Chlorobium tepidum* which was also dissolved in chloroform; both results were based on $^1$H-NMR spectroscopy. These authors ascribed each pair of split H signals to the spectroscopically nonequivalent BChl molecules in the dimer which was formed in pure chloroform. However, the absorption spectrum of BChl **c** I obtained for pure chloroform solution exhibited both the 675 nm (Form I) and the 705 nm (Form II) peaks with comparative intensity. Therefore, I focused my

attention on the dimeric species (Form I) which was created when the amount of methanol in chloroform solution was decreased. In this Chapter, I have concluded the piggy-back stacking of the macrocycles for a dimer which gives rise to only one signal for each H in the BChl **c** molecule.

Figure 8 shows another model with a face-to-face stacking of a pair of macrocycles as well as a pair of Mg···OH coordination bonds [3]. An examination of the front view and the top view will reveal that the hfs of the 5-H, $3^1$-H, $3^1$Me-H and 2Me-H signals can be explained in terms of this particular model as well, a fact which has left some ambiguity in the previous structural assignment. However, it is absolutely clear that no NOE correlation should take place between the 20Me-H and the 7Me-H signals in this face-to-face stacking configuration. Thus, a definitive answer to question (1), which was addressed in the Introduction, has been found; the dimer takes the "piggy-back" stacking configuration.

Olson and Pedersen [4] as well as Chiefari et al. [5] assigned Form I to a dimer, and therefore I analyzed the $^1$H-NMR data of Form I in terms of a dimer. Here I point out that the progressive changes in chemical shift in phase B suggests possible formation of a lower oligomer, in which the dimers are stacked to form a straight column; this stacking configuration substantiates all the $^1$H-NMR characteristics as does the single dimeric unit. Further, no drastic changes in the $Q_y$ absorption should be caused by this type of stacking of the dimers, a fact which may have prevented the detection of this additional species by electronic absorption spectroscopy. I certainly need additional information on the number of BChl **c** molecules in Form I to make the final conclusion.

Nozawa et al. [9] and Chiefari et al. [5] assigned Form II to a linear aggregate of dimers formed through hydrogen bondings. However, it is highly unlikely that hydrogen bonds are formed in the present system, i.e., BChl **c** dissolved in a mixture of methanol and chloroform. In the present investigation, I have proposed a new model for spectroscopically the same "Form II" species based on the changes in chemical shift and in peak intensity when the amount of methanol in chloroform was reduced substantially. Our model is completely different from those of the previous authors in the arrangement of the dimers. Further, the "piggy-back" dimer used by Nozawa et al. [9] is essentially the same as, but the "face-to-face" dimer used by Chiefari et al. [5] is different from, the dimers I used here. My present model consisting of the piggy-back dimers stacked to form an inclined column explains nicely the $^1$H-NMR data. However, this structure needs to be established by $^{13}$C-NMR spectroscopy.

## 6. REFERENCES


(1) R. E. Blankenship, J. M. Olson and M. Miller, Anoxygenic Photosynthetic Bacteria, ed. by R. E. Blankenship, M. T. Madigan and C. E. Bauer, Kluwer Academic Publishers, The Netherlands (1995) 399.

(2) M. Mimuro, K. Matsuura, K. Shimada, Y. Nishimura, I. Yamazaki, M. Kobayashi, Z.-Y. Wang and T. Nozawa, Molecular Networks and Funneling Process of Energy Transfer in Green Photosynthetic Bacteria, in: proceeding of the Xth International Photosynthesis Congress, Montpellier, France (1995) in press.

(3) K. M. Smith, L. A. Kehres and J. Fajer, J. Am. Chem. Soc., 105 (1983) 1387.

(4) J. M. Olson and J. P. Pedersen, Photosynth. Res., 25 (1990) 25.

(5) J. Chiefari, K. Griebenow, N. Griebenow, T. S. Balaban, A. R. Holzwarth and K. Schaffner, J. Phys. Chem., 99 (1995) 1357.

(6) R. J. Abraham, K. M. Smith, D. A. Goff and J.-J. Lai, J. Am. Chem. Soc., 104 (1982) 4332.

(7) K. M. Smith, F. W. Bobe, D. A. Goff and R. J. Abraham, J. Am. Chem. Soc., 108 (1986) 1111.

(8) T. Nozawa, K. Ohtomo, Y. Morishita, H. Konami and M. T. Madigan, Chem. Lett., (1992) 261.

(9) T. Nozawa, K. Ohtomo, M. Suzuki, Y. Morishita and M. T. Madigan, Bull. Chem. Soc. Jpn., 66 (1993) 231.

(10) T. M. Wahlund, C. R. Woese, R. W. Castenholz and M. T. Madigan, Arch. Microbiol., 156 (1991) 81.

(11) H.-C. Chow, R. Serlin and C. E. Strouse, J. Am. Chem. Soc., 97 (1975) 7230.

(12) R. Serlin, H.-C. Chow and C. E. Strouse, J. Am. Chem. Soc., 97 (1975) 7237.

(13) M. Lutz and G. van Brakel, Green Photosynthetic Bacteria, ed. by J. M. Olson, Plenum Press, New York (1988) 23.

(14) P. Hildebrandt, H. Tamiaki, A. R. Holzwarth and K. Schaffner, J. Phys. Chem., 98 (1994) 2192.

Table1. Chemical shifts (in ppm) of the H signals of 8-ethyl-12-ethyl farnesyl bacteriochlorophyll **c**

| | Amount of methanol (μl) added to chloroform (550 μl) | | | | | | | | | | | |
|---|---|---|---|---|---|---|---|---|---|---|---|---|
| | 50 | 40 | 30 | 25 | 20 | 18 | 16 | 14 | 12 | 11 | 10 | 9.0 |
| 5 | 9.68 | 9.67 | 9.66 | 9.66 | 9.64 | 9.63 | 9.61 | 9.58 | | | 9.49 | 9.43 |
| 10 | 9.53 | 9.53 | 9.53 | 9.54 | 9.54 | 9.54 | 9.55 | 9.55 | 9.55 | 9.55 | 9.56 | 9.56 |
| $3^1$ | 6.35 | 6.34 | 6.33 | 6.33 | 6.30 | 6.28 | 6.26 | 6.22 | 6.17 | 6.14 | 6.09 | 6.02 |
| $13^2$ | 5.22 | 5.22 | 5.21 | 5.21 | 5.21 | 5.21 | 5.21 | 5.21 | 5.20 | 5.20 | 5.20 | 5.20 |
| 18 | 4.58 | 4.58 | 4.57 | 4.57 | 4.58 | 4.58 | 4.58 | 4.58 | 4.58 | 4.58 | 4.59 | 4.59 |
| 17 | 4.14 | 4.14 | 4.15 | 4.15 | 4.15 | 4.15 | 4.15 | 4.16 | 4.16 | 4.16 | 4.17 | 4.17 |
| $12^1$ | 4.08 | 4.08 | 4.08 | 4.08 | 4.07 | 4.07 | 4.07 | 4.07 | 4.07 | 4.06 | 4.06 | 4.06 |
| 20Me | 3.81 | 3.81 | 3.82 | 3.82 | 3.82 | 3.82 | 3.82 | 3.82 | 3.82 | 3.82 | 3.82 | 3.82 |
| $8^1$ | 3.77 | 3.77 | 3.77 | 3.77 | 3.78 | 3.78 | 3.78 | 3.78 | 3.78 | 3.79 | 3.79 | 3.79 |
| 2Me | 3.35 | 3.35 | 3.34 | 3.34 | 3.32 | 3.32 | 3.30 | | 3.26 | 3.23 | 3.21 | 3.17 |
| 7Me | 3.29 | 3.29 | 3.29 | 3.29 | 3.29 | 3.29 | 3.29 | 3.29 | 3.29 | 3.28 | 3.28 | 3.28 |
| $3^1$Me | 2.12 | 2.12 | 2.11 | 2.11 | 2.10 | 2.09 | 2.08 | 2.06 | | | | |
| $12^1$Me | 1.91 | 1.91 | 1.92 | 1.92 | 1.92 | 1.92 | 1.92 | 1.91 | 1.91 | 1.91 | 1.91 | 1.90 |
| $8^1$Me | 1.71 | 1.71 | 1.71 | 1.71 | 1.72 | 1.72 | 1.72 | 1.72 | 1.73 | 1.73 | 1.73 | 1.74 |
| 18Me | 1.52 | 1.52 | 1.52 | 1.52 | 1.52 | 1.52 | 1.52 | 1.52 | 1.52 | 1.52 | 1.52 | 1.52 |

Table1. (continued)

| | Amount of methanol (μl) added to chloroform (550 μl) | | | | | | | | | | | | |
|---|---|---|---|---|---|---|---|---|---|---|---|---|---|
| | 8.0 | 7.0 | 6.0 | 5.0 | 4.5 | 4.0 | 3.5 | 3.0 | 2.5 | 2.0 | 1.5 | 1.0 | 0.5 |
| 5 | 9.37 | 9.27 | 9.12 | | | | | | | | | | |
| 10 | 9.56 | 9.57 | 9.58 | 9.59 | 9.59 | 9.60 | 9.61 | 9.62 | 9.63 | 9.65 | 9.66 | 9.67 | 9.69 |
| $3^1$ | 5.93 | | | | | | | | | | | | |
| $13^2$ | 5.19 | 5.19 | 5.18 | 5.18 | 5.18 | 5.18 | 5.18 | 5.18 | 5.19 | 5.20 | 5.20 | 5.18 | |
| 18 | 4.60 | 4.61 | 4.62 | 4.65 | 4.65 | 4.66 | 4.68 | 4.70 | 4.71 | 4.74 | 4.77 | 4.80 | 4.83 |
| 17 | 4.18 | 4.19 | 4.20 | | | 4.23 | 4.26 | 4.28 | 4.30 | 4.31 | | | |
| $12^1$ | 4.05 | 4.04 | 4.05 | 4.05 | 4.04 | 4.03 | 4.02 | 4.01 | 4.00 | | | | |
| 20Me | 3.82 | 3.82 | 3.82 | 3.82 | 3.82 | 3.83 | 3.83 | 3.84 | 3.84 | 3.84 | | | |
| $8^1$ | 3.79 | 3.80 | | 3.85 | 3.86 | 3.86 | 3.87 | 3.89 | (3.90) | 3.93 | | | |
| 2Me | 3.12 | 3.05 | | | | | | | | | | | |
| 7Me | 3.27 | 3.27 | 3.26 | 3.25 | 3.25 | 3.25 | 3.24 | 3.24 | 3.24 | 3.24 | 3.24 | | |
| $3^1$Me | | | | | | | | | | | | | |
| $12^1$Me | 1.90 | | 1.87 | 1.85 | | | | | | | | | |
| $8^1$Me | 1.75 | 1.76 | 1.77 | 1.80 | 1.81 | 1.82 | 1.84 | 1.86 | 1.91 | 1.91 | | | |
| 18Me | 1.53 | | | | | | | | | | | | |

Table 2. Changes in chemical shift and in peak intensity of H signals found for different phases of BChl **c** in mixed solvent when the amount of methanol added to chloroform is increased. The origin of the changes is shown in a pair of parentheses

| Phase | Chemical shifts (ring current effects) | Peak intensity (steric interactions) |
|---|---|---|
| P | No clear changes | A quasi-linear decrease<br>2Me-H, $3^1$Me-H, 5-H, $3^1$-H<br>(overlap with the macrocycle)<br><br>Gradual decrease<br>the rest of Hs |
| A | Gradual hfs<br>5-H, $3^1$-H, 2Me-H, $3^1$Me-H<br>(inside the macrocycle contour) | Continuous quasi-linear decrease<br>2Me-H, $3^1$Me-H, 5-H, $3^1$-H<br>(overlap with the macrocycle)<br><br>Progressive decrease<br>$12^1$-H, $12^1$Me-H<br><br>Gradual decrease<br>the rest of Hs |
| B | Progressive hfs<br>5-H, $3^1$-H, 2Me-H<br>(inside the macrocycle contour)<br><br>Gradual lfs<br>10-H, 17-H; 18-H, $8^1$-H, $8^1$Me-H<br>(outside the macrocycle contour) | Further quasi-linear decrease<br>2Me-H, 5-H, $3^1$-H<br>(overlap with the macrocycle)<br><br>Rapid quasi-linear decrease<br>$12^1$-H, $12^1$Me-H<br>(overlap with the macrocycle)<br><br>Progressive decrease or disappearance<br>the rest of the signals<br>(overlap with the macrocycle or interaction among peripheral groups) |
| C | Progressive hfs<br>$12^1$-H<br>(inside the macrocycle contour)<br><br>Progressive lfs<br>10-H, 18-H, 17-H, $8^1$-H, $8^1$Me-H<br>(outside the macrocycle contour) | Continuous decrease<br>18-H, 10-H, 17-H, $13^2$-H, 7Me-H<br>(among peripheral Hs)<br><br>Disappearance<br>all the rest of the signals<br>(overlap with the macrocycle or interaction among peripheral groups) |

Table 3. Intramolecular (○) and intermolecular (◎) NOE corelations for a 8-ethyl-12-ethyl farnesyl bacteriochlorophyll *c* solution (11 μl methanol + 550 μl chloroform).

| | 2Me | $3^1$ | $3^1$ Me | 5 | 7Me | $8^1$ | $8^1$ Me | 10 | $12^1$ | $12^1$ Me | $13^2$ | 17 | 18 | 18Me | 20Me |
|---|---|---|---|---|---|---|---|---|---|---|---|---|---|---|---|
| 2Me | | | | | | | | | | | | | | | ○ |
| $3^1$ | | | | | | | | | | | | | | | |
| $3^1$Me | | | | | | | | | | | | | | | |
| 5 | | | | | | | | | | | | | | | |
| 7Me | | | | | | ○ | ○ | | | | | | | | ◎ |
| $8^1$ | | | | | ○ | | ○ | ○ | | | | | | | |
| $8^1$Me | | | | | ○ | ○ | | ○ | | | | | | | |
| 10 | | | | | | ○ | ○ | | ○ | | | | | | |
| $12^1$ | | | | | | | | ○ | | ○ | | | | | |
| $12^1$Me | | | | | | | | | ○ | | | | | | |
| $13^2$ | | | | | | | | | | | | ○ | | | |
| 17 | | | | | | | | | | | ○ | | | ○ | |
| 18 | | | | | | | | | | | | | | ○ | ○ |
| 18Me | | | | | | | | | | | | ○ | ○ | | ○ |
| 20Me | ○ | | | | ◎ | | | | | | | | ○ | ○ | |

## FIGURE CAPTIONS

**Figure 1.** A molecular model of 8-ethyl-12-ethyl farnesyl bacteriochlorophyll **c** (BChl **c**) based on the X-ray structures of ethyl chlorophyllide **a** dihydrate (Chow et al. 1975) and ethyl chlorophyllide **b** dihydrate (Serlin et al. 1975). The farnesyl group is replaced by a methyl group for simplicity (see text).

**Figure. 2**. Dependence of the electronic absorption spectrum of BChl **c** on the solvent composition, i.e., (a) 50, (b) 18, (c) 14, (d) 11, (e) 8, (f) 6, (g) 4, (h) 2 and (i) 1 $\mu$l methanol added to 550 $\mu$l chloroform.

**Figure 3.** Dependence of the $^1$H-NMR spectrum of BChl **c** on the solvent composition, i.e., (a) 50, (b) 18, (c) 14, (d) 11, (e) 8, (f) 6, (g) 4, (h) 2 and (i) 1 $\mu$l methanol added to 550 $\mu$l chloroform.

**Figure 4.** Dependence of the chemical shift of each H signal on the solvent composition shown as a function of the amount of methanol ($\mu$l) added to 550 $\mu$l chloroform.

**Figure 5.** Dependence of the peak intensity of each H signal on the solvent composition shown as a function of the amount of methanol ($\mu$l) added to 550 $\mu$l chloroform.

**Figure 6.** A ROESY spectrum for the solution of 11 $\mu$l methanol added to 550 $\mu$l chloroform. Both intramolecular and intermolecular NOE correlations are shown.

**Figure 7.** Models for the aggregate forms of BChl **c** present in the mixtures of methanol and chloroform: (a) The dimer with a piggy-back stacking of the macrocycles and (b) an oligomer in which the dimers are stacked to form an inclined column. Those Hs which played key roles in determining the structures are shown by indicating the carbon atoms to which they are attached.

**Figure 8.** A rejected model of dimer having a face-to-face stacking of the macrocycle and a pair of Mg···OH coordination bonds.

Fig. 1

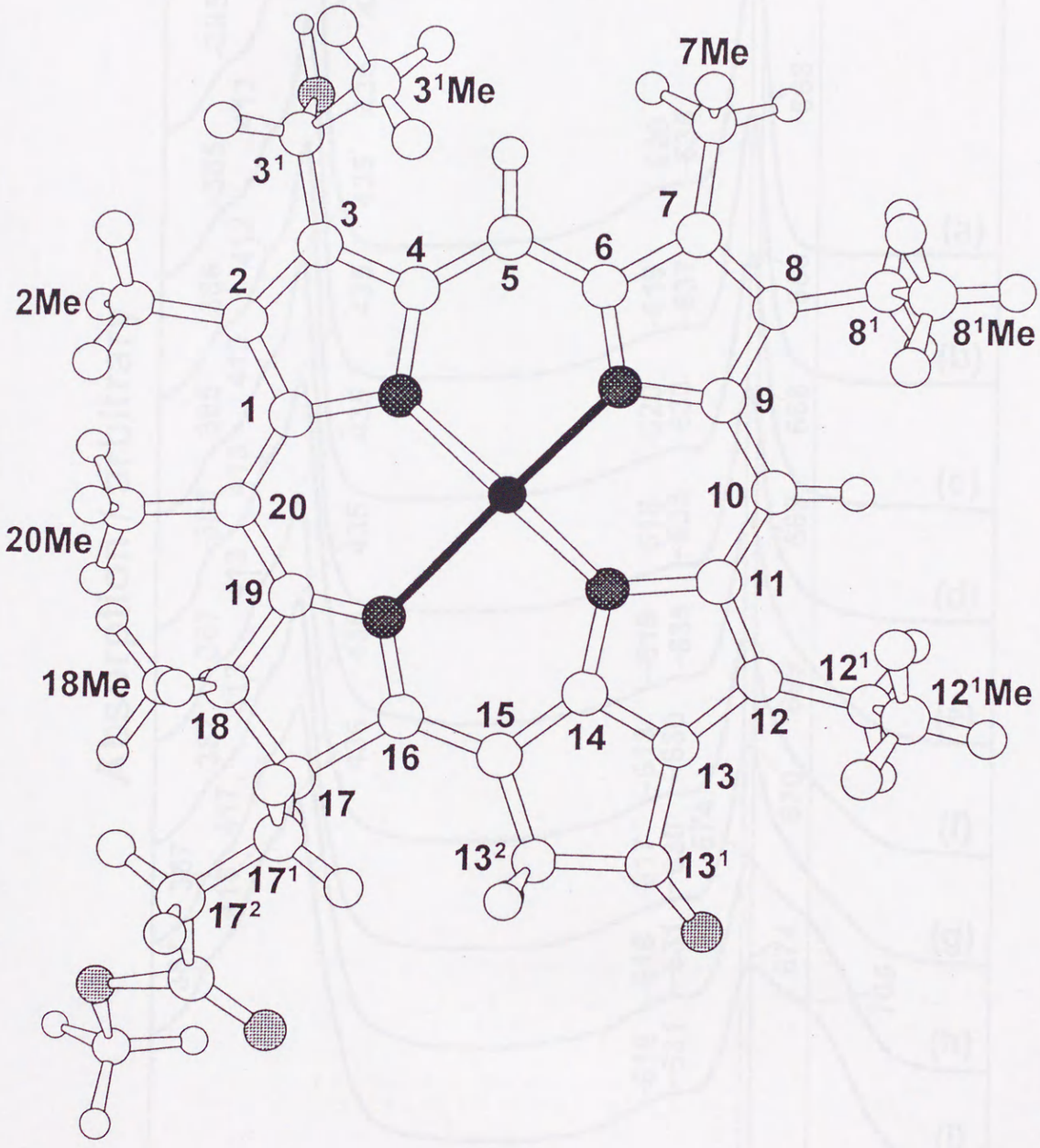
7Me
3¹Me
3¹
3
7
4
6
8
2
5
2Me
8¹
8¹Me
1
9
10
20
20Me
11
19
12¹
12¹Me
18Me
18
15
12
14
16
13
17
13²
13¹
17¹
17²

Fig. 2

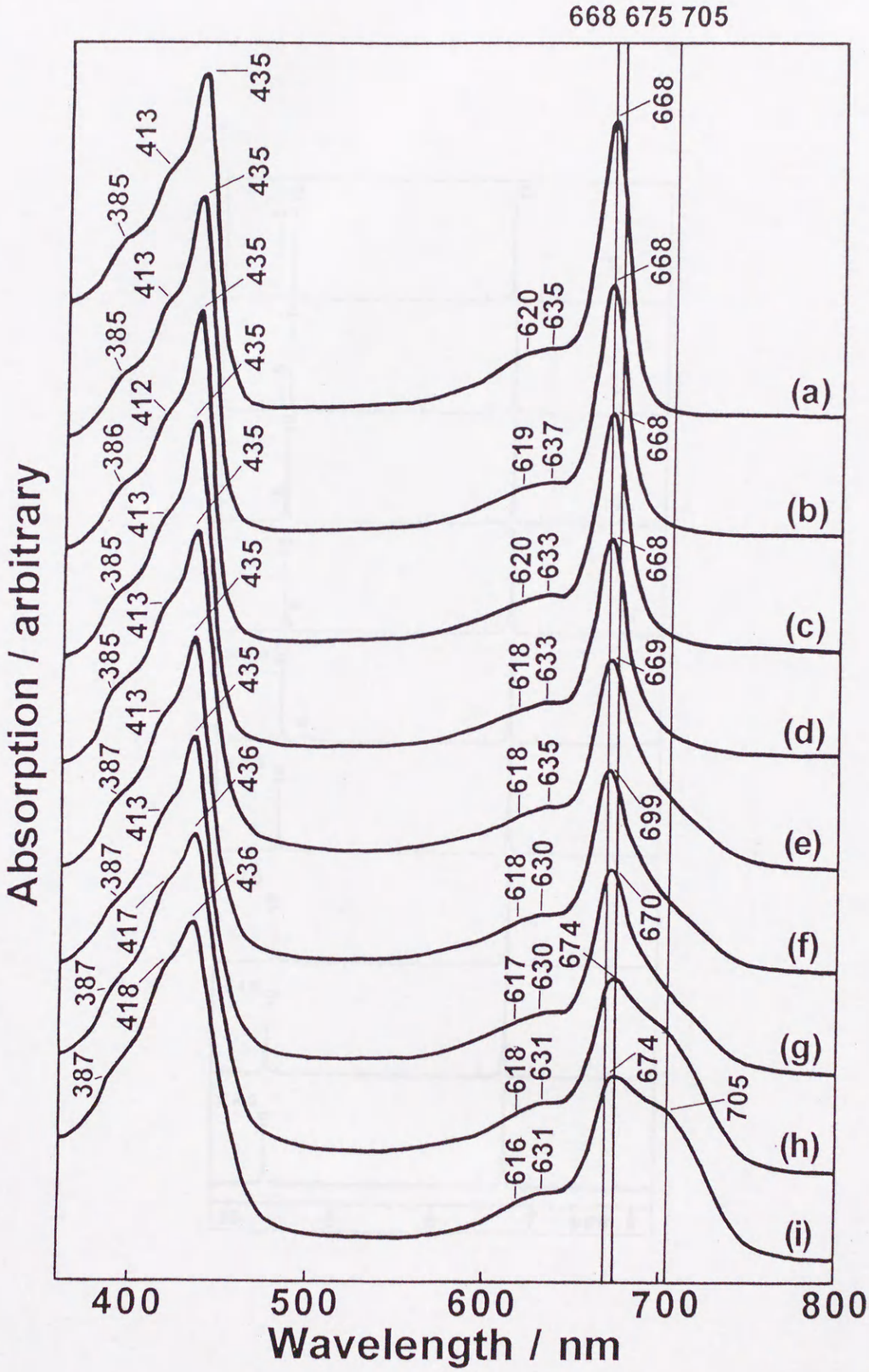
668 675 705
Absorption / arbitrary
Wavelength / nm
400
500
600
700
800
(a)
(b)
(c)
(d)
(e)
(f)
(g)
(h)
(i)

Fig. 3

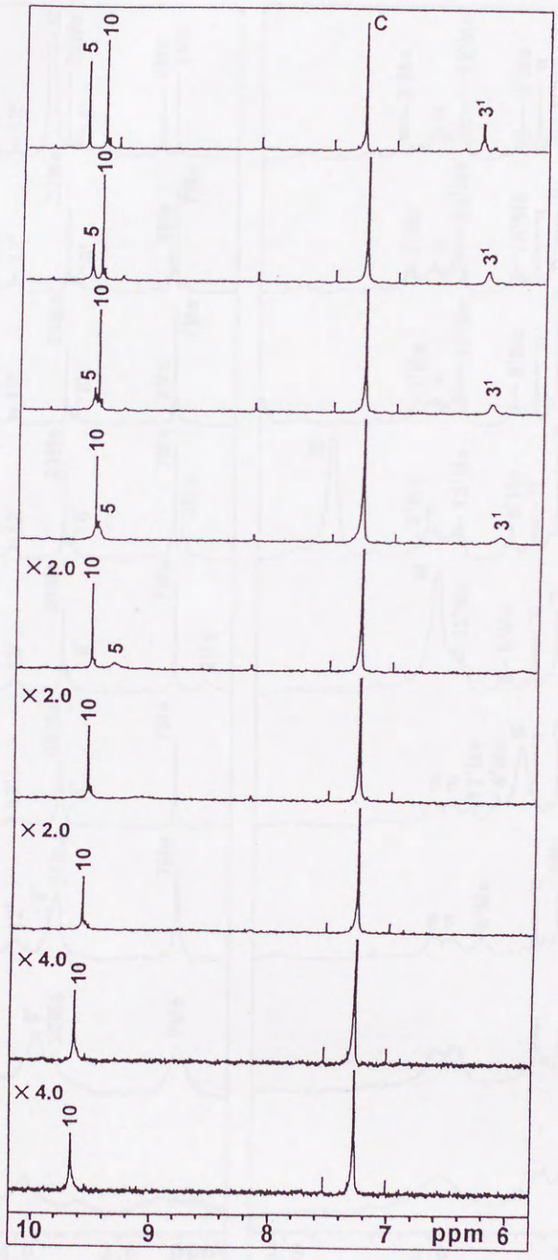

Fig. 3 (Continued)

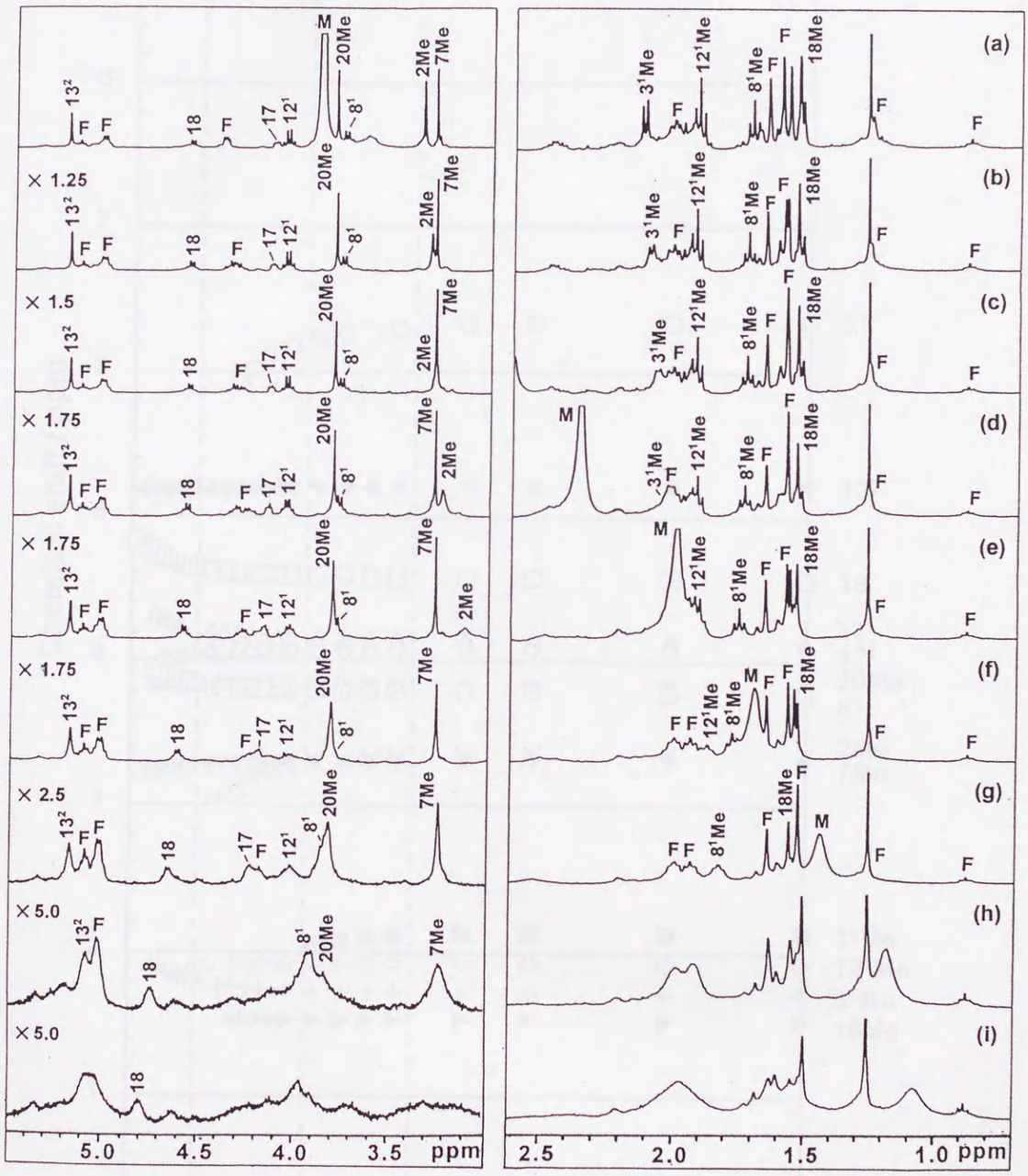

Fig. 4

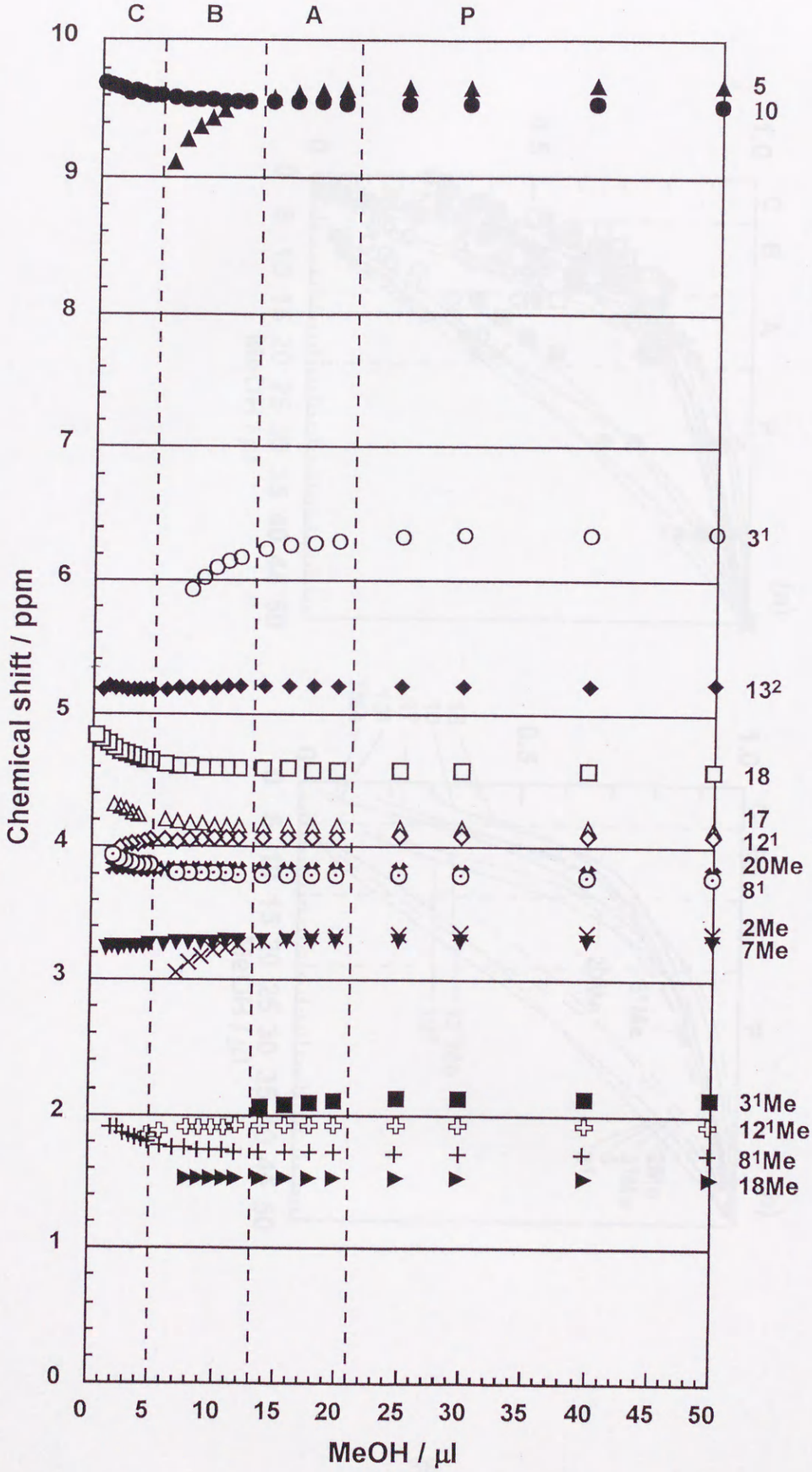
C
B
A
P
10
9
8
7
6
5
4
3
2
1
0
Chemical shift / ppm
0
5
10
15
20
25
30
35
40
45
50
MeOH / µl
5
10
3¹
13²
18
17
12¹
20Me
8¹
2Me
7Me
3¹Me
12¹Me
8¹Me
18Me

Fig. 5

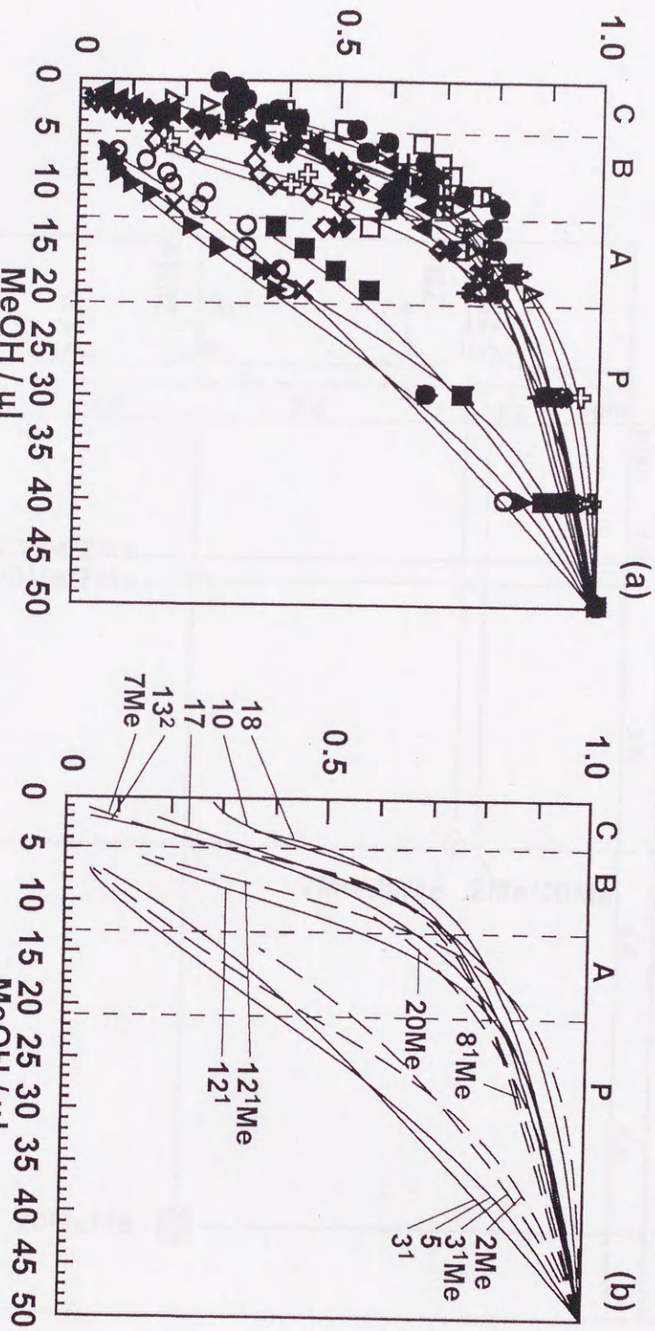
1.0
0.5
0
C B A P
(a)
0 5 10 15 20 25 30 35 40 45 50
MeOH / µl
(b)
18
10
17
13²
7Me
8¹Me
2bMe
12¹Me
12¹
2Me
3¹Me
5
3¹

Fig. 6

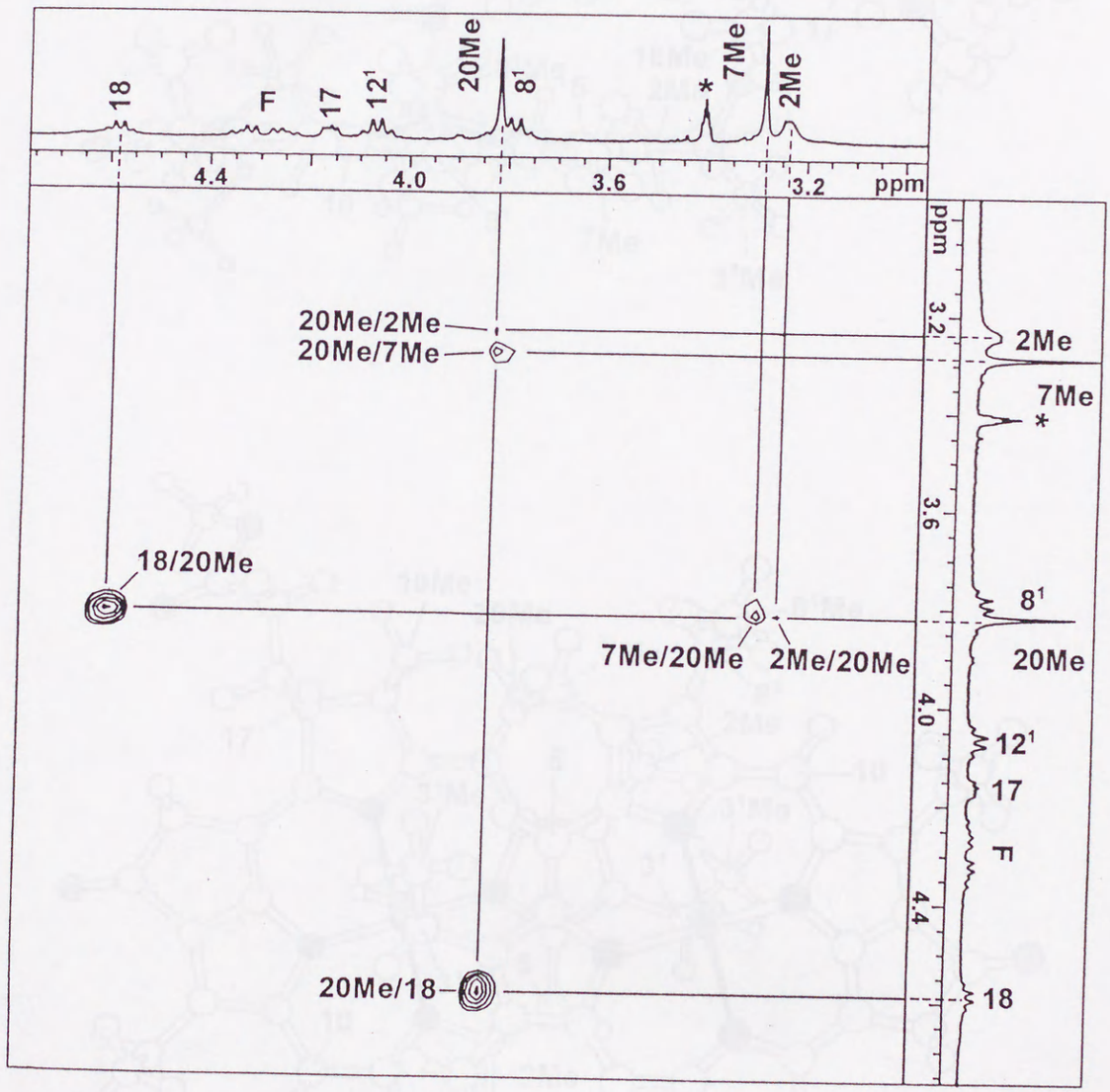
18
F
17
12¹
20Me
8¹
*
7Me
2Me
4.4
4.0
3.6
3.2
ppm
20Me/2Me
20Me/7Me
18/20Me
7Me/20Me
2Me/20Me
20Me/18
ppm
3.2
3.6
4.0
4.4
2Me
7Me
*
8¹
20Me
12¹
17
F
18

Fig. 7

(a)

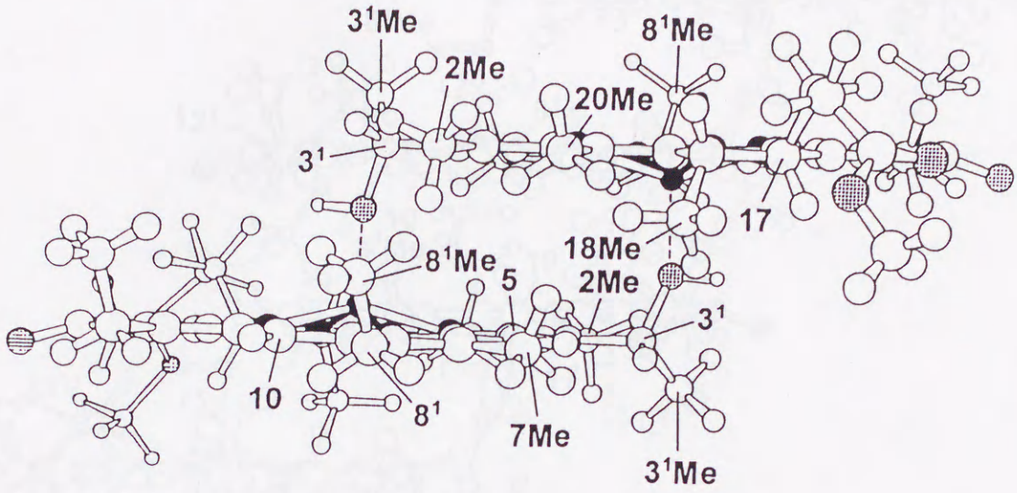
3¹Me
2Me
8¹Me
20Me
3¹
17
18Me
8¹Me
5
2Me
3¹
10
8¹
7Me
3¹Me

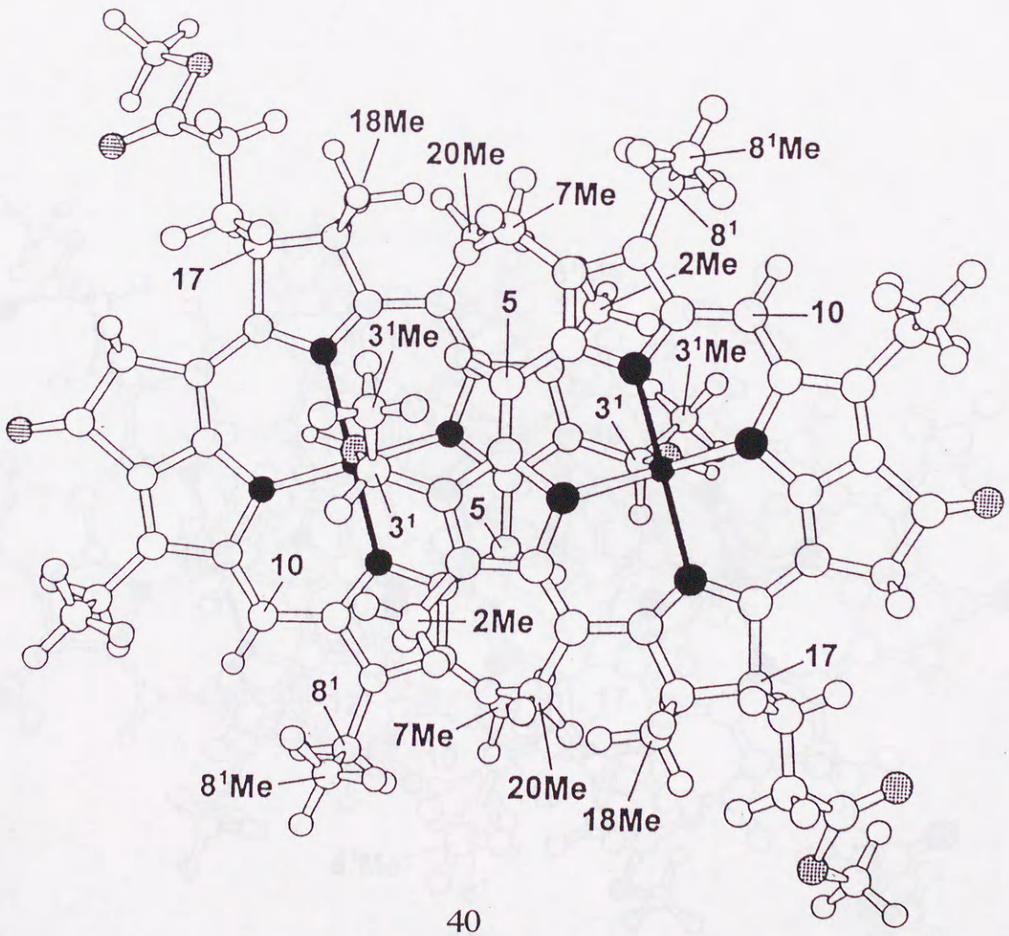
18Me
20Me
7Me
8¹Me
8¹
17
2Me
5
10
3¹Me
3¹Me
3¹
3¹
5
10
2Me
17
8¹
7Me
8¹Me
20Me
18Me

Fig. 7 (Continued)

(b)

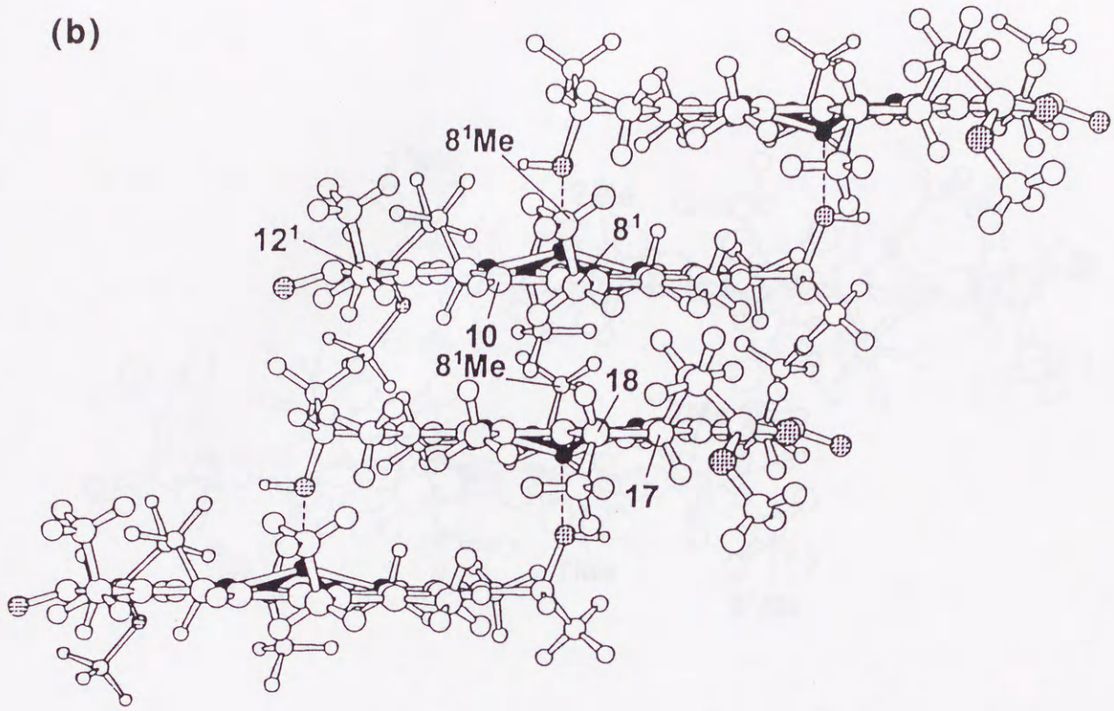


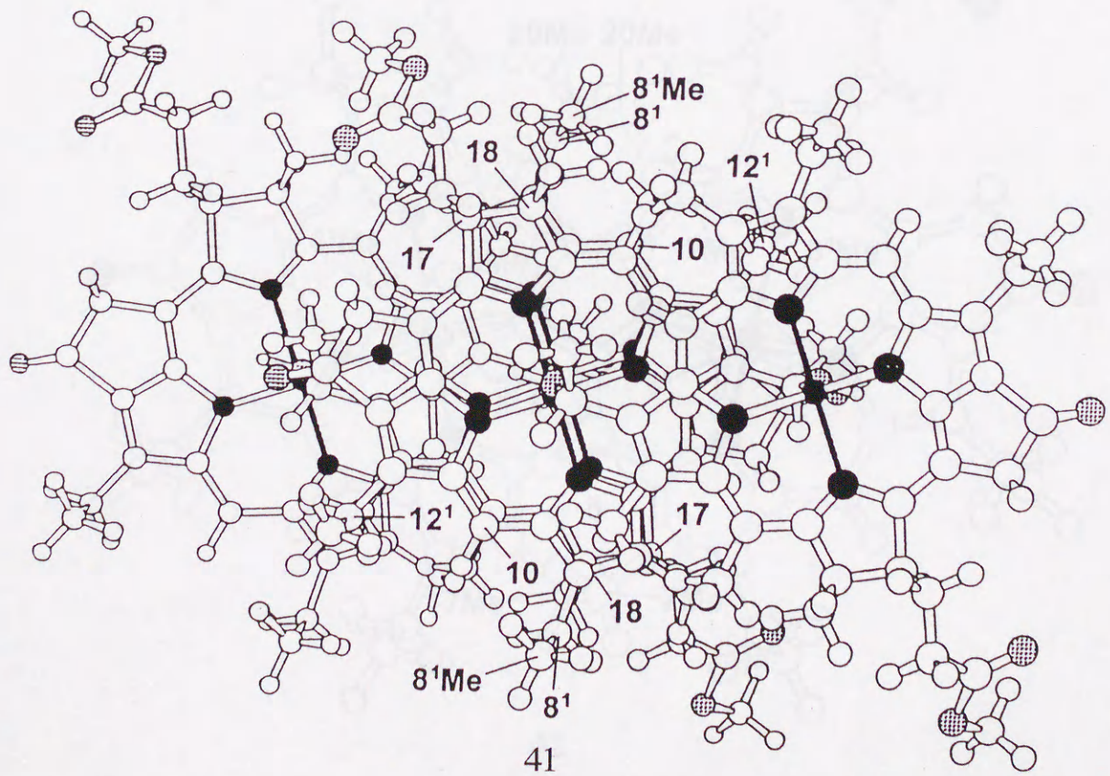

Fig. 8

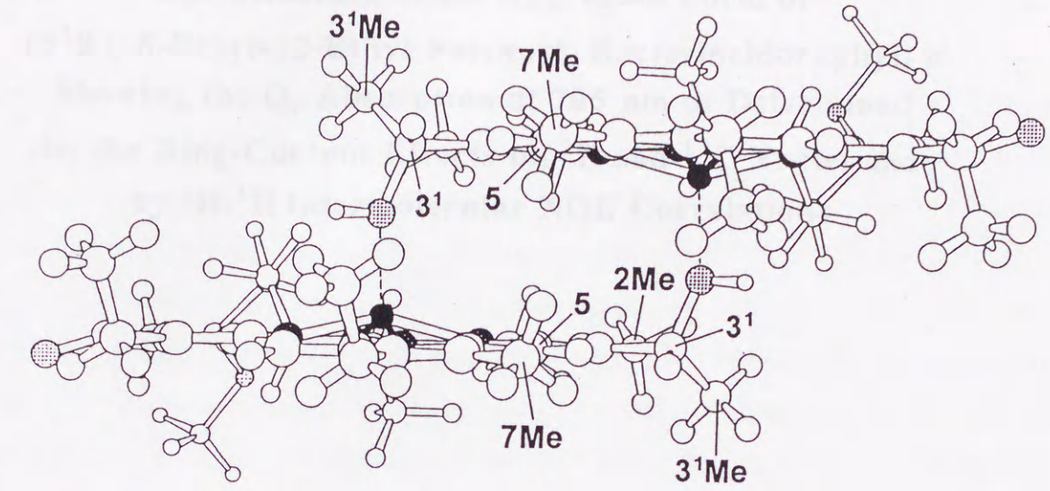
3¹Me
7Me
3¹
5
2Me
5
3¹
7Me
3¹Me

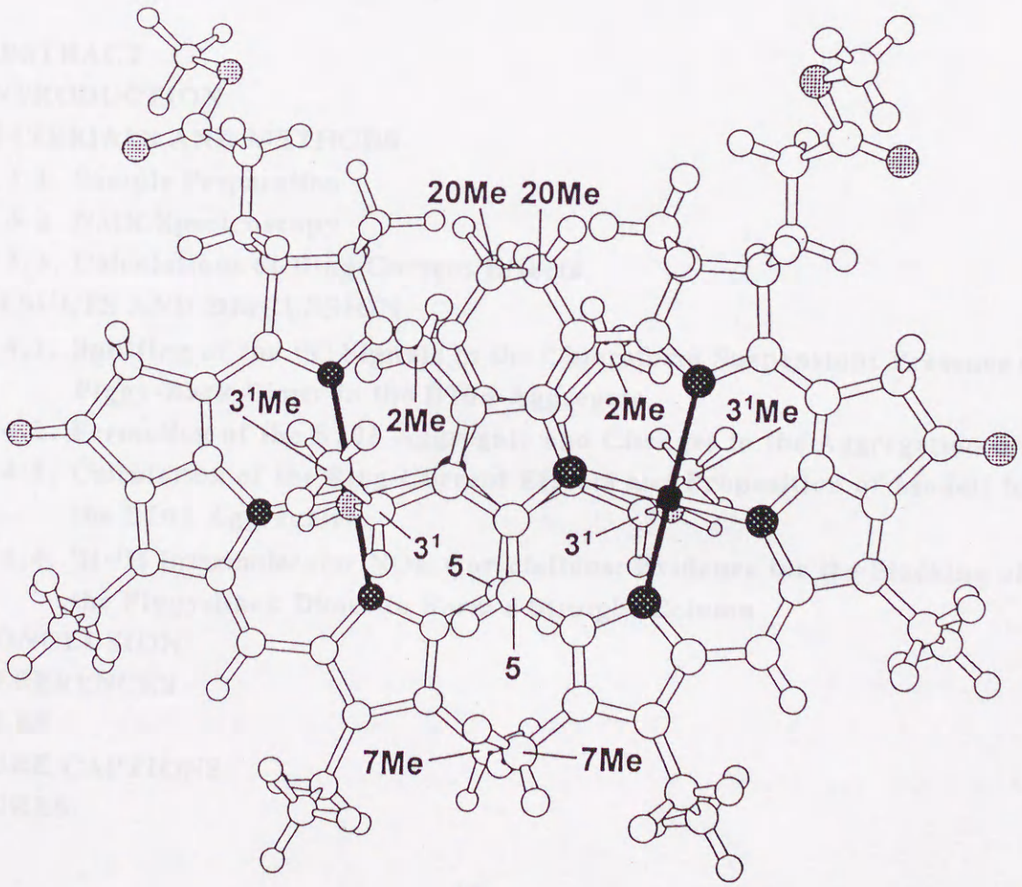
20Me 20Me
3¹Me
2Me
2Me
3¹Me
3¹
5
3¹
5
7Me
7Me

Chapter 2

# The Structure of the Aggregate Form of (3$^1$R), 8-Ethyl-12-Ethyl Farnesyl Bacteriochlorophyll *c* Showing the $Q_y$ Absorption at 705 nm as Determined by the Ring-Current Effects on $^1$H and $^{13}$C Nuclei and by $^1$H-$^1$H Intermolecular NOE Correlations

## 1. ABSTRACT

$^{13}$C-Enriched bacteriochlorophyll **c** (R[E, E] BChl $\mathbf{c}_F$) was suspended in chloroform to form an aggregate showing the $Q_y$ absorption at 705 nm. (1) The aggregate exhibited several largely-split $^{13}$C-NMR signals suggesting the presence of non-equivalent BChl **c** molecules in the form of the piggy-back dimer. (2) Changes in the $^{13}$C chemical shifts were traced when methanol was titrated to dissolve the aggregate, and the aggregation shifts (in reference to the monomeric state) were determined as a function of the amount of methanol titrated, and they were analyzed empirically. (3) The ring-current effects were calculated based on the loop-current approximation, and the results were compared with the observed aggregation shifts for $^{13}$C and $^{1}$H nuclei (the $^{1}$H aggregation shifts were determined by extrapolation of the data taken from Chapter 1). The results showed that the assembly of two straight columns consisting of the piggy-back dimer stacked in the antiparallel orientation is the best choice as a model for the B705 aggregate. (4) Three dimensional F1 $^{13}$C-edited F3 $^{13}$C-filtered heteronuclear single-quantum nuclear-Overhauser-effect spectroscopy was applied to the aggregate consisting of a 1:1 mixture of $^{13}$C-labeled and unlabeled BChl **c** in order to selectively detect the intermolecular $^{1}$H-$^{1}$H NOE correlations. The NOE correlations were explained in terms of a straight column, supporting the above model.

## 2. INTRODUCTION

Green photosynthetic bacteria have an antenna complex called 'chlorosomes' that contain bacteriochlorophyll **c** (BChl **c**) as the major component, and the self-assembly of the BChl **c** molecules is supposed to play a key role in forming the chlorosome structure [1-5]. Here, NMR spectroscopy has been used as a useful tool, one of the strategies to be chosen for the elucidation of the assembly of BChl **c** in chlorosomes is structural determination by NMR of better-defined *in vitro* aggregates followed by structural correlation with the real chlorosomes on the basis of spectral comparison; spectroscopies to be used include electronic absorption, resonance-Raman and circular dichroism.

*In vitro* aggregate forms of BChl **c** have been classified by the wavelength of the $Q_y$ absorption [6, 7]: (1) a dimer absorbing around 675 nm, (2) a 'lower aggregate' absorbing around 705 nm and (3) a 'higher aggregate' absorbing above 740 nm. Here, we note that no definitive information has been available concerning the size of these aggregates except for the dimer. I previously called the aggregate forms 'Form I', 'Form II' and 'Form III', respectively (Chapter 1) [8], but hereafter, I will call them 'the

B675 dimer', 'the B705 aggregate' and 'the B745 aggregate' according to the $Q_y$ absorption. The composition of these aggregate forms in a BChl **c** suspension depends on the stereoisomeric configuration of the hydroxyethyl group and the sidechains attached to 8 and 12 carbons of the BChl **c** molecule, and the BChl **c** concentration and the solvent in the suspension [6-10].

Most recently, the isotope-filtering method has been developed in order to selectively observe the $^1$H-$^1$H intermolecular NOE correlations between the $^{13}$C-labeled and unlabeled molecules [11]. This first application of the isotope-filtering technique to an aggregate consisting of a 1:1 mixture of $^{13}$C-labeled BChl **c** and unlabeled BChl **c** has enabled us to detect selectively the $^1$H-$^1$H intermolecular NOE correlations.

Concerning the structure of the B705 aggregate, two contradictory models have been proposed based on $^1$H-NMR spectroscopy: Nozawa et al. proposed a linear array of the piggy-back dimer to form the –C=O···H–O– hydrogen bonds (Figure 1b) [12], whereas Mizoguchi et al. proposed a stacking of the piggy-back dimer in the parallel orientation to form an inclined column (Figure 1c in Chapter 1) [8]. In order to solve this contradiction, I have applied the following two independent NMR techniques to this particular aggregate: (1) Comparison of the observed aggregation shifts (changes in chemical shifts due to aggregate formation in reference to the monomeric state) with the calculated ring-current effects due to the neighboring macrocycles: The $^1$H and $^{13}$C aggregation shifts were determined by tracing the changes in chemical shifts when methanol was titrated to dissolve the aggregate which was formed in chloroform, whereas the ring-current effects were calculated by using the loop-current approximation. (2) Determination of intermolecular $^1$H-$^1$H NOE correlations: Three dimensional F1 $^{13}$C-edited F3 $^{13}$C-filtered heteronuclear single-quantum correlation nuclear-Overhauser-effect spectroscopy (HSQC-NOESY) [11] was applied to a 1:1 mixture of $^{13}$C-labeled and unlabeled BChl **c** in order to selectively determine the intermolecular $^1$H-$^1$H NOE correlations. The results indicated that both models are to be abandoned, and that an assembly of two straight columns in which the piggy-back dimers are stacked in the antiparallel orientation (Figure 1f) should be proposed, instead, as a model for the B705 aggregate.

## 3. MATERIALS AND METHODS

### 3.1. Sample Preparation

(a) For the Measurements of Aggregation Shifts. The cells of *Chlorobium limicola* f. sp. *thiosulfatophilum* were grown in the medium of Wahlund et al. [13] containing both 1.0 g / l $NaH^{13}CO_3$

and 0.5 g / l $NaH^{12}CO_3$ as carbon sources. $^{13}$C-Enriched R[E, E] BChl $\mathbf{c}_F$, i.e., bacteriochlorophyll **c** ($3^1$R, 8-ethyl-12-ethyl, farnesyl; hereafter, abbreviated as 'BChl **c**') was extracted from the above cells, and then, it was isolated by HPLC from a mixture of BChl **c** components as described previous Chapter 1 except for the following HPLC conditions to collect the present isomer: column, a 20 mm $\phi$ x 300 mm ODS (octadecylsilane) column (Shinawa Chemical Industries, VX-ODS 5 $\mu$m); eluent, methanol; and flow rate, 3.0 - 3.5 ml· $min^{-1}$. The enrichment factor was determined to be ~ 45 % by the use of the relative intensities of the split and unsplit $^1$H signals from 5-H and 10-H (substituted $^{13}$C nuclei causes a pair of split $^1$H signals due to the $^{13}$C-$^1$H coupling, whereas $^{12}$C nuclei does not). The incorporation of $^{13}$C was not completely uniform because of the presence of an additional carbon source, 0.5 g / l $^{12}CH_3{}^{12}COONH_4$. This isomer of BChl **c** exhibited a single peak at the detection wavelength of 435 nm. BChl **c**, i.e., R[E,E] BChl $\mathbf{c}_F$, was suspended, at the concentration of 1.6 x $10^{-2}$ M, in 660 $\mu$l chloroform-$d_1$ (99.8 %, Nacalai tesque) which had been dried over 3 Å molecular sieve (Kishida Chemicals). Then, methanol-$d_4$ (99.8 %, Nacalai tesque) was titrated stepwise (0 ~ 100 $\mu$l) to the suspension.

(b) For the Determination of $^1$H-$^1$H Intermolecular NOE Correlations. The cells were grown in the medium of Wahlund et al. [13], in which sodium bicarbonate was replaced by 99% $NaH^{13}CO_3$ (SHOKO Co. Ltd., Japan), and the amount of natural-abundance ammonium acetate was reduced from 0.5 g / l to 0.1 g / l. The growth rate was approximately 2.5 times slower; the culturing was repeated twice. The enrichment factor was determined by the relative intensities of the split and unsplit H signals from 5-H, 10-H and $3^1$-H; it was > 95 % for 5-C and 10-C attached to the macrocycle, whereas it was > 83 % for $3^1$-C in the peripheral. A 1:1 mixture of the labeled and unlabeled BChl **c** was suspended in 660 $\mu$l chloroform-$d_1$ at the concentration of 2.5 x $10^{-3}$ M, and then 5.0 $\mu$l methanol-$d_4$ was added to partially dissolve the aggregate.

### 3.2. NMR Spectroscopy

For the determination of the aggregation shifts, a set of $^{13}$C-NMR spectra was recorded at 0 °C by the use of a JEOL JNM-A400 FT NMR Spectrometer; TMS (tetramethylsilane) was used as an internal standard. A set of assignments of $^{13}$C signals was obtained by the use of two-dimensional HMQC (heteronuclear multiple-quantum correlation), HMBC (heteronuclear multiple-bond correlation) and DEPT (distortionless enhancement by polarization transfer) spectra.

For the determination of the $^1$H-$^1$H intermolecular NOE correlations, the three dimensional F1 $^{13}$C-

edited F3 $^{13}$C-filtered HSQC-NOESY spectrum of the above particular solution was recorded at 0 °C by the use of a Varian Unity plus 600 MHz FT-NMR spectrometer. The spectrum was obtained by the use of the pulse scheme shown in Fig. 7a of ref.11. Experimental conditions were summarized as follows: the NOE mixing time, 400 ms; 3D spectrum, 32 increments in the F1 dimension, 69 increments in the F2 dimension, 960 complex points in the F3 dimension, and 16 scans for each increment; the spectral widths, 7334 Hz for the F1, 8000 Hz for the F2, and 8000 Hz for the F3. The $^{13}$C carrier frequency was set to 74.2 ppm. The total measuring time was 90.5 h.

The aggregation shift of each signal at '0 μl' methanol was determined, when necessary, by extrapolation of chemical-shift values at low methanol concentrations by the use of a function of the type, y=a[1 - exp(±x/b)]+c, where x is the amount of methanol, y is the chemical shift, and a, b and c are constants.

### 3.3. Calculations of Ring-Current Effects

The ring-current effects were calculated based on the loop-current approximation. This method was first developed by Johnson and Bovey [14] and applied to the benzene ring. Independently, I derived an equation to calculate the z-component of the magnetic flux from a circular loop current, and wrote a computer program to calculate the ring-current effects. The derivation of the equation is as follows: First, I assume circular current (I) with a radius (a) which is located at the origin and on the xy-plane. Then, the vector potential ($\mathbf{A}$) at a point P specified in the circular cylindrical coordinates, P(p, θ, z), can be given by

$$\mathbf{A} = \frac{\mu I}{4\pi} \oint \frac{d\mathbf{s}}{r}, \tag{1}$$

where μ is the magnetic susceptibility, and r is the distance between the point P and the infinitesimal line element $d\mathbf{s}$ on the circle. The components of $\mathbf{A}$ are given, by symmetry, as (0, $A_\theta$, 0), where

$$A_\theta = \frac{\mu I}{4\pi} \oint \frac{ds_\theta}{r}. \tag{2}$$

By making use of the complete elliptic integrals of the first and the second kinds, i.e.,

$$\mathbf{K}(k) \equiv \int_0^{\frac{\pi}{2}} \frac{d\phi}{\sqrt{1 - k^2 \sin^2 \phi}} \tag{3}$$

$$\mathbf{E}(k) \equiv \int_0^{\frac{\pi}{2}} \sqrt{1 - k^2 \sin^2 \phi} \cdot d\phi \tag{4}$$

where

$$k^2 = \frac{4a\rho}{(a+\rho)^2 + z^2}, \tag{5}$$

Eq. 2 turns out to be

$$A_\theta = \frac{\mu I}{\pi k}\sqrt{\frac{a}{\rho}}\left[(1-\frac{k^2}{2})\mathbf{K}(k) - \mathbf{E}(k)\right]. \tag{6}$$

Then, the magnetic flux $\mathbf{B}$ ($B_\rho$, 0, $B_z$) can be obtained by using the relation $\mathbf{B}$=rot $\mathbf{A}$ as follows;

$$B_\rho = -\frac{\partial}{\partial z}A_\theta \tag{7}$$

$$B_z = \frac{1}{\rho}\frac{\partial}{\partial \rho}(\rho A_\theta). \tag{8}$$

Using the relations

$$K'(k) \equiv \frac{d}{dk}K(k) = \frac{E(k)}{k(1-k^2)} - \frac{K(k)}{k} \tag{9}$$

$$E'(k) \equiv \frac{d}{dk}E(k) = \frac{1}{k}[E(k) - K(k)], \tag{10}$$

I finally obtain the following expressions,

$$B_\rho = \frac{\mu I}{4\pi}\frac{zk}{\rho\sqrt{\rho a}}\left\{\frac{1-\frac{k^2}{2}}{1-k^2}E(k) - K(k)\right\} \tag{11}$$

$$\mathrm{Bz} = \frac{\mu I}{2\pi}\frac{1}{\sqrt{(a+\rho)^2+z^2}}\left[\mathrm{K}(k) + \frac{a^2-\rho^2-z^2}{(a-\rho)^2+z^2}\mathrm{E}(k)\right]. \tag{12}$$

In writing a computer program, I expanded $K(k)$ and $E(k)$ into a pair of power series,

$$K(k) = \frac{(1+\kappa)\pi}{2}\sum\left\{\frac{(2r-1)!!}{(2r)!!}\right\}^2 \kappa^{2r} \tag{13}$$

$$E(k) = \frac{\pi}{2(1+\kappa)}\sum\left\{\frac{(2r-3)!!}{(2r)!!}\right\}^2 \kappa^{2r} \tag{14}$$

where

$$\kappa = \frac{1-\sqrt{1-k^2}}{1+\sqrt{1-k^2}}, \qquad (15)$$

and then, I took power up to r=3. I set the parameters as follows: $a$=4.5 Å, $n_e$=4.0, the interlayer distance within the piggy-back dimer, 3.0 Å, and the interlayer distance between the piggy-back dimers, 4.0 Å. Detailed arrangements of the BChl **c** molecules in models will be shown in figures.

## 4. RESULTS AND DISCUSSION

### 4.1. Splitting of the $^{13}C$ Signals in the Chloroform Suspension: Presence of Piggy-Back Dimer in the B705 Aggregate

Figure 2 shows a molecular model of BChl **c**, i.e., R[E,E] BChl $\mathbf{c}_F$, which has been used in the present investigation. This is the same model as used in the previous Chapter 1 except for the conformations of the ethyl groups attached to the 8 and 12 positions, which are now modified to facilitate molecular packing in the aggregates. The geometry of the macrocycle is taken from the results of X-ray crystallography of ethyl chlorophyllide **a** [15] and ethyl chlorophyllide **b** [16] dihydrates. See the previous Chapter 1 for the details of the model. Hereafter, each carbon atom will be referred to by the use of the labeled number, whereas a methyl hydrogen atom will be named after the carbon atom to which the particular methyl group is attached (concerning the methyl group in the hydroxyethyl group, for example, the carbon atom will be called '$3^2$-C', whereas the hydrogen atoms '$3^1$Me-H'). In building a model for the piggy-back dimer, the shift of the Mg atom out of the macrocycle plane and the conformation of the hydroxyethyl group were set differently to form a pair of Mg···OH coordination bonds (*vide infra*).

Figure 3 shows a set of representative $^{13}C$-NMR spectra of $^{13}C$-enriched BChl **c** (concentration 1.6 x $10^{-2}$ M) for (a) a monomer in the mixture of 100 μl methanol and 660 μl chloroform, (b) aggregates formed in 6 μl methanol and 660 μl chloroform, and (c) aggregates formed in chloroform without methanol. The monomer exhibited the $Q_y$ absorption at 668 nm. The aggregate for 6 μl methanol in chloroform exhibited an electronic absorption spectrum similar to that shown in Figure 2g of Chapter 1, which shows that the ratio of the B675 dimer : the B705 aggregate is 2:1. The electronic absorption spectrum of the aggregate in pure chloroform showed a pair of comparative $Q_y$ absorptions at 683 and 699 nm, indicating the ratio is approximately 1:1. When the amount of methanol titrated into the suspension of BChl **c** in chloroform is in the range

of 0 - 12 $\mu$l, the B675 dimer is always the major component and the B705 aggregate is the second major component; on the other hand, no indication of the B745 aggregate (see Figure 2 of ref. 10) was seen. These facts should be kept in mind in the analysis of the NMR data.

Because of the present $^{13}C$ enrichment factor of 45%, each $^{13}C$ signal consists of two components, i.e., split peaks due to coupling with the neighboring $^{13}C$ nuclei (nucleus) and a single peak without coupling. The signals of 4 carbon atoms out of 35 could not be identified for the following reasons: (1) the signal of 2-C due to overlap with that of the farnesyl group, (2) the 3-C and (3) 4-C signals which overlap with each other, and (4) the $13^2$-C signal due to overlap with that of methanol. A peak denoted as S is due to methanol in the solvent, and peaks denoted as F originate from the farnesyl group of BChl **c**.

Most importantly, the $^{13}C$-NMR spectrum of the aggregates in chloroform (without methanol) exhibits several widely-split peaks, which are circled in Figure 3c and listed in Table I. The result indicates that at least two BChl **c** molecules are located in different environments. Among them, the three largest splittings of the signals due to 5-C, 19-C and 14-C can be explained in terms of two different conformations of the hydroxyethyl groups in the piggy-back dimer to form a pair of Mg$\cdots$OH coordination bonds (see Figure 4). Table I lists the different distances between the $3^1$ Me group ($3^2$-C) and 5-C, 19-C and 14-C. Direct steric interaction between the methyl group and each relevant carbon atom or indirect interaction through another neighboring carbon or nitrogen atom may affect the electronic structure, and as a result, give rise to the different chemical shifts of the relevant carbon atoms. The splitting of the $3^1$-C signal is also ascribable to the two different conformations of the hydroxyethyl group; the local electronic structure around the particular carbon atom may be varied due to different steric and coordination interactions of the neighboring atoms. The splittings of the $17^3$-C and the $7^1$-C signals can be ascribed to the different conformations of the ester group and the ethyl group attached to the 8 position, respectively; these different conformations may originate from either the formation of the piggy-back dimer or further association of the dimers.

Thus, the splittings of the 5-C, 19-C, 14-C and $3^1$-C signals strongly suggest the presence of the piggy-back dimer in the B705 aggregate, a conclusion which is consistent to the previous propositions of the aggregate models using this piggy-back dimer as a structural component [8, 12].

### 4.2. Formation of the B705 Aggregate and Changes in the Aggregation Shifts

Figure 5 shows changes in the aggregation shifts for $^{13}C$ nuclei in reference to those in a monomeric state (100 $\mu$l methanol) when the amount of methanol is reduced toward zero (actual experiments were performed in the opposite direction by increasing the amount of methanol titrated). Different phases, P, A, B and C, are defined according to previous $^{1}H$ NMR spectroscopy (Chapter 1), by correlating the $^{1}H$-NMR spectra of the present suspension of 16 mM BChl **c** to those recorded previously using a suspension of 2.5 mM BChl **c** (Chapter 1). Table II lists the $^{13}C$ chemical shifts for 0, 14, 36, 52 and 100 $\mu$l methanol (in 660 $\mu$l chloroform) which are used in the division of different phases; aggregation shifts in each phase and the total aggregation shifts of 0 $\mu$l minus 100 $\mu$l methanol are also shown in the table.

When the amount of methanol is reduced, all the $^{13}C$ aggregation shifts show monotonous changes in Phases P and A. In Phase B, different patterns of the aggregation-shift changes emerge; see, for example, the changes in the $13^{1}$-C, $2^{1}$-C and $3^{2}$-C signals showing progressive high-field-shifts (hfs), the change in the 13-C signal turning from low-field-shift (lfs) to hfs, and the change in the $7^{1}$-C signal which gradually starts lfs. In Phase C, a completely different patterns of the aggregation-shift changes appear as continuation of the transformation in Phase B. Figure 6 depicts the signs of the aggregation shifts of $^{13}C$ nuclei for (a) Phase P, (b) Phases P + A and (c) Phase C; Figure 6d depicts the total aggregation shifts. Table III summarizes the $^{1}H$ aggregation shifts which are taken from Chapter 1; the values for 0 $\mu$l have been determined by extrapolation in the present investigation. The signs of the aggregation shifts of H nuclei in each phase and in total are also depicted in Figure 6.

When the schematic presentation of the stacked structures in Figure 1 and the molecular model in Figure 2 are taken into account, the aggregation shifts in each phase shown in Figure 6 suggest the following types of association or aggregation of the BChl **c** molecules. (a) Phase A: Hfs are seen for $3^{1}$-C in the hydroxyethyl group as well as for 1-C, 6-C, 9-C, 14-C, 16-C and 19-C all adjacent to the four nitrogen atoms ligating the central Mg atom. These changes strongly suggest the formation of the Mg$\cdots$OH coordination bond(s), which causes changes in the electronic structure. (b) Phase P+A: Additional hfs are seen in 2Me-H, $3^{1}$Me-H, $3^{1}$-H and 5-H as well as in $2^{1}$-C and $3^{1}$-C all located at the upper-left corner of the molecule, a fact which strongly suggests the formation of the piggy-back dimer. Based on the aggregation shifts, stacking of the piggy-back dimers to form an inclined or a straight column (Figures 1c and 1d) can also take place

in this phase because the hfs of the carbon atoms forming the 16-membered ring may be an indication of these structures (*vide infra*). (c) Phase C: Clearly split hfs regions, i.e., one at the upper-left corner (2Me-H, $3^1$-H, $3^1$Me-H and 5-H as well as $20^1$-, $2^1$-, $3^1$-, $3^2$- and 5-C) and the other at the lower-right corner ($12^1$Me-H and $12^1$-H as well as $12^1$-, 12-, 13- and $13^1$-C) are found. On the other hand, a clear lfs region is seen in-between crossing the center from the lower-left corner to the upper-right corner (18-H, $17^1$-H, $8^1$-H, $8^1$Me-H and 10-H as well as 19-, 18-, 17-, $17^2$-, $17^3$-, $13^2$-, 14-, 11-, 10-, 9-, $8^1$-, $8^2$-, $7^1$- and 6-C). The results strongly suggest the presence of the linear array of the piggy-back dimer (Figure 1b) or an assembly of either stacked column (Figure 1e or 1f).

The classification of each phase is somewhat arbitrary, and some of the hfs and lfs are left unexplained. This type of qualitative analysis is based on the ring-current effects due to the adjacent overlapping macrocycle, and the long-range ring-current effects can never be included. Therefore, calculations of the ring-current effects for various models are absolutely necessary to propose a model for the B705 aggregate.

### 4.3. Calculation of the Ring-Current Effects and Proposition of Models for the B705 Aggregates

The ring-current effects were calculated for all the models shown in Figure 1 except for those at the top (Structure 1 and Structure 2) that have been proposed as the basic structures of the B745 aggregate [17]; Figure 7 shows the results. The ring-current effects calculated for each model can be characterized as follows (see the panel indicated at the beginning of each characterization). (a): The formation of the piggy-back dimer gives rise to the hfs region at the upper-left corner and the rest of the part becomes the lfs region. This is due to the overlap of the upper left corners of the pair of macrocycles (see also Figure 1b). (b): A linear array of the piggy-back dimer (along the y-direction) produces the hfs regions at the upper-left and the lower-right corners; the rest of the part crossing the center from the lower-left to the upper-right corner becomes the lfs region. This is due to the shifted stackings of the macrocycles (Figure 1b). (c) and (d): Stacking of the piggy-back dimer in the parallel (antiparallel) orientation to form an inclined (straight) column causes an additional hfs region on the carbon atoms forming the 16-membered ring in the macrocycle. This is probably due to the complete overlap of the neighboring macrocycles newly introduced (Figures 1c and 1d). No clear difference is seen between the

inclined and straight columns. (e) and (f): When the stacked columns are assembled with each other along the y-direction, the clear hfs regions appear at the upper-left and the lower-right corners and the lfs region appears in-between crossing the central part from the lower-left to the upper-right corner. This is obviously due to the introduction of the shifted stacking of the macrocycles (similar to the case of the linear array of the piggy-back dimers). (g) and (h): The hfs regions shrink when the number of assembled columns increases further to 3. No clear difference is seen between the inclined and the straight columns, irrespective of the number of columns assembled.

The above results of the calculations of the ring-current effects confirm the qualitative analysis of the aggregation shifts described in the previous section: The observed aggregation shifts could be explained nicely in terms of an aggregate structure in which the basic unit of the piggy-back dimer is stacked together to form an inclined or a straight column, and it is assembled each other in the y-direction. However, I have tried more quantitative comparison between the observed aggregation shifts and the calculated ring-current effects.

Table IV compares for $^{1}H$ nuclei the signs of the observed aggregation shifts and those of the calculated ring-current effects for the various models mentioned above. The hfs and lfs are shown by - and +, respectively, and wrong predictions are marked by $\surd$. As far as the number of correct predictions of the signs (I call this 'score') is concerned, the highest score is found for the assembly of 2 inclined or straight columns (both 13/15); no difference is seen between the inclined and the straight columns to be assembled. When each correct prediction is weighted against the absolute value of the aggregation shift (I call this 'weighted score'), the highest score for the assembly of two columns becomes as high as 0.97, but no difference is seen between the different types of column.

Table V shows the same type of comparison for $^{13}C$ nuclei. Here, the highest score (24/31) and the highest weighted score (0.87) are found for the assembly of two straight columns. The second-highest score (23/31) and weighted score (0.86) are seen for the assembly of two inclined columns. Difference between the straight and the inclined columns is now found, even though it is very small.

Dependence of the ring-current effects on the number of layers on each side of the BChl **c** molecule in question was examined. However, it turned out that the pair of neighboring layers plays a dominant role, and that additional layers on both side showed little additional effects. On

the other hand, the dependence of the ring-current effects on the number of the piggy-back dimers in their linear array exhibited continuous lfs for all the nuclei, and the dependence became almost saturated when the number of the piggy-back dimer on each side became 2 (5 piggy-back dimers in total). Similar dependence was found for the number of the inclined or straight columns assembled. Therefore, the sizes of the models shown in Figure 1 are considered to bc large enough to characterize the ring-current effects for each model.

Thus, the calculations of the ring-current effects for the set of models show that the assembly of the two straight columns consisting of the piggy-back dimers stacked in the antiparallel orientation, is the most likely model for the B705 aggregate.

### 4.4. $^{1}$H-$^{1}$H Intermolecular NOE Correlations: Evidence for the Stacking of the Piggy-Back Dimer to Form a Straight Column

In general, $^{1}$H-$^{1}$H NOE correlations to be detected in the mixed aggregate of $^{13}$C-labeled and unlabeled BChl **c** can be classified into the following three types: (1) the NOE correlation between a pair of protons both of which are attached to the $^{13}$C atoms; (2) the NOE correlation between a pair of protons both of which are attached to the $^{12}$C atoms; and (3) the NOE correlation between a proton attached to the $^{12}$C atom and another proton attached to the $^{13}$C atom. In the present aggregate consisting of mixed $^{13}$C-labeled and unlabeled BChl **c**, type 1 and type 2 correlations can be ascribed to intramolecular NOE correlations within either the $^{13}$C-labeled or unlabeled BChl **c** molecule. On the other hand, type 3 correlation is ascribable to *intermolecular* NOE correlation between the $^{13}$C-labeled and unlabeled BChl **c** molecules. Thus, the isotope-filtering method can be applied to facilitate the selective observation of type 3 intermolecular NOE correlations [11].

Figure 8 shows the strip plots from the three dimensional intermolecular NOESY spectrum of a 1:1 mixture of the $^{13}$C-labeled and unlabeled BChl **c** molecules. Intermolecular $^{1}$H-$^{1}$H NOE correlations are selectively detected by the isotope-filtering technique (see Introduction). Table VI lists 9 independent NOE correlations found in the figure; here, the correlations among ten $^{1}$H signals are detected out of the fifteen $^{1}$H signals listed in Table III. Five signals including 2Me-H, 3$^{1}$Me-H, 3$^{1}$-H, 5-H and 12$^{1}$Me-H could not be detected; geometrically, these $^{1}$Hs are covered by the pair of macrocycles in the piggy-back dimer or in the assembly of the stacked columns.

Figure 9 shows that all the NOE correlations can be explained in terms of the straight column, i.e., the stacking of the piggy-back dimers in the antiparallel orientation. All the

correlations, (1) to (9), are labeled in the panels which include (a) a front view from a direction perpendicular to the direction of assembly, (b) another front view from the opposite direction, (c) a top view showing overlap between molecule I and molecule II, and (d) a top view showing overlap between molecule II and molecule III. Table VI lists also the distance of each $^1$H-$^1$H pair found in the NOE correlations which is estimated based on the present model. Since the positions of the H atoms in a methyl group vary depending on the internal-rotation angle around the C–Me bond, the C–C distances are also shown for reference. All the $^1$H-$^1$H distances listed in the table are within the detection limit of NOE correlation, 5 Å.

The intermolecular NOE correlations listed in Table VI, originating from close $^1$H-$^1$H contacts between the peripherals of the stacked BChl c pairs, can be classified into three different categories (see Figure 2 for the definition of Region L and Region R): Correlations between Region L and Region R, correlations between Region L and Region L, and correlations between Region R and Region R. Specific assignments of the NOE correlations are as follows: (a) Correlations 1, 2 and 3 (between Region L and Region R) can be assigned to the close $^1$H-$^1$H contacts on both sides of the piggy-back dimer; (b) correlations 4, 5 and 6 (between Region L and Region L) can be assigned to the close $^1$H-$^1$H contacts on one side of a completely-overlapped macrocycle pair; and (c) correlations 7, 8 and 9 (between Region R and Region R) can be assigned to the close $^1$H-$^1$H contacts on the other side of the completely-overlapped macrocycle pair. Therefore, all the intermolecular $^1$H-$^1$H NOE correlations predicted by the model could be actually observed except for the correlation of 18Me-H and 18-H, which escaped from the NOE detection.

Thus, selective detection of the intermolecular $^1$H-$^1$H NOE correlation provided us with definitive evidence for the presence of the straight column in the B705 aggregate.

## 5. CONCLUSION

(1) Splitting of the $^{13}$C-NMR signals in the aggregate formed in chloroform, (2) the aggregation shifts for $^1$H and $^{13}$C nuclei when the amount of titrated methanol is reduced, (3) the calculated ring-current effects on both nuclei in various models, and (4) $^1$H-$^1$H intermolecular NOE correlations have lead us to the conclusion that an assembly of two straight columns, each of which consists of the piggy-back dimer stacked in the antiparallel orientation, is the most likely model for the structure of the B705 aggregate, which is being formed when the amount of

methanol in the chloroform suspension of R[E,E] BChl $\mathbf{c}_F$ is reduced.

The model proposed by Nozawa et al., i.e., a linear array of the piggy-back dimers [12] (Figure 1b), explains neither the $^1H$ and $^{13}C$ aggregation shifts (see the lowest scores in Tables IV and V) nor the $^1H$-$^1H$ intermolecular NOE correlations listed in Table VI. The model proposed by Mizoguchi et al., i.e., the inclined column of stacked piggy-back dimers (Chapter 1) (Figure 1c) explains fairly well the $^1H$ and $^{13}C$ aggregation shifts (see Tables IV and V), but it does not explain completely the intermolecular $^1H$-$^1H$ NOE correlations. Thus, these two models should be abandoned.

## 6. REFERENCES


(1) R. E. Blankenship, J. M. Olson, and M. Miller, "Antenna complexes from green photosynthetic bacteria", in *Anoxygenic Photosynthetic Bacteria*, ed. by R. E. Blankenship, M. T. Madigan and C. E. Bauer, Kluwer Academic Publishers, The Netherlands, 1995, pp. 399-435.

(2) H. Tamiaki, "Supramolecular structure in extramembraneous antennae of green photosynthetic bacteria", *Coord. Chem. Rev.*, **148**, 183-197 (1996).

(3) J. M. Olson, "Chlorophyll organization and function in green photosynthetic bacteria", *Photochem. Photobiol.*, **67**, 61-75 (1998).

(4) T. Nozawa, K. Ohtomo, M. Suzuki, H. Nakagawa, Y. Shikama, H. Konami, and Z.-Y. Wang, "Structures of chlorosomes and aggregated BChl *c* in *Chlorobium tepidum* from solid state high resolution CP/MAS $^{13}C$ NMR", *Photosynth. Res.*, **41**, 211-223 (1994).

(5) T. S. Balaban, A. R. Holzwarth, K. Schaffner, G.-J. Boender, and H. J. M. de Groot, "CP-MAS $^{13}C$-NMR dipolar correlation spectroscopy of $^{13}C$-enriched chlorosomes and isolated bacteriochlorophyll *c* aggregates of *Chlorobium tepidum*: The self-organization of pigments is the main structural feature of chlorosomes", *Biochemistry*, **34**, 15259-15266 (1995).

(6) J. M. Olson, and J. P. Pedersen. "Bacteriochlorophyll *c* monomers, dimers, and higher aggregates in dichloromethane, chloroform, and carbon tetrachloride", *Photosynth. Res.*, **25**, 25-37 (1990).

(7) J. Chiefari, K. Griebenow, N. Griebenow, T. S. Balaban, A. R. Holzwarth, and K.

Schaffner.", Models for the pigment organization in the chlorosomes of photosynthetic bacteria: Diastereoselective control of *in-vitro* bacteriochlorophyll $c_s$ aggregation", *J. Phys. Chem.*, **99**, 1357-1365 (1995).

(8) T. Mizoguchi, L. Limantara, K. Matsuura, K. Shimada, and Y. Koyama, "Aggregation forms of 8-ethyl-12-ethyl farnesyl bacteriochlorophyll *c* in methanol-chloroform mixtures as revealed by $^1$H NMR spectroscopy", *J. Mol. Struct.*, **379**, 249-265 (1996).

(9) D. C. Brune, G. H. King, and R. E. Blankenship, "Interactions between bacteriochlorophyll *c* molecules in oligomers and in chlorosomes of green photosynthetic bacteria", in *Photosynthetic Light-Harvesting Systems*, ed. by H. Scheer and S. Schneider, Walter de Gruyter & Co., Berlin, New York, 1988, pp. 141-151.

(10) T. Mizoguchi, K. Matsuura, K. Shimada, and Y. Koyama, "The structure of the aggregate form of bacteriochlorophyll *c* showing the $Q_y$ absorption above 740 nm: A $^1$H-NMR study", *Chem. Phys. Lett.*, **260**, 153-158 (1996).

(11) K. Ogura, H. Terasawa, and F. Inagaki, "An improved double-tuned and isotope-filtered pulse scheme based on a pulsed field gradient and a wide-band inversion shaped pulse". *J. Biomol. NMR*, **8**, 492-498 (1996).

(12) T. Nozawa, K. Ohtomo, M. Suzuki, Y. Morishita, and M. T. Madigan, "Structures and organization of bacteriochlorophyll *c*'s in chlorosomes from a new thermophilic bacterium *Chlorobium tepidum*", *Bull. Chem. Soc. Jpn.*, **66**, 231-237 (1993) .

(13) T. M. Wahlund, C. R. Woese, R. W. Castenholz and M. T. Madigan, "A Thermophilic Green Sulfur Bacterium from New Zealand Hot Springs, *Chlorobium Tepidum* sp. nov", *Arch. Microbiol.* **156**, 81-90 (1991).

(14) C. E. Johnson, and F. A. Bovey "Calculation of Nuclear Magnetic Resonance Spectra of Aromatic Hydrocarbons", *J. Chem. Phys.* **29**, 1012-1014 (1958).

(15) H.-C. Chow, R. Serlin, and C. E. Strouse, "The crystal and molecular structure and absolute configuration of ethyl chlorophyllide *a* dihydrate. A model for the different spectral forms of chlorophyll *a*", *J. Am. Chem. Soc.*, **97**, 7230-7237 (1975).

(16) R. Serlin, H.-C. Chow, and C. E. Strouse, "The crystal and molecular structure of ethyl chlorophyllide *b* dihydrate at -153°", *J. Am. Chem. Soc.*, **97**, 7237-7242 (1975).

(17) T. Mizoguchi, S. Sakamoto, Y. Koyama, K. Ogura, and F. Inagaki, "The structure of the aggregate form of bacteriochlorophyll *c* showing the $Q_y$ absorption above 740 nm as

determined by the ring-current effects on $^{1}H$ and $^{13}C$ nuclei and by $^{1}H$-$^{1}H$ intermolecular NOE correlations", *Photochem. Photobiol.*, **67**, 239-248 (1998).

Table I. Some of large splittings of the $^{13}C$ signals of the 705 nm aggregate in chloroform without methanol (ppm).

| Carbon atom | Chemical shifts | Splitting | Distance and correlation[a] to $3^2$-C (Å) | |
|---|---|---|---|---|
| 5-C | 95.25, 101.10 | 5.85 | (a) 5.3 | (a') 4.9 |
| 19-C | 167.54, 169.62 | 2.08 | (b) 4.4 | (b') 6.0 |
| 14-C | 161.28, 162.88 | 1.60 | (c) 5.1 | (c') 4.9 |
| $17^3$-C | 173.44, 174.96 | 1.52 | | |
| $3^1$-C | 63.69, 64.83 | 1.14 | | |
| $7^1$-C | 11.15, 11.61 | 0.46 | | |

[a]See Figure 4.

Table II. The $^{13}C$ chemical shifts and the aggregation shifts for the B705 nm aggregate.

| Carbon atom | Amount of methanol titrated | | | | | Aggregation shifts in phase | | | | $\delta_{0\mu l}-\delta_{100\mu l}$ |
|---|---|---|---|---|---|---|---|---|---|---|
| | 0 µl | 14 µl | 36 µl | 52 µl | 100 µl | P | A | B | C | |
| 1-C | 153.55 | 153.54 | 153.68 | 153.79 | 153.96 | -0.17 | -0.11 | -0.14 | 0.01 | -0.41 |
| 5-C | 98.20 | 99.64 | 100.16 | 100.27 | 100.41 | -0.14 | -0.11 | -0.52 | -1.44 | -2.21 |
| 6-C | 150.85 | 150.61 | 150.66 | 150.74 | 150.94 | -0.20 | -0.08 | -0.05 | 0.24 | -0.09 |
| 7-C | 132.80 | 133.62 | 133.84 | 133.87 | 133.95 | -0.08 | -0.03 | -0.22 | -0.82 | -1.15 |
| 8-C | 143.65 | 143.68 | 143.71 | 143.75 | 143.84 | -0.09 | -0.04 | -0.03 | -0.03 | -0.19 |
| 9-C | 146.55 | 146.24 | 146.20 | 146.22 | 146.32 | -0.10 | -0.02 | 0.04 | 0.31 | 0.23 |
| 10-C | 106.35 | 105.98 | 105.92 | 105.93 | 106.02 | -0.09 | -0.01 | 0.06 | 0.37 | 0.33 |
| 11-C | 147.25 | 146.81 | 146.77 | 146.77 | 146.81 | -0.04 | 0 | 0.04 | 0.44 | 0.44 |
| 12-C | 140.20 | 141.06 | 141.24 | 141.24 | 141.24 | 0 | 0 | -0.18 | -0.86 | -1.04 |
| 13-C | 129.75 | 130.76 | 130.88 | 130.86 | 130.76 | 0.10 | 0.02 | -0.12 | -1.01 | -1.01 |
| 14-C | 162.10 | 161.42 | 161.41 | 161.45 | 161.57 | -0.12 | -0.04 | 0.01 | 0.68 | 0.53 |
| 15-C | 105.10 | 105.14 | 105.14 | 105.18 | 105.20 | -0.02 | -0.04 | 0 | -0.04 | -0.10 |
| 16-C | 153.40 | 153.98 | 154.20 | 154.26 | 154.35 | -0.09 | -0.06 | -0.22 | -0.58 | -0.95 |
| 17-C | 50.65 | 50.24 | 50.21 | 50.22 | 50.27 | -0.05 | -0.01 | 0.03 | 0.41 | 0.38 |
| 18-C | 49.45 | 48.52 | 48.33 | 48.33 | 48.39 | -0.06 | 0 | 0.19 | 0.93 | 1.06 |
| 19-C | 168.75 | 168.06 | 167.92 | 167.94 | 168.06 | -0.12 | -0.02 | 0.14 | 0.69 | 0.69 |
| 20-C | 105.10 | 105.14 | 105.14 | 105.18 | 105.20 | -0.02 | -0.04 | 0 | -0.04 | -0.10 |
| $2^1$-C | 14.65 | 16.83 | 17.33 | 17.39 | 17.45 | -0.06 | -0.06 | -0.50 | -2.18 | -2.80 |
| $3^1$-C | 64.10 | 65.14 | 65.39 | 65.41 | 65.41 | 0 | -0.02 | -0.25 | -1.04 | -1.31 |
| $3^2$-C | 23.45 | 25.14 | - | 25.87 | 26.11 | -0.24 | - | - | -1.69 | -2.66 |
| $7^1$-C | 11.40 | 11.15 | 11.07 | 11.07 | 11.06 | 0.01 | 0 | 0.08 | 0.25 | 0.34 |
| $8^1$-C | 19.95 | 19.66 | 19.61 | 19.62 | 19.66 | -0.04 | -0.01 | 0.05 | 0.29 | 0.29 |
| $8^2$-C | 17.95 | 17.73 | 17.69 | 17.69 | 17.71 | -0.02 | 0 | 0.04 | 0.22 | 0.24 |
| $12^1$-C | 20.60 | 21.11 | 21.23 | 21.25 | 21.30 | -0.05 | -0.02 | -0.12 | -0.51 | -0.70 |
| $12^2$-C | 17.10 | 17.03 | 17.10 | 17.14 | 17.20 | -0.06 | -0.04 | -0.07 | 0.07 | -0.10 |
| $13^1$-C | 196.35 | 197.11 | 197.56 | 197.73 | 197.99 | -0.26 | -0.17 | -0.45 | -0.76 | -1.64 |
| $17^1$-C | 29.70 | 29.86 | 29.90 | 29.91 | 29.96 | -0.05 | -0.01 | -0.04 | -0.16 | -0.26 |
| $17^2$-C | 31.20 | 30.84 | 30.80 | 30.82 | 30.89 | -0.07 | -0.02 | 0.04 | 0.36 | 0.31 |
| $17^3$-C | 174.25 | 173.99 | 174.00 | 174.03 | 174.12 | -0.09 | -0.03 | -0.01 | 0.26 | 0.13 |
| $18^1$-C | 20.85 | 20.89 | 20.91 | 20.92 | 20.96 | -0.04 | -0.01 | -0.02 | -0.04 | -0.11 |
| $20^1$-C | 21.40 | 21.55 | 21.58 | 21.59 | 21.61 | -0.02 | -0.01 | -0.03 | -0.15 | -0.21 |

Table III. The $^1$H chemical shifts and the aggregation shifts for the B705 nm aggregate[a].

| Proton atom | Amount of methanol titrated | | | | | Aggregation shifts in phases | | | | $\delta_{0\mu l}-\delta_{50\mu l}$ |
|---|---|---|---|---|---|---|---|---|---|---|
| | 0 µl | 5 µl | 12 µl | 20 µl | 50 µl | P | A | B | C | |
| 5 | 8.00 | 8.95 | 9.48 | 9.64 | 9.68 | -0.04 | -0.16 | -0.53 | -0.95 | -1.68 |
| 10 | 9.70 | 9.59 | 9.55 | 9.54 | 9.53 | 0.01 | 0.01 | 0.04 | 0.11 | 0.17 |
| $3^1$ | 4.90 | 5.60 | 6.17 | 6.30 | 6.35 | -0.05 | -0.13 | -0.57 | -0.70 | -1.45 |
| $13^2$ | 5.20 | 5.18 | 5.20 | 5.21 | 5.22 | -0.01 | -0.01 | -0.02 | 0.02 | -0.02 |
| 18 | 4.85 | 4.65 | 4.58 | 4.58 | 4.58 | ~0 | ~0 | 0.07 | 0.20 | 0.27 |
| 17 | 4.40 | 4.20 | 4.16 | 4.15 | 4.14 | 0.01 | 0.01 | 0.04 | 0.20 | 0.26 |
| $12^1$ | 3.95 | 4.05 | 4.07 | 4.07 | 4.08 | -0.01 | ~0 | -0.02 | -0.10 | -0.13 |
| 20Me | 3.85 | 3.82 | 3.82 | 3.82 | 3.81 | 0.01 | ~0 | ~0 | 0.03 | 0.04 |
| $8^1$ | 4.00 | 3.85 | 3.78 | 3.78 | 3.77 | 0.01 | ~0 | 0.07 | 0.15 | 0.23 |
| 2Me | 2.25 | 2.90 | 3.26 | 3.32 | 3.35 | -0.03 | -0.06 | -0.36 | -0.65 | -1.10 |
| 7Me | 3.25 | 3.25 | 3.29 | 3.29 | 3.29 | ~0 | ~0 | -0.04 | ~0 | -0.04 |
| $3^1$Me | 1.85 | 1.95 | 2.04 | 2.10 | 2.12 | -0.02 | -0.06 | -0.09 | -0.10 | -0.27 |
| $12^1$Me | 1.65 | 1.85 | 1.91 | 1.92 | 1.91 | 0.01 | -0.01 | -0.06 | -0.20 | -0.26 |
| $8^1$Me | 2.05 | 1.80 | 1.73 | 1.72 | 1.71 | 0.01 | 0.01 | 0.07 | 0.25 | 0.34 |
| 18Me | 1.55 | 1.55 | 1.52 | 1.52 | 1.52 | ~0 | ~0 | 0.03 | ~0 | 0.03 |

[a]Based on data from ref. 8.

Table IV. Comparison for the $^1H$ nuclei between the observed aggregation shifts and the calculated ring-current effects.

| Proton atom | Aggregation shifts | Piggy-back dimer | 'Linear array' | Inclined column | | | Straight column | | |
|---|---|---|---|---|---|---|---|---|---|
| | | | | 1 column | 2 columns[d] | 3 columns | 1 column | 2 columns[d] | 3 columns |
| 5-H | —[a] | — | — | — | — | — | — | — | — |
| 10-H | + | + | + | + | + | + | + | + | + |
| $3^1$-H | — | — | +✓ | — | — | — | — | — | — |
| $13^2$-H | — | +✓[b] | — | — | — | — | +✓ | — | — |
| 18-H | + | + | + | + | + | + | + | + | + |
| 17-H | + | + | + | + | + | + | + | + | + |
| $12^1$-H | — | +✓ | — | +✓ | +✓ | — | +✓ | +✓ | — |
| 20Me-H | + | + | + | + | + | + | + | + | + |
| $8^1$-H | + | + | + | + | + | + | + | + | + |
| 2Me-H | — | — | +✓ | — | — | +✓ | — | — | +✓ |
| 7Me-H | — | — | +✓ | +✓ | +✓ | +✓ | — | +✓ | +✓ |
| $3^1$Me-H | — | — | +✓ | — | — | +✓ | — | — | — |
| $12^1$Me-H | — | +✓ | — | +✓ | — | — | +✓ | — | — |
| $8^1$Me-H | + | + | + | + | + | + | + | + | + |
| 18Me-H | + | + | + | + | + | + | + | + | + |
| Score | | 12/15 | 11/15 | 12/15 | 13/15 | 12/15 | 12/15 | 13/15 | 13/15 |
| Weighted score[c] | | 0.94 | 0.55 | 0.93 | 0.97 | 0.78 | 0.94 | 0.97 | 0.82 |

[a]High-field shift and low-field shift are denoted as — and +, respectively.
[b]Wrong predictions are shown by ✓.
[c]A sum of the absolute values of observed aggregation shift for correct prediction devided by the sum of all the absolute values of observed aggregation shift.
[d]In the case of two columns, the ring-current effects for a pair BChl c molecules in the same central layer but in different environments are averaged.

Table V. Comparison for the $^{13}C$ nuclei between the observed aggregation shifts and the calculated ring-current effects.

| Carbon atom | Aggregation shifts | Piggy-back dimer | 'Linear array' | Inclined column | | | Straight column | | |
|---|---|---|---|---|---|---|---|---|---|
| | | | | 1 column | 2 columns[d] | 3 columns | 1 column | 2 columns[d] | 3 columns |
| 1-C | −[a] | − | +✓[b] | − | − | − | − | − | − |
| 5-C | − | − | − | − | − | − | − | − | − |
| 6-C | − | − | +✓ | − | − | − | − | − | − |
| 7-C | − | +✓ | +✓ | − | +✓ | +✓ | − | +✓ | +✓ |
| 8-C | − | +✓ | +✓ | +✓ | +✓ | +✓ | − | +✓ | +✓ |
| 9-C | + | + | + | −✓ | + | + | −✓ | + | + |
| 10-C | + | + | + | −✓ | + | + | −✓ | + | + |
| 11-C | + | + | + | −✓ | −✓ | −✓ | −✓ | −✓ | −✓ |
| 12-C | − | +✓ | − | − | − | − | − | − | − |
| 13-C | − | +✓ | − | − | − | − | − | − | − |
| 14-C | + | + | −✓ | −✓ | −✓ | −✓ | −✓ | −✓ | −✓ |
| 15-C | − | +✓ | +✓ | − | − | − | − | − | − |
| 16-C | − | +✓ | +✓ | − | − | +✓ | − | − | +✓ |
| 17-C | + | + | + | −✓ | + | + | + | + | + |
| 18-C | + | + | + | + | + | + | + | + | + |
| 19-C | + | + | + | −✓ | + | + | −✓ | + | + |
| 20-C | − | +✓ | +✓ | − | +✓ | +✓ | − | − | +✓ |
| $2^1$-C | − | − | +✓ | − | − | +✓ | − | − | +✓ |
| $3^1$-C | − | − | − | − | − | − | − | − | − |
| $3^2$-C | − | − | +✓ | − | − | − | − | − | − |
| $7^1$-C | + | + | + | + | + | + | −✓ | + | + |
| $8^1$-C | + | + | + | + | + | + | + | + | + |
| $8^2$-C | + | + | + | + | + | + | + | + | + |
| $12^1$-C | − | +✓ | − | +✓ | − | − | +✓ | − | − |
| $12^2$-C | − | +✓ | − | +✓ | − | − | +✓ | − | − |
| $13^1$-C | − | +✓ | − | − | − | − | +✓ | − | − |
| $17^1$-C | − | +✓ | +✓ | +✓ | +✓ | +✓ | +✓ | +✓ | +✓ |
| $17^2$-C | + | + | + | + | + | + | + | + | + |
| $17^3$-C | + | + | + | + | + | + | + | + | + |
| $18^1$-C | − | +✓ | +✓ | +✓ | +✓ | +✓ | +✓ | +✓ | +✓ |
| $20^1$-C | − | +✓ | +✓ | +✓ | +✓ | +✓ | +✓ | +✓ | +✓ |
| Score | | 18/31 | 18/31 | 19/31 | 23/31 | 21/31 | 19/31 | 24/31 | 21/31 |
| Weighted score[c] | | 0.66 | 0.57 | 0.81 | 0.86 | 0.69 | 0.75 | 0.87 | 0.69 |

[a]High-field shift and low-field shift are denoted as − and +, respectively.
[b]Wrong predictions are shown by ✓.
[c]A sum of the absolute values of observed aggregation shift for correct prediction devided by the sum of all the absolute values of observed aggregation shift.
[d]In the case of two columns, the ring-current effects for a pair BChl c molecules in the same central layer but in different environments are averaged.

Table VI. Observed intermolecular NOE correlations and the H-H and C-C atomic distances estimated on the basis of the partial straight-column structure shown in Figure 9.

| Intermolecular NOE correlations | Interacting regions | Estimated distances ( Å ) | |
|---|---|---|---|
| | | H-H | C-C |
| (1) 7Me-H ◄► 18-H | Region L ◄► Region R | 3.2 | 4.6 |
| (2) 7 Me-H ◄► 20 Me-H | | 1.4 | 2.8 |
| (3) 18 Me-H ◄► $8^1$ Me-H | | 3.9 | 5.8 |
| (4) 17-H ◄► $13^2$-H | Region L ◄► Region L | 3.5 | 5.0 |
| (5) 17-H ◄► 18-H | | 3.1 | 4.1 |
| (6) 20 Me-H ◄► 18-H | | 3.1 | 4.8 |
| (7) 10-H ◄► $8^1$-H | Region R ◄► Region R | 2.8 | 4.9 |
| (8) 10-H ◄► $12^1$-H | | 3.9 | 5.0 |
| (9) $8^1$-H ◄► $8^1$ Me-H | | 3.2 | 4.1 |

## FIGURE CAPTIONS

**Figure 1.** Schematic presentation of the real and hypothetical stackings of the macrocycles in the BChl **c** aggregates. (a) Structure 1 and Structure 2, in which the monomeric units are stacked together to form an inclined column with different sliding directions. (b) Piggy-back dimer, in which the second molecule is stacked back-to-face, after 180° rotation, to form a pair of the Mg··OH coordination bonds, and its 'linear array' along the y-axis. (c) Inclined column, which is formed by the stacking of the piggy-back dimer in the parallel orientation. (d) Straight columns which is formed by the stacking of the piggy-back dimer in the antiparallel orientation. (e) The assembly of two inclined columns and (f) the assembly of two straight columns both along the y-axis. For each monomeric unit (see Figure 2 for the molecular model), the front surface of the macrocycle is painted in black; its left-hand-side (Region L) is shaded and its right-hand-side (Region R) is left open. The y-direction of the macrocycle is indicated by the keto-carbonyl group, and the shift of the Mg atom out of the macrocycle plane is shown by a small solid circle with a triangle.

**Figure 2.** A molecular model for BChl **c** (R[E, E] BChl $\mathbf{c}_F$) used in the present investigation. Small open bullets, large open bullets, shaded bullets, dotted bullets and a solid bullet indicate the H, C, N, O and Mg atoms, respectively. The typification of carbon atoms, the definition of Region L and Region R as well as of the X and Y axes are also shown.

**Figure 3.** Representative $^{13}$C-NMR spectra of (a) a monomer, (b) a mixture of the B675 dimer and the B705 aggregate (2:1), and (c) another mixture of the B675 dimer and the B705 aggregate (1:1). BChl c is suspended in 660 $\mu$l chloroform at the concentration of $1.6 \times 10^{-2}$ M, and (a) 100 $\mu$l, (b) 6 $\mu$l and (c) 0 $\mu$l methanol were added to the suspension. Peaks marked S and F are due to methanol in the solvent and the farnesyl group of BChl **c**, respectively. Large splittings of the $^{13}$C signals in spectrum (c) are marked with circles.

**Figure 4.** Different conformations of the hydroxyethyl groups of BChl **c** in the piggy-back dimer. Those carbon atoms which give rise to largely split signals in the NMR spectrum shown in Figure 3c are marked. Distances between the 3$^1$Me group and those carbon atoms giving rise to the

three largest splittings (5-C, 19-C and 14-C) are indicated (see Table I).

**Figure 5.** Changes in the $^{13}C$ aggregation shifts as a function of the amount of methanol titrated. Different phases, P, A, B and C, in the process of the B705 aggregate formation, are those defined previously by the changes in the $^{1}H$ aggregation shifts (Chapter 1). BChl **c** was dissolved in 660 $\mu$l chloroform at the concentration of $1.6 \times 10^{-2}$ M.

**Figure 6.** The $^{1}H$ and $^{13}C$ aggregation shifts for (a) Phase P, (b) Phase P+A and (c) Phase C. Those aggregation shifts whose absolute values are larger than 0.08 alone are shown for simplicity. The $^{1}H$ aggregation shifts were determined by extrapolation of the data from the previous Chapter 1. Solid bullet indicate high-field-shift (hfs) and shaded bullet low-field-shift (lfs); open bullet show either the $^{1}H$ and $^{13}C$ nuclei whose shifts are not observed (less than 0.08) or the N, O or Mg nuclei which are not relevant. (d) The $^{1}H$ and $^{13}C$ aggregation shifts in total, i.e., 0 $\mu$l - 100 $\mu$l methanol, are also shown (small shifts are also shown in this case).

**Figure 7.** The calculated ring-current effects on $^{1}H$ and $^{13}C$ nuclei for (a) the piggy-back dimer, (b) the linear array of the piggy-back dimer, (c) a single inclined column, (d) a single straight column, the assembly of (e) 2 and (g) 3 inclined columns, and the assembly of (f) 2 and (h) 3 straight columns. See Figure 1 for the definition of the structural models, and see Figure 6 for the expression of hfs and lfs (small shifts are also included).

**Figure 8.** Strip plots from the three dimensional, intermolecular $^{1}H$-$^{1}H$ NOESY spectrum of a 1:1 mixture of $^{13}C$-labeled and unlabeled BChl **c** . Diagonal peaks are labeled 'D'.

**Figure 9.** A partial structure of the straight column (Figure 1d) as a basic unit of the B705 aggregate, (a) a front view from a direction perpendicular to the direction of assembly, (b) another front view form the opposite direction, (c) a top view showing the overlap between molecule I and molecule II, and (d) another top view showing the overlap between molecule II and molecule III. Nine different types of intermolecular $^{1}H$-$^{1}H$ correlations, which are listed in Table VI, are shown based on this partial structure.

Fig. 1

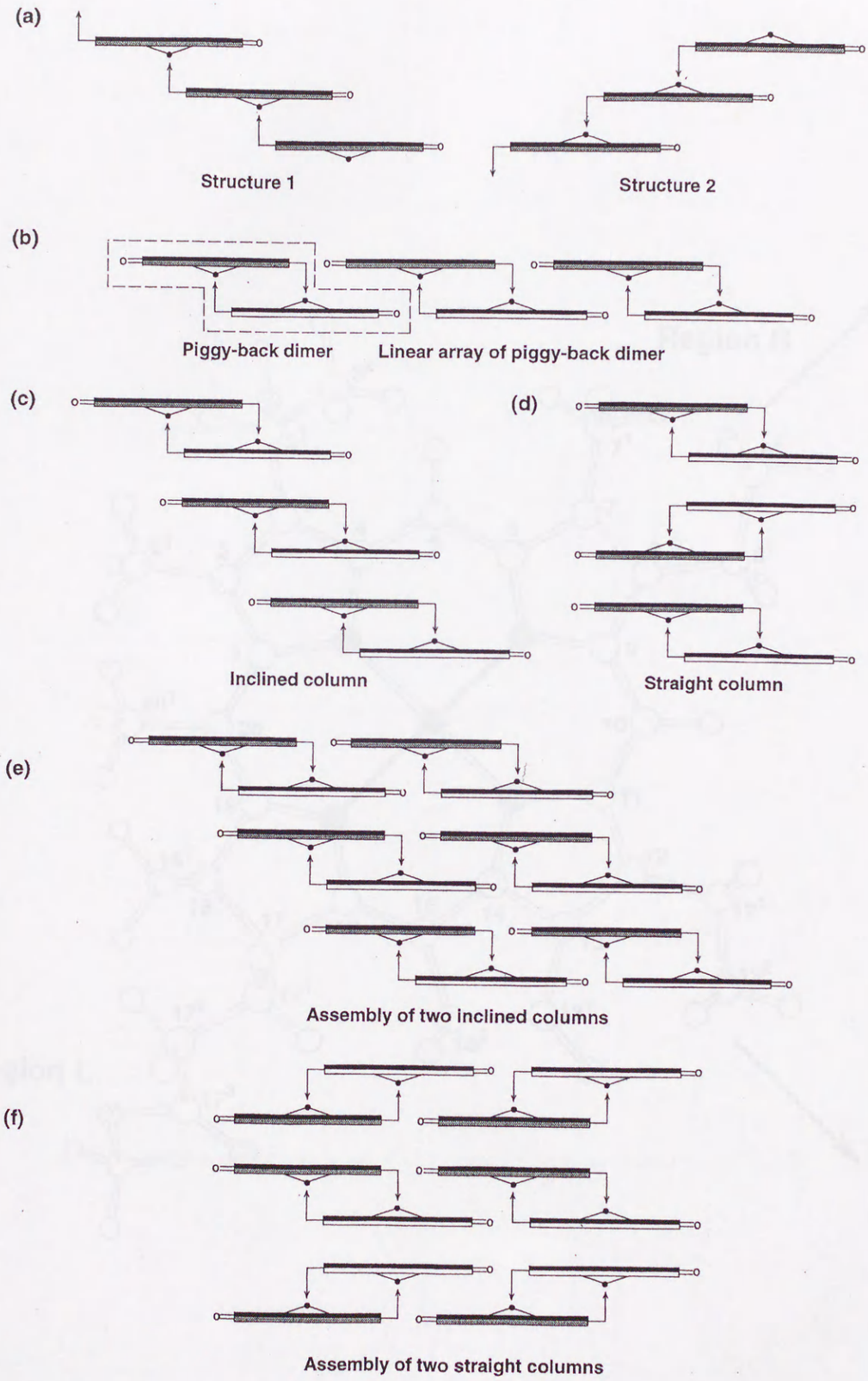
(a)
Structure 1
Structure 2
(b)
Piggy-back dimer
Linear array of piggy-back dimer
(c)
Inclined column
(d)
Straight column
(e)
Assembly of two inclined columns
(f)
Assembly of two straight columns

Fig. 2

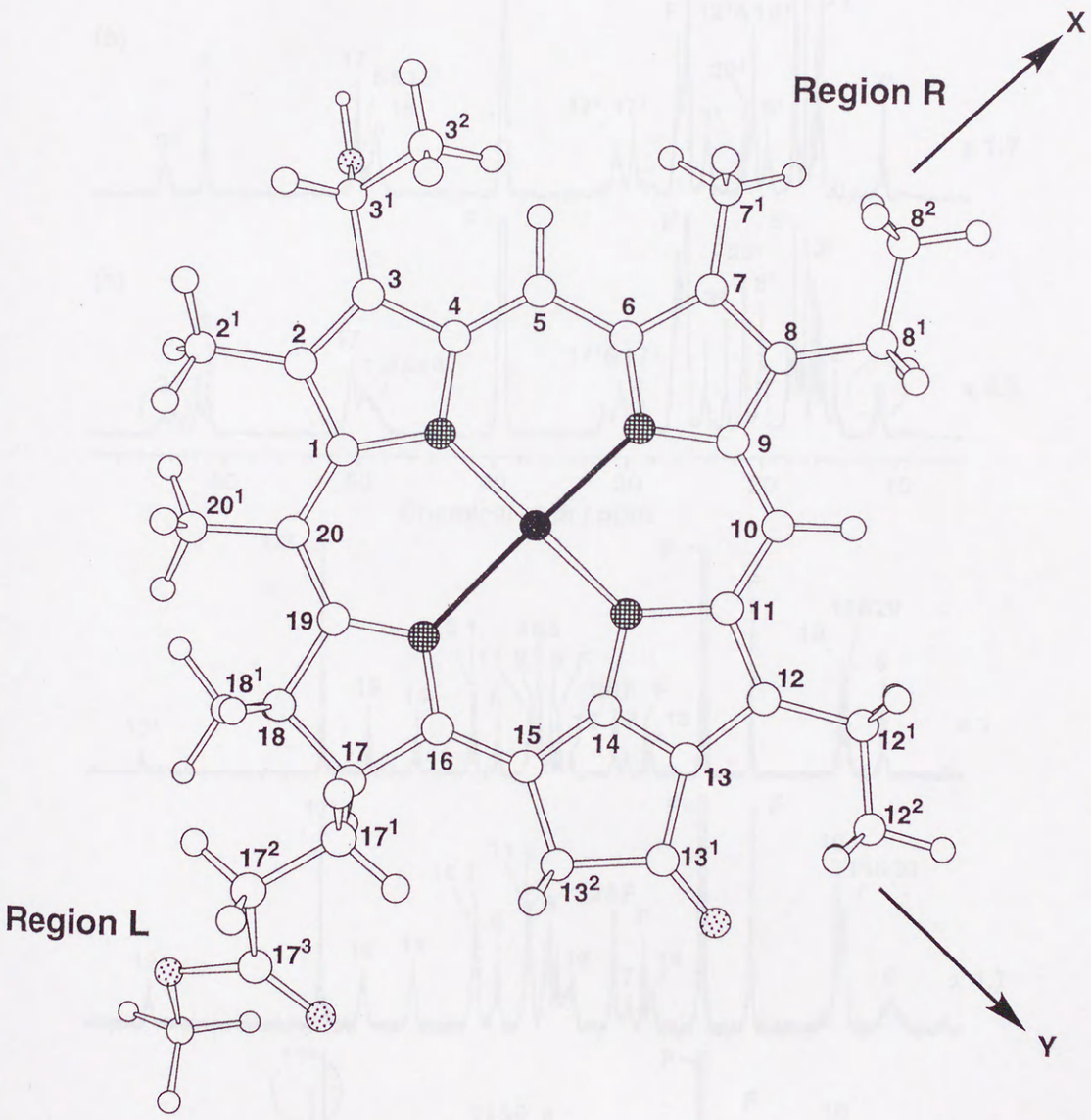
X
Region R
Region L
Y
1
2
2¹
3
3¹
3²
4
5
6
7
7¹
8
8¹
8²
9
10
11
12
12¹
12²
13
13¹
13²
14
15
16
17
17¹
17²
17³
18
18¹
19
20
20¹

Fig. 3

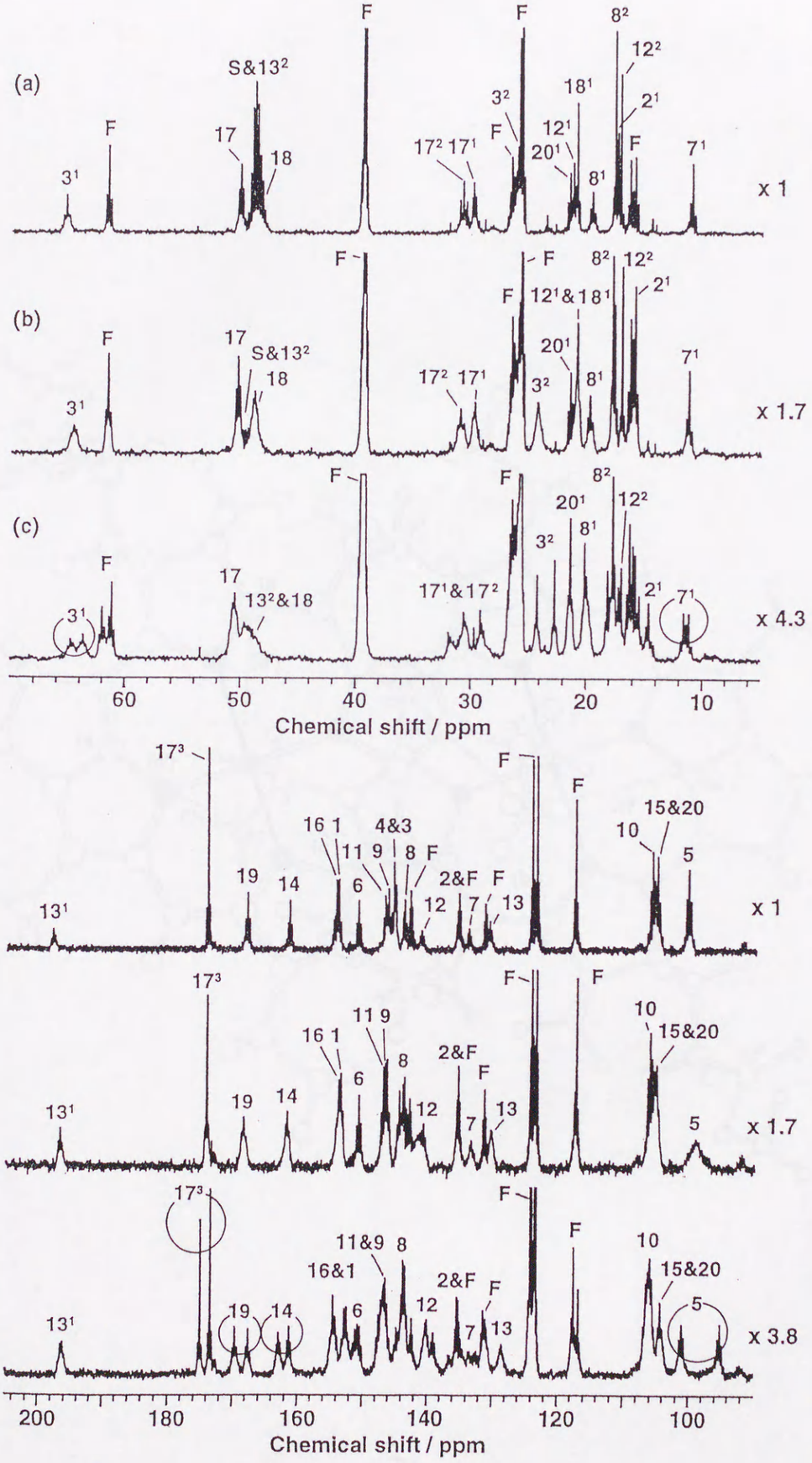
(a)
(b)
(c)
x 1
x 1.7
x 4.3
x 1
x 1.7
x 3.8
F
S&13²
17
18
3¹
17²
17¹
3²
12¹
20¹
18¹
8¹
8²
12²
2¹
7¹
12¹&18¹
13²&18
17¹&17²
16 1
11 9
4&3
8
2&F
19
14
6
12
7
13
10
15&20
5
11&9
16&1
60
50
40
30
20
10
200
180
160
140
120
100
Chemical shift / ppm

Fig. 4

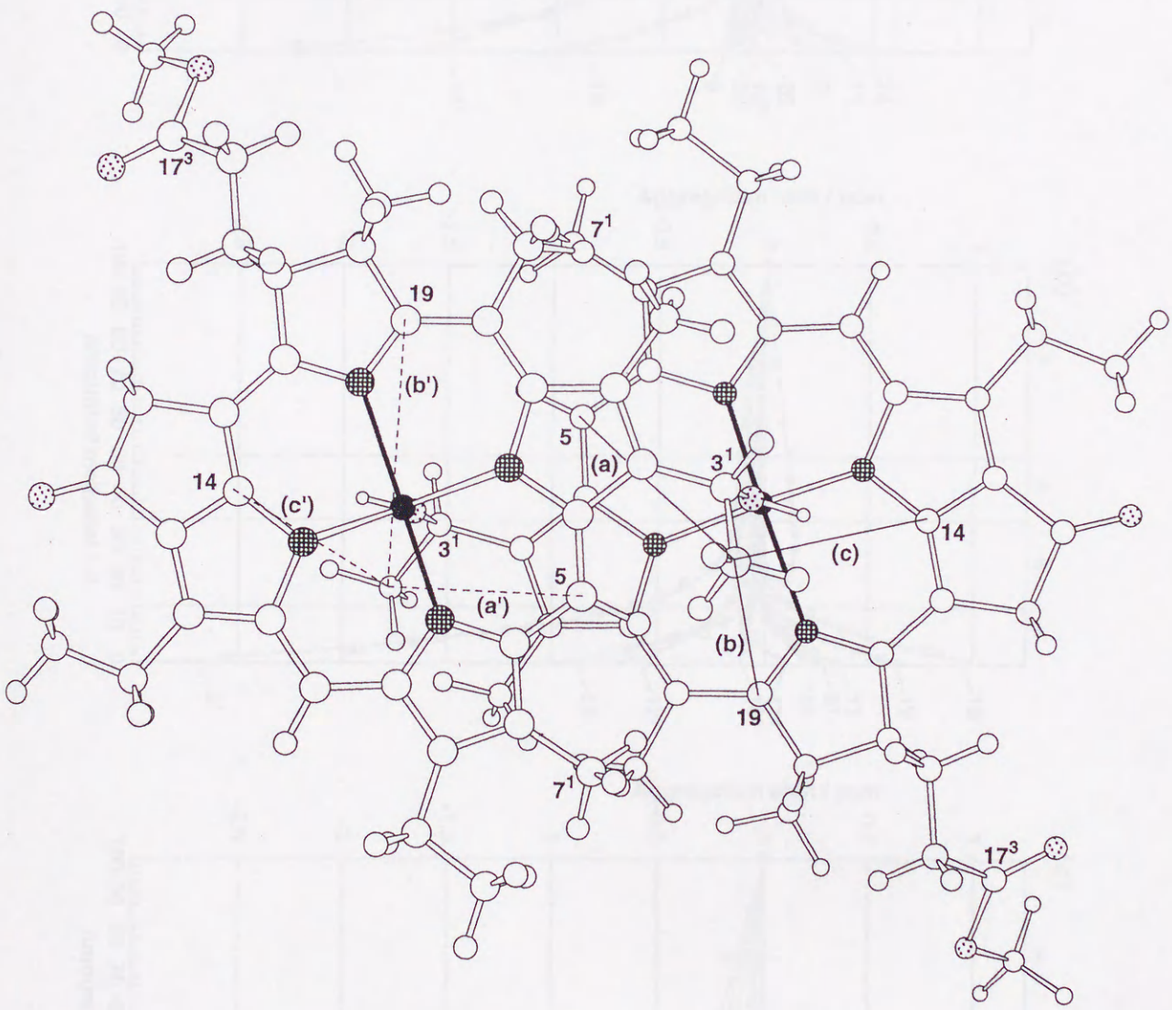

Fig. 5

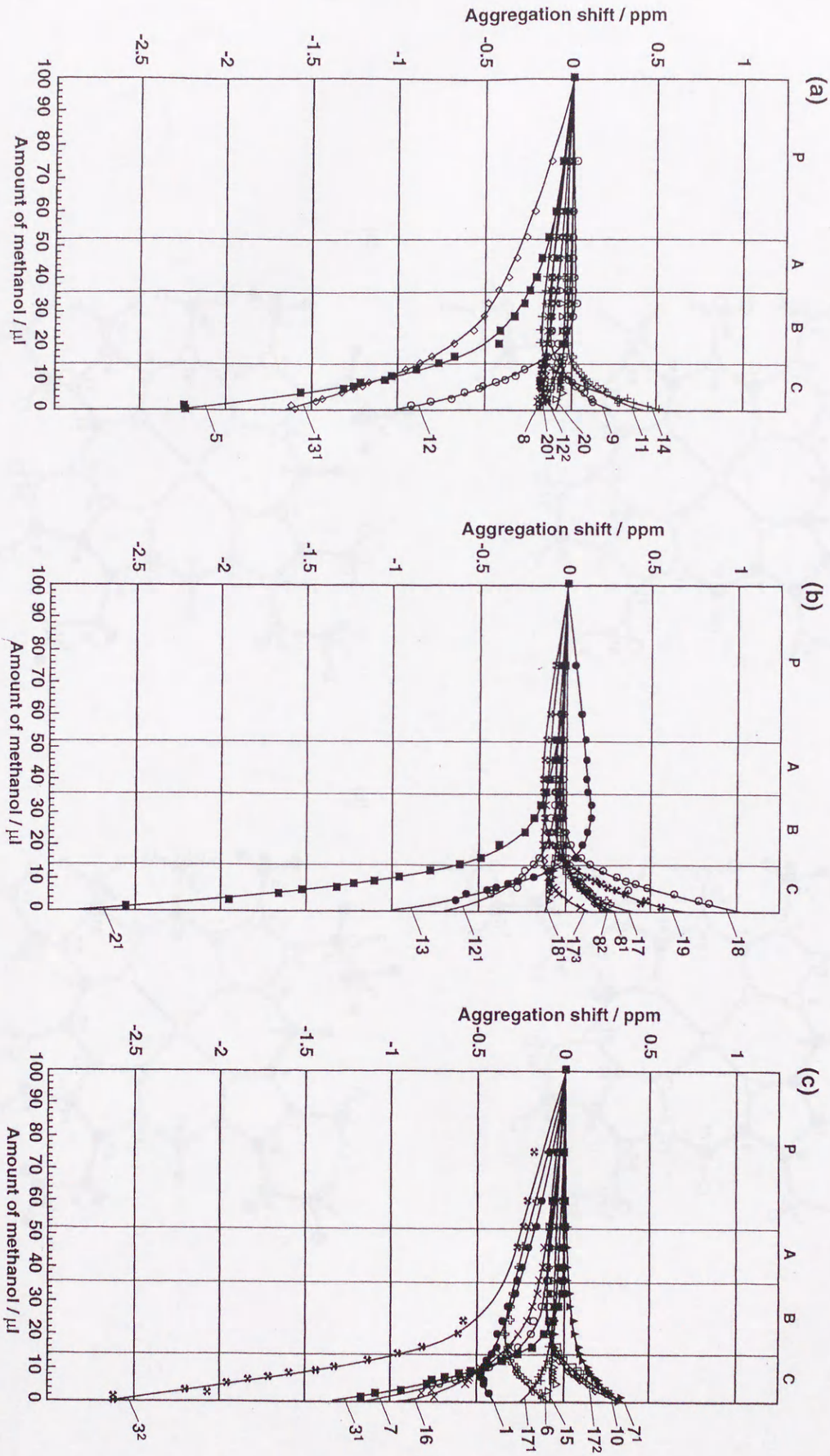
(a)
Aggregation shift / ppm
1
0.5
0
-0.5
-1
-1.5
-2
-2.5
P
A
B
C
Amount of methanol / µl
100 90 80 70 60 50 40 30 20 10 0
5
13¹
12
8
20¹
12²
20
9
11
14
(b)
Aggregation shift / ppm
1
0.5
0
-0.5
-1
-1.5
-2
-2.5
P
A
B
C
Amount of methanol / µl
100 90 80 70 60 50 40 30 20 10 0
21
13
12¹
18¹
17³
8²
8¹
17
19
18
(c)
Aggregation shift / ppm
1
0.5
0
-0.5
-1
-1.5
-2
-2.5
P
A
B
C
Amount of methanol / µl
100 90 80 70 60 50 40 30 20 10 0
32
31
7
16
1
17¹
6
15
17²
10
7¹

Fig. 6

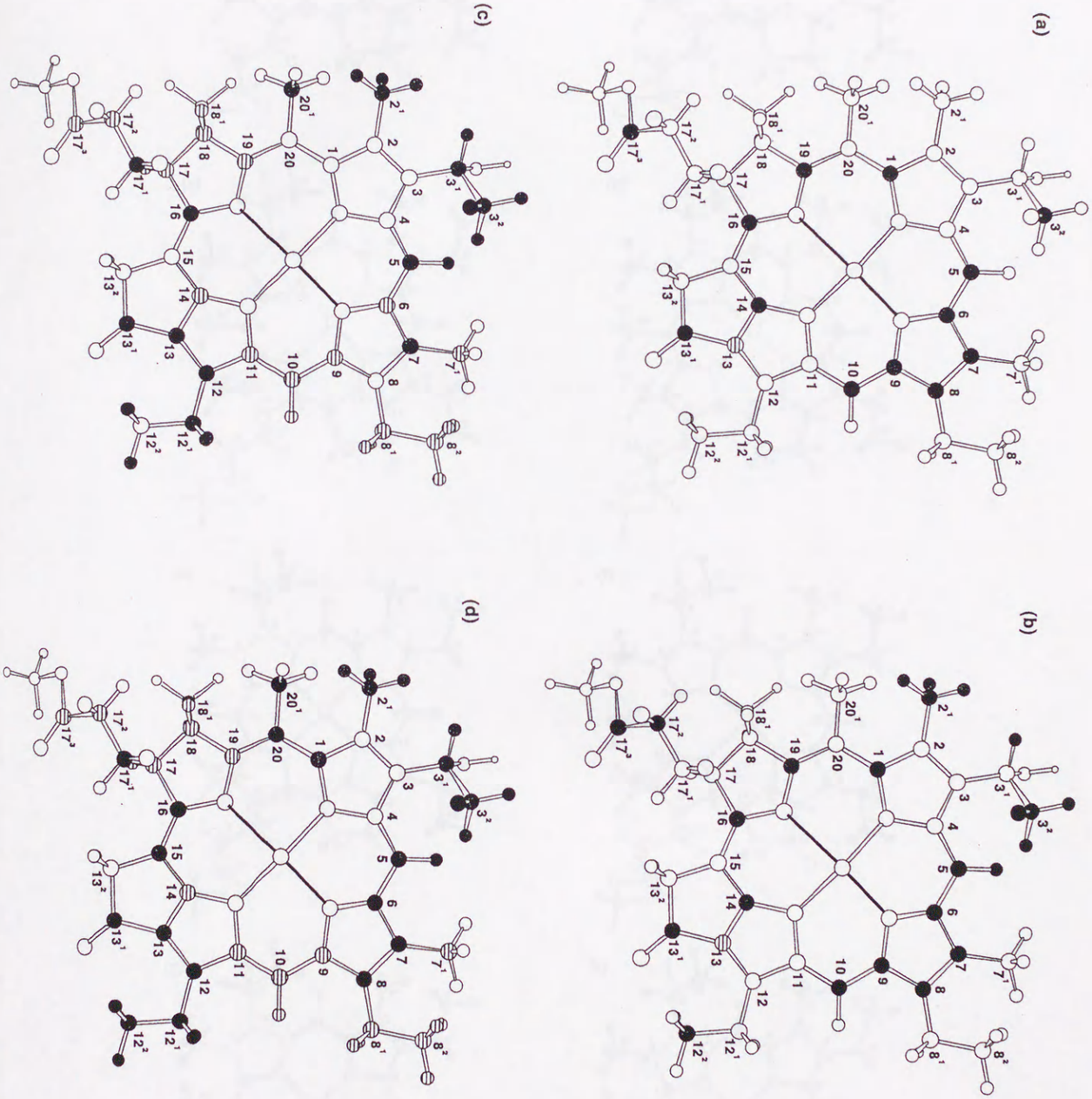

Fig. 7

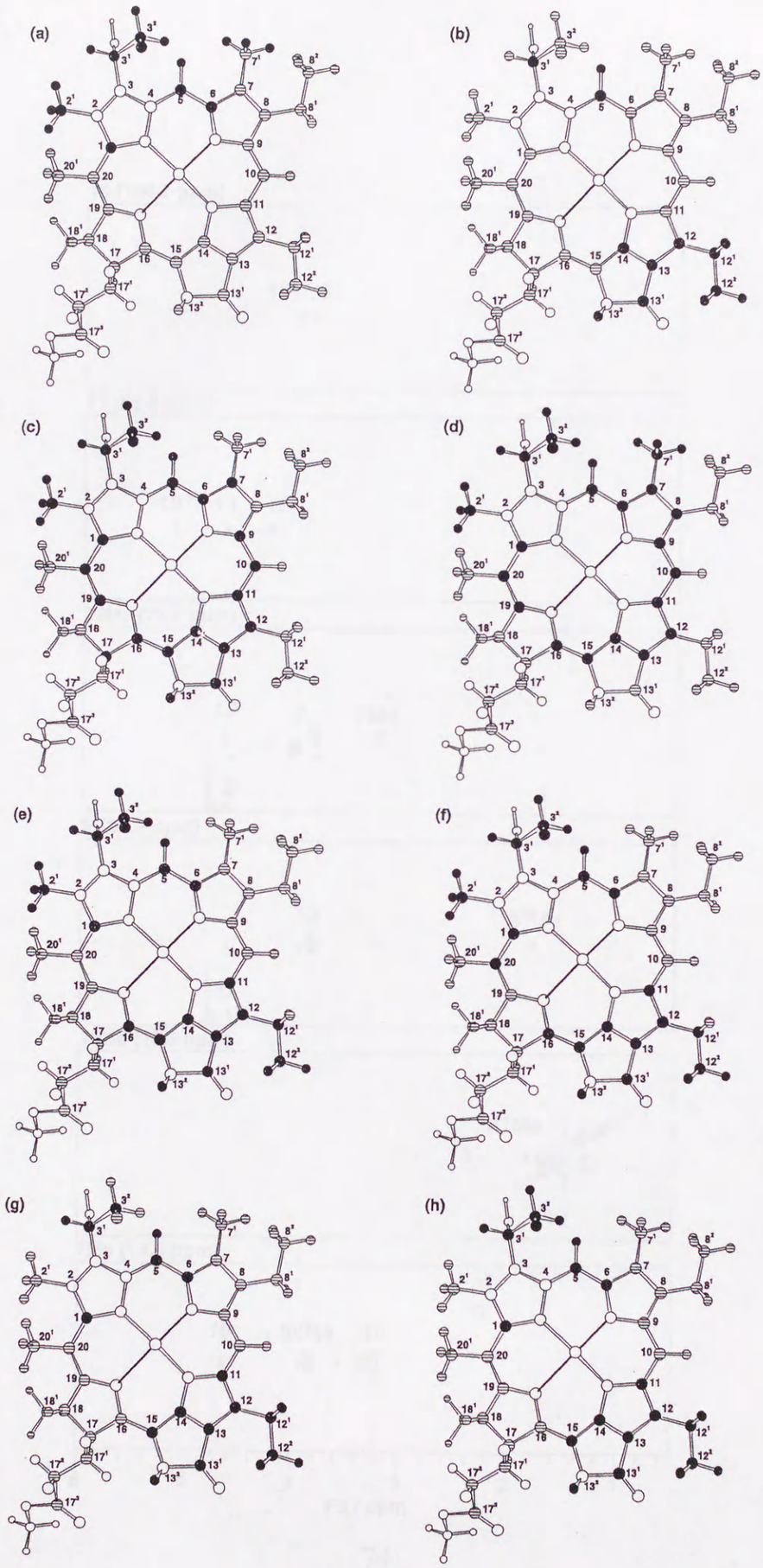

Fig. 8

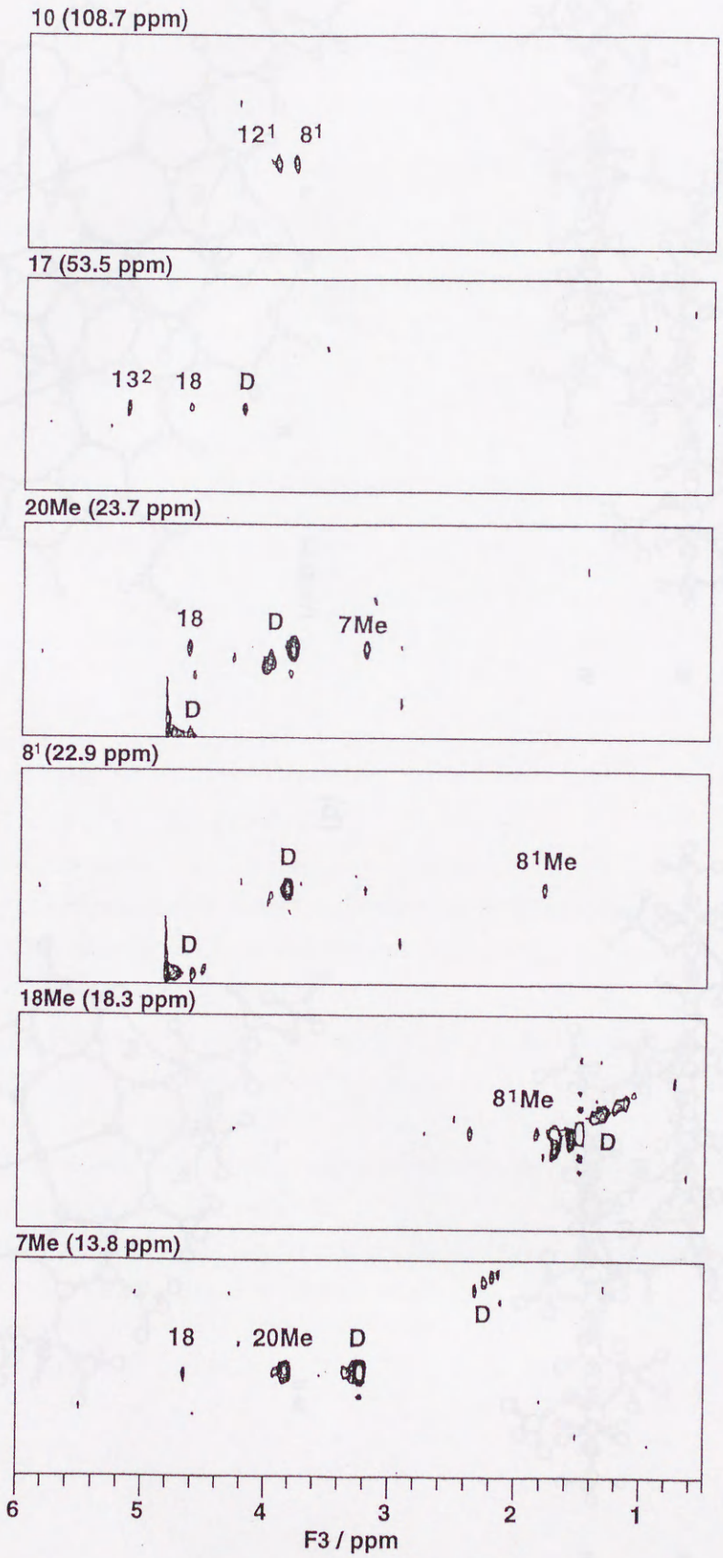
10 (108.7 ppm)
12¹ 8¹
17 (53.5 ppm)
13² 18 D
20Me (23.7 ppm)
18 D 7Me
D
8¹ (22.9 ppm)
D
8¹Me
D
18Me (18.3 ppm)
8¹Me
D
7Me (13.8 ppm)
D
18 20Me D
6 5 4 3 2 1
F3 / ppm

Fig. 9

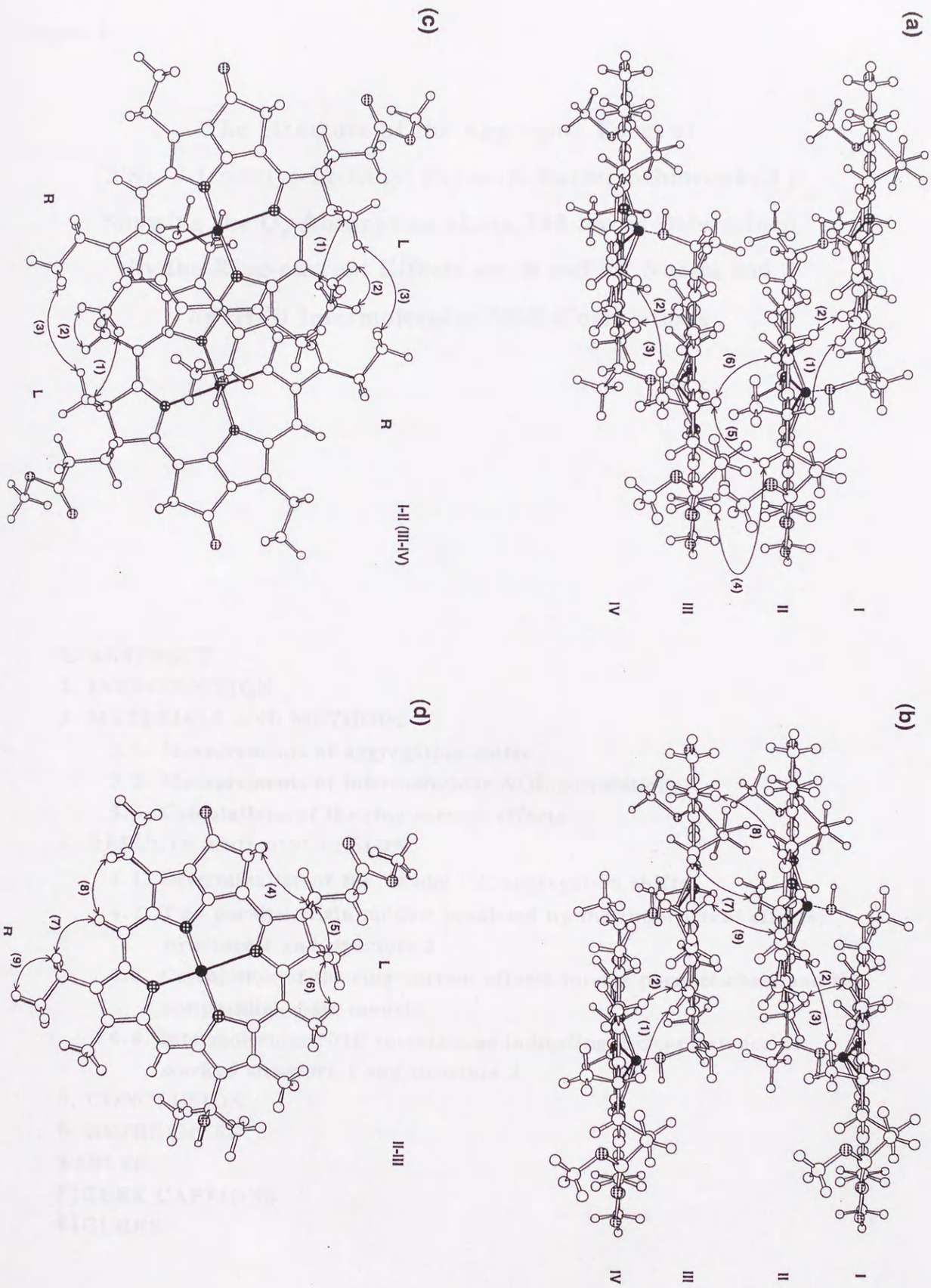
(a)
I
II
III
IV
(1)
(2)
(3)
(4)
(5)
(6)
(b)
I
II
III
IV
(1)
(2)
(3)
(7)
(8)
(9)
(c)
I-II (III-IV)
R
L
L
R
(1)
(2)
(3)
(d)
II-III
R
L
(4)
(5)
(6)
(7)
(8)
(9)

Chapter 3

# The Structure of the Aggregate Form of (3$^1$S), 8-Isobutyl-12-Ethyl Farnesyl Bacteriochlorophyll *c* Showing the $Q_y$ Absorption above 740 nm as Determined by the Ring-current Effects on $^1$H and $^{13}$C Nuclei and by $^1$H-$^1$H Intermolecular NOE Correlations

## 1. ABSTRACT

$^{13}$C-Enriched bacteriochlorophyll **c** (S[I, E] BChl $\mathbf{c}_F$) was suspended in a 1:3 mixture of methylene chloride and carbon tetrachloride to form an aggregate showing the $Q_y$ absorption above 740 nm; changes in the both $^1$H and $^{13}$C chemical shifts were traced when methanol was titrated to dissolve the aggregate, and then, the changes were correlated to the ring-current effects due to the neighboring macrocycles in the aggregate. A pair of aggregate structures has been proposed based on the ring-current effects on both $^1$H and $^{13}$C nuclei; the monomeric units are stacked together to form an inclined column with different sliding directions, in which the y-axis of the molecule is parallel to the long axis of the column. In order to confirm this pair of models, the ring-current effects on the $^1$H and $^{13}$C nuclei were calculated based on both the magnetic-dipole and the loop-current approximations. Further, an application of three dimensional F1 $^{13}$C-edited F3 $^{13}$C-filtered HSQC-NOESY NMR spectroscopy to the above aggregate consisting of a 1:1 mixture of $^{13}$C-labeled and unlabeled BChl **c** succeeded in detecting selectively the $^1$H-$^1$H intermolecular NOE correlations, which established the coexistence of the above pair of stacked structures in the aggregate.

## 2. INTRODUCTION

Green photosynthetic bacteria have a unique antenna complex called chlorosomes which contain bacteriochlorophyll **c** (BChl **c**) as the major component (see ref. [1] for a comprehensive review). The BChl **c** molecules are organized as aggregate where proteins do not serve any direct structural functions: direct pigment-pigment interaction in the aggregate plays a key role in forming the chlorosome structure [2, 3]. In this sense, we can mimic the structure of the native chlorosomes by forming an *in vitro* BChl **c** aggregate in nonpolar solvents, because both of which are characterized by the $Q_y$ absorption above 740 nm. Numerous spectroscopic studies have been performed on both the native chlorosomes and the artificial aggregates, and various models for their structures have been proposed [1, 4]. In particular, the large red shift of the $Q_y$ absorption [5-8] as well as changes in the $^1$H and $^{13}$C chemical shifts upon aggregate formation in reference to those in the monomeric state [2, 3, 8-10] have been used extensively to predict those structures. Concerning the basic structural motif of the stacking of BChl **c** macrocycles, two different models have been proposed most recently (see Fig. 1): (1) A model consisting of stacked monomers to form an inclined column proposed by

Holzwarth, de Groot and co-workers [3, 11]; this model is often referred to as the 'parallel-chain model' [1]. (Actually, two different ways of stacking, i.e., structure 1 and structure 2, are possible in this model.) (2) Another model consisting of stacked linear arrays of 'piggy-back' dimeric units proposed by Nozawa and co-workers which they call the "direct overlap model"[8]; this model is referred to as the 'antiparallel-chain model' [1]. Either type of stacking needs to be verified before building a model for the real structure of chlorosomes.

The idea underlying my series of investigations concerning the aggregate structures (Chapter 1 and Chapter 2) is that I trace continuously the changes in chemical shift when an aggregate form is being dissolved by stepwise titration of methanol; then, I build a model which explains the chemical-shift changes in terms of the ring-current effects. I used the signals from 15 peripheral protons and the signals originating from a total of 31 skeletal and peripheral $^{13}C$ nuclei which were enriched up to ~45 % to build the particular model. Further, I have newly written a program to calculate the ring-current effects on both the $^{1}H$ and $^{13}C$ nuclei based on the magnetic-dipole and the loop-current approximations.

Most recently, the isotope-filtering method has been developed in order to selectively observe the $^{1}H$-$^{1}H$ intermolecular NOE correlations between the $^{13}C$-labeled and unlabeled molecules [12]. This application of the isotope-filtering technique to an aggregate consisting of a 1:1 mixture of $^{13}C$-labeled BChl **c** and unlabeled BChl **c** has enabled us to detect selectively the $^{1}H$-$^{1}H$ intermolecular NOE correlations.

On the basis of the ring-current effects and the intermolecular $^{1}H$-$^{1}H$ NOE correlations, I am going to propose a pair of coexistent stacked structures in the aggregate of BChl **c** showing the $Q_y$ absorption above 740 nm. The results give a strong support of the 'parallel-chain model'.

## 3. MATERIALS AND METHODS

### 3.1. Measurements of aggregation shifts

S[I,E] BChl $\mathbf{c}_F$ (simply called 'BChl **c**' in this chapter) showing an $^{13}C$ enrichment factor of ~ 45 % was obtained by exactly the same method as in the case of R[E, E] BChl $\mathbf{c}_F$ (Chapter 2).

The higher aggregate form was produced by dissolving the BChl **c** into a 1:3 mixture of methylene chloride-$d_2$ (99.6 %, Nacalai Tesque) and carbon tetrachloride (99.7 % spectral grade, Kishida Chemicals Lot J4934) at the concentration of 2.5 x $10^{-3}$ M (the mixed solvent had been dried

over 3 Å molecular sieve), and then by titrating methanol-$d_4$ (99.8 %, Nacalai Tesque). The $^1$H-NMR as well as the electronic absorption spectra were recorded as described the previous Chapter. However, a higher BChl **c** concentration (4.7 x $10^{-3}$ M) was used this time to facilitate the $^{13}$C-NMR measurements.

The $^{13}$C-NMR spectrum of each sample solution (digital resolution, 1.65 Hz) was recorded at 0 °C by the use of a JEOL JNM-A400 FT NMR spectrometer and a JEOL NM-VT 1A temperature controller. $^1$H-$^{13}$C COSY spectra were recorded to aid the assignment of the $^{13}$C signals. Its DEPT spectra using the 45°, 90° and 135° pulses were also recorded. HMQC and HMBC spectra were recorded under the following conditions: 128 increments in the F1 dimension, 512 complex points in the F2 dimension, and 64 or more scans for each increment; the spectral width, 22500 Hz for F1 and 4600 Hz for F2.

### 3.2. Measurements of intermolecular NOE correlations

BChl **c** showing $^{13}$C enrichment factors of > 95 % for 5-C and 10-C and > 83 % for $3^1$-C was obtained as in the previous case of R[E,E] BChl $\mathbf{c}_F$ (Chapter 2).

The aggregate form of BChl **c** was prepared by dissolving a 1:1 mixture of $^{13}$C-labeled and unlabeled BChl **c** into a mixture of dichloromethane and carbon tetrachloride (1:3) at the concentration of $2.5 \times 10^{-3}$ M, and then 1.5 $\mu$l methanol was added in order to partially dissolve the aggregate and to facilitate a higher resolution in NMR spectroscopy.

For the determination of the $^1$H-$^1$H intermolecular NOE correlations, F1 $^{13}$C-edited F3 $^{13}$C-filtered HSQC-NOESY spectra were recorded at 0 °C by the use of a Varian Unity plus 600 MHz FT NMR Spectrometer. Detailed conditions for the above measurements were described the previous Chapter 2.

### 3.3. Calculations of the ring-current effects

The ring-current effects were calculated based on two different approximations, i.e., the magnetic-dipole approximation and the loop-current approximation. *(a) The magnetic-dipole approximation.* This method was first developed by Abraham [13] and Abraham et al. [14] in order to calculate the ring-current effects in porphyrin and chlorin molecules, and then it was applied to BChl **c** by Nozawa et al. [2, 10]. In the present molecule, the conjugated macrocycle consists of three pyrrole rings and one sixteen-membered ring, the latter of which was split into four hexagonal rings

according to their methods. The ring-current effect due to each ring was approximated by a pair of magnetic-dipoles above and below the ring separated by a distance p. In the present calculations of the 'ring-current effects', the value of p=0.64 Å [14] and the dipole-moment values for the pyrrole and the hexagonal rings, i.e., $\mu_p$=17.3 and $\mu_H$=19.0 [2, 15] were used. *(b) The loop-current approximation.* This method was first developed by Johnson and Bovey [16] and applied to the benzene ring. The ring-current effects were calculated based on the loop-current approximation as described the previous Chapter 2: Equation (12) in Chapter 2 expressing the z-component of the magnetic flux at point P($\rho$, $\theta$, z) was used:

$$\mathrm{Bz} = \frac{\mu I}{2\pi} \frac{1}{\sqrt{(a+\rho)^2 + z^2}} \left[ \mathrm{K}(k) + \frac{a^2 - \rho^2 - z^2}{(a-\rho)^2 + z^2} \mathrm{E}(k) \right]$$

where $a$ is a radius of the loop current, $\mu$ is the magnetic susceptibility, and K(k) and E(k) are the complete elliptic integrals of the first and the second kinds expressed in terms of

$$\mathrm{k} = \frac{2\sqrt{a\rho}}{\sqrt{(a+\rho)^2 + z^2}} \quad .$$

Concerning the loop current $I$, the relation,

$$I = -\frac{n_e e^2}{4\pi mc} H_0$$

was used, where $n_e$ is an effective number of electrons under the influence of the external magnetic field, $H_0$; $e$ and $m$ are the charge and the mass of electron; and $c$ is the velocity of light. In the practical calculations of the ring-current effects, I assumed a current loop with a radius 4.0 Å, which was centered on the magnesium atom and located on the macrocycle plane.

## 4. RESULTS AND DISCUSSION

### 4.1. Determination of the $^1$H and $^{13}$C aggregation shifts

*A molecular model of BChl* ***c***. Figure 2a shows a molecular model of BChl **c** used in the present investigation; each skeletal or peripheral carbon atom is typified. The closed bars indicate the Mg···N coordination bonds along the $Q_x$ axis, which can be used to visualize the orientation of the macrocycle in a complicated stacked structure.

The molecular model is essentially the same as that used in the previous Chapter except for (1)

the stereoisomeric configuration of the hydroxylethyl group attached to C3 is changed from R to S, and (2) the ethyl group attached to C8 is replaced by the isobutyl group. The farnesyl group is replaced by the methyl group in both cases, because I will not discuss its conformation. The conformation of the peripheral groups of the present model is in accord with the X-ray structure of methyl bacteriopheophorbide **d** ($3^1$S, 8-isobutyl-12-ethyl) [17].

*Dependence of the electronic absorption spectrum on the solvent composition.* In order to facilitate $^1$H-NMR spectroscopy of BChl **c** in the aggregate form relevant to the chlorosomes, a solvent system which satisfies the following conditions was searched for: (1) An aggregate form exhibiting the $Q_y$ absorption band in the 740-750 nm region can be formed. (2) BChl **c** can be dissolved (suspended) at the concentration of ~ $10^{-3}$ M without sedimentation. (3) A deuterated solvent is contained in a solvent mixture to facilitate locking by the use of trace $^1$H. A mixture of methylene chloride and carbon tetrachloride (1:3) turned out to satisfy these conditions.

Figure 3 shows the changes in the electronic absorption spectrum when the amount of methanol which was titrated into the above solution was reduced from 25 $\mu$l (the methanol / BChl **c** mole ratio = 450 / 1) to none. The spectrum for 25 $\mu$l methanol is essentially the same as that of the monomer in the pure methanol solution (Soret 436 nm; $Q_y$ 668 nm), and therefore, it can mainly be ascribed to the monomer. On the other hand, the spectrum for without methanol is similar to that of the intact chlorosomes which was suspended in 50 mM Tris-HCl (pH 8.0) buffer (Soret, 454 nm; $Q_y$, 747 nm), although the contribution of the $Q_y$ absorption of the dimer (671 nm) is negligible in the latter spectrum. Therefore, this spectrum can be ascribed to a mixture of the higher aggregate (the major component) and the dimer (a minor component).

When the amount of methanol was decreased, a shoulder appeared around 703 nm (8 $\mu$l methanol). When it was decreased further, the shoulder built up and the absorption maximum shifted to the red continuously (7 - 0.5 $\mu$l methanol). This pattern of spectral changes suggest (1) first, a smaller aggregate was formed in the solution, (2) then, the average number of the BChl **c** molecules in the aggregate increased gradually, and (3) finally, what I call 'a higher aggregate' was formed. Neither an isosbestic point nor a discrete change was found in the spectral pattern, a fact which supports the above interpretation.

*Dependence of $^1$H chemical shift and peak intensity on the solvent composition.* Figure 4 shows the changes in the $^1$H chemical shifts (hereafter, each $^1$H will be abbreviated as H) as functions of the amount of methanol titrated. (The signals of $8^2$-H, $17^1$-H and $17^2$-H could not be

observed clearly due to the multiple splittings and to the resultant low intensities.) When the amount of methanol was decreased from 50 to 0 $\mu$l, the following changes took place in the H signals in the figure: (1) Practically no changes were found in the preliminary phase P, (2) clear changes started in phase A, and (3) continuous but progressive changes took place in phase B. (Some of the H signals became invisible in the last phase, because of the extensive broadening of the signals.) The results indicate that essentially the same type of aggregates were being formed in phase A and phase B.

The changes in the $^1$H chemical shifts can be summarized as follows: (1) Large high-field-shifts (hfs) are found for the 5-H, $3^1$-H, $13^2$-H, $12^1$-H, 2Me-H, $3^1$Me-H, $12^1$Me-H signals, while small hfs is seen for the 7Me-H signal. (2) Large low-field-shifts (lfs) are found for the 18-H, $8^1$-H and 18Me-H signals, while small lfs are seen for the 10-H, 17-H, 20Me-H and $8^2$Me-H signals. Since some H signals could not be traced completely at lower concentrations of methanol, the above classification of 'large' and 'small' is somewhat arbitrary. In the $^1$H-NMR study, I define the aggregation shifts as chemical-shift differences between the higher aggregate (without methanol) and the monomer (with 50 $\mu$l methanol); the chemical-shift values for '0 $\mu$l' methanol were obtained by extrapolation of the data shown in Fig. 4 (Their observed points can be fitted by the use of functions, $y=a\{1-\exp(\pm x/b)\}$, where x is the decrease in the amount of methanol and y is the change in the $^1$H chemical shift (a and b are constants)).

Figure 5 shows changes in peak intensities as functions of the solvent composition. When the amount of methanol was decreased, all the H signals decreased in intensity in a similar way, although the $3^1$-H, 5-H, 2Me-H, $12^1$Me-H, $12^1$-H and $3^1$Me-H signals tend to decrease first, and the 18-H signal to decrease last. This observation of a single pattern of intensity decrease supports strongly the above idea that essentially the same type of aggregates are being formed in phases A and B.

*Dependence of $^{13}$C chemical shift on the solvent composition.* In the $^{13}$C-NMR study, I used a higher BChl **c** concentration of $4.7 \times 10^{-3}$ M; here, based on changes in the electronic-absorption and the $^1$H-NMR spectra, I regard the states with 30 $\mu$l, 7 $\mu$l and < 1 $\mu$l of methanol as representing the monomer, the starting point of high-aggregate formation, and a typical higher-aggregate state. It is noted that electronic absorption spectroscopy showed the coexistence of the higher aggregate and the dimer even at the last stage of higher-aggregate formation (see Fig. 3).

The assignment of the carbon signals was made by the use of HMQC and HMBC ($^1$H, $^{13}$C-COSY and long-range COSY) as well as DEPT spectra. A total of 31 $^{13}$C signals could be traced out of the 36 labeled carbon atoms; carbon signals which could not be traced at all were as follows: (1)

the signals of $13^2$-C and 18-C due to overlap with that of the solvent, methanol, and (2) the signals of 2-C, 7-C and 13-C due to overlap with those of the farnesyl group. Among the remaining 29 independent $^{13}C$ signals (the signals of 9-C and 11-C as well as those of 8-C and 12-C were overlapped), 11 of them could not be traced until 1 μl methanol due to their broadening; therefore, an extrapolation procedure was necessary to determine the chemical shifts at '0 μl' methanol.

Figure 6 depicts the changes in the $^{13}C$ chemical shifts as functions of decreasing amount of titrated methanol in reference to those at 30 μl methanol. (The effects of molecular association actually started before 30 μl methanol; the value for the $^{13}C$-chemical shift of $13^1$-C (the most sensitive signal) was 196.99 and 197.22 ppm at 50 and 100 μl methanol, respectively). Uniqueness of the changes in the $^{13}C$ chemical shifts, in comparison with the changes in the $^1H$ chemical shifts seen in Fig. 4, is that large chemical-shift changes take place even in the region of 30 - 7 μl methanol. The changes in the entire region may be classified into three groups: (1) Signals of (a) $13^1$-C, 3-C, $17^1$-C, $20^1$-C, 9-C, 11-C; (b) 4-C, 17-C; and (c) $17^2$-C, $7^1$-C, $3^1$-C which change in a similar trend in the entire region. (2) Signals of (a) 5-C, $12^2$-C, 14-C; (b) $8^2$-C, 19-C; and (c) 6-C, 1-C, 16-C, 15-C which change the sign of curvature at a certain point (e.g., show an inflection point). (3) Signals of (a) 8-C, 12-C, 20-C, $18^1$-C; (b) $12^1$-C, $2^1$-C, $17^3$-C, $8^1$-C, $8^3$-C; and (c) $3^2$-C, 10-C which start to change progressively after a certain point.

The above classification suggests the presence of at least two different origins for the chemical-shift changes, i.e., one predominates at an early stage and the other predominates at the later stage of the aggregate formation. I assume that the former is due to the electronic redistribution on the $^{13}C$ nuclei in the macrocycle which is mainly caused by the formation of the Mg···OH coordination bond, and that the latter is due to the ring-current effects of the neighboring macrocycles which are caused by the formation of a higher aggregate structure. The following observations support these assumptions: (1) The changes before 7 μl methanol are one of the largest (except for $13^1$-C) for 3-C and $3^1$-C which are located near the hydroxylethyl group and also for 1-C, 4-C, 6-C, 9-C and 11-C which are adjacent to the nitrogen atoms. (2) The changes after 7 μl tend to be progressive (irrespective of the directions) and their observed points can be fitted by the use of functions, $y=a\{1-\exp(\pm x/b)\}$, where x is the decrease in the amount of methanol and y is the change in the $^{13}C$ chemical shift (a and b are constants). Actually, these functions were taken into account when I extrapolated the chemical-shift values to '0 μl' methanol. This observation strongly suggests the formation of a regular stacking of the macrocycles in the higher aggregate. (3) The progressive changes in the $^{13}C$

chemical shifts start at 7 μl, when the changes in the $^{1}H$ chemical shifts ascribable to the ring-current effects do.

Close examination of each curve fitting shows that the above two origins, i.e., the coordination effects and the ring-current effects, are difficult to separate, and that the relative contribution of the two kinds of effect, at a certain amount of methanol, seems to differ from one carbon atom to another. Thus, a strict definition of the observed ring-current effects solely ascribable to the stacking of the macrocycles is rather difficult. Therefore, I can define the changes in the $^{13}C$ chemical shifts due to the aggregate formation (hereafter, I will call them 'the $^{13}C$ aggregation shifts') by two *practical* ways: one way is in reference to those at 7 μl methanol (the starting point of the higher aggregate formation) and the other is in reference to the chemical shifts at 30 μl methanol (the monomeric state), although the above discussion suggests that the former definition is more reasonable. The aggregation shifts of the two definitions are in agreement as far as their directions are concerned. Table 1 lists the values of the $^{13}C$ chemical-shifts at amounts of methanol, 30 μl, 7 μl and '0 μl', and the values of aggregation shifts defined as '0 μl' methanol minus 30 μl methanol.

### 4.2. Two parallel-chain models predicted by the ring-current effects; structure 1 and structure 2

Figure 2b depicts the observed aggregation shifts thus determined for the $^{1}H$ and $^{13}C$ nuclei. It shows that there is clear geometrical distinction between the high-field-shift (hfs) region and the low-field-shift (lfs) region. Generally speaking, the hfs regions appear at the upper-left and the lower-right corners of the BChl **c** molecule shown in this figure, and the lfs region crosses the central part from the lower-left to the upper-right corner. The hfs of the three carbons, i.e., $17^{1}$, $17^{2}$ and $17^{3}$, are exceptions.

I measured also the $^{1}H$ and $^{13}C$ NMR spectra, with 1.5 μl methanol, when the sample solution was cooled down to -20 °C, but no additional splitting of the signals was observed. Further, I measured the $^{1}H$ and $^{13}C$ NMR spectra for the solution without methanol, but those spectra were similar to those with 1 μl methanol. The results strongly suggest that each BChl **c** molecule is located in the same environment in the aggregate.

Figures 7 and 8 show a pair of models, i.e., stacked 'structure 1' and 'structure 2', which I propose in the present investigation; schematic presentation of the structures is given in Fig. 1a, as

well. They consist of a stepwise stacking of the monomeric BChl **c** molecules to form an inclined column. The models were built based on the following assumptions: (1) Translational symmetry: The macrocycles of all the BChl **c** molecules in the aggregate should take the same orientation. (This assumption is based on the above observations.) (2) The ring-current effect [18]: The hfs (lfs) of the signal should take place for a H or a C atom which is located inside (outside) of the contour of the macrocycle of the neighboring BChl **c** molecule when the particular atom is projected onto the macrocycle plane. (3) The Mg···OH axial coordination: Both the deviation of the Mg atom out of the macrocycle plane in the penta-coordinated state and the conformation of the hydroxylethyl group around the 3 - $3^1$ axis can be adjusted to form the Mg···OH coordination bond to stabilize the aggregated form. (4) The Mg···OH coordination bond is assumed to be 1.7 Å, and the distance between a pair of parallel macrocycles is assumed to be 3.5 Å.

Structure 1 and structure 2 are different in the sliding direction of the stacked column (see Figs. 7a and 8a), which results in difference in the conformation of the hydroxylethyl group around the C3 - $C3^1$ axis and also in the direction of the central magnesium atom out of the macrocycle plane in order to form a stacked structure. Structure 1 is the same as the model which I proposed in the previous $^1$H-NMR study (see Fig. 5 of ref. [19]). Structure 2 is obviously different from structure 1. However, the latter can explain the aggregation shifts (in terms of the ring-current effects) in exactly the same way as the former, because their projections (Figs. 7c and 8c) are basically the same. In these figures, the aggregation shifts are indicated for the central BChl **c** molecule. The two separate regions of hfs and lfs in the central molecule can be explained nicely in terms of the overlapping macrocycles of the upper or the lower BChl **c** molecule; namely, the atoms showing the hfs (lfs) are projected inside (outside) of the neighboring macrocycle.

Some exceptions are found in the aggregation shifts (see also Fig. 2b): The lfs of $3^1$-C may be explained in terms of the effects of coordination between the Mg atom and the hydroxyl group, whereas the hfs of $17^3$-C may be explained in terms of hydrogen bonding to the ester carbonyl group. These coordination and hydrogen bonding can change in number when the formation of the aggregate proceeds progressively.

I tried to explain the observed aggregation shifts (ring-current effects) in terms of the antiparallel-chain model (based on Fig. 8b of ref. [8]). However, this model failed to explain the hfs region in the lower-right corner of the BChl **c** molecule shown in Fig. 2b. In order to establish the superiority of the parallel-chain model over the antiparallel-chain model, I performed the calculations

of the ring-current effects.

### 4.3. Calculation of the ring-current effects for the parallel-chain and the antiparallel-chain models

Since the calculations of the ring-current effects based on the loop-current approximation are going to be applied to the aggregates of BChl **c** molecules, I have first examined various parameters which can affect the ring-current effects by the use of the parallel-chain model as an example. The results can be summarized as follows: (a) The size of the current loop which stands for the neighboring macrocycle drastically affects the divergence of the $^{1}H$ and $^{13}C$ signals of the BChl **c** molecule in question; when the current loop expands, the signals of those nuclei which get into the loop (after projection) exhibit hfs, and the signals of those nuclei remaining outside the loop shift continuously to the lower field. I assumed a single loop with a radius of 4.0 Å which is centered at the Mg atom and covers all the conjugated systems in the macrocycle. (b) The distance between the model loop and the BChl **c** molecule in question also drastically affects the divergence of the signals from it; when the current loop moves apart along the z-direction, the split signals of the BChl **c** molecule tend to converge due to decrease in the ring-current effects. (c) The overlap of the current loop with the BChl **c** molecule, of course, affects the divergence of the signals; when the neighboring current loop slides away in the xy-plane, the split signals tend to converge eventually to the zero ring-current effect. (d) When the number of the stacked current loops on both sides of the BChl **c** molecule in question which is located in a single parallel chain increases, all the signals shift gradually to the low field; however, the shifts become almost saturated for the number of loops on each side becomes 5. (e) Approach of another stacked 'parallel' chain affects little the ring-current shifts of the BChl **c** molecule in the parallel chain in question as far as the approaching chain stays out of the limit of van der Waals contacts.

Tables 2 and 3 compare, for the $^{1}H$ and the $^{13}C$ nuclei, the observed aggregation shifts with the ring-current effects calculated for the parallel-chain and the antiparallel-chain models based on both the magnetic-dipole and the loop-current approximations. Since the aggregation shifts can originate not only from the ring-current effects of the π-electrons in the conjugated macrocycle but also from the effects of coordination and hydrogen bonding, and since the calculations of the ring-current effects are based on such simple approximations, I will confine myself to a qualitative comparison of the signs (directions) of the observed aggregation shifts with those of the calculated ring-current

effects:

Concerning the $^{1}H$ nuclei (see Table 2), the ring-current effects which were calculated for the parallel-chain model based on the magnetic-dipole approximation show perfect agreement with the observed aggregation shifts (the score of agreement, 15 / 15); on the other hand, the ring-current effects calculated for the antiparallel-chain model gives rise to a much lower score of agreement (10 / 15). The score of the parallel-chain model (12 / 15) is slightly higher than that of the antiparallel-chain model (11 / 15) when the ring-current effects are calculated based on the loop-current approximation. Thus, the superiority of the parallel-chain model over the antiparallel-chain model is shown.

Concerning the $^{13}C$ nuclei (Table 3), the ring-current effects which were calculated for the parallel-chain model based on the loop-current approximation exhibit the highest score of agreement (25 / 31); the score for the antiparallel-chain model is definitely lower (21 / 31). In the case of the magnetic-dipole approximation, the score of agreement for the parallel-chain model (21 / 31) is much higher than that for the antiparallel-chain model (12 / 31). Here, the superiority of the parallel-chain model is shown much more clearly.

In the case of the magnetic-dipole approximation, the calculated values of 'the ring-current shifts' can be directly compared to the observed values of the aggregation shifts (scaling of the calculated ring-current effects is necessary in the loop-current approximation). Therefore, I defined a residual factor $\sum |\Delta_{obs}-\Delta_{calc}| / \sum |\Delta_{obs}|$, and calculated this value using the observed and calculated 'ring-current shifts'. The results were as follows: concerning the $^{1}H$ nuclei, the values were 3.03 and 3.40 for the parallel-chain and the antiparallel-chain models, respectively; concerning the $^{13}C$ nuclei, they were 2.89 and 3.52 for the parallel-chain and the antiparallel-chain models. The residual factor is much smaller for the parallel-chain model, showing again its superiority over the antiparallel-chain model.

### 4.4. Intermolecular NOE correlations indicating the coexistence of stacked structure 1 and structure 2

In general, $^{1}H$-$^{1}H$ NOE correlations to be detected in the mixed aggregate of $^{13}C$-labeled and unlabeled BChl **c** can be classified into the following three types: (1) the NOE correlation between a pair of protons both of which are attached to the $^{13}C$ atoms; (2) the NOE correlation between a pair of protons both of which are attached to the $^{12}C$ atoms; and (3) the NOE correlation between a proton attached to the $^{12}C$ atom and another proton attached to the $^{13}C$ atom. In the present aggregate

consisting of mixed $^{13}$C-labeled and unlabeled BChl **c**, type 1 and type 2 correlations can be ascribed to intramolecular NOE correlations within either the $^{13}$C-labeled or unlabeled BChl **c** molecule. On the other hand, type 3 correlation is ascribable to *intermolecular* NOE correlation between the $^{13}$C-labeled and unlabeled BChl **c** molecules. Thus, the isotope-filtering method can be applied to facilitate the selective observation of type 3 intermolecular NOE correlations [12].

Under the present experimental conditions, I could use the following 10 $^{1}$H signals to detect the intermolecular NOE correlations; they include 10-H, 13$^{2}$-H, 18-H, 17-H, 20Me-H, 8$^{1}$-H, 7Me-H, 8$^{2}$-H, 18Me-H and 8$^{2}$Me-H. The signals originating from 2Me-H, 3$^{1}$-H, 3$^{1}$Me-H, 5-H, 12$^{1}$-H and 12$^{1}$Me-H could not be used because of their broadening due to severe steric interaction when the aggregate was being formed. The signals from 17$^{1}$-H and 17$^{2}$-H were not useful because of multiple splitting. The intermolecular NOE correlation is supposed to be detected when the distance between a pair of protons attached to different molecules is less than 5 Å.

Figure 9 shows the strip plots from the 3D intermolecular NOESY spectrum of a 1:1 mixture of the $^{13}$C-labeled and unlabeled BChl **c** molecules. Twelve independent intermolecular $^{1}$H-$^{1}$H NOE correlations are seen; they are listed in Table 4. If I define 'region R' and 'region L' in the BChl **c** molecule, as shown in Fig. 2a, corresponding to the right-hand-side and the left-hand-side of the molecule with respect to the stacking axis, I can classify the intermolecular NOE correlations into the following three groups: (1) NOE correlations due to proton-proton close contact between region L of one BChl **c** molecule and region L of another BChl **c** molecule (correlation L↔L), which include 17-H⇔18-H, 17-H⇔20Me-H, 18Me-H⇔20Me-H, 17-H⇔13$^{2}$-H and 18-H⇔20Me-H correlations. (2) NOE correlations due to close contact between region R of one BChl **c** molecule and region R of another BChl **c** molecule (correlation R↔R), which include 8$^{1}$-H⇔7Me-H, 8$^{1}$-H⇔8$^{2}$Me-H, 8$^{2}$Me-H ⇔7Me-H, 10-H⇔8$^{2}$Me-H, 10-H⇔8$^{2}$-H and 10-H⇔8$^{1}$-H correlations. (3) An NOE correlation due to close contact between region L of one BChl **c** molecule and region R of another BChl **c** molecule (correlation L↔R), including a single 7Me-H⇔20Me-H correlation.

The above intermolecular NOE correlations L↔L and R↔R can be explained nicely in terms of structure 1 and structure 2: Figure 7 depicts each close contact of a pair of protons in structure 1 responsible for the intermolecular NOE correlation by the use of its numbering listed in Table 4. Each atomic distance between a pair of relevant protons is also listed in the table. In the case of methyl-H; I did not try to adjust the internal rotation angle around the C-Me axis; here, the carbon-carbon distance can be used as a measure to examine whether the proton-proton distance can take an acceptable value.

Concerning the L↔L correlation, the intermolecular NOE correlations (1), (2) and (3) can be explained in terms of structure 1 as shown by arrows in Fig. 7a. Table 4 shows the values of $^1$H-$^1$H distance can be less than 5 Å. However, NOE correlations (4) and (5) are left unexplained by this structure; the $^1$H-$^1$H distances are too long. Concerning the R↔R correlation, NOE correlations (6), (7), (8), (9) and (10) can be explained by this structure as shown in Fig. 7b and Table 4, but an intermolecular NOE correlation (11) is left unexplained.

Figure 8 depicts each close contact of protons in structure 2 responsible for NOE correlation, and the distance between the relevant protons is listed in Table 4. Concerning the L↔L correlation, the NOE correlations (4) and (5) can be explained in terms of this structure as shown by arrows in Fig. 8a and Table 4 (the proton-proton distances are less than 5 Å), but correlations (1), (2) and (3) are left unexplained. Concerning the R↔R correlation, all the intermolecular NOE correlations (6), (7), (8), (9), (10) and (11) can be explained by this structure as shown in Fig. 8b and Table 4.

As described above, the proton-proton distances listed in Table 4 show that some intermolecular NOE correlations which can not be explained by one stacked structure can be explained by the other stacked structure. Specifically, intermolecular NOE correlations (4), (5) and (11) can not be explained by structure 1, but they can be explained by structure 2, instead. On the other hand, the NOE correlations (1), (2) and (3) can not be explained by structure 2, but they can be explained by structure 1. In other words, only a combination of structure 1 and structure 2 can explain *all* the observed L↔L and the R↔R intermolecular NOE correlations. The results establish the coexistence of structure 1 and structure 2 in the present BChl **c** aggregate.

One single L↔R intermolecular NOE correlation, i.e., (12), is left unexplained. This can be ascribed to a piggy-back dimer which coexists in the aggregate suspension; the presence of this dimeric form has been shown by electronic absorption spectroscopy (*vide supra*). This type of intermolecular NOE correlation has already been detected by conventional ROESY measurements in the dimeric form of R[E, E] BChl $\mathbf{c}_F$ in chloroform (Chapter 1).

Thus, all the observed NOE correlations have been explained (in other words, no artificial NOE correlations have been detected). Close examination of the models of structure 1 and structure 2 suggest that the following additional pairs of protons were supposed to give rise to intermolecular NOE correlations: 7Me-H⇔10-H, 8$^1$-H⇔8$^2$-H, 13$^2$-H⇔20Me-H and 13$^2$-H⇔18-H for both structure 1 and structure 2; 18Me-H⇔17-H for structure 1; and 13$^2$-H and 18Me-H for structure 2 (concerning the methyl groups, the $^1$H-$^1$H distance depends on their conformations). Actually, all of

these correlations were not detected. On the other hand, the model for the piggy-back dimer (see Fig. 7a in Chapter 1) suggests that the following proton-pairs potentially give rise to intermolecular NOE correlation, although they depend on the conformation of the methyl and the *iso*-butyl groups: 7Me-H ⇔18Me-H, 20Me-H⇔8-*iso*-butyl-H and 18Me-H⇔8-*iso*-butyl-H. They were actually not observed, either. The results indicate that some proton-pairs can escape NOE detection.

The observed intermolecular $^1$H-$^1$H NOE correlations could never be explained in terms of the antiparallel-chain model. Thus, the parallel-chain model including two different stacked structures (structure 1 and structure 2) has been established, and at the same time, the antiparallel-chain model is questioned, by this NOE measurement.

## 5. CONCLUSION

The present $^1$H- and $^{13}$C-NMR spectroscopy of the aggregate of S[I, E] BChl $\mathbf{c}_F$ showing the $Q_y$ absorption above 740 nm has identified two different types of stacked structures, i.e., structure 1 and structure 2, both of which can be classified into the parallel-chain model. Both structure 1 and structure 2 consist of a stepwise stacking of the monomeric BChl **c** molecules to form an inclined column, but they are different in the sliding direction of the column. The proposition of these models is based on (1) comparison between the observed aggregation shifts and the ring-current effects calculated on the basis of the magnetic-dipole and the loop-current approximations and (2) the observed intermolecular $^1$H-$^1$H NOE correlations. The latter established the coexistence of structure 1 and structure 2. (No attempts were made to build a model for higher-order organization of these different structures.)

The present results strongly suggest that the structural motif in the aggregates absorbing above 740 nm both *in vitro* and *in vivo* is the parallel-chain stacking. The antiparallel-chain stacking (at least what is called the 'direct ring overlap' model [8]) is highly unlikely as a motif in this type of aggregate.

## 6. REFERENCES

(1) Blankenship, R. E., J. M. Olson and M. Miller (1995) Antenna Complexes from Green Photosynthetic Bacteria. In *Anoxygenic Photosynthetic Bacteria* (Edited by R. E.

Blankenship, M. T. Madigan and C. E. Bauer), pp. 399-435. Kluwer Academic Publishers, The Netherlands.

(2) Nozawa, T., K. Ohtomo, M. Suzuki, H. Nakagawa, Y. Shikama, H. Konami and Z.-Y. Wang (1994) Structures of Chlorosomes and Aggregated BChl *c* in *Chlorobium Tepidum* from Solid State High Resolution CP/MAS $^{13}C$ NMR. *Photosynth. Res.* **41**, 211-223.

(3) Balaban, T. S., A. R. Holzwarth, K. Schaffner, G.-J. Boender and H. J. M. de Groot (1995) CP-MAS $^{13}C$-NMR Dipolar Correlation Spectroscopy of $^{13}C$-Enriched Chlorosomes and Isolated Bacteriochlorophyll *c* Aggregates of *Chlorobium Tepidum*: The Self-Organization of Pigments Is the Main Structural Feature of Chlorosomes. *Biochemistry* **34**, 15259-15266.

(4) Tamiaki, H (1996) Supramolecular Structure in Extramembraneous Antennae of Green Photosynthetic Bacteria. *Coord. Chem. Reviews* **148**, 183-197.

(5) Smith, K. M., L. A. Kehres and J. Fajer (1983) Aggregation of the Bacteriochlorophylls *c*, *d*, and *e*. Models for the Antenna Chlorophylls of Green and Brown Photosynthetic Bacteria. *J. Am. Chem. Soc.* **105**, 1387-1389.

(6) Brune, D. C., G. H. King and R. E. Blankenship (1988) Interactions between Bacteriochlorophyll *c* Molecules in Oligomers and in Chlorosomes of Green Photosynthetic Bacteria. In *Photosynthetic Light-Harvesting Systems* (Edited by H. Scheer and S. Schneider), pp. 141-151. Walter de Gruyter, Berlin·New York.

(7) Alden, R. G., S. H. Lin and R. E. Blankenship (1992) Theory of Spectroscopy and Energy Transfer of Oligomeric Pigments in Chlorosome Antennas of Green Photosynthetic Bacteria. *J. Luminescence* **51**, 51-66.

(8) Nozawa, T., K. Ohtomo, M. Suzuki, Y. Morishita and M. T. Madigan(1993) Structures and Organization of Bacteriochlorophyll *c*'s in Chlorosomes from a New Thermophilic Bacterium *Chlorobium Tepidum*. *Bull. Chem. Soc. Jpn.* **66**, 231-237.

(9) Smith, K. M., F. W. Bobe, D. A. Goff and R. J. Abraham (1986) NMR Spectra of Porphyrins. 28. Detailed Solution Structure of a Bacteriochlorophyllide *d* Dimer. *J. Am. Chem. Soc.* **108**, 1111-1120.

(10) Nozawa, T., K. Ohtomo, Y. Morishita, H. Konami and M. T. Madigan (1992) Dimer Structures of Bacteriochlorophyll *c* from *Chlorobium Tepidum* in $CDCl_3$. *Chem. Lett.*, 261-264.

(11) Holzwarth, A. R. and K. Schaffner (1994) On the Structure of Bacteriochlorophyll Molecular

Aggregates in the Chlorosomes of Green Bacteria. A Molecular Modelling Study. *Photosynth. Res.* **41**, 225-233.

(12) Ogura, K., H. Terasawa and F. Inagaki (1996) An Improved Double-Tuned and Isotope-Filtered Pulse Scheme Based on a Pulsed Field Gradient and a Wide-Band Inversion Shaped Pulse. *J. Biomol. NMR* **8**, 492-498.

(13) Abraham, R. J. (1961) The Proton Magnetic Resonance Spectra of Porphyrins Part II. Ring Current Effects in the Porphyrins. *Mol. Phys.* **4**, 145-152.

(14) Abraham, R. J., S. C. M. Fell and K. M. Smith (1977) The N.m.r. Spectra of Porphyrins 13 - A Ring Current Model for the Porphyrin and Chlorin (7,8-Dihydroporphyrin) Rings. *Org. Magn. Reson.* **9**, 367-373.

(15) Nozawa, T., M. Suzuki, K. Ohtomo, Y. Morishita, H. Konami and M. T. Madigan (1991) Aggregation Structure of Bacteriochlorophyll *c* in Chlorosomes from *Chlorobium Tepidum*. *Chem.* Lett., 1641-1644.

(16) Johnson, C. E. and F. A. Bovey (1958) Calculation of Nuclear Magnetic Resonance Spectra of Aromatic Hydrocarbons. *J. Chem. Phys.* **29**, 1012-1014.

(17) Smith, K. M., D. A Goff, J. Fajer and K. M. Barkigia (1982) Chirality and Structures of Bacteriochlorophylls *d*. *J. Am. Chem. Soc.* **104**, 3747-3749.

(18) Abraham, R. J., K. M. Smith, D. A. Goff and J.-J Lai (1982) NMR Spectra of Porphyrins. 18. A Ring-Current Model for Chlorophyll Derivatives. *J. Am. Chem. Soc.* **104**, 4332-4337.

(19) Mizoguchi, T., K. Matsuura, K. Shimada and Y. Koyama (1996) The Structure of the Aggregate Form of Bacteriochlorophyll *c* Showing the $Q_y$ Absorption above 740 nm: A $^1$H-NMR Study. *Chem. Phys. Lett.* **260**, 153-158.

**Table 1**. The $^{13}C$ aggregation shifts for the aggregate absorbing above 740 nm.

| Carbon atom | Amount of methanol titrated | | | Aggregation shifts | |
|---|---|---|---|---|---|
| | '0' µl | 7 µl | 30 µl | $\Delta=\delta_{0\mu l} - \delta_{30\mu l}$ | $\Delta=\delta_{0\mu l} - \delta_{7\mu l}$ |
| 1-C | 153.60 | 153.24 | 153.44 | 0.16 | 0.36 |
| 3-C | 144.35 | 144.47 | 144.80 | -0.45 | -0.12 |
| 4-C | 144.70 | 144.83 | 145.18 | -0.48 | -0.13 |
| 5-C | 99.80 | 100.47 | 100.47 | -0.67 | -0.67 |
| 6-C | 150.30 | 149.90 | 150.13 | 0.17 | 0.40 |
| 8-C | 140.85 | 140.70 | 140.73 | 0.12 | 0.15 |
| 9-C | 146.75 | 146.69 | 146.57 | 0.18 | 0.06 |
| 10-C | 106.55 | 106.16 | 106.16 | 0.39 | 0.39 |
| 11-C | 146.75 | 146.69 | 146.57 | 0.18 | 0.06 |
| 12-C | 140.85 | 140.70 | 140.73 | 0.12 | 0.15 |
| 14-C | 161.60 | 161.02 | 161.10 | 0.50 | 0.58 |
| 15-C | 104.90 | 105.18 | 105.08 | -0.18 | -0.28 |
| 16-C | 153.90 | 153.72 | 153.86 | 0.04 | 0.18 |
| 17-C | 50.40 | 50.30 | 50.30 | 0.10 | 0.10 |
| 19-C | 167.90 | 167.27 | 167.34 | 0.56 | 0.63 |
| 20-C | 104.90 | 104.52 | 104.53 | 0.37 | 0.38 |
| $2^1$-C | 16.60 | 17.21 | 17.26 | -0.66 | -0.61 |
| $3^1$-C | 65.35 | 65.32 | 65.18 | 0.17 | 0.03 |
| $3^2$-C | 25.50 | 25.90 | 26.06 | -0.56 | -0.40 |
| $7^1$-C | 11.65 | 11.49 | 11.40 | 0.25 | 0.16 |
| $8^1$-C | 35.70 | 35.51 | 35.49 | 0.21 | 0.19 |
| $8^2$-C | 32.20 | 32.07 | 32.10 | 0.10 | 0.13 |
| $8^3$-C | 23.50 | 23.25 | 23.20 | 0.30 | 0.25 |
| $12^1$-C | 20.40 | 20.93 | 21.09 | -0.69 | -0.53 |
| $12^2$-C | 16.70 | 16.70 | 16.88 | -0.18 | 0.00 |
| $13^1$-C | 195.45 | 195.94 | 196.71 | -1.26 | -0.49 |
| $17^1$-C | 29.70 | 29.90 | 29.95 | -0.25 | -0.20 |
| $17^2$-C | 30.45 | 30.52 | 30.62 | -0.17 | -0.07 |
| $17^3$-C | 172.85 | 173.23 | 173.28 | -0.43 | -0.38 |
| $18^1$-C | 21.00 | 20.70 | 20.67 | 0.33 | 0.30 |
| $20^1$-C | 21.55 | 21.49 | 21.46 | 0.09 | 0.06 |

**Table 2.** Comparison, for the $^1H$ nuclei, between the observed aggregation shifts and the calculated ring-current effects based on different models and approximations.

| Proton atom | Aggregation shift $\Delta=\delta_{0\mu l} - \delta_{50\mu l}$ | Magnetic-dipole approximation | | Loop-current approximation | |
|---|---|---|---|---|---|
| | | parallel-chain model | antiparallel-chain model | parallel-chain model | antiparallel-chain model |
| 5-H | −[a] | − | − | − | − |
| 10-H | +[b] | + | −✓[c] | + | + |
| $3^1$-H | − | − | − | − | − |
| $13^2$-H | − | − | − | − | +✓ |
| 18-H | + | + | + | + | + |
| 17-H | + | + | −✓ | + | + |
| $12^1$-H | − | − | − | − | +✓ |
| 20Me-H | + | + | −✓ | + | + |
| $8^1$-H | + | + | + | + | + |
| 2Me-H | − | − | − | +✓ | − |
| 7Me-H | − | − | − | +✓ | +✓ |
| $3^1$Me-H | − | − | − | − | − |
| $12^1$Me-H | − | − | +✓ | +✓ | +✓ |
| 18Me-H | + | + | −✓ | + | + |
| $8^2$Me-H | + | + | + | + | + |
| | | 15 / 15 | 10 / 15 | 12 / 15 | 11 / 15 |

[a, b]High-field-shift and low-field-shift are denoted as − and +.

[c]Wrong prediction are shown by ✓.

**Table 3**. Comparison, for the $^{13}C$ nuclei, between the observed aggregation shifts and the calculated ring-current effects based on different models and approximations.

| Carbon atom | Aggregation shifts | Magnetic-dipole approximation | | Loop-current approximation | |
|---|---|---|---|---|---|
| | $\Delta=\delta_{0\mu l} - \delta_{30\mu l}$ | parallel-chain model | antiparallel-chain model | parallel-chain model | antiparallel-chain model |
| 1-C | +[a] | −✓[c] | −✓ | + | −✓ |
| 3-C | −[b] | − | − | − | − |
| 4-C | − | − | − | − | − |
| 5-C | − | − | − | − | − |
| 6-C | + | −✓ | −✓ | + | −✓ |
| 8-C | + | + | −✓ | + | + |
| 9-C | + | + | −✓ | + | + |
| 10-C | + | + | −✓ | + | + |
| 11-C | + | −✓ | −✓ | + | + |
| 12-C | + | −✓ | −✓ | −✓ | + |
| 14-C | + | −✓ | −✓ | −✓ | + |
| 15-C | − | − | − | − | +✓ |
| 16-C | + | −✓ | −✓ | + | + |
| 17-C | + | + | + | + | + |
| 19-C | + | + | −✓ | + | + |
| 20-C | + | + | −✓ | + | + |
| 21-C | − | − | − | − | − |
| 31-C | + | −✓ | −✓ | −✓ | −✓ |
| $3^2$-C | − | − | − | − | − |
| $7^1$-C | + | −✓ | −✓ | + | + |
| $8^1$-C | + | + | + | + | + |
| $8^2$-C | + | + | + | + | + |
| $8^3$-C | + | + | + | + | + |
| $12^1$-C | − | − | − | − | +✓ |
| $12^2$-C | − | − | +✓ | − | +✓ |
| $13^1$-C | − | − | − | − | +✓ |
| $17^1$-C | − | − | +✓ | +✓ | +✓ |
| $17^2$-C | − | +✓ | +✓ | +✓ | +✓ |
| $17^3$-C | − | +✓ | +✓ | +✓ | +✓ |
| $18^1$-C | + | + | −✓ | + | + |
| $20^1$-C | + | + | −✓ | + | + |
| | | 21 / 31 | 12 / 31 | 25 / 31 | 21 / 31 |

[a, b]Low-field-shift and high-field-shift are denoted as + and −.
[c]Wrong prediction are shown by ✓.

Table 4. Observed intermolecular NOE correlations and estimated H-H atomic distances.

| | Intermolecular NOE correlations | | Correlations between molecular regions | H-H distance (Å) | | C-C distance (Å) | |
|---|---|---|---|---|---|---|---|
| | | | | Structure 1 | Structure 2 | Structure 1 | Structure 2 |
| (1) | 17-H | 18-H | L ⟷ L | 4.0 | (8.5) | 6.0 | 8.5 |
| (2) | 17-H | 20Me-H | | 2.0 | (10.5) | 4.0 | 11.0 |
| (3) | 18Me-H | 20Me-H | | 3.0 | (7.0) | 4.5 | 8.5 |
| (4) | 17-H | $13^2$-H | | (9.0)[a] | 4.5 | 9.5 | 5.5 |
| (5) | 18-H | 20Me-H | | (8.0) | 3.5 | 9.5 | 4.5 |
| (6) | $8^1$-H | 7Me-H | R ⟷ R | 2.5 | 3.0 | 5.0 | 4.5 |
| (7) | $8^1$-H | $8^2$Me-H | | 4.5 | 4.5 | 6.0 | 5.5 |
| (8) | $8^2$Me-H | 7Me-H | | 4.5 | 4.5 | 5.5 | 5.5 |
| (9) | 10-H | $8^2$Me-H | | 4.0 | 4.0 | 6.0 | 6.0 |
| (10) | 10-H | $8^2$-H | | 4.5 | 4.5 | 6.0 | 6.0 |
| (11) | 10-H | $8^1$-H | | (5.5) | 5.0 | 6.5 | 6.0 |
| (12) | 7Me-H | 20Me-H | L ⟷ R | 2.0 | | 3.0 | |

[a]Proton-proton distances too large for the NOE correlation to be detected are shown in parentheses.

## FIGURES CAPTIONS

**Figure 1.** Schematic presentations of (a) the parallel-chain model and (b) the antiparallel-chain model. The parallel-chain model includes both structure 1 and structure 2 which differ in the sliding direction of the stacked column.

**Figure 2.** (a) A molecular model of BChl **c**, typification of the carbon atoms, and the definition of region L and region R; and (b) the observed aggregation shifts for the $^{1}H$ and $^{13}C$ signals. Those nuclei exhibiting high-field-shift (hfs) and low-field-shift (lfs) are shown by ● and ▨, respectively.

**Figure 3.** Dependence of the electronic absorption spectrum of BChl **c** on the solvent composition; the amount of methanol which was added to 550 $\mu$l of the solvent mixture of methylene chloride and carbon tetrachloride (1:3) is shown for each spectrum.

**Figure 4.** Dependence of the chemical shift of each H signal on the solvent composition; the abscissa scales the amount of methanol added to 550 $\mu$l of the solvent mixture of methylene chloride and carbon tetrachloride (1:3).

**Figure 5.** Dependence of the peak intensity of each H signal on the solvent composition; see the caption of Fig. 3 for the abscissa scale. (a) Curve fitting to the observed points; (b) the curve for each H signal obtained by the fitting in (a).

**Figure 6.** Changes in the $^{13}C$ chemical shifts as the functions of decreasing amount of titrated methanol.

**Figure 7.** A stacking model of 'structure 1'. The side views (a) from region L and (b) from region R, and (c) the top view: The observed hfs (●) and lfs (▨) are indicated in reference to the neighboring macrocycles, and those intermolecular NOE correlations which can be explained in terms of this structure are shown by using arrows and their numbering listed in Table 4.

**Figure 8.** A stacking model of 'structure 2'. The side views (a) from region L and (b) from region

R, and (c) the top view: The observed hfs (●) and lfs (◍) are indicated in reference to the neighboring macrocycles, and those intermolecular NOE correlations which can be explained in terms of this structure are shown by using arrows and their numbering listed in Table 4.

**Figure 9.** F2($^1$H)-F3($^1$H) slices from the 3D 600 MHz F1 $^{13}$C-edited-F3 $^{13}$C-filtered HSQC-NOESY spectrum of a 1:1 mixture of $^{13}$C-labeled and unlabeled BChl **c** dissolved at the concentration of $2.5 \times 10^{-3}$ M in a 1:3 mixture of dichloromethane and carbon tetrachloride, to which 1.5 $\mu$l methanol-$d_4$ was added. Assignment is given to each NOE correlation between a proton attached to the $^{12}$C nuclei in unlabeled BChl **c** and a proton attached to the $^{13}$C nuclei in $^{13}$C-labeled BChl **c**; the diagonal peaks are labeled "D".

Fig. 1

(a)

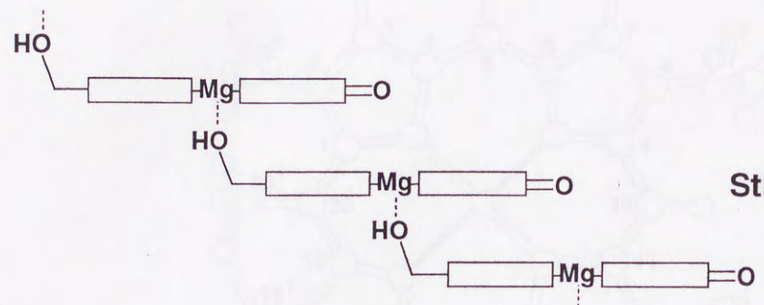


Structure 1

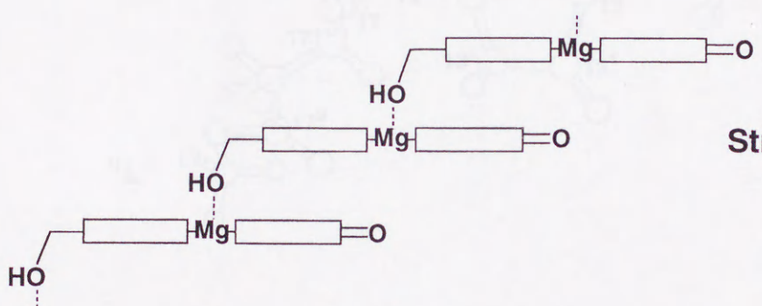


Structure 2

(b)

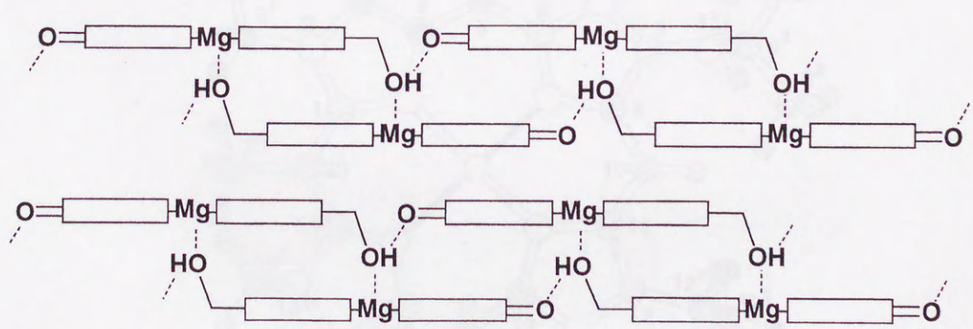

Fig. 2

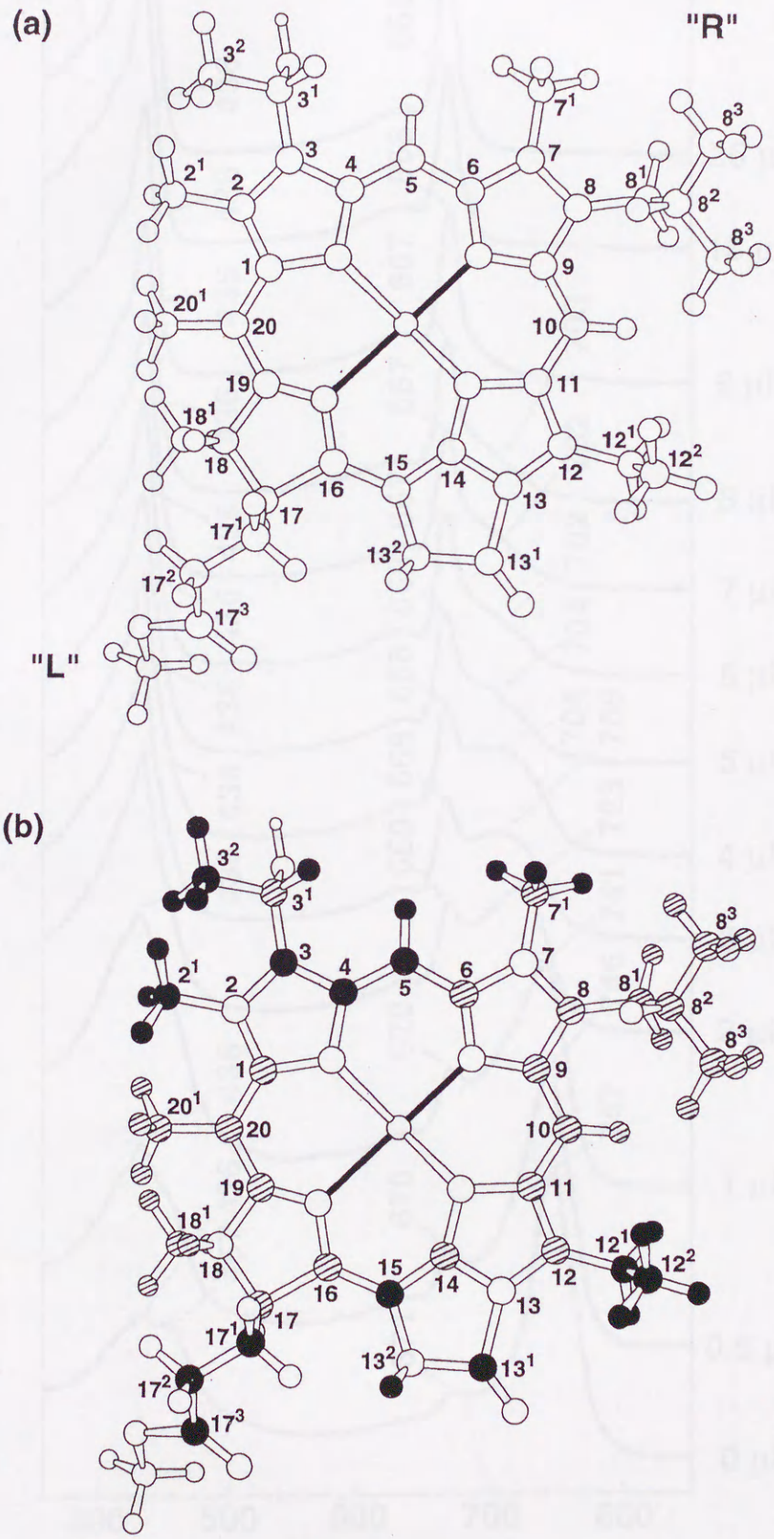

Fig. 3

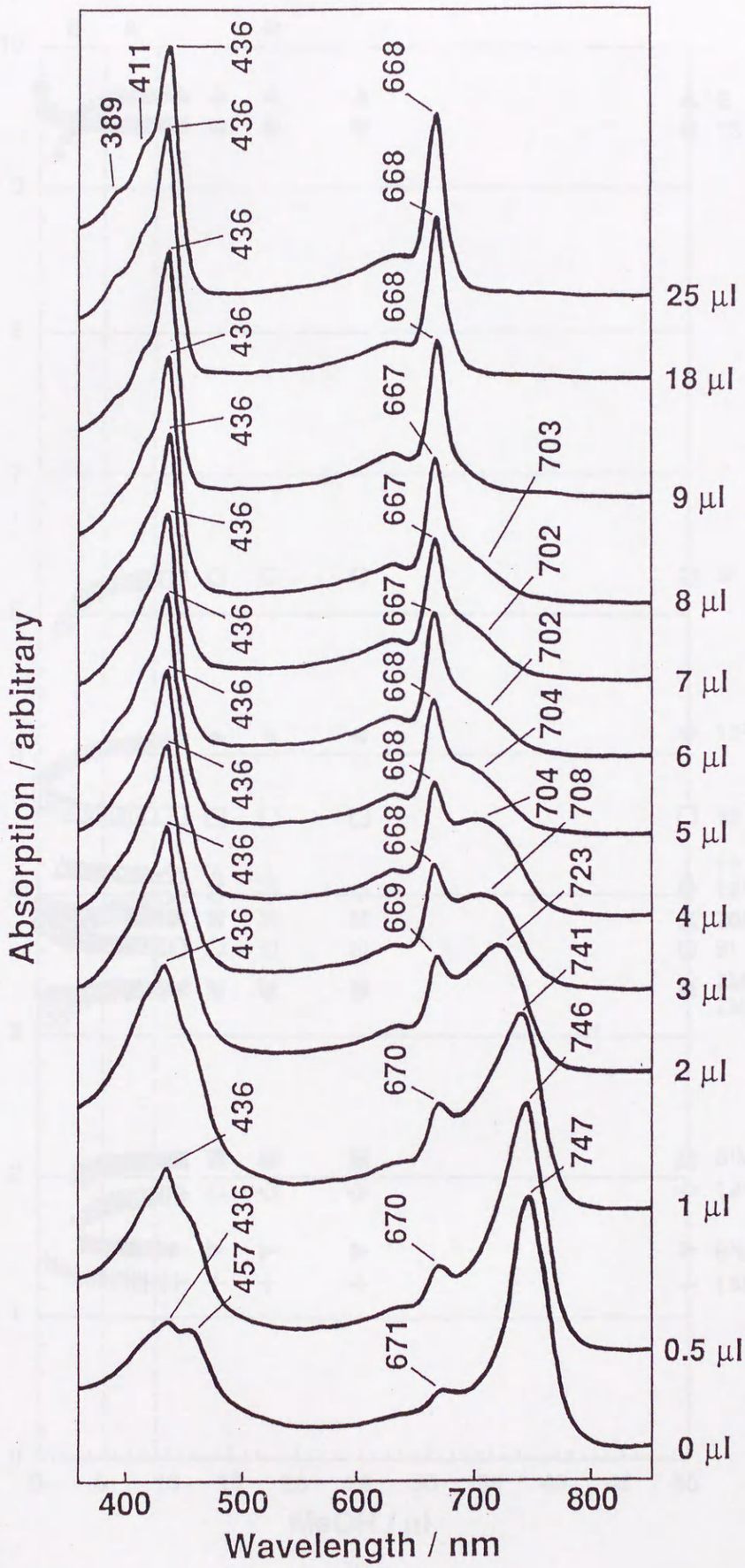
Absorption / arbitrary
Wavelength / nm
400
500
600
700
800
389
411
436
668
667
703
702
704
708
723
669
741
746
670
747
457
671
25 µl
18 µl
9 µl
8 µl
7 µl
6 µl
5 µl
4 µl
3 µl
2 µl
1 µl
0.5 µl
0 µl

Fig. 4

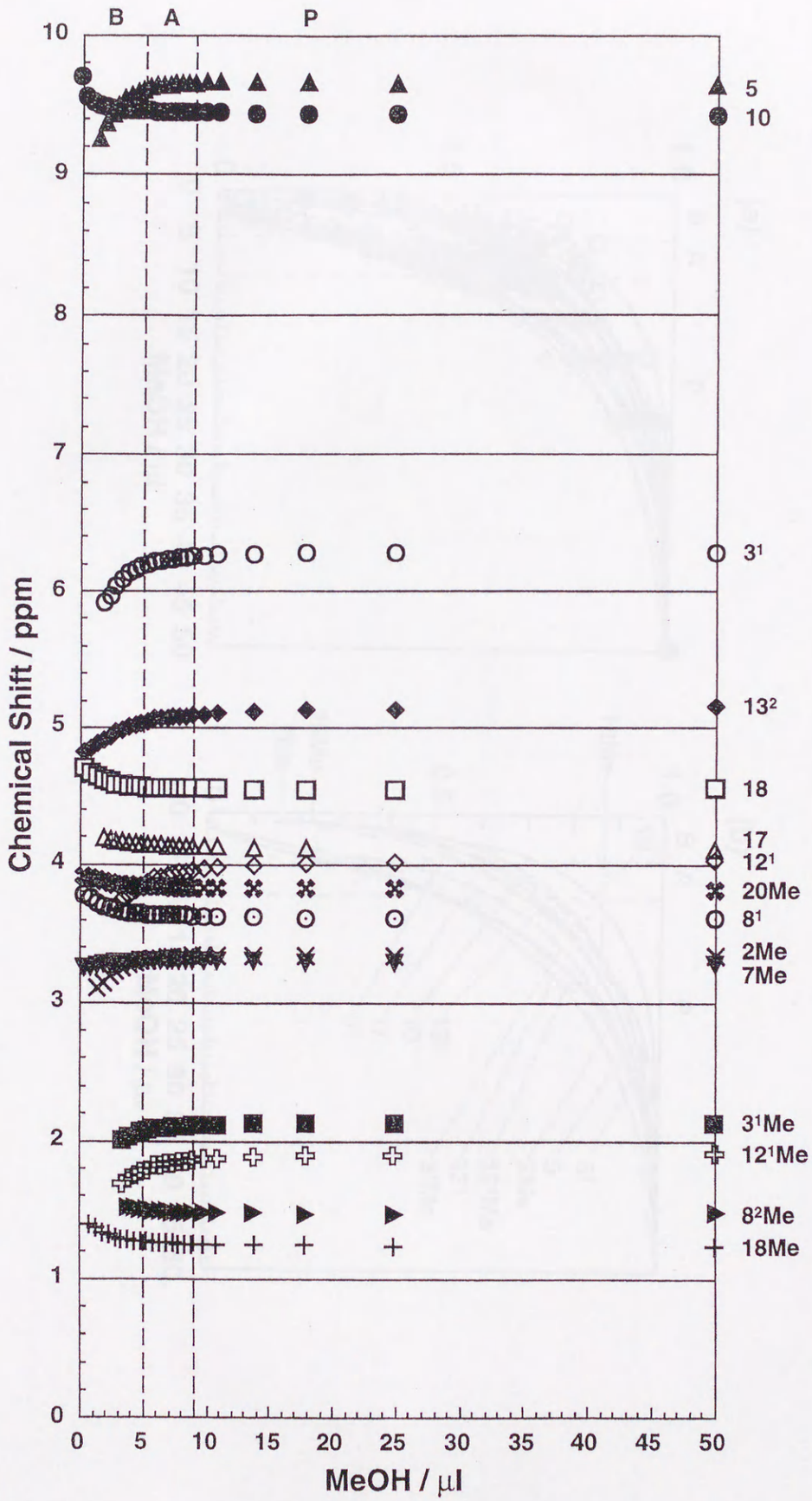
B
A
P
10
9
8
7
6
5
4
3
2
1
0
Chemical Shift / ppm
0
5
10
15
20
25
30
35
40
45
50
MeOH / µl
5
10
3¹
13²
18
17
12¹
20Me
8¹
2Me
7Me
3¹Me
12¹Me
8²Me
18Me

Fig. 5

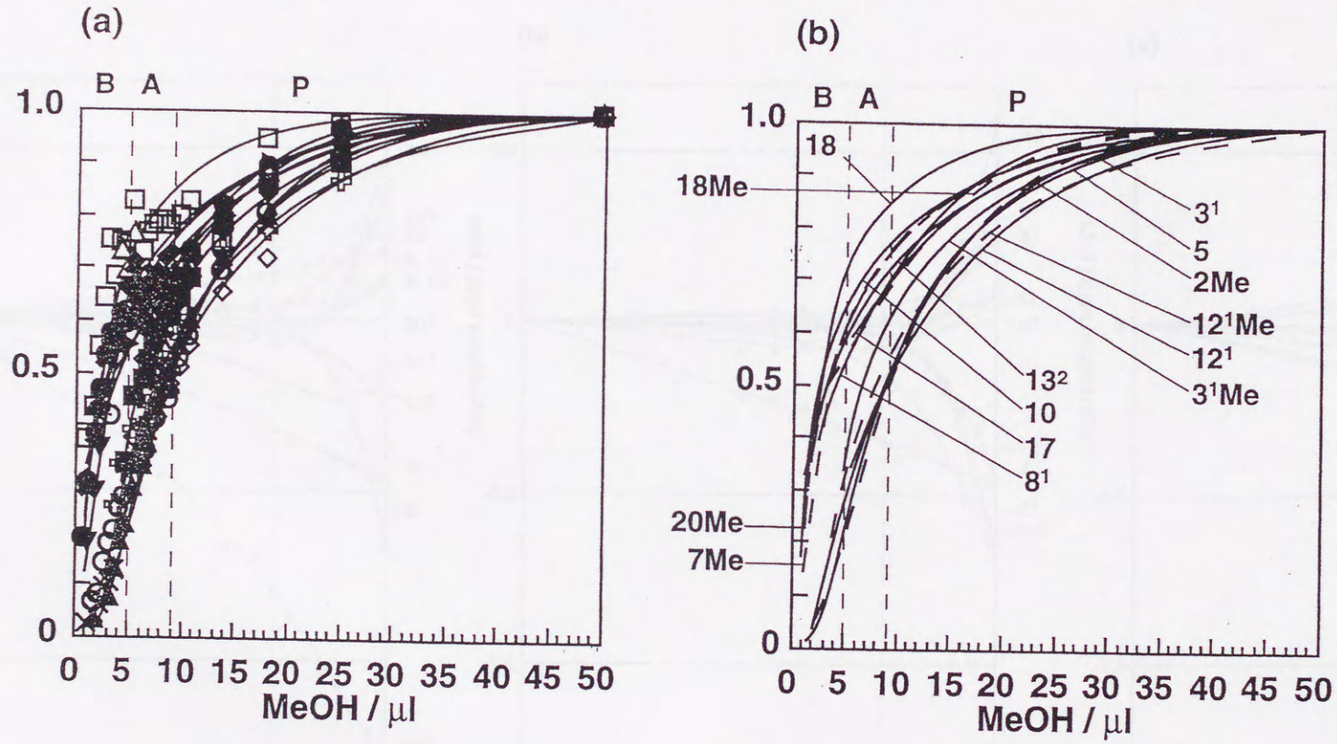
(a)
B A P
1.0
0.5
0
0 5 10 15 20 25 30 35 40 45 50
MeOH / µl
(b)
B A P
1.0
0.5
0
18
18Me
20Me
7Me
3¹
5
2Me
12¹Me
12¹
3¹Me
13²
10
17
8¹
0 5 10 15 20 25 30 35 40 45 50
MeOH / µl

Fig. 6

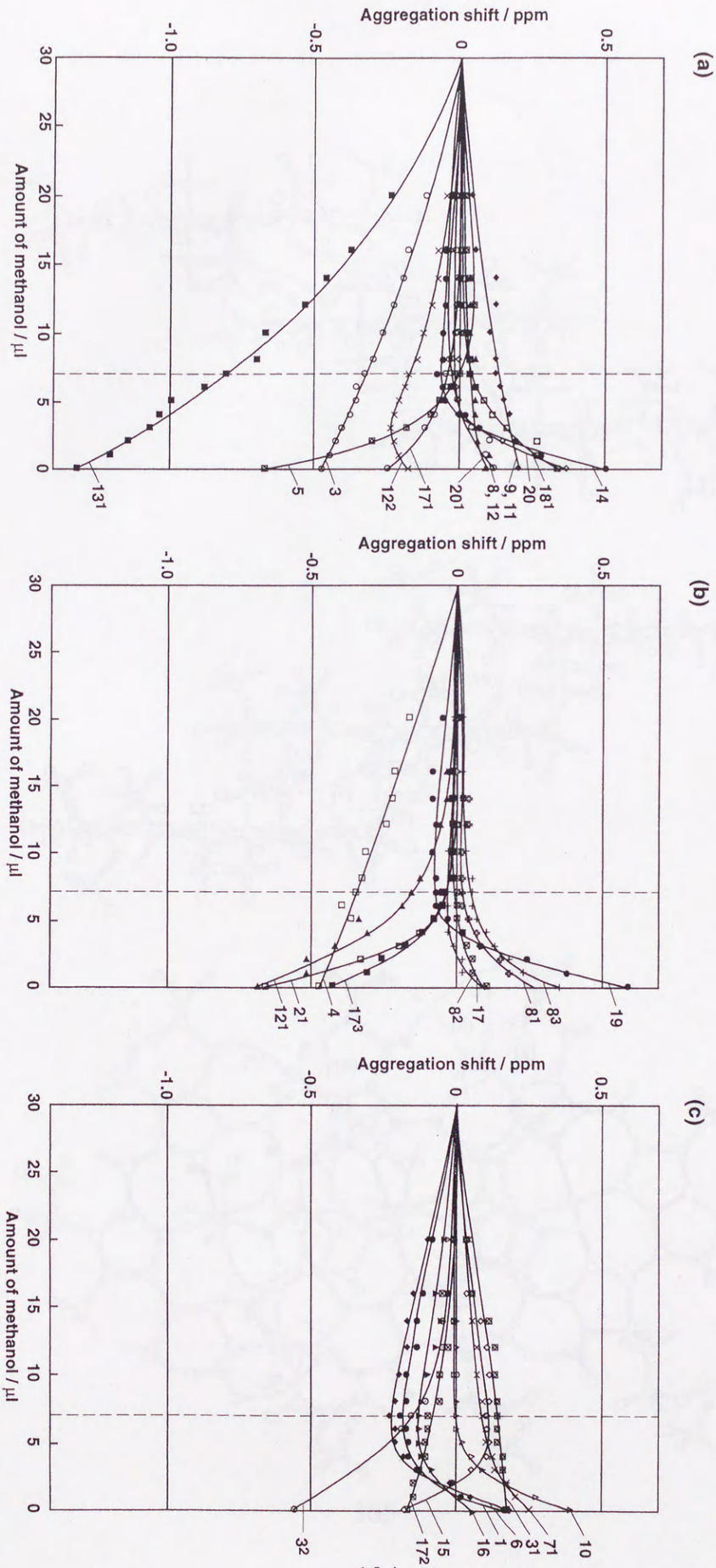
Aggregation shift / ppm
-1.0
-0.5
0
0.5
Amount of methanol / µl
0
5
10
15
20
25
30
(a)
131
5
3
122
171
201
8, 12
9, 11
20
181
14
(b)
121
21
4
173
82
17
81
83
19
(c)
32
172
15
16
1
6
31
71
10

Fig. 7

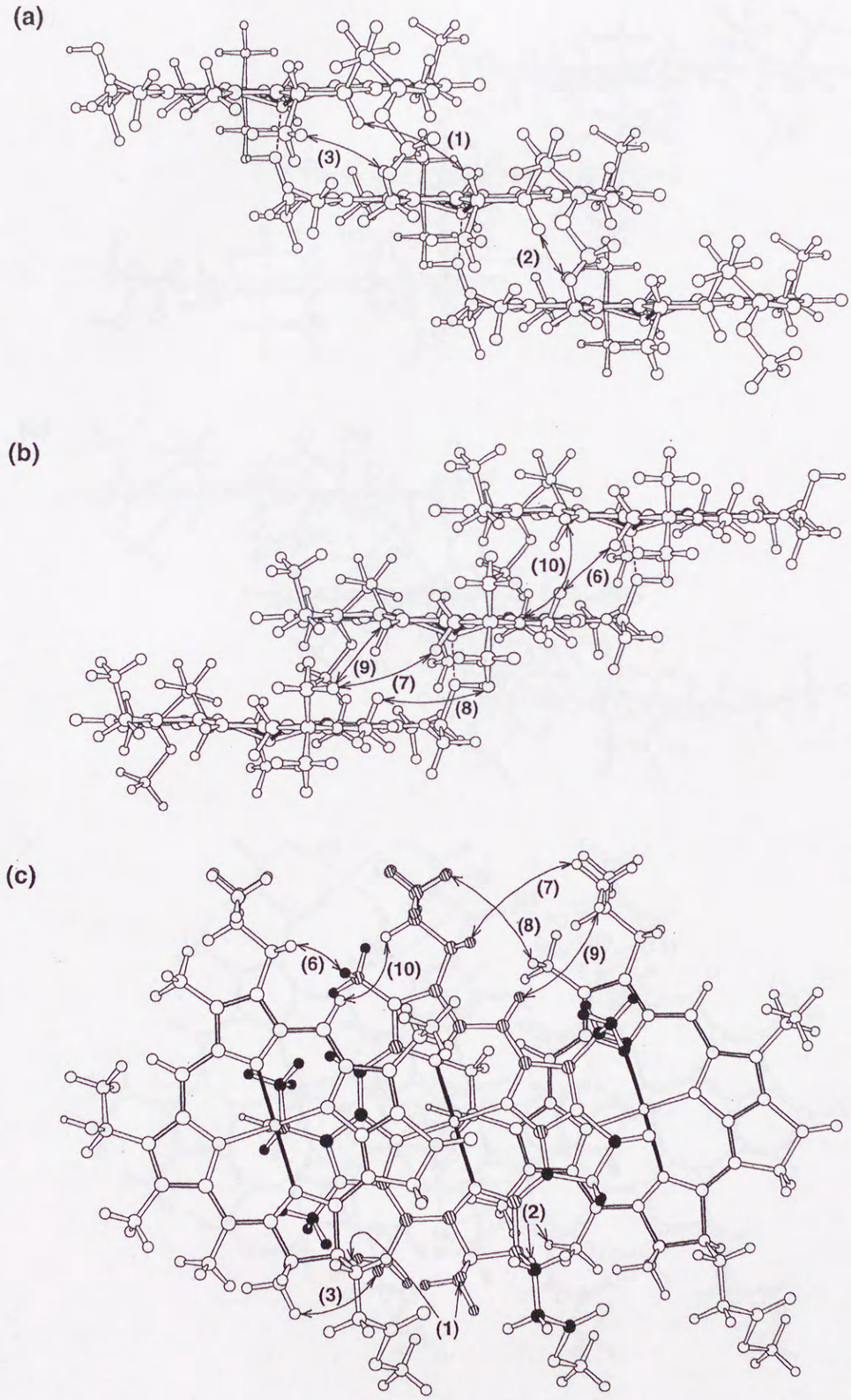

Fig. 8

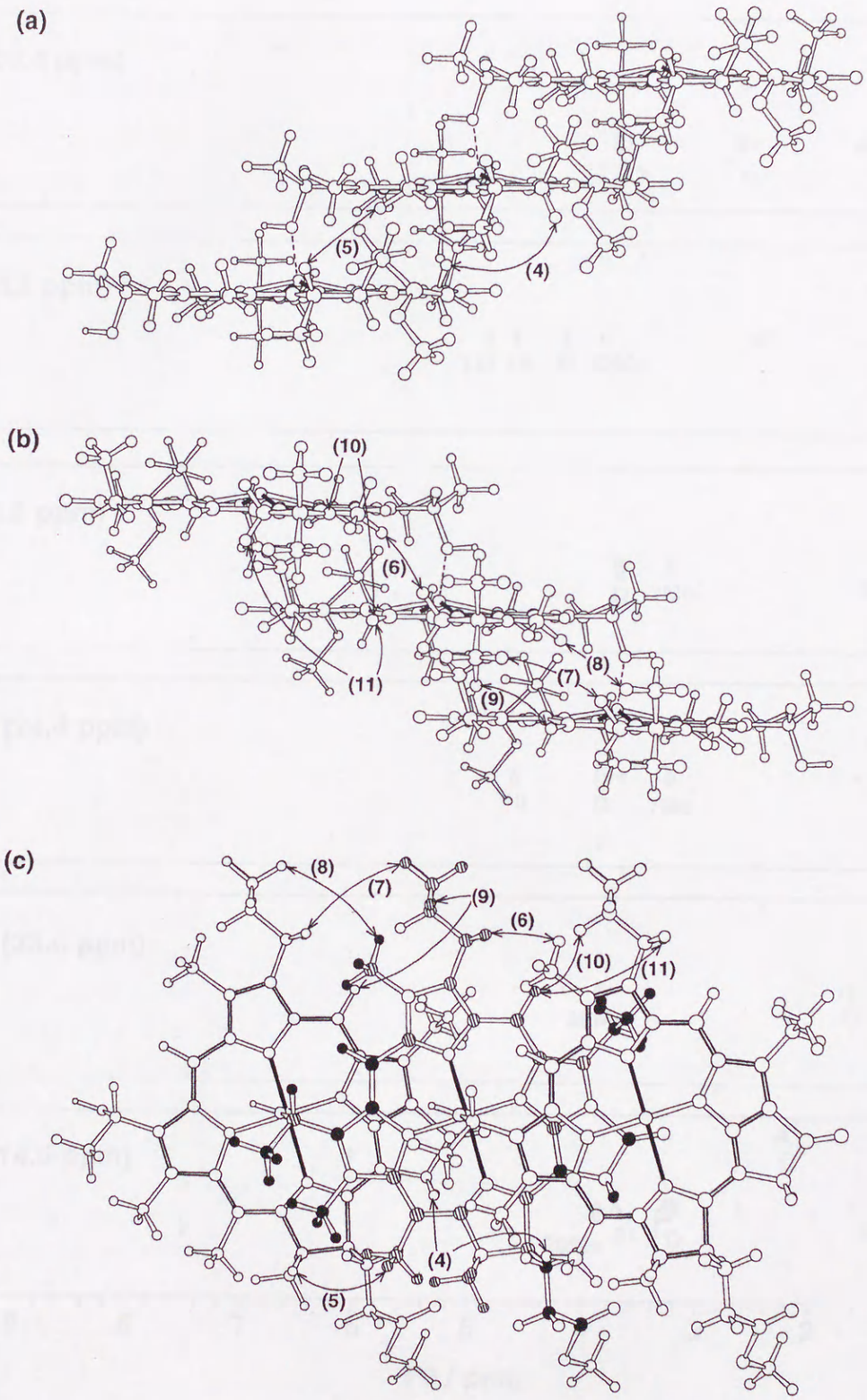

Fig. 9

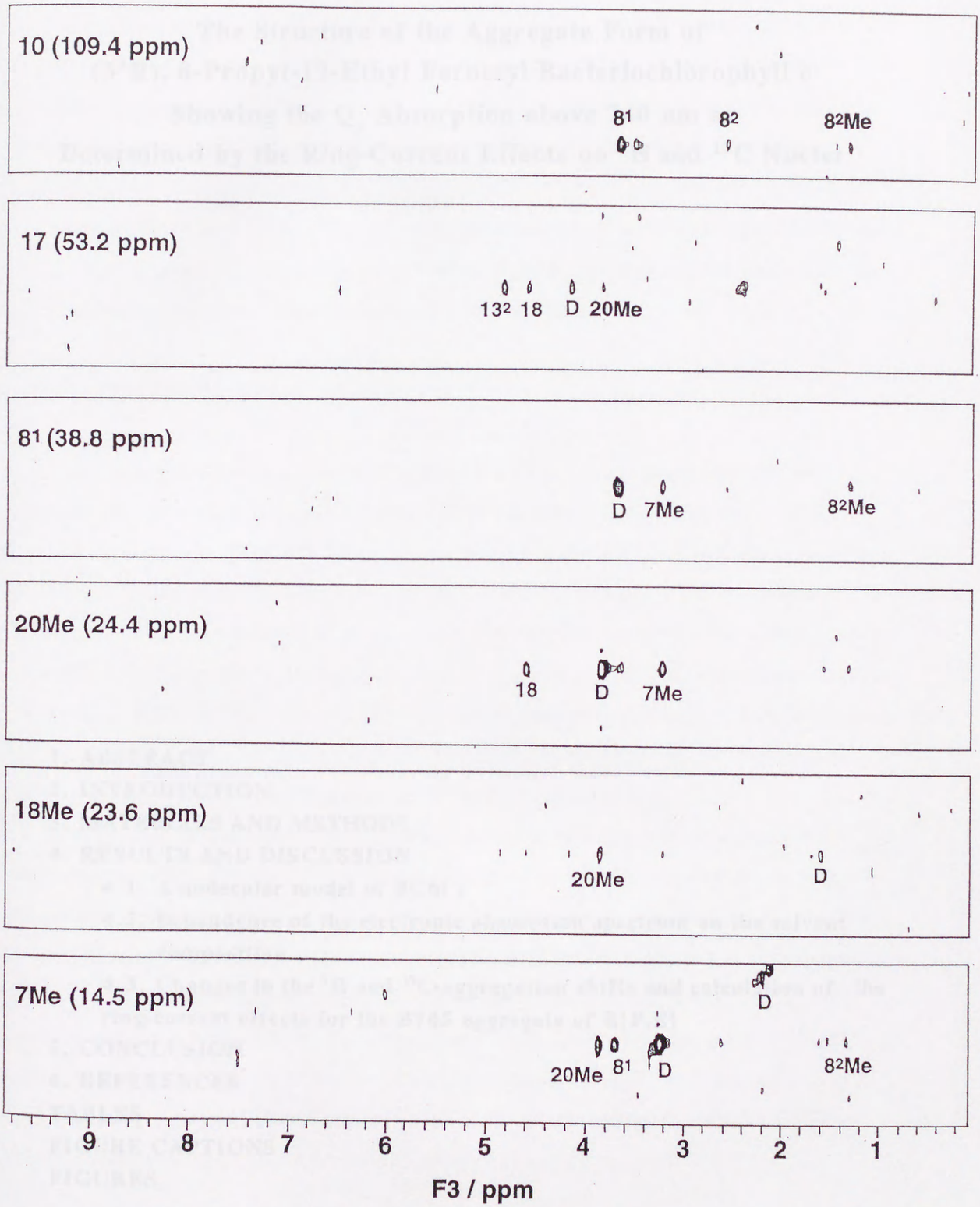
10 (109.4 ppm)
8¹
8²
8²Me
17 (53.2 ppm)
13² 18 D 20Me
8¹ (38.8 ppm)
D 7Me
8²Me
20Me (24.4 ppm)
18 D 7Me
18Me (23.6 ppm)
20Me
D
7Me (14.5 ppm)
D
20Me 8¹ D
8²Me
9 8 7 6 5 4 3 2 1
F3 / ppm

Chapter 4

# The Structure of the Aggregate Form of (3$^1$R), 8-Propyl-12-Ethyl Farnesyl Bacteriochlorophyll *c* Showing the $Q_y$ Absorption above 740 nm as Determined by the Ring-Current Effects on $^1$H and $^{13}$C Nuclei

## 1. ABSTRACT

$^{13}$C-Enriched bacteriochlorophyll **c** ($3^1$R, 8-propyl-12-ethyl, farnesyl) was suspended in a 1:14 mixture of methylene chloride and cyclohexane to form an aggregate showing the $Q_y$ absorption above 740 nm; changes in the $^1$H- and $^{13}$C chemical shifts were traced when ethanol was titrated to dissolve the aggregate, and then, the changes were correlated to the ring-current effects due to the neighboring macrocycles in the aggregate. The aggregate structure has been proposed based on the ring-current effects on both $^1$H and $^{13}$C nuclei; the piggy-back dimers are stacked together to form an inclined column. In order to confirm the above stacked structure, the ring-current effects on the $^1$H and $^{13}$C nuclei were calculated based on the loop-current approximation.

## 2. INTRODUCTION

The photosynthetic system of green bacteria contains a unique antenna complex called 'chlorosomes', whose structural motif is believed to be the same as that of the aggregate of the bacteriochlorophyll **c** (BChl **c**) molecules extracted from the membrane [1-3]. Both the chlorosomes and the aggregate are characterized by the $Q_y$ absorption above 740 nm [1-3] and by the similar $^{13}$C-NMR spectra [4-6]. Two different models have been proposed concerning the type of stacking of the macrocycles: (1) Nozawa and coworkers [7] proposed a model consisting of stacked linear arrays of dimeric units ('direct overlap model'). (2) Holzwarth, de Groot and coworkers [4, 5, 8] proposed a model consisting of stacked monomers to form an inclined column. Either type of stacking needs to be proved in order to build a structural model of the entire chlorosomes.

Green photosynthetic bacteria having chlorosomes as antenna complexes are characterized by a unique feature of BChl **c** molecules they contain: One is the stereoisomeric configuration of the hydroxylethyl group at the $C3^1$ position, and the other is the bulkiness of the sidechain at the C8 and C12 positions (see Figure 2 in the Introduction section). Each isomer is known to form a series of artificial aggregates characterized by different wavelengths of the $Q_y$ absorption depending on the stereoisomeric configuration [9-11]. Those aggregates include the dimer absorbing at ~ 675 nm, a lower aggregate absorbing at ~ 705 nm, a medium aggregate absorbing at ~ 720 nm, and a higher aggregate absorbing above 745 nm; hereafter, I call them 'the dimer' (B675), 'B705', 'B720' and 'B745', respectively, according to the apparent wavelengths of the $Q_y$ absorption.

In order to understand the structural basis for the transformation among aggregate forms, I need to determine 'the structural motifs' of key aggregates: I have determined the structure of B675 of R[E,E] to be the piggy-back dimer (Chapter 1), the structural motif of B705 of R[E,E] to be a stacking of the piggy-back dimer to form a straight column (Chapter 2), and that of B745 of S[I,E] to be a parallel, stepwise stacking of the monomers (Chapter 3). Here, I used two different techniques of $^{1}$H- and $^{13}$C-NMR spectroscopy; one is a comparison between the aggregation shifts (the changes in chemical shift upon aggregate formation) and the theoretically calculated ring-current effects, and the other is the detection of $^{1}$H-$^{1}$H intermolecular NOE (nuclear Overhauser effect) correlations. In this Chapter, I focused on another higher aggregates, B745, of R[P,E], because the Nozawa group proposed an antiparallel-chain model for the B745 formed by the use of the entire extract of BChl **c** (a mixture of isomers whose major component is the R isomers [12]) from *Chlorobium tepidum* [7]; the Nozawa model is completely different from our parallel-chain model for the B745 of S[I,E] as described in Chapter 3. This contradiction could originate from a pair of different B745s consisting of the R and S isomers. Thus, I addressed a question: What is 'the structural motif' of B745 of R[P,E] as determined by NMR spectroscopy?

## 3. MATERIALS AND METHODS

*Chlorobium limicola* f. sp. *thiosulfatophilum* was grown, and R[P,E]BChl **c** (3$^{1}$R, 8-propyl-12-ethyl, farnesyl) was obtained from it as described the previous Chapters. R[P,E] was suspended in a mixture of $CH_2Cl_2$ and cyclohexane (1 : 14 v/v) at the concentration of $2.5 \times 10^{-3}$ M to form a B745 aggregate, to an aliquot (550 μL) of which ethanol (0 - 100 μL) was titrated; the deuterium contents of those solvents were 99.9, 99.6 and 99.0 % for $CH_2Cl_2$, cyclohexane (both ISOTEC Inc., Chiba) and ethanol (Nacalai tesque, Osaka), respectively. The $^{1}$H and $^{13}$C-NMR spectra of the suspensions were recorded at room temperature by the use of a JEOL JNM-A400 FT NMR spectrometer as described the previous Chapters. Tetramethylsilane was used as an internal standard. $^{1}$H-$^{1}$H COSY (correlation spectroscopy) and $^{1}$H-$^{1}$H ROESY (rotating-frame Overhauser effect spectroscopy) spectra as well as $^{13}$C-$^{1}$H COSY, HMBC (heteronuclear multiple-bond correlation) and DEPT (distortionless enhancement by poralization transfer) spectra were recorded to aid the assignments of the $^{1}$H as well as $^{13}$C signals. Decomposition of the aggregate was traced, for exactly the same suspensions as used for NMR measurements, by electronic-absorption spectroscopy using a

25 μm cell. Spectral deconvolution was performed by assuming five Gaussian components, i.e., the monomer, the (B675) dimer, the B705, B720 and B745 aggregates. The ring-current effects were calculated by the use of the loop-current approximation as described previous Chapter 2 & 3.

## 4. RESULTS AND DISCUSSION

### 4.1. A molecular model of BChl c

Figure 1 shows a molecular model of BChl **c** which is used in this Chapter. The large and small open circles indicate the carbon and hydrogen atoms; the dotted, shaded and closed circles indicate the atoms of oxygen, nitrogen and magnesium, respectively. The closed bars indicate the Mg···N coordination bonds along the $Q_x$ axis, which can be used to visualize the orientation of the macrocycle in a complicated stacked structure.

The molecular model is essentially the same as that used in the previous Chapter 1 & 2 except for the C8 sidechain is replaced by the propyl group. The farnesyl group is replaced by the methyl group in both cases, because I will not discuss its conformation. The molecular structure in the Figure is based on the results of the X-ray structures of ethyl chlorophyllide **a** [13] dihydrate.

### 4.2. Dependence of the electronic absorption spectrum on the solvent composition

Figure 2 shows changes in the $Q_y$ absorption when the B745 of R[P,E] was formed in a mixture of $CH_2Cl_2$ and cyclohexane (1 : 14 v/v) at the concentration of $2.5 \times 10^{-3}$ M, and then it was decomposed by titration of ethanol into the lower aggregates and eventually into the monomer.

Figure 3 shows changes in the composition of all those components in this process. When the amount of ethanol titrated is reduced, the changes are characterized as follows: After the formation of certain amounts of the dimer, B705 and B720, in the initial phase, at the expense of the monomer, B745 is suddenly generated at the expense of those components except for B720. Here, changes in the amount of B720 suggests the formation of B720 as well. Thus, I tried to determine, by means of $^1$H- and $^{13}$C- NMR spectroscopy, the structural motif of B745 and B720 being generated in the final stage.

### 4.3. Changes in the $^1$H and $^{13}$C-aggregation shifts and calculation of the ring-current effects for the B745 aggregate of R[P,E]

Table 1 lists the $^{1}H$ chemical shifts at 0 $\mu$L ethanol (extrapolated values) and those at 50 $\mu$L ethanol, and their differences ('the aggregation shifts'). When the amount of ethanol titrated is reduced systematically, I observed monotonous change in the aggregation shifts, a fact which supports the idea that B720 is a lower homologue of B745. Figure 4 shows their structural motif which I have determined by the use of those aggregation shifts (Hara et al., unpublished results): Panels b and c depict the pattern of the aggregation shifts in reference to the molecular structure; those $^{1}H$ and $^{13}C$ showing the high-field-shift are painted, and those showing the low-field-shift are shaded. This pattern of aggregation shifts as well as the splitting of the $^{1}H$ signals (data not shown) proved that the piggy-back dimer [14, 15] is the basic structure in this structural motif. Actually, those panels show that the atoms showing high-field-shift are located inside of the neighboring macrocycle ring whereas the atoms showing low-field-shift are located outside of it, when they are projected on its plane. (In this comparison, I need to take into account the long-range ring-current effects as well.) Then, I tried to determine the positional shift of the neighboring dimeric unit by calculating the ring-current effects due to the conjugated macrocycles of the neighboring BChl **c** molecules in the aggregate; in this calculation, I only used the loop-current approximation as described in Chapter 2.

Table 1 compares the signs of the observed aggregation shifts and the calculated ring-current effects for the structural motif shown in Figure 4, which gave rise to the best agreement. The positional shift of the neighboring piggy-back dimer along the y-direction was determined to be 8.75 Å, the Mg to Mg distance in the same layer being 15.25 Å (thus, the positional shift is 8.75 / 15.25 = 0.57 in terms of the unit along the y-direction). I call this structural motif 'a shifted-inclined column'. Correct prediction of the signs of the aggregation shifts (score) is 11 / 14 = 0.79, and the weighted score, which is defined as a sum of the absolute values of the observed aggregation shifts correctly predicted divided by the sum of the absolute values of all the observed aggregation shifts, is as high as 0.95. I believe that the weighted score is more reliable, because the absolute values of shift are taken into account.

Table 2 lists, for the $^{13}C$ nuclei, the observed aggregation shifts, $\delta$(0 $\mu$L ethanol) - $\delta$(100 $\mu$L ethanol), the signs of the observed aggregation shifts and the calculated ring-current effects. The best values of the score, 24 / 30 = 0.80, and the weighted score, 0.87, were obtained for the positional shift of the neighboring dimer, 8.75Å, as in the case of the $^{1}H$ nuclei.

All the above results lead us to the conclusion that the structural motif of B745 (and B720) is

the shifted-inclined column of the piggy-back dimers as shown in Figure 4. A unique feature of this structure is the complete overlap between the next nearest neighbors along the z-direction just like bricks in a brick wall (see Fig. 3 in the Introduction section).

'A direct ring overlap model' proposed by Nozawa et al. [7] for the B745 form of the BChl **c** extract (a mixture containing R[E,E] and R[P,E] as the major component [12]) is compared with, and contrasted to, our present model for the B745 of R[P,E] as follows: (1) The piggy-back dimer is the basic structural unit in both models. (2) The Nozawa model consists of a linear array of a pair of piggy-back dimers extending to the y-direction (see Figure 8b of [7]), whereas our model consists of columns of stacked dimers extending in both the y- and the z-directions (see Fig. 3 in the Introduction section). (3) The positional shift between the neighboring dimers is 11.60 Å / 15.50 Å = 0.75 in the Nozawa model (estimated from Figure 8 of [7]), whereas it is 8.75 Å / 15.25 Å = 0.57 in our model as mentioned above.

## 5. CONCLUSION

A stacking of the piggy-back dimers to form a shifted inclined column has been proposed as the structural motif in the B745 of R[P,E]. This structural motif is completely different from that in the B745 of S[I,E], i.e., a parallel, stepwise stacking of the monomers. The results lead us to the idea that there are two different B745 forms, one the piggy back dimer-based structure for the R isomers and the other the monomer-based structure for the S isomers.

## 6. REFERENCES


1. Blankenship, R. E., J. M. Olson and M. Miller (1995) Antenna complexes from green photosynthetic bacteria. In *Anoxygenic Photosynthetic Bacteria* (Edited by R. E. Blankenship, M. T. Madigan and C. E. Bauer), pp. 399-435. Kluwer Academic Publishers, The Netherlands.
2. Tamiaki, H. (1996) Supramolecular structure in extramembraneous antennae of green photosynthetic bacteria. *Coord. Chem. Rev.* **148**, 183-197.
3. Olson, J. M. (1998) Chlorophyll organization and function in green photosynthetic bacteria. *Photochem. Photobiol.* **67**, 61-75.

4. Balaban, T. S., A. R. Holzwarth, K. Schaffner, G.-J. Boender and H. J. M. de Groot (1995) CP-MAS $^{13}$C-NMR dipolar correlation spectroscopy of $^{13}$C-enriched chlorosomes and isolated bacteriochlorophyll *c* aggregates of *Chlorobium tepidum*: The self-Organization organization of pigments is the main structural feature of chlorosomes. *Biochemistry* **34**, 15259-15266.

5. van Rossum, B.-J., G. J. Boender, F. M. Mulder, J. Raap, T. S. Balaban, A. Holzwarth, K. Schaffner, S. Prytulla, H. Oschkinat and H. J. M. de Groot (1998) Multidimensional CP-MAS $^{13}$C NMR of uniformly enriched chlorophyll. *Spectrochim. Acta Part A* **54**, 1167-1176.

6. Nozawa, T., K. Ohtomo, M. Suzuki, H. Nakagawa, Y. Morishita, H. Konami and Z.-Y. Wang (1994) Structures of chlorosomes and aggregated BChl **c** in *Chlorobium tepidum* from solid state high resolution CP/MAS $^{13}$C NMR. *Photosynth. Res.* **41**, 211-223.

7. Nozawa, T., K. Ohtomo, M. Suzuki, Y. Morishita and M. T. Madigan(1993) Structures and organization of bacteriochlorophyll *c*'s in chlorosomes from a new thermophilic bacterium *Chlorobium tepidum*. *Bull. Chem. Soc. Jpn.* **66**, 231-237.

8. Holzwarth, A. R. and K. Schaffner (1994) On the structure of bacteriochlorophyll molecular aggregates in the chlorosomes of green bacteria. A molecular modelling study. *Photosynth. Res.* **41**, 225-233.

9. Olson, J. M. and J. P. Pedersen (1990) Bacteriochlorophyll c monomers, dimers, and higher aggregates in dichloromethane, chloroform, and carbon tetrachloride. *Photosynth. Res.* **25**, 25-37.

10. Tamiaki, H., S. Takeuchi, R. Tanikaga, T. S. Balaban, A. R. Holzwarth and K. Schaffner (1994) Diastereoselective control of aggregation of 3$^1$-epimeric zinc methyl bacteriopheophorbides-*d* in apolar solvents. *Chem. Lett.*, 401-402.

11. Chiefari, J., K. Griebenow, N. Griebenow, T. S. Balaban, A. R. Holzwarth and K. Schaffner (1995) Models for the pigment organization in the chlorosomes of photosynthetic bacteria: Diastereoselective control of *in-vitro* bacteriochlorophyll $c_s$ aggregation. *J. Phys. Chem.* **99**, 1357-1365.

12. Nozawa, T., K. Ohtomo, M. Suzuki, Y. Morishita and M. T. Madigan(1991) Structures of bacteriochlorophyll c's in chlorosomes from a new thermophilic bacterium *Chlorobium tepidum*. *Chem. Lett.*, 1763-1766.

13. Chow, H.-C., R. Serlin and C. E. Strouse (1975) The crystal and molecular structure and absolute configuration of ethyl chlorophyllide *a* dihydrate. A model for the different spectral forms of chlorophyll *a*. *J. Am. Chem. Soc.* **97**, 7230-7237.

14. Smith, K. M., F. W. Bobe, D. A. Goff and R. J. Abraham (1986) NMR spectra of porphyrins. 28. Detailed solution structure of a bacteriochlorophyllide *d* dimer. *J. Am. Chem. Soc.* **108**, 1111-1120.

15. Wang, Z.-Y., M. Umetsu, M. Kobayashi and T. Nozawa (1999) Complete assignment of $^{1}H$ NMR spectra and structural analysis of intact bacteriochlorophyll *c* dimer in solution. *J. Phys. Chem. B* **103**, 3742-3753.

**Table 1.** Comparison, for the $^1H$ nuclei, between the observed aggregation shifts and the calculated ring-current effects for the structural motif of the B745d and B720d aggregate forms.

| Proton | Amount of ethanol titrated | | Aggregation shifts | Shifts | |
|---|---|---|---|---|---|
| | 0 μL | 50 μL | $\delta_{0\mu L} - \delta_{50\mu L}$ | obs | calc |
| 5-H | 7.33 | 9.73 | -2.40 | − | − |
| 10-H | 9.72 | 9.49 | 0.23 | + | + |
| 17-H | 4.33 | 4.12 | 0.21 | + | + |
| 18-H | 4.88 | 4.54 | 0.34 | + | + |
| 2Me-H | 1.59 | 3.30 | -1.71 | − | − |
| $3^1$-H | 3.10 | 6.25 | -3.15 | − | − |
| 7Me-H | 3.14 | 3.26 | -0.12 | − | + |
| $8^1$-H | 3.98 | 3.67 | 0.31 | + | + |
| $8^2$-H | 2.40 | 2.17 | 0.23 | + | + |
| $8^2$Me-H | 1.45 | 1.22 | 0.23 | + | + |
| $12^1$-H | 3.74 | 4.01 | -0.27 | − | + |
| $12^1$Me-H | 1.86 | 1.93 | -0.07 | − | − |
| $13^2$-H | 5.11 | 5.18 | -0.07 | − | + |
| 20Me-H | 3.95 | 3.81 | 0.14 | + | + |
| Score | | | | 11 / 14 | |
| Weighted score* | | | | 0.95 | |

*A sum of the absolute values of observed aggregation shift for correct prediction divided by the sum of all the absolute values of observed aggregation shift.

**Table 2.** Comparison, for the $^{13}C$ nuclei, between the observed aggregation shifts and the calculated ring-current effects for the structural motif of the B745d and B720d aggregate forms.

| Carbon | Amount of ethanol titrated | | Aggregation shifts | Shifts | |
|---|---|---|---|---|---|
| | 0 μL | 100 μL | $\delta_{0\mu L} - \delta_{100\mu L}$ | obs | calc |
| 1-C | 154.18 | 154.75 | -0.57 | − | − |
| 3-C | 144.55 | 146.33 | -1.78 | − | − |
| 4-C | 144.55 | 146.33 | -1.78 | − | − |
| 5-C | 100.05 | 101.70 | -1.65 | − | − |
| 6-C | 150.95 | 151.40 | -0.45 | − | + |
| 7-C | 133.67 | 134.38 | -0.71 | − | + |
| 9-C | 148.17 | 147.72 | 0.45 | + | + |
| 10-C | 107.30 | 106.71 | 0.59 | + | + |
| 11-C | 148.17 | 147.72 | 0.45 | + | + |
| 14-C | 162.74 | 162.40 | 0.34 | + | + |
| 15-C | 105.48 | 105.16 | 0.32 | + | + |
| 16-C | 154.18 | 154.75 | -0.57 | − | + |
| 17-C | 51.82 | 51.34 | 0.48 | + | + |
| 18-C | 50.27 | 49.18 | 1.09 | + | + |
| 19-C | 168.43 | 168.00 | 0.43 | + | + |
| 20-C | 105.48 | 105.16 | 0.32 | + | + |
| $2^1$-C | 16.13 | 17.53 | -1.40 | − | − |
| $3^1$-C | 65.40 | 65.88 | -0.48 | − | − |
| $7^1$-C | 11.82 | 11.40 | 0.42 | + | + |
| $8^1$-C | 29.39 | 29.01 | 0.38 | + | + |
| $8^3$-C | 15.13 | 14.67 | 0.46 | + | + |
| $12^1$-C | 21.61 | 21.83 | -0.22 | − | + |
| $12^2$-C | 17.16 | 17.22 | -0.06 | − | − |
| $13^1$-C | 195.60 | 197.44 | -1.84 | − | − |
| $13^2$-C | 49.13 | 49.53 | -0.40 | − | + |
| $17^1$-C | 30.61 | 30.67 | -0.06 | − | + |
| $17^2$-C | 31.71 | 31.43 | 0.28 | + | + |
| $17^3$-C | 173.91 | 173.78 | 0.13 | + | + |
| $18^1$-C | 21.16 | 21.00 | 0.16 | + | + |
| $20^1$-C | 21.94 | 21.73 | 0.21 | + | + |
| Score | | | | 24 / 30 | |
| Weighted score* | | | | 0.87 | |

*A sum of the absolute values of observed aggregation shift for correct prediction divided by the sum of all the absolute values of observed aggregation shift.

## FIGURE CAPTIONS

**Figure 1.** A molecular model of ($3^1$R), 8-propyl-12-ethyl farnesyl bacteriochlorophyll **c** (R[P, E]BChl **c**); the farnesyl group is replaced by a methyl group for simplicity.

**Figure 2.** Changes in the $Q_y$ absorption when the B745 aggregate of R[P,E] was formed in a mixture of $CH_2Cl_2$ and cyclohexane (1 : 14 v/v, 550 μL) at the concentration of $2.5 \times 10^{-3}$ M, and titrated with 0 - 50 μL ethanol. Each spectrum is deconvoluted, by Gaussian fitting, into components including the monomer absorbing at 665 nm (dotted broken line), the dimer (B675, dotted line), B705 (shorter broken line), B720 (longer broken line) and B745 (solid line).

**Figure 3.** Changes in the composition of the aggregate components when the B745 aggregate of R[P,E] was formed in a mixture of $CH_2Cl_2$ and cyclohexane (1 : 14 v/v, 550 μL) at the concentration of $2.5 \times 10^{-3}$ M, and titrated with 0 - 50 μL ethanol. Each component is distinguished as the monomer (square), the dimer (cross), B705 (triangle), B720 (diamond) and B745 (circle).

**Figure 4.** The structural motif in the B745 of R[P,E] as determined by NMR spectroscopy; (a) a front view, and (b) and (c) top views showing the overlap of layer I and layer II (layer III and layer IV) and that of layer II and layer III, respectively. For the BChl **c** molecule in layer II, the $^1$H and $^{13}$C nuclei showing high-field-shift and low-field-shift are painted and shaded, respectively.

Fig. 1

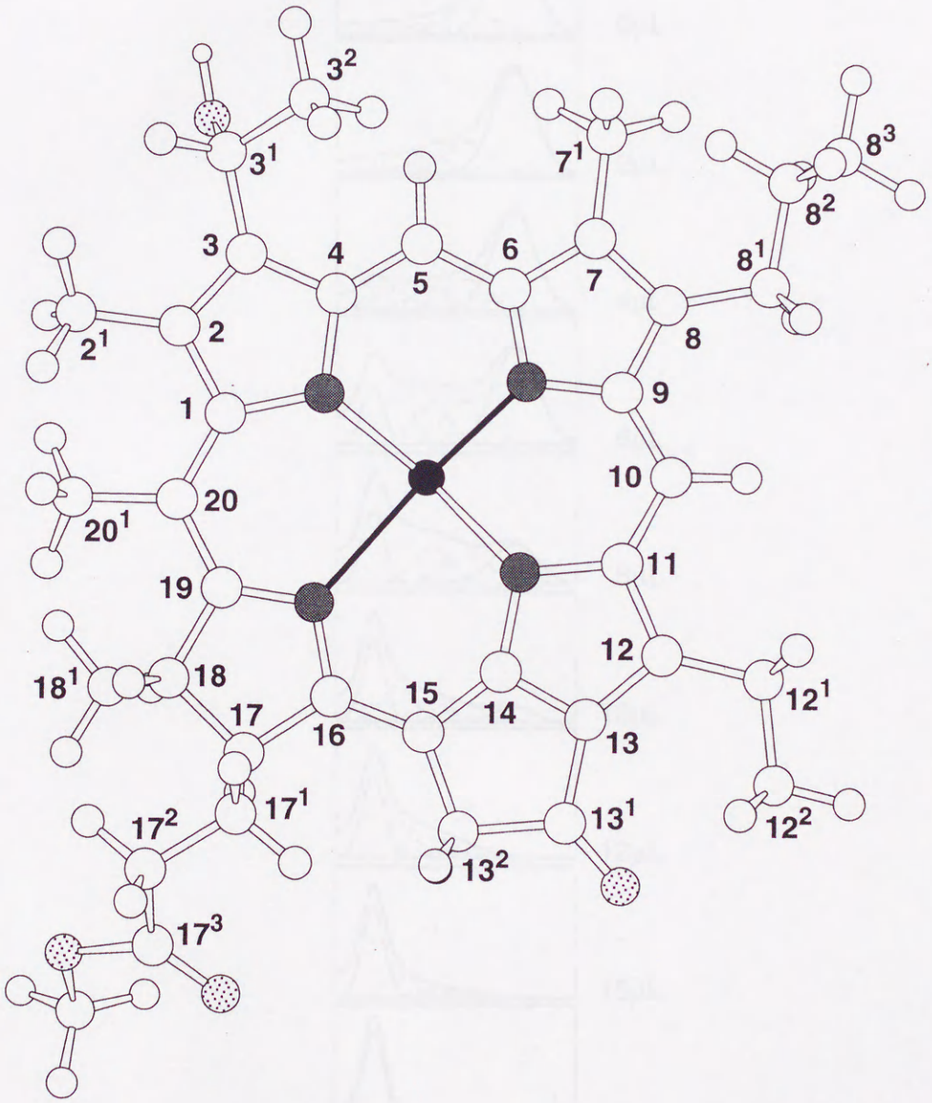
3²
3¹
7¹
8³
8²
3
4
6
5
7
8¹
2
2¹
8
1
9
10
20
20¹
11
19
12
18¹
18
15
12¹
17
16
14
13
17¹
13¹
17²
12²
13²
17³

Fig. 2

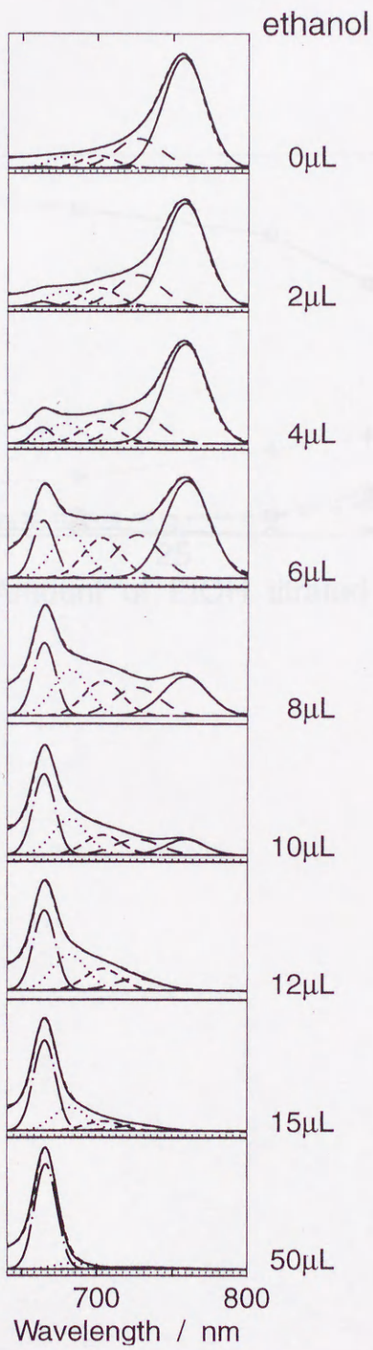
ethanol
0μL
2μL
4μL
6μL
8μL
10μL
12μL
15μL
50μL
700
800
Wavelength / nm

Fig. 3

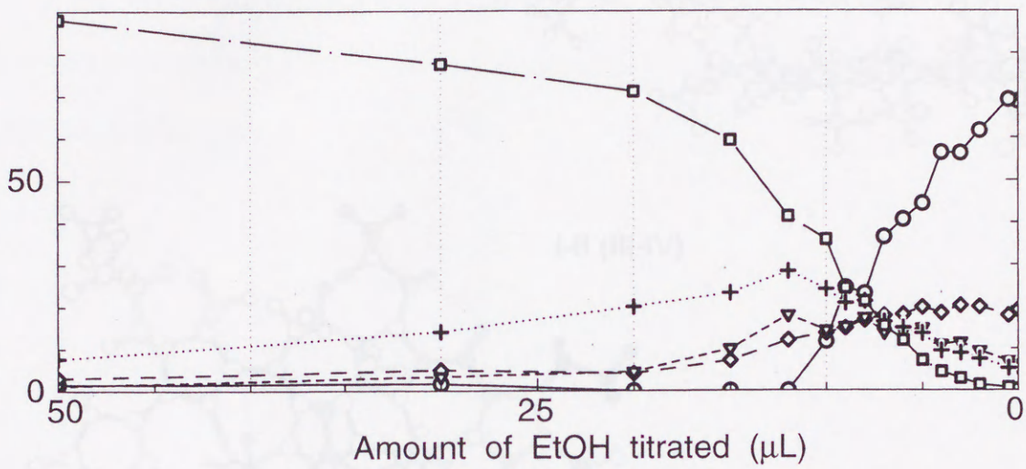

Fig. 4

(a)

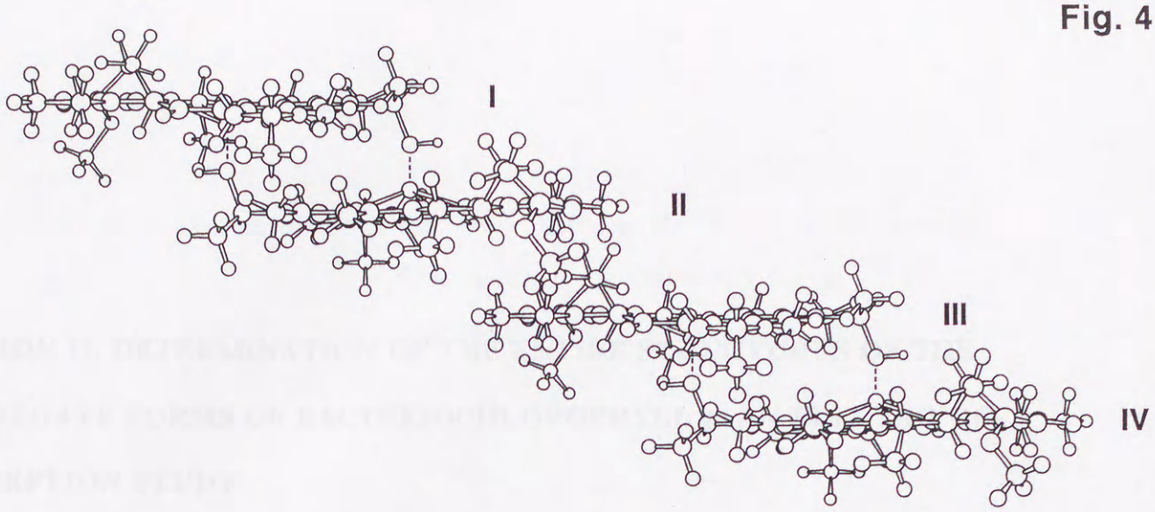


(b)

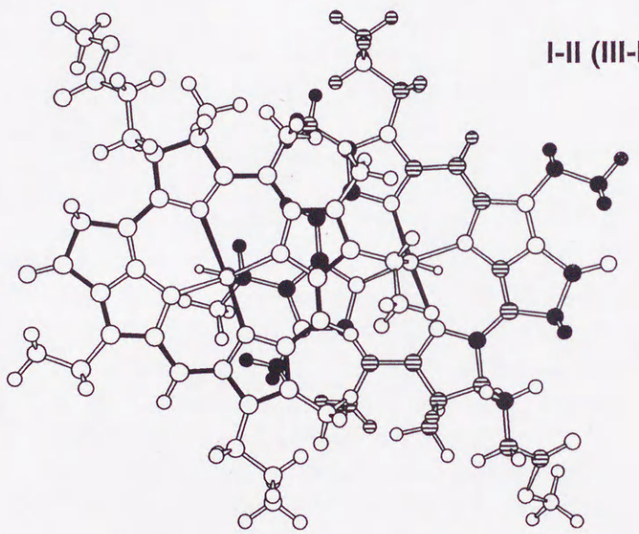


(c)

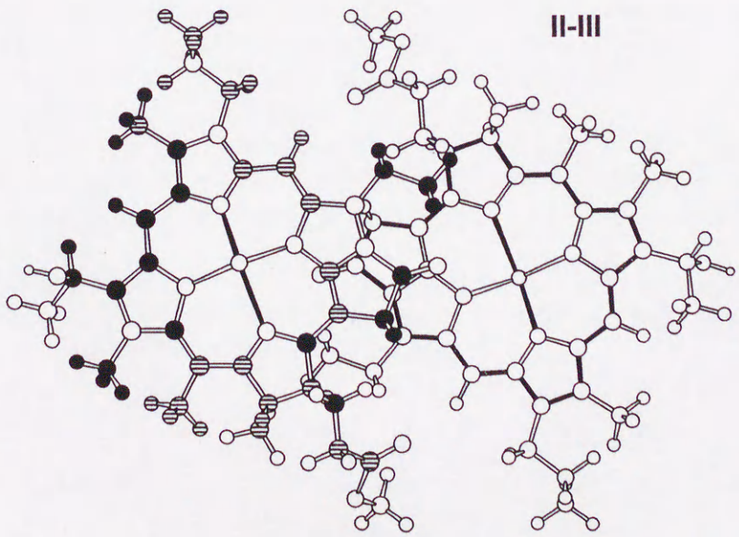

## SECTION II. DETERMINATION OF THE ENTIRE STRUCTURES OF THE AGGREGATE FORMS OF BACTERIOCHLOROPHYLL *c*: AN ELECTRONIC-ABSORPTION STUDY

Chapter 5

# Structural Transformation among the Aggregate Forms of Bacteriochlorophyll *c* as Determined by Electronic-Absorption and NMR Spectroscopies: Dependence on the Stereoisomeric Configuration and on the Bulkiness of the 8-C Sidechain

## 1. ABSTRACT

Transformation among the aggregate forms of bacteriochlorophyll *c* characterized by the wavelength of the $Q_y$ absorption, i.e., the dimer (B675), B705, B720 and B745, was traced by electronic-absorption spectroscopy for each of the isomers including R[E,E], R[P,E], R[I,E], S[P,E] and S[I,E] suspended in the mixtures of methylene chloride and *n*-hexane. Combination of NMR spectroscopy determining the structural motifs and calculation of the shift of the $Q_y$ absorption reflecting the long-range, transition dipole - transition dipole interactions among the macrocycles, in the entire aggregate structures, proposed the following models: B705d (B705d'), a linear array of straight (inclined) columns consisting of a pair of the piggy-back dimers; B720d and B745d, an assembly of two and five shifted-inclined columns consisting of more than six piggy-back dimers; and B720m and B745m, an assembly of one and two parallel, stepwise stacking of ~ 30 monomers. Calculations of the steric energies rationalized two different pathways of transformations, (1) the dimer → B705d (B705d') → B720d → B745d for the R isomers, and (2) the monomer → (B720m) → B745m for the S isomers. Addition of S[I,E] seems to trigger the B745d → B745m transformation of the R isomers.

## 2. INTRODUCTION

Green photosynthetic bacteria have an antenna complex called 'chlorosomes' characterized by the $Q_y$ absorption above 745 nm, whose structure is believed to be an aggregate of bacteriochlorophyll (BChl) *c* [1-3]. Two different models have been proposed for this structure, one, a parallel stepwise stacking of the monomers often referred to as the parallel-chain model [4-6], and the other, a stacked linear array of the 'piggy-back' dimers referred to as the antiparallel-chain model [7]. A most recent NMR study supports the former model [8].

Figure 1 shows the HPLC elution profile of an extract from the chlorosomes from *Chlorobium limicola* f. sp. *thiosulfatophilum*; it contains BChl *c* isomers in the ratio of R[E,E] ($3^1$R, 8-ethyl-12-ethyl BChl *c*) : R[P,E] ($3^1$R, 8-propyl-12-ethyl BChl *c*) : S[I,E] ($3^1$S, 8-isobutyl-12-ethyl BChl *c*) : S[P,E] ($3^1$S, 8-propyl-12-ethyl BChl *c*) = 39 : 48 : 8 : 5 (an approximate ratio of R[E,E] : R[P,E] : S[I,E] = 4 : 5 : 1). A trace of R[I,E] ($3^1$R, 8-isobutyl-12-ethyl BChl *c*) is also present. Concerning the stereoisomeric configurations at the $3^1$-C, the R configuration is the major component and the S

configuration is the minor component. Concerning the sidechains attached to the 8-C, the amount is in the order, P ≥ E > I (propyl ≥ ethyl > isobutyl). Since S[I,E] can form a higher aggregate consisting of a parallel, stepwise stacking of the monomers (Chapter 3) [6, 9] as in the case of chlorosomes [4, 5, 8], I wondered if the presence of S[I,E] in a minimal amount may have any physiological relevance. Thus, I addressed a first question: Does S[I,E] play any structural role in forming the chlorosome structure?

Each isomer is known to form a series of artificial aggregates characterized by different wavelengths of the $Q_y$ absorption depending on the stereoisomeric configuration [10-12]. Those aggregates include the dimer absorbing at ~ 675 nm, a lower aggregate absorbing at ~ 705 nm, a medium aggregate absorbing at ~ 720 nm, and a higher aggregate absorbing above 745 nm; hereafter, I call them 'the dimer' (B675), 'B705', 'B720' and 'B745', respectively, according to the apparent wavelengths of the $Q_y$ absorption. In order to answer the above question, I need to systematically compare the formation and transformation of those aggregates for all the component isomers, i.e., R[E,E], R[P,E], R[I,E], S[P,E] and S[I,E]. Based on the characterization of each isomer from this viewpoint, I hoped to find a key to the implication of the isomeric composition in chlorosomes. Thus, I addressed a second question: How do the R and S stereoisomeric configurations and the bulkiness of the 8-C sidechain affect the formation of various aggregate forms? Actually, Chiefari et al. [12] showed, by means of electronic-absorption and infrared spectroscopies, that the R and S isomers can give rise to different kinds of aggregate form. They changed the composition of the aggregate forms, for stearyl BChl *c* from *Chloroflexus aurantiacus,* changing its concentration in methylene chloride ($CH_2Cl_2$) and chloroform. In this Chapter, I used, as solvent, a mixture of $CH_2Cl_2$ and *n*-hexane, and reduced the amount of $CH_2Cl_2$ to form higher aggregates of farnesyl BChl *c* from *Chlorobium limicola.* In both cases, the aggregates were formed under completely hydrophobic environment without affecting the coordination bond between the central Mg and the oxygen in the hydroxyethyl group as well as the hydrogen bond between the keto-carbonyl and the hydroxyl groups. Concerning the bulkiness of the sidechains, no systematic studies have been made.

The wavelength of the $Q_y$ absorption plays a key role in classifying the aggregate forms. The red shift of the $Q_y$ absorption is determined by the transition dipole - transition dipole interactions among the conjugated macrocycles in a particular aggregate, which depend, in general, on the positional shift of a pair of neighboring BChl *c* molecules aligned in parallel, the number of stacked molecules to form a column, and the number of assembled columns. It is particularly interesting why

such a classification of the BChl *c* aggregates can be made based on the $Q_y$ absorption, because there must be a variety of aggregates having different forms and sizes in the system in question. There have been no clear explanations for the discrete $Q_y$ absorption for each aggregate form. Thus, I addressed a third question: How can the wavelengths of the $Q_y$ absorption in the various aggregate forms be predicted by theoretical calculation of transition dipole - transition dipole interactions? I have tried to determine the entire structures of the medium and higher aggregate forms by the use of the wavelength of the $Q_y$ absorption. Here, I used the structural motifs determined by NMR spectroscopy as the bases, and then tried to determine the entire aggregate structures by extending them in the y- and/or z-direction(s).

The models for the aggregate forms thus proposed should be energetically feasible. Therefore, I tried to calculate the intermolecular steric energies for all the aggregate models. The energies in each aggregate should include the enthalpy terms such as van der Waals interactions among the atoms, the coordination and hydrogen-bonding energies, and the interaction of the $\pi$ conjugated systems as well as the entropy term of hydrophobic interaction. In this Chapter, I focused on van der Waals interactions among the carbon and hydrogen atoms calculated by using a Lennard-Jones type potential, and tried to compare 'the steric energies' between the R and S isomers and among the isomers having different 8-C sidechains. (More sophisticated calculation including all the different energies mentioned above is necessary, of course, to predict an aggregate structure on a completely theoretical basis [5].) Thus, the last question I addressed was: How do the R and S stereoisomeric configurations and the bulkiness of the 8-C sidechain energetically govern the formation and transformation of those aggregates?

## 3. MATERIALS AND METHODS

### 3.1. Sample preparation and HPLC analysis

*Chlorobium limicola* f. sp. *thiosulfatophilum* was grown, and the BChl *c* isomers were obtained from it as described the previous Section [13, 14]. In this Chapter, the analysis and preparation of the BChl *c* isomers, i.e., R[E,E], R[P,E], R[I,E], S[P,E] and S[I,E], were performed under the following HPLC conditions: For analysis, column, VX-ODS (5 μm) 4.6 mmϕ × 250 mm (Shinwa Chemical Co. Ltd, Kyoto); eluent, 9.0 % water in methanol; flow rate, 0.5 mL·min$^{-1}$; and detection wavelength, 435 nm. For preparation, VX-ODS (5 μm) 20 mmϕ × 250 mm; eluent, 5.0 %

water in methanol; flow rate, 3.0 mL·min$^{-1}$; and detection wavelength, 455 nm. Each isomer isolated was identified by NMR spectroscopy. Chlorosomes were prepared by the method of Gerola and Olson [15]. HPLC analysis of the isomeric composition of BChl *c* in chlorosomes was performed as follows: pigments were extracted from chlorosomes with methanol, the carotenoid and BChl *a* components were removed by passing through a crystalline-cellulose column, and the eluting BChl *c* component (with a trace of BChl *d*) was subjected to the above HPLC analysis using a Shimadzu LC-10AS liquid chromatograph equipped with a Waters 996 diode-array detector.

### 3.2. Electronic-absorption measurements and spectral deconvolution

Electronic-absorption spectra were measured by the use of a Hitachi U-2000 spectrophotometer for each of the above BChl *c* isomers suspended in the mixtures of $CH_2Cl_2$ and *n*-hexane at the concentration of $1.0 \times 10^{-5}$ M (optical pathlength, 10 mm). Sample suspension in each mixed solvent with various composition was prepared as follows: Each isomer was dissolved into $CH_2Cl_2$ at the concentration of $2.0 \times 10^{-3}$ M, 25 μL of this solution was injected into 5.0 mL of the mixture of $CH_2Cl_2$ and *n*-hexane with a specified composition, the suspension was homogenized for 10 s by using a vortex mixer, and kept in the dark for more than 30 min at room temperature. Both solvents were dehydrated before use with 3 Å molecular sieve; $CH_2Cl_2$ was then passed through an alumina column. The effect of adding S[I,E] to R[E,E] or to a mixture of R[E,E] + R[P,E] (4 : 5 w/w) was examined for suspensions having various isomeric compositions by keeping the total BChl *c* concentration ($1.0 \times 10^{-5}$ M) and the solvent composition (4.8% $CH_2Cl_2$).

Hexanol treatment of chlorosomes was preformed by the method of Matsuura and Olson [16], and samples of various degrees of decomposition were prepared as follows: 45 μL of concentrated chlorosomes ($OD_{747}$ = 81.7) was suspended into 3.0 mL of 50 mM Tris-HCl, 1 mM Na-EDTA (pH 8.0) containing a specified amount of 1-hexanol (0 ~ 59.0 mM, saturated), and then left to stand in the dark for 30 min at room temperature.

Spectral deconvolution was performed by assuming five Gaussian components. The following wavelength of the $Q_y$ absorption was actually observed after deconvolution into each aggregate form: the monomer (660 - 665 nm in isomeric BChl *c*, and 665 - 669 nm in chlorosomes), the dimer(B675) (673 - 680 nm), B705 (695 - 704 nm), B720 (715 - 726 nm), and B745 (745 - 753 nm). The bandwidth of each component was: the monomer (15 nm in isomeric BChl *c*, and 18 nm in chlorosomes), B675 (25 - 26 nm), B705 (25 - 27 nm), B720 (33 - 35 nm) and B745 (37 - 40 nm).

### 3.3. Calculation of the shift of the $Q_y$ absorption

The transition dipole - transition dipole interactions among the BChl *c* molecules in each model aggregate were calculated by using the point-monopole approximation described by Sauer et al. [17]. The interaction energy $V_{12}$ between BChl *c* 1 and 2 can be expressed by

$$V_{12} = \sum_i \sum_j \rho_{1i}\rho_{2j} / |R_{1i} - R_{2j}| \qquad (1)$$

where $\rho_{1i}$ is the transition monopole of BChl *c* 1 at atom i, $\rho_{2j}$ is the transition monopole of BChl *c* 2 at atom j, and $|R_{1i} - R_{2j}|$ is the distance between the two atoms. The transition monopole on each atom was calculated by the same method as Weiss [18]; their values were scaled to agree with the spectroscopically determined value of the $Q_y$ transition dipole of Chl *a* (0.88 eÅ). Here, the dielectric constant was set to 1.0 by assuming that the dielectric constant of the surrounding medium is approximately equal to that of the spectroscopic medium. In order to improve the approximation to the transition charge density of the π-orbitals, each π-orbital was split into two rings, i.e., 1 Å above and below the porphyrin plane. The coordinates for BChl *c* were obtained by some modification of those of ethyl chlorophyllide *a* dihydrate determined by x-ray crystallography [19].

### 3.4. Calculation of van der Waals interactions

The van der Waals interactions among the H and C atoms ('the steric energy') were calculated by the use of an Insight II ver. 98.0 program (Molecular Simulations Inc., San Diego) using a Lennard-Jones potential function. No structural optimization was performed in this calculation.

In both calculations, the models of BChl *c* aggregates were built based on the following assumptions: (1) The interlayer distance is 3.5 Å in the calculations of van der Waals energy (the interdimer distance was changed to 5.0 Å and 4.5 Å in the straight and inclined columns, respectively); (2) the intercolumn distance is 15.25 Å for all the medium and higher aggregates; and (3) the BChl *c* macrocycles in the same layer are always in the same plane.

## 4. RESULTS AND DISCUSSION

### 4.1. Dependence of transformation among the bacteriochlorophyll *c* aggregate forms on the stereoisomeric configuration and on the bulkiness of the 8-C sidechain as

**probed by electronic-absorption spectroscopy**

Figure 2 shows changes in the $Q_y$ absorption when each of the BChl *c* isomers is suspended in the mixtures of $CH_2Cl_2$ and *n*-hexane, and the amount of the former solvent is reduced from 100 to 1.0 % (from the bottom to the top of each panel). In this process, the monomer-to-dimer, the dimer-to-lower aggregate and the lower aggregate-to-higher aggregate transformations are expected to take place, because the solubility of the solvent mixture is reduced systematically. The spectral changes in each isomer are characterized, in general, by decrease in a component on the blue side and increase in a component on the red side. Therefore, a plausible interpretation of the set of spectral changes is: when the size of aggregate increases, the $Q_y$ absorption shifts further to the red.

First, I compare the spectra of the set of isomers in 100 % $CH_2Cl_2$: Concerning the R stereoisomers (hereafter, simply denoted as 'isomers'), B675 which has been assigned to the piggy-back dimer [13, 20, 21] is the major component in R[E,E] and R[P,E], but the monomer becomes comparable to the dimer in R[I,E]. Concerning the S isomers, the monomer (absorbing at 665 nm) is predominant in S[P,E], but it becomes comparable to the dimer (B675) in S[I,E]. Thus, for the isomers having a smaller 8-C sidechain, the dimer is the major component in the R isomer, whereas the monomer is the major component in the S isomer. The dimer and the monomer become comparable for the R and S isomers having a large sidechain. Second, I compare the spectra of the isomers in 1.0 % $CH_2Cl_2$: Concerning the R isomers, a mixture of the dimer and the lower and medium aggregates (B705 and B720) are formed in R[E,E] (no B745 is present), but the higher aggregate (B745) is formed as the major component in R[P,E] and R[I,E]. Concerning the S isomers, both B720 and B745 are formed in S[P,E], and B745 is formed as the major component in S[I,E]. Thus, in both the R and S isomers, those isomers having a large 8-C sidechain readily form the higher aggregate, B745. Third, I compare transformation from the monomer eventually to the higher aggregate in the isomers having a large 8-C sidechain: In R[P,E] and R[I,E], a gradual transformation of the dimer $\rightarrow$ B705 + B720 $\rightarrow$ B745 takes place, whereas in S[I,E], a direct transformation of the monomer $\rightarrow$ B745 takes place, the amounts of the dimer, B705 and B720 being much smaller in amount in this case. Fourth, I compare the solvent composition where the formation of B745 starts: Concerning the R isomers, B745 is not formed at all in R[E,E] at the present concentration (it can be formed at the concentration of $3.0 \times 10^{-5}$ M); the formation of B745 becomes evident in R[P,E] at 15 - 10 % $CH_2Cl_2$, and in R[I,E] at 30 % $CH_2Cl_2$ (a solvent having much higher solubility). Concerning the S isomers, in S[P,E], B745 appears at 10 - 5 % $CH_2Cl_2$ but it does not become the major

component even in 1.0 % $CH_2Cl_2$, and, in S[I,E], the B745 formation becomes evident at 20 - 15 % $CH_2Cl_2$. These trends lead us to the same conclusion as in the second comparison. Finally, I compare the formation of B745 in chlorosomes with that in S[I,E]. The spectral changes showing the direct transformation from the monomer to B745, with small contributions of the dimer, B705 and B720, parallel to those of S[I,E], a fact which strongly suggests structural similarity of the BChl *c* aggregates formed in those two systems.

Figure 3 compares, among the five BChl *c* isomers and chlorosomes, changes in the composition of the five components including the monomer, the dimer (B675), B705, B720 and B745. This figure derived from Figure 2 is useful for quantitative comparison of the composition and for characterization of the transformations from one aggregate to another. Concerning the relative stability of the dimer vs. the monomer in 50 % $CH_2Cl_2$ in *n*-hexane, for example, it is 8.18, 4.79, 1.93, 0.32 and 1.13 in R[E,E], R[P,E], R[I,E], S[P,E] and S[I,E], respectively. Those values quantitize the conclusion drawn from the first comparison mentioned above. Concerning the starting point of the B745 formation, it is in the order, in terms of the amount of $CH_2Cl_2$ in the solvent, S[I,E] (20.0 %) > R[I,E] (12.5 %) ≈ R[P,E] (11.1 %) > S[P,E] (6.25 %). The values quantitize the conclusion of the fourth comparison. Concerning the pattern of the aggregate transformation, much more clear difference is seen between the R and S isomers: In R[P,E] and R[I,E], the dimer to B705 + B720 transformation takes place first, and the transformation from those forms to B745 follows (R[E,E] exhibits only the first transformation under the present concentration). In S[P,E], transformation from the monomer to both B720 and B745 takes place. In S[I,E], a sudden generation of B745 at the expense of all the other components is clearly seen, although an indication of the B720 formation is also observed. The amounts of B705 and B720 in the S isomers are much smaller than those in the R isomers during the transformation, supporting the conclusion of the third comparison mentioned above.

The changes in the aggregate composition in all the isomers suggest that the formation of both B745 and B720 are taking place at the final stage, and that the relative contribution of the former is enhanced when the size of the 8-C sidechain increases, irrespective of the R and S configurations.

In chlorosomes, a clear transformation from the monomer to B745 predominates when the amount of 1-hexanol titrated was reduced; decrease in the dimer is additionally seen during the transformation. The amounts of B705 and B720 are negligible. The changes in the composition are similar to those in the case of S[I,E] when the amount of $CH_2Cl_2$ is reduced down to less than 20 %,

suggesting again the structural similarity between the chlorosomes and the B745 aggregate of S[I,E] as mentioned above.

Figure 4 shows changes in the $Q_y$ absorption when (a) the ratio of S[I,E] vs. R[E,E] and (b) the ratio of S[I,E] vs. a 4 : 5 mixture of R[E,E] and R[P,E] are varied from 0 to 100 % (from the bottom to the top of each panel). In order to extract the net effect of mixing S[I,E] with the R isomer(s) due to the intermolecular interaction between the S and R isomers in the suspension, I calculated each composite spectrum by the use of the composition and the representative spectra of the 0 and 100 % S[I,E], and also the difference of the observed minus the composite spectrum.

First, I describe the effect of mixing S[I,E] with R[E,E]: In the 0 % S[I,E] suspension, there is no indication of B745, whereas in the 100 % S[I,E] suspension, B745 is predominant. The observed spectra in the region of 10 - 80 % S[I,E] exhibit much stronger contribution of B745 and much weaker contribution of the dimer and B705 than the composite spectra. As a result, the corresponding difference spectra give rise to a positive peak due to B745 in the longer wavelength region and double negative peaks due to the dimer and B705 in the shorter wavelength region. Thus, a minimal amount of S[I,E] (not smaller than 10 %) triggers the transformation from the dimer and B705 to B745 in R[E,E] that is the major component. The contribution of B720 is not clear most probably because its wavelength is very close to that of the zero point of the difference spectrum, although it must be affecting the slope of the difference spectrum in this region.

Next, I proceed to the effect of mixing S[I,E] with the mixture of the R isomers: The composition of 10 % S[I,E] corresponds to the isomeric ratio of S[I,E] : R[E,E] : R[P,E] $\approx$ 1 : 4 : 5 found in chlorosomes (*vide supra*). (If I assume that the functions of S[I,E] and S[P,E] were the same, the composition should correspond to 13 % S, instead.) Here again, the positive peak of B745 and the negative peaks of the dimer and B705 are clearly seen, suggesting the transformation of the dimer + B705 $\rightarrow$ B745 in the mixed R isomers. It is to be noted that this transformation can take place even at 5 % S[I,E]; this is probably due to the contribution of R[P,E] which enhances the formation of B745. Most importantly, the difference spectrum at 80 % S[I,E] gives rise to a weak negative peak around 745 nm, even though the two negative peaks around 675 and 705 nm are still present. This must originate from difference in the molar extinction coefficient between the two different kinds of B745s, one which is generally formed by the R isomers and the other which is generally formed by S[I,E]. The negative peak at 745 nm indicates that the latter aggregate structure must have a lower extinction coefficient. This observation suggests a transformation from 'B745d' (a

dimer-based higher aggregate) to 'B745m' (the monomer-based higher aggregate), because the R isomers tend to form the piggy-back dimer than the S isomers; the details proving this idea will be described later after the proposition of the models for those two different B745 aggregates.

Figure 5 shows changes in the composition of the five apparent components detected by the deconvolution of the set of observed spectra shown in Figure 4. In the first case of the addition of S[I,E] to R[E,E], all the dimer, B705 and B720 decrease in parallel and B745 is formed, reflecting transformation from the former group of aggregates to the latter. Here, B720 is clearly detected as an independent component, a fact which supports the above explanation of why B720 could not be detected as a negative peak in the difference spectra. The monomer is negligible in the amount throughout the transformation. In the second case of the addition of S[I,E] to a mixture of R[E,E] and R[P,E], exactly the same conclusion can be drawn except for the formation of B745 in an earlier stage, reflecting the presence of R[P,E] enhancing the formation of the higher aggregate.

### 4.2. Higher assembly of the aggregate forms as revealed by a combination of electronic-absorption spectroscopy and calculation of the transition dipole - transitio n dipole interactions

As described in the Introduction, NMR spectroscopy has been powerful to determine 'the structural motifs' in various aggregate forms of BChl *c* [6, 9, 13, 14]. Now, I have the structure of the piggy-back dimer of R[E,E] (Chapter 1), and the structural motifs of the B705 of R[E,E] (Chapter 2), the B745 of S[I,E] (Chapter 3) and the other B745 of R[P,E] (Chapter 4). Here, changes in the $^{1}H$ and $^{13}C$ chemical shifts were traced for a BChl *c* suspension when the amount of methanol or ethanol, titrated to decompose the particular aggregates, is reduced, and then 'the aggregation shifts' were determined experimentally. Next, the ring-current effects on a BChl *c* molecule due to the surrounding molecules were calculated theoretically to predict the aggregation shifts. The structural parameters were determined to obtain the best agreement in signs between the observed aggregation shifts and the calculated ring-current effects. In some cases, I applied three dimensional NMR spectroscopy to a 1 : 1 mixture of $^{13}C$-labeled and unlabeled BChl *c* to detect the $^{1}H$-$^{1}H$ intermolecular NOE correlations (Chapter 2 & 3) [6, 14]. A unique point of this type of NMR spectroscopy is that I am applying high-resolution NMR spectroscopy to smaller fragments that are generated by decomposition of an aggregate. Another unique points is that the NOE correlations detect direct $^{1}H$-$^{1}H$ contacts and that the aggregation shifts reflect the ring-current effects due to the first and possibly the

second nearest-neighbor macrocycles. Thus, NMR spectroscopy determines 'the structural motifs' (the fragments) by the use of short-range magnetic interactions.

Electronic-absorption spectroscopy, on the other hand, is useful to determine the entire structure of an aggregate, because it is based on the transition dipole - transition dipole interactions among the BChl *c* macrocycles that is basically a long-range interaction. In this Chapter, I tried to form various aggregates by changing the composition of hydrophobic solvents to keep the structures of higher aggregates intact. An important question I addressed in the Introduction section was why each aggregate form can give rise to a well-defined, electronic-absorption band despite of the distribution in the aggregate size. In order to rationalize this observation, I have tried to calculate the transition dipole - transition dipole interaction to predict the shift of the $Q_y$ absorption for higher assemblies of all the structural motifs so far proposed. Figure 6 summarizes the entire structures of B705, B720 and B745 which I am going to propose; their structural motifs determined by NMR spectroscopy are enclosed by broken lines. Note also the definition of the x-, y- and z-axes.

*(a) The structures of the B720 and B745 aggregates of R[P,E].* In the Chapter 4, I have determined the structural motif of B720 and B745 of R[P,E] to be a stacking of the piggy-back dimer to form a shifted-inclined column. Since this structural motif contains the dimer as a basic unit, I will call the models of the medium and higher aggregates 'B720d' and 'B745d', respectively. I have tried to reproduce the two different $Q_y$ absorptions by the use of the higher-order assembly of this structural motif. Figure 7a shows the calculated red shifts of the $Q_y$ absorption for the assemblies of one, two and five shifted-inclined columns having different numbers of the stacked piggy-back dimer. When the number of stacked dimers is increased for a certain fixed number of columns (see each line), the value of red shift increases slightly and converges very quickly to a certain value. (This is actually the mechanism why a particular aggregate form gives rise to a discrete $Q_y$ absorption; when its red shift converges to a certain value, it hardly depends on the number of the stacked structural units any more.) When the number of stacked columns is increased, on the other hand, a group of red shifts increases stepwise (see the lines) and converges again to a certain value, which is slightly above the line denoted as B745. (After the expansion of the structural motif along the y- and z-axes, the relative contribution of the blue-shift component becomes negligible.) Based on those results as well as on the results concerning a variety of aggregate forms which will be described later, I multiplied the calculated shifts of the $Q_y$ absorption by a factor of 3, when they are compared with the observed shifts. On the basis of this scaling factor, Figure 7a leads to the conclusion that B720d and

B745d consist of two and five shifted-inclined columns of approximately six stacked piggy-back dimers (24 and 60 molecules) as shown in Figure 6. Thus, B720d is regarded as a lower analogue of B745d.

*(b) The structures of the B705 (B705') aggregate of R[E,E].* The structural motif of B705 of R[E,E] was determined by NMR spectroscopy to be an assembly of two columns of stacked piggy-back dimers (Chapter 2) [13, 14]: Comparison of the observed aggregation shifts with those predicted by the calculation of the ring-current effects lead us to a pair of models, one, an assembly of two straight columns (Chapter 2) [14], and the other, an assembly of two inclined columns (Chapter 1) [13, 14]; I will call the higher-order assembly of them 'B705d' and 'B705d' ', respectively. The former model has been confirmed by $^{1}H$-$^{1}H$ NOE correlations (Chapter 2) [14]. The calculation of the wavelength of the $Q_y$ absorption based on the transition dipole - transition dipole interactions showed that further stacking of this structural motifs along the z-axis gave rise to both a slightly red-shifted component and a strongly blue-shifted component. However, increase in the number of the structural motifs (consisting of a pair of piggy-back dimers) along the y-axis gave rise to progressive red shift of the red-shifted component, and decrease in relative intensity of the blue-shifted component. Figure 7b shows the progressive red shifts of the $Q_y$ absorption for both the straight and the inclined columns. For both models, the value of calculated red shift multiplied by the factor of 3 approximately converges to the observed red shift of B705, and therefore, those linear arrays of the straight and the inclined columns of two piggy-back dimers can be regarded as models of B705 (named B705d and B705d'); see Figure 6. B705d' seems to fit the line of B705 better than B705d, although it has not been identified by NMR spectroscopy.

*(c) The structures of the B720 and B745 aggregates of S[I,E].* $^{1}H$- and $^{13}C$- NMR spectroscopy of the B745 of S[I,E] lead us to propose a parallel, stepwise stacking of monomers as 'the structural motif' (Chapter 3) [6, 9]. Since this aggregate structure uses the monomer as the basic structural unit, I will call it 'B745m'; its structural motif is indicated by broken line in Figure 6. A pair of models, i.e., structure 1 and structure 2, has been proposed based on comparison between the observed and the predicted aggregation shifts; here, the ring-current effects were calculated by the use of both the magnetic-dipole and the loop-current approximations, which showed similar results (Chapter 3) [6]. Both structures were confirmed by the $^{1}H$-$^{1}H$ NOE correlations (Chapter 3) [6]. I observed, in S[I,E], a much clear indication of the formation of both B720 and B745 by electronic-absorption spectroscopy (Figure 3 of Chapter 3), and further, monotonous aggregation shifts in both

$^{1}$H-NMR [9] and $^{13}$C-NMR (Chapter 3) [6], when the amount of methanol titrated into a suspension of methylene chloride and carbon tetrachloride (1 : 3) was reduced. Therefore, I regard B720 as a lower analogue of B745, and tried to determine their entire structures using the above structure 1 as the structural motif (structure 1 and structure 2 give rise to the same transition-dipole interactions). Figure 7c shows the results of calculation for the red shift of the $Q_y$ absorption. It is clearly seen that one and two columns of the parallel, stepwise stacking explain very nicely the observed $Q_y$ absorptions of B720 and B745, after multiplying the calculated shifts by the scaling factor of 3. Larger numbers of columns gave rise to further red shift, and therefore, those models were abandoned. I call these structures 'B720m' and 'B745m' indicating both the $Q_y$ absorption and the monomeric structural unit. Thus, I have obtained a basis to regard B720m (a smaller analogue of B745m) as a candidate of the apparent B720 in the case of the S isomer.

Figure 8 compares, with the observed red shifts of the $Q_y$ absorption, the calculated red shifts multiplied by the factor of 3 for various aggregate forms depicted in Figure 6. The agreement between the observed and the calculated red shifts is satisfactory. The models used for the calculations can be classified into two categories, i.e., one dimer-based (denoted as 'd') and the other monomer-based (denoted as 'm').

### 4.3. Dependence of the steric energies on the R and S stereoisomeric configuration and on the bulkiness of the 8-C sidechain: how it governs the formation and transformation among various aggregates

As mentioned above, I focused my attention to van der Waals interactions among the H and C atoms, and tried to calculate the steric energy in order to rationalize the observed formation and transformation of various aggregates depending on the R and S configurations and on the ethyl, propyl and isobutyl 8-C sidechains. Here, I ignore the obviously important interactions such as coordination, hydrogen bonding, overlap of the conjugated rings and hydrophobic interaction, an assumption which may be justified because those interactions are more or less similar in the various aggregate forms depicted in Figure 6, when suspended in a hydrophobic solvent. Table 1 lists the results of calculation of the steric energy. Here, I am going to explain the following four major observations described in the first section of 'Results and Discussion' in terms of the structure and the steric energy of each aggregate.

(1) In the case of the isomers having a small 8-C sidechain suspended into a mixed solvent with

high solubility, the dimer is the major component in the R isomer, whereas the monomer is the major component in the S isomer. This difference becomes less clear when the size of the sidechain increases (*vide supra*): Table 1 (the first column) shows that, in the piggy-back dimer, the steric energies of the R isomers are approximately 1/3 of those of the S isomers, and that the R isomers are preferable for the structure of the piggy-back dimer than the S isomers. Further, the steric energy of the dimeric structure tends to decrease when the sidechain becomes more bulky for both isomers. Figures 9a and b depict the structural origin of those characteristics: If all the sidechains were in the macrocycle plane, there were no difference in the steric energy at all between the R and S isomers. The difference in the steric energy originates from the steric interactions among sidechains attached to the optically-active carbons (see the asterisks). Here, I need to notice that the stereoisomeric configurations of the sidechains attached to the 17-C and 18-C can cause different steric interactions with the $3^1$Me between the two isomers (shown by solid arrows). The $3^1$Me-to-$17^1$ distance in the R isomer (5.5Å) is larger than the $3^1$Me-to-18Me distance in the S isomer (5.1Å), one of the factors which causes the smaller steric energy in the R isomer.

Figures 9a and b also show that, the piggy-back stacking gives rise to van der Waals interaction between the 20Me and the 8-C sidechain (shown by broken arrows). On the other hand, Table 1 shows that the steric energy decreases when the size of the 8-C sidechain increases, a result which supports the idea that the structure of the piggy-back dimer is stabilized by the *attractive* van der Waals interaction between the two groups. Thus, the structure of the piggy-back dimer is stabilized, when the size of the 8-C sidechain increases.

Holzwarth and co-workers [12] have already shown that the R isomer contains a mixture of the dimeric species than the S isomer, and that the S isomer contains more monomers in the case of stearyl BChl *c* from *Chloroflexus aurantiacus*. This important finding is now confirmed in farnesyl BChl *c*, and a possible interpretation of the difference is now proposed from a viewpoint of stereochemistry. The dependence on the bulkiness of the 8-C sidechain is a completely new piece of information obtained in this Chapter.

(2) When the solubility of the solvent mixture is reduced, sequential transformations of the dimer → B705 + B720 → B745 take place in the R isomer, whereas direct transformation of the monomer → B745 takes place in the S isomer, the amounts of B705 and B720 being much smaller in the latter case (*vide supra*): Here, I need to note that the analysis of the $Q_y$ absorption described in the previous section has elucidated the presence of two different kinds of B720 and B745, i.e., the

dimer-based (B720d and B745d) and the monomer-based (B720m and B745m), as shown in Figure 6. Table 1 shows that the steric energies of the R isomers in the forms of the dimer and the dimer-based lower and medium aggregates (B705d, B705d' and B720d) are substantially lower than those of the S isomers, explaining the larger contributions of the apparent B705 and B720 during the transformations in the R isomers. In contrast, the much larger steric energies of the S isomers in B705d (B705d') and B720d explain their much smaller contribution during the above 'direct' transformation.

(2') In the final stage of the B745 formation, clear transformation of the dimer + B705 + B720 → B745 takes place in the R isomers, whereas an indication of the formation of both B745 and B720 was seen in the S isomers (*vide supra*): Table 1 explains this difference. In the R isomers, gradual increase in the steric energy takes place in the order, the dimer → B705d (B705d') → B720d → B745d. This increase in the steric energy may be compensated by stabilization through the hydrogen bonding between the keto-carbonyl and the hydroxyethyl groups (between columns) [5], and the hydrophobic interaction between the long, farnesyl sidechains (within a column). (Even if this is not the case, reducing solubility causes the formation of the higher aggregates). In the S isomers, on the other hand, the interdimer and intercolumn steric energies in the form of the shifted-inclined column stacking of the dimers (B720d and B745d) become too high to be compensated, and the formation of the parallel, stepwise stacking of the monomers (B720m and B745m), instead, becomes energetically much more favorable, because of the much smaller interlayer and intercolumn energies of this structure (see the last four columns of Table 1). Thus, the parallel generation of B745m and B720m are now energetically explained.

For the R isomers, the parallel, stepwise stacking using the monomers as the structural subunit is energetically unfavorable. Table 1 shows that their total steric energies are almost three times larger than those of the S isomers. Figures 9c and d show that the steric environment of the $3^1$Me, in the parallel, stepwise stacking, drastically changes depending on the R and S configurations (shown by solid arrows). In the R isomers, there are two close contacts one between the $3^1$Me and the 18Me (5.0 Å) and the other between the $3^1$Me and the 20Me (5.4 Å); in the S isomers, there is only one close contact between the $3^1$Me and the $8^1$-C (6.1 Å). This gives rise to 1.6 times larger interlayer steric energy in the R isomers; the intercolumn steric energy is approximately four times larger.

Thus, completely different pathways of aggregate formation can be proposed based on the analysis of the $Q_y$ absorption and the calculations of the steric energy: (a) the monomer → the dimer

→ B705d (or B705d') → B720d → B745d for the R isomers, and (b) the monomer → (B720m) → B745m for the S isomers.

Holzwarth and co-workers [12] have proposed a similar scheme based on electronic-absorption , infrared and NMR spectroscopies of stearyl BChl *c* mentioned above. Their scheme is compared with, and contrasted to, our present scheme as follows: (i) The Holzwarth scheme uses the closed dimer and the open dimer (actually a pair of parallel, stacked monomers) [22] as the basic units to form Type I (703 nm) and Type II (750 nm) aggregates [12], whereas our model uses the dimer and the monomer as basic units to form B745d and B745m. (ii) Holzwarth model prefers the face-to-face stacking (for 'the closed dimer'), but our model uses the piggy-back stacking, instead, because the calculated steric energy is much lower in the piggy-back stacking than the face-to-face stacking, and the presence of the piggy-back dimer has been evidenced by NMR spectroscopy [13, 20, 21]. (iii) The Holzwarth scheme does not include the higher aggregate (~ 750 nm) consisting of the dimers, but our scheme does.

(3) When the solubility of the solvent is reduced, those R and S isomers having a bulky 8-C sidechain generate B745 more efficiently (*vide supra*): Table 1 actually shows that the steric energies of both B745d and B745m tend to decrease when the 8-C sidechain becomes larger. This is actually the reflection of the trend in their basic subunits, i.e., the piggy-back dimer and the parallel, stepwise stacking of the monomers, respectively. The stabilization of the structure of the piggy-back dimer in the R isomer when the size of the 8-C sidechain is increased has been explained above. Here, I explain the case of the parallel, stepwise stacking. Table 1 as well as Figures 9c and d show that, irrespective of the R and S isomers, the association between the 8-C sidechain and the 7Me of the neighboring molecule (shown by broken lines in the figure) stabilizes the parallel, stepwise stacking. Thus, the bulky 8-C sidechain plays an important role in forming the higher aggregates irrespective of the R and S isomers.

### 4.4. Possible structural role of S[I,E] in chlorosomes: A minimal amount of it may trigger formation of B745d and subsequent transformation from B745d to B745m

(4) When S[I,E] was added to the aggregates of R[E,E] or to those of R[E,E] + R[P,E] (4 : 5), transformation from the dimer, B705 and B720 to B745 took place as a result of newly-introduced intermolecular interaction between the R and S isomers. In the latter case of the mixture of three isomers, a decrease in the molar-extinction coefficient of the apparent B745 was also observed,

suggesting transformation between two different types of B745s (*vide supra*): Since I now know that the R isomers tend to form B745d and that S[I,E] tends to form B745m, an intriguing idea is that the addition of S[I,E] not only triggers the transformation of the dimer → B705d (B705d') → B720d → B745d in the R isomers themselves but also the B745d-to-B745m transformation in the particular R isomers (or in other words, the formation of B745m using both the R and S isomers).

Figure 6 shows that the formation of B745d in the former transformation is structurally feasible, because the stacking of each BChl *c* molecule in B745m is very similar to that in B745d except for the molecular orientation (all parallel in the former and alternative in the latter). Thus, B745m of the S isomer can function as a template in forming B745d of the R isomers, when those structures are close-by.

The structural similarity between B745d and B745m should make the transformation between them structurally feasible as well. Further, the steric energies listed in Table 1 show that the latter transformation from B745d to B745m in a mixture of the R and S isomers is also energetically feasible. Since the energy of the S isomer in B745m (121 kcal· $mol^{-1}$) is much smaller than that of the R isomer in B745d (170 kcal· $mol^{-1}$), the increase in the steric energy in the B745d to B745m transformation in the R isomer (345 - 170 = 175 kcal· $mol^{-1}$) can be compensated by the decrease in the steric energy due to the replacement of the R isomer in B745d by the S isomer in B745m (120 - 171 = -49 kcal· $mol^{-1}$), when enough amount of the S isomer is present. Setting the mole fraction of the S isomer in the mixed aggregate to be $x_S$, a relation of the complete compensation, 175 $(1 - x_S)$ = 49 $x_S$, leads to a value of $x_S = 0.78$. Thus, more than 78 % S isomer is necessary for the transformation to take place in this particular case of a small assembly of two columns consisting of four stacked molecules, whose results are listed in Table 1.

As a more realistic case, I consider the B745d to B745m transformation using the models shown in Figure 6. More specifically, I consider the transformation from B745d having 5 columns of 6 stacked dimers to B745m having 2 columns of 30 stacked monomers, the number of the BChl *c* molecules being 60 in both cases. By the use of values listed in Table 1 (mind that the values listed are all for four layers of the BChl *c* molecules and two columns), the steric energies of B745d (containing 60 R isomers), B745m (60 S isomers) and B745m (60 R isomers) can be calculated to be 2634, 1026 and 2777 kcal· $mol^{-1}$. Then, I consider two cases, i.e., case A when B745d contains only the R isomers ($x_R = 1$), and case B when B745m contains both the R ($x_R = 1 - x_S$) and the S ($x_S$) isomers. When case A and case B have the same steric energy in total, a relation holds, $2634 \times 1 =$

2777 (1 - $x_S$) + 1026 $x_S$, which leads to a value of $x_S = 0.08$. The result indicates that the transformation from B745d to B745m is energetically advantageous, when more than 8 % of the S isomer is mixed with the R isomers. This value is very close to the composition in the chlorosomes, i.e., R[E,E] : R[P,E] : S[I,E] ≈ 4 : 5 : 1. Further investigation is necessary to experimentally establish this B745d to B745m transformation in the mixed isomers.

Thus, the structural and the energetic bases for the role of S[I,E] in supporting the formation of B745d and the subsequent B745d to B745m transformation of the R isomers have been proposed. Recent NMR spectroscopy [4, 8] as well as comparison of transformations in this study strongly support the idea that the structure of B745m is very similar to that of chlorosomes, another important basis for the present proposal concerning the structural role of S[I,E].

## 5. CONCLUSION

The following answers to the questions addressed in the Introduction section have been obtained: (1) Does S[I,E] play any role in forming the chlorosome structure? Electronic-absorption spectroscopy showed that addition of S[I,E] to R[E,E] as well as to a 4 : 5 mixture of R[E,E] and R[P,E] assists the transformation of the dimer + 705d + 720d → B745d and the subsequent transformation of B745d → B745m in the R isomers (see below for the structural and the energetic bases of these transformations). The structure of B745m is considered to be similar to that of chlorosomes, and therefore, the answer is 'yes'.

(2) How do the R and S stereoisomeric configurations and the bulkiness of the 8-C sidechain affect the formation of various aggregate forms? The following characteristic features have been found by electronic-absorption spectroscopy of the five isomers (R[E,E], R[P,E], R[I,E], S[P,E] and S[I,E]) in suspension: (a) In a hydrophobic solvent with high solubility ($CH_2Cl_2$), the R isomers are much more stable in the piggy-back dimer than the S isomers when the 8-C sidechain is small. When the size of the sidechain increases, the stability of the dimers tends to become similar. (b) In a hydrophobic solvent with low solubility (*n*-hexane), both the R and S isomers having a larger 8-C sidechain readily form the higher aggregate, B745. (c) When the solubility is reduced systematically by changing the composition of the two solvents, the R isomers exhibit gradual transformation of the dimer → B705 + B720 → B745, whereas the S isomers exhibit a direct transformation of the monomer → B745. The latter transformation is similar to that of chlorosomes when the amount of 1-

hexanol titrated is reduced.

(3) How can the wavelength of the $Q_y$ absorption be predicted by theoretical calculation of the transient dipole - transient dipole interaction in various aggregate forms? The calculations elucidated the mechanism how each aggregate form can give rise to a well-defined absorption, irrespective of the obvious distribution of the aggregate size; that is the convergence of the red shift in the $Q_y$ absorption when the aggregate size is increased. The results lead us to the proposition of models for B705d and B705d', B720d and B720m, and B745d and B745m as shown in Figure 6. The stackings of the molecules themselves in B745d and B745m were found to be very similar to each other except for the molecular orientation (alternative and parallel, respectively).

(4) How do the R and S stereoisomeric configurations and the bulkiness of the 8-C sidechain energetically govern the formation and the transformation of the aggregate forms? Calculations of the steric energies (van der Waals interaction) rationalized the above characteristic features of the aggregate formation and transformation found by electronic-absorption spectroscopy. (a) The higher stability of the R isomers in the piggy-back dimer than the S isomers was substantiated by the smaller (1/3) steric energy in the former. (b) The higher efficiency in the formation of the higher aggregate (B745) for the isomers (both R and S) having a larger 8-C sidechain was also realized in terms of the steric energy (attractive van der Waals interaction), although the calculated differences were rather small. Stereochemically, the effect was ascribed to the association between the 8-C sidechain and the near-by methyl group of the neighboring molecule. (c) The gradual transformation in the R isomer was explained in terms of the higher stability of its piggy-back dimer mentioned above. The direct transformation in the S isomer was explained by the lower stability of its piggy-back dimer and also by the extremely low energy of the parallel, stepwise stacking of the monomers. The results lead us to the proposition of a pair of completely different pathways of transformation between the R and S isomers; the dimer → B705d (B705d') → B720d → B745d for the R isomers, and the monomer → B720m → B745m for the S isomers.

Concerning the effect of adding S[I,E] to R[E,E] or to a mixture of R[E,E] and R[P,E] (4 : 5), the structural basis for the first and the second transformations mentioned above is given as the structural similarity between B745d and B745m. Concerning the energetic basis, calculations of the steric energies lead us to an estimation of a minimal amount of S[I,E] to be 8 % to trigger the second, B745d-to-B745m transformation to take place. This result strongly suggests the role of S[I,E] in forming the aggregate structure of chlorosomes, which is believed to be similar to that of S[I,E].

## 6. REFERENCES


1. Blankenship, R. E., J. M. Olson and M. Miller (1995) Antenna complexes from green photosynthetic bacteria. In *Anoxygenic Photosynthetic Bacteria* (Edited by R. E. Blankenship, M. T. Madigan and C. E. Bauer), pp. 399-435. Kluwer Academic Publishers, The Netherlands.
2. Tamiaki, H. (1996) Supramolecular structure in extramembraneous antennae of green photosynthetic bacteria. *Coord. Chem. Rev.* **148**, 183-197.
3. Olson, J. M. (1998) Chlorophyll organization and function in green photosynthetic bacteria. *Photochem. Photobiol.* **67**, 61-75.
4. Balaban, T. S., A. R. Holzwarth, K. Schaffner, G.-J. Boender and H. J. M. de Groot (1995) CP-MAS $^{13}$C-NMR dipolar correlation spectroscopy of $^{13}$C-enriched chlorosomes and isolated bacteriochlorophyll *c* aggregates of *Chlorobium tepidum*: The self-organization of pigments is the main structural feature of chlorosomes. *Biochemistry* **34**, 15259-15266.
5. Holzwarth, A. R. and K. Schaffner (1994) On the structure of bacteriochlorophyll molecular aggregates in the chlorosomes of green bacteria. A molecular modelling study. *Photosynth. Res.* **41**, 225-233.
6. Mizoguchi, T., S. Sakamoto, Y. Koyama, K. Ogura and F. Inagaki (1998) The structure of the aggregate form of bacteriochlorophyll *c* showing the $Q_y$ absorption above 740 nm as determined by the ring-current effects on $^1$H and $^{13}$C nuclei and by $^1$H-$^1$H intermolecular NOE correlations. *Photochem. Photobiol.* **67**, 239-248.
7. Nozawa, T., K. Ohtomo, M. Suzuki, Y. Morishita and M. T. Madigan(1993) Structures and organization of bacteriochlorophyll *c*'s in chlorosomes from a new thermophilic bacterium *Chlorobium tepidum*. *Bull. Chem. Soc. Jpn.* **66**, 231-237.
8. van Rossum, B.-J., G. J. Boender, F. M. Mulder, J. Raap, T. S. Balaban, A. Holzwarth, K. Schaffner, S. Prytulla, H. Oschkinat and H. J. M. de Groot (1998) Multidimensional CP-MAS $^{13}$C NMR of uniformly enriched chlorophyll. *Spectrochim. Acta Part A* **54**, 1167-1176.
9. Mizoguchi, T., K. Matsuura, K. Shimada and Y. Koyama (1996) The structure of the aggregate form of bacteriochlorophyll *c* showing the $Q_y$ absorption above 740 nm: A $^1$H-NMR study. *Chem. Phys. Lett.* **260**, 153-158.

10. Olson, J. M. and J. P. Pedersen (1990) Bacteriochlorophyll c monomers, dimers, and higher aggregates in dichloromethane, chloroform, and carbon tetrachloride. *Photosynth. Res.* **25**, 25-37.

11. Tamiaki, H., S. Takeuchi, R. Tanikaga, T. S. Balaban, A. R. Holzwarth and K. Schaffner (1994) Diastereoselective control of aggregation of $3^1$-epimeric zinc methyl bacteriopheophorbides-*d* in apolar solvents. *Chem. Lett.*, 401-402.

12. Chiefari, J., K. Griebenow, N. Griebenow, T. S. Balaban, A. R. Holzwarth and K. Schaffner (1995) Models for the pigment organization in the chlorosomes of photosynthetic bacteria: Diastereoselective control of *in-vitro* bacteriochlorophyll $c_s$ aggregation. *J. Phys. Chem.* **99**, 1357-1365.

13. Mizoguchi, T., L. Limantara, K. Matsuura, K. Shimada and Y. Koyama (1996) Aggregation forms of 8-ethyl-12-ethyl farnesyl bacteriochlorophyll *c* in methanol-chloroform mixtures as revealed by $^1$H NMR spectroscopy. *J. Mol. Struct.* **379**, 249-265.

14. Mizoguchi, T., K. Ogura, F. Inagaki and Y. Koyama (1999) The structure of an aggregate form of bacteriochlorophyll *c* showing the $Q_y$ absorption at 705 nm as determined by the ring-Current current effects on $^1$H and $^{13}$C nuclei and by $^1$H-$^1$H intermolecular NOE correlations. *Biospectroscopy* **5**, 63-77.

15. Gerola, P. D. and J. M. Olson (1986) A new bacteriochlorophyll a-protein complex associated with chlorosomes of green sulfur bacteria. *Biochim. Biophys. Acta* **848**, 69-76.

16. Matsuura, K. and J. M. Olson (1990) Reversible conversion of aggregated bacteriochlorophyll c to the monomeric form by 1-hexanol in chlorosomes from *Chlorobium* and *Chloroflexus*. *Biochim. Biophys. Acta* **1019**, 233-238.

17. Sauer, K., R. J. Cogdell, S. M. Prince, A. Freer, N. W. Isaacs and H. Scheer (1996) Structure-based calculations of the optical spectra of the LH2 bacteriochlorophyll-protein complex from *Rhodopseudomonas acidophila*. *Photochem. Photobiol.* **64**, 564-576.

18. Weiss, C. (1972) The pi electron and absorption spectra of chlorophylls in solution. *J. Mol. Spectrosc.* **44**, 37-80.

19. Chow, H.-C., R. Serlin and C. E. Strouse (1975) The crystal and molecular structure and absolute configuration of ethyl chlorophyllide *a* dihydrate. A model for the different spectral forms of chlorophyll *a*. *J. Am. Chem. Soc.* **97**, 7230-7237.

20. Smith, K. M., F. W. Bobe, D. A. Goff and R. J. Abraham (1986) NMR spectra of

porphyrins. 28. Detailed solution structure of a bacteriochlorophyllide *d* dimer. *J. Am. Chem. Soc.* **108**, 1111-1120.

21. Wang, Z.-Y., M. Umetsu, M. Kobayashi and T. Nozawa (1999) Complete assignment of $^{1}H$ NMR spectra and structural analysis of intact bacteriochlorophyll *c* dimer in solution. *J. Phys. Chem. B* **103**, 3742- 3753.
22. Balaban, T. S., H. Tamiaki, A. R. Holzwarth and K. Schaffner (1997) Self-assembly of methyl zinc ($3^{1}R$)- and ($3^{1}S$)-bacteriopheophorbides *d*. *J. Phys. Chem. B* **101**, 3424-3431.

**Table 1.** Steric energies for various aggregate forms consisting of 4 layers of BChl *c* (kcal · mol$^{-1}$).

| Aggregate | B675d* | B705d† | | B705d' * | | B720d & B745d | | | B720m & B745m‡ | | |
|---|---|---|---|---|---|---|---|---|---|---|---|
| Base | dimer | dimer | | dimer | | dimer | | | monomer | | |
| *Stacking* | *piggy-back dimer* | *straight column* | | *inclined column* | | *shifted inclined column* | | | *stepwise* | | |
| | interlayer§ | interdimer‖ | total | interdimer¶ | total | interdimer§ | intercolumn** | total | interlayer§ | intercolumn** | total |
| R[E,E] | *17.0* | 15.8 | *32.8* | -0.2 | *16.8* | 42.0 | 112.2 | *171.2* | *83.7* | 261.9 | *345.6* |
| [P,E] | *16.2* | 17.1 | *33.3* | 164 | *180* | 42.0 | 111.9 | *170.1* | *83.4* | 261.8 | *345.2* |
| [I,E] | *15.2* | — †† | — | 208 | *223* | 41.9 | 111.4 | *168.5* | *82.5* | 261.5 | *344.0* |
| S[E,E] | *51.6* | 16.5 | *68.1* | -0.8 | *50.8* | 42.0 | 653.3 | *746.9* | *50.4* | 71.3 | *121.7* |
| [P,E] | *50.8* | 17.8 | *68.6* | 163 | *214* | 42.0 | 653.1 | *745.9* | *50.1* | 71.2 | *121.3* |
| [I,E] | *49.8* | — | — | 207 | *257* | 41.9 | 652.4 | *744.1* | *49.2* | 70.8 | *120.0* |

*, †, ‡Structural motifs determined by $^{1}$H- & $^{13}$C-NMR; *(13), †(14) and ‡(6, 9).

Center-to-center distances §3.5 Å, ‖5.0 Å, ¶4.5 Å and **15.25 Å.

††Energies larger than $10^{3}$ kcal · mol$^{-1}$ are not shown.

## FIGURE CAPTIONS

**Figure 1.** (a) The composition of the BChl *c* isomers in an extract from the chlorosomes of *Chlorobium limicola* f. sp. *thiosulfatophilum* as determined by HPLC. Peaks labeled with 'd' are due to isomeric BChl *d*. (b) Chemical structures of the BChl *c* isomers. The typification of carbon atoms in the macrocycle is given by numbering. Optically-active carbon atoms are indicated by asterisk; the R and S stereoisomers are defined for the $3^1$-C. The R isomers having the ethyl group at the 12-C, and the ethyl, propyl and isobutyl group at the 8-C are named R[E,E], R[P,E] and R[I,E], respectively; the S stereoisomers are named similarly.

**Figure 2.** Changes in the $Q_y$ absorption in each of the BChl *c* isomers, i.e., R[E,E], R[P,E], R[I,E], S[P,E] and S[I,E], which is suspended in the mixtures of $CH_2Cl_2$ and *n*-hexane (BChl *c* concentration, $1.0 \times 10^{-5}$ M); higher aggregates absorbing at longer wavelengths are formed by reducing the amount of $CH_2Cl_2$. Changes in the $Q_y$ absorption in chlorosomes, which are suspended in 50 mM Tris-HCl, 1 mM Na-EDTA (pH 8.0) containing different amounts of 1-hexanol, are also shown for comparison. The chlorosome concentration was $OD_{747} = 1.2$, and the 1-hexanol concentration was reduced from 59 mM (saturated) to 0 mM. Each spectrum is deconvoluted, by Gaussian fitting, into components including the monomer absorbing at 665 nm (dotted broken line), the dimer (B675, dotted line), B705 (shorter broken line), B720 (longer broken line) and B745 (solid line).

**Figure 3.** Changes in the composition of the monomer, dimer (B675), B705, B720 and B745 components in each of the isomers, R[E,E], R[P,E], R[I,E], S[P,E] and S[I,E], when the amount of $CH_2Cl_2$ is reduced from 50 to 0 %. Changes in the composition in chlorosomes when the amount of 1-hexanol titrated is reduced from 59 to 30 mM are also shown for comparison. Each component is distinguished as the monomer (square), the dimer (cross), B705 (triangle), B720 (diamond) and B745 (circle).

**Figure 4.** (a) Changes in the $Q_y$ absorption when S[I,E] is added to (a) R[E,E] and (b) a mixture of R[E,E] and R[P,E] (4 : 5). The amount of S[I,E] is increased from 0 to 100 %. The solvent composition ($CH_2Cl_2$ : *n*-hexane = 1 : 20 v/v), and the total BChl *c* concentration ($1.0 \times 10^{-5}$ M) were

kept unchanged. (1) The original spectra, (2) composite spectra calculated by the use of the isomeric composition and the spectra of 0 and 100 % S[I,E], and (3) the difference spectra of (1) - (2).

**Figure 5.** Changes in the composition of the monomer, dimer (B675), B705, B720 and B745 components in (a) S[I,E] added to R[E,E] and (b) S[I,E] added to a mixture of R[E,E] and R[P,E] (4 : 5). Each component is distinguished as the monomer (square), the dimer (cross), B705 (triangle), B720 (diamond) and B745 (circle).

**Figure 6.** Schematic presentation of the aggregate forms consisting of the piggy-back dimers (labeled 'd') and the monomers (labeled 'm'): The former include B675d, i.e., the piggy-back dimer; B705d (B705d') a linear array of straight (inclined) columns consisting of a pair of the piggy-back dimers; B720d and B745d, an assembly of two and five shifted-inclined columns of more than six piggy-back dimers. The latter include B720m and B745m, an assembly of one and two parallel, stepwise stacking of ~ 30 monomers (only 20 monomers are shown in the figure). The open and shaded sides indicate the left-hand-side and the right-hand-side of the BChl *c* plane shown in Figure 1.

**Figure 7.** Calculated shifts of the $Q_y$ absorption (multiplied by a factor of 3) due to the transition dipole - transition dipole interactions among the BChl *c* molecules depending on the number of stacked (piggy-back) dimers or monomers, and on the number of columns assembled; (a) shifted inclined columns consisting of the dimers, (b) linear arrays of straight and inclined columns consisting of two dimers, and (c) parallel, stepwise stacking of the monomers. The dotted lines indicate the observed shifts for the apparent aggregate forms (B705, B720 and B745).

**Figure 8.** Comparison of the observed red shifts of the apparent aggregate forms including the dimer (B675), B705, B720 and B745, and the calculated red shifts (multiplied by a factor of 3) of the aggregate forms based on the piggy-back dimers including B675d, B705d (B705d'), B720d and B745d, and those based on the monomers including B720m and B745m.

**Figure 9.** The environment of the $3^1$Me and the 8-C sidechain of (a) R[I,E] and (b) S[I,E] in the piggy-back dimer, and (c) R[I,E] and (d) S[I,E] in the parallel, stepwise stacking of the monomers.

Repulsive van der Waals interactions associated with the $3^1$Me (see the solid lines) more destabilize the S isomer in the piggy-back dimer, and the R isomer in the parallel, stepwise stacking (relevant atoms are painted). Attractive van der Waals interactions associated with the 8-C sidechain (see the dotted lines) stabilizes both the R and S isomers having a bulky 8-C sidechain (relevant atoms are shaded).

Fig. 1

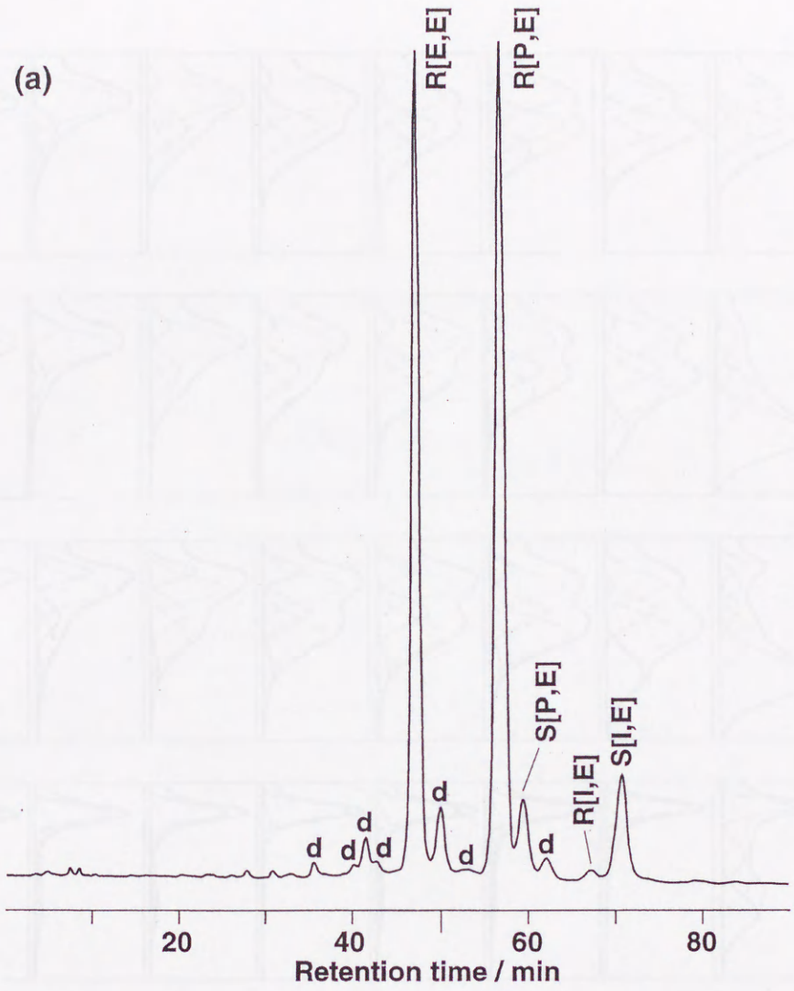
(a)
R[E,E]
R[P,E]
S[P,E]
R[I,E]
S[I,E]
d
20
40
60
80
Retention time / min

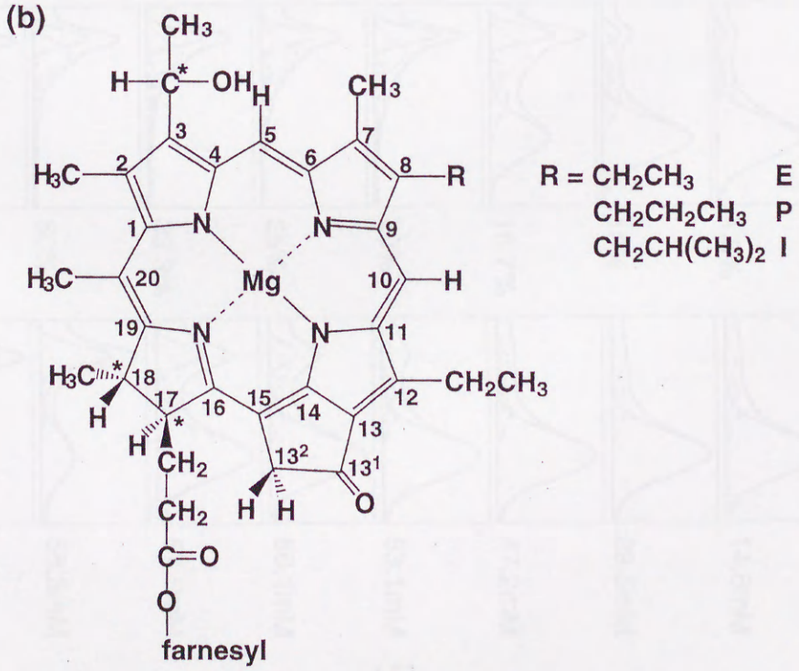
(b)
farnesyl
R = CH2CH3 E
CH2CH2CH3 P
CH2CH(CH3)2 I

Fig. 2

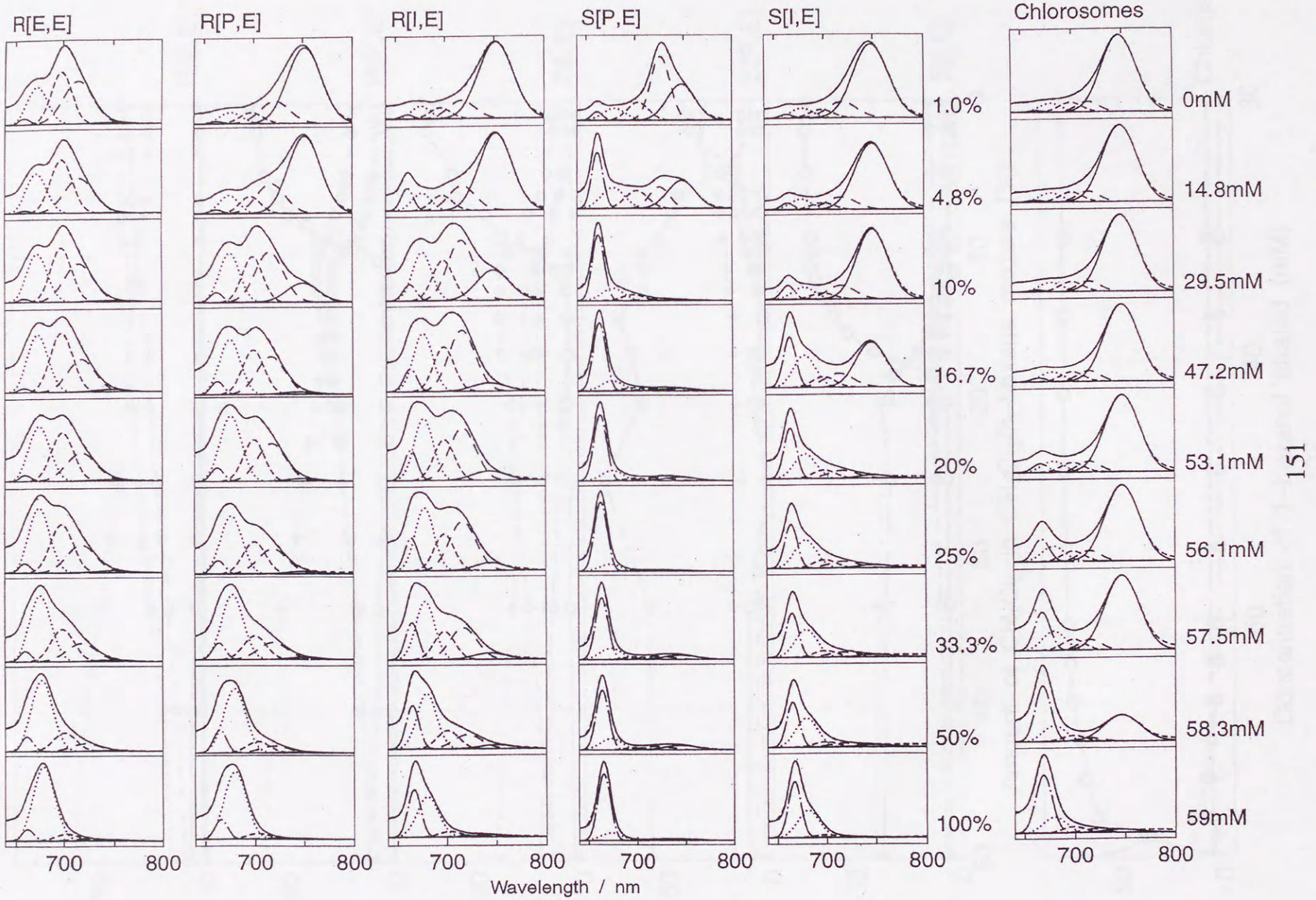
R[E,E]
R[P,E]
R[I,E]
S[P,E]
S[I,E]
Chlorosomes
1.0%
4.8%
10%
16.7%
20%
25%
33.3%
50%
100%
0mM
14.8mM
29.5mM
47.2mM
53.1mM
56.1mM
57.5mM
58.3mM
59mM
700
800
Wavelength / nm

151

Fig. 3

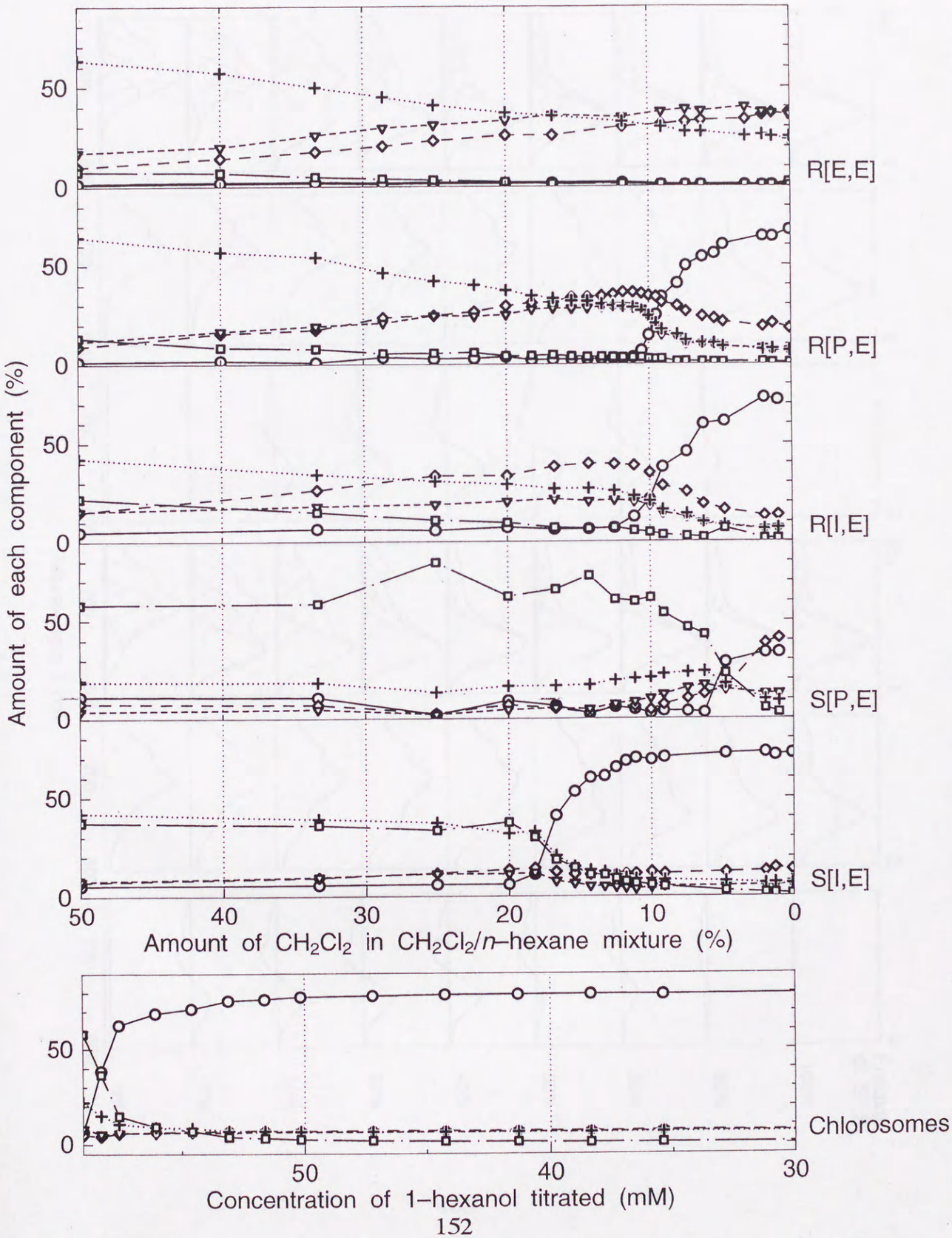
Amount of each component (%)
R[E,E]
R[P,E]
R[I,E]
S[P,E]
S[I,E]
50
0
50
40
30
20
10
0
Amount of $CH_2Cl_2$ in $CH_2Cl_2$/*n*–hexane mixture (%)
Chlorosomes
50
40
30
Concentration of 1–hexanol titrated (mM)

Fig. 4

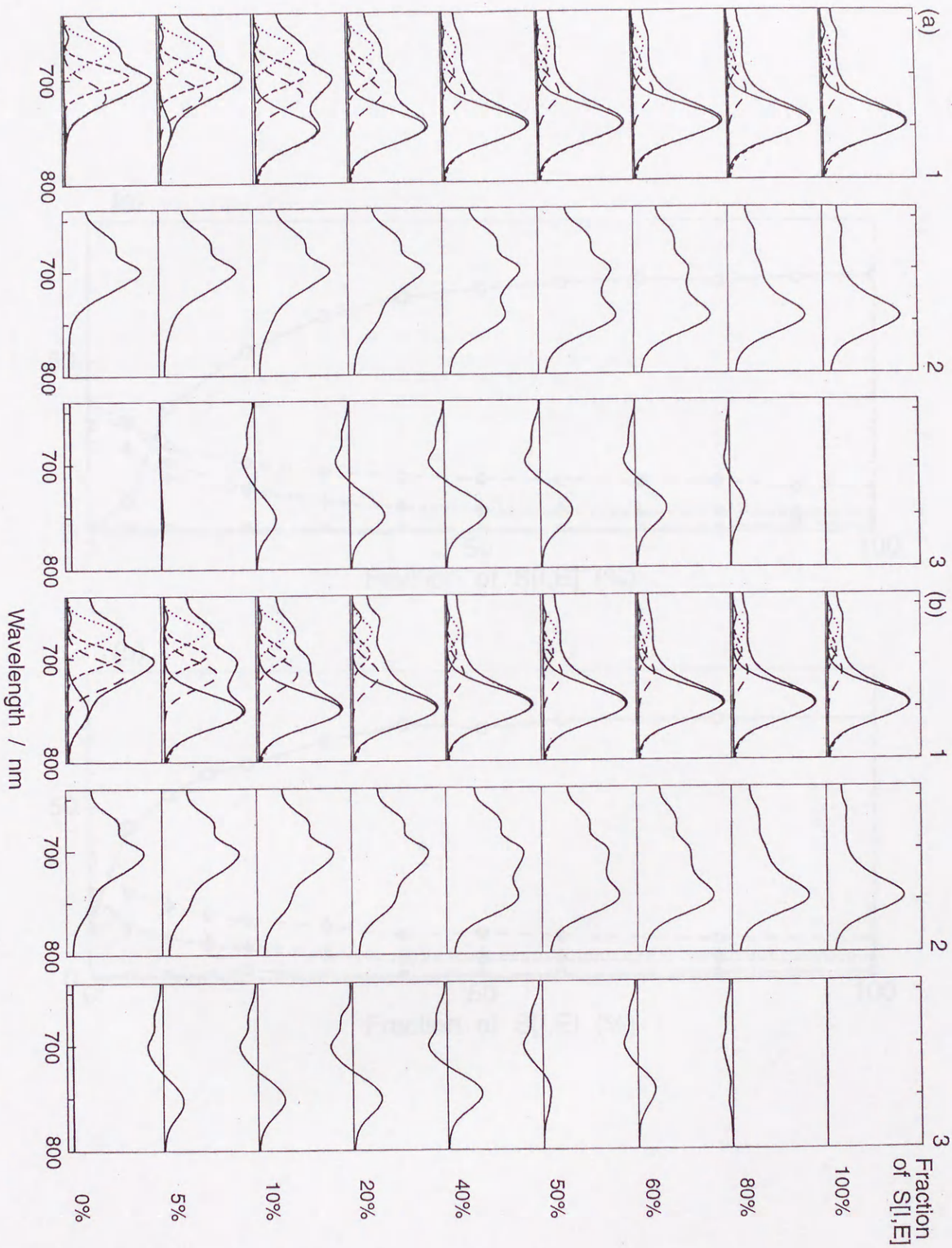
(a)
(b)
1
2
3
700
800
Wavelength / nm
0%
5%
10%
20%
40%
50%
60%
80%
100%
Fraction of S[I,E]

Fig. 5

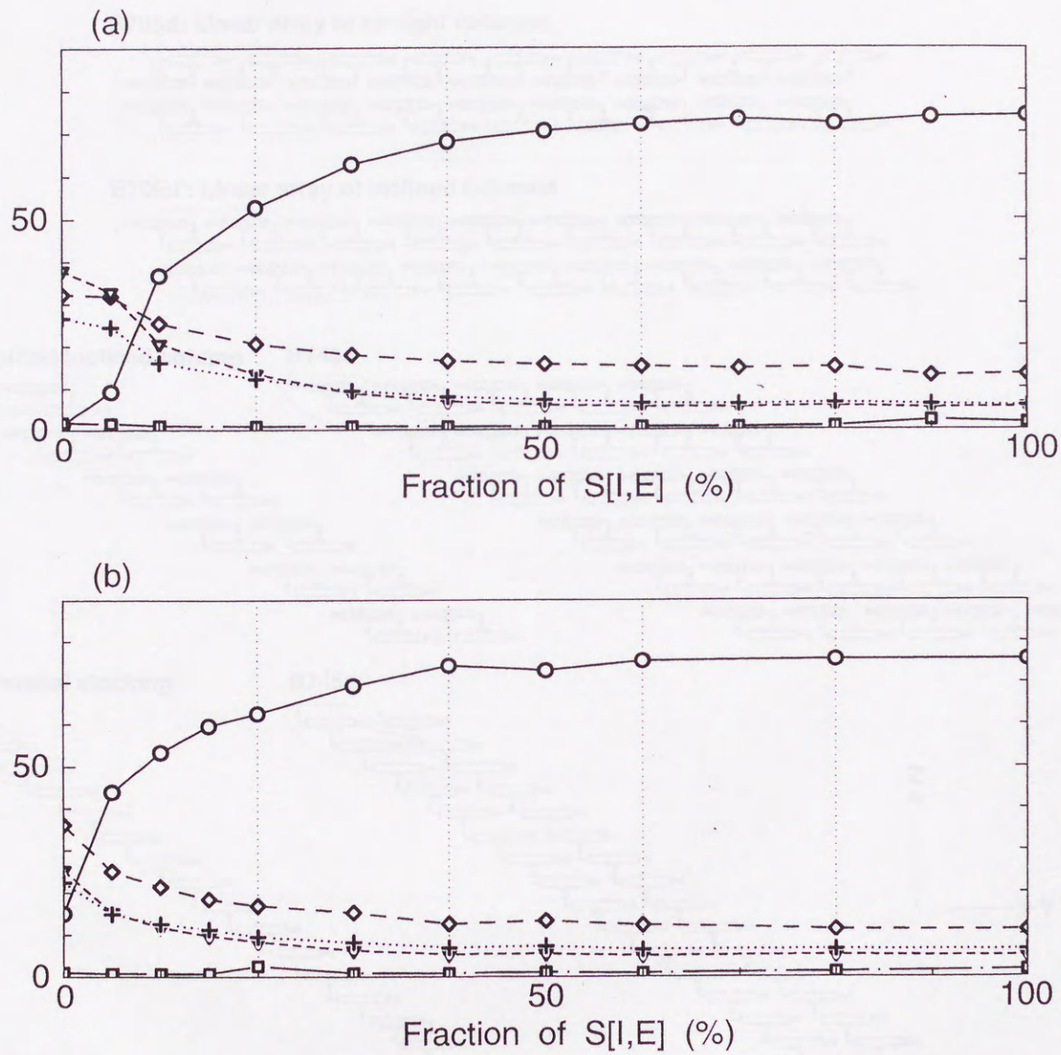

Fig. 6

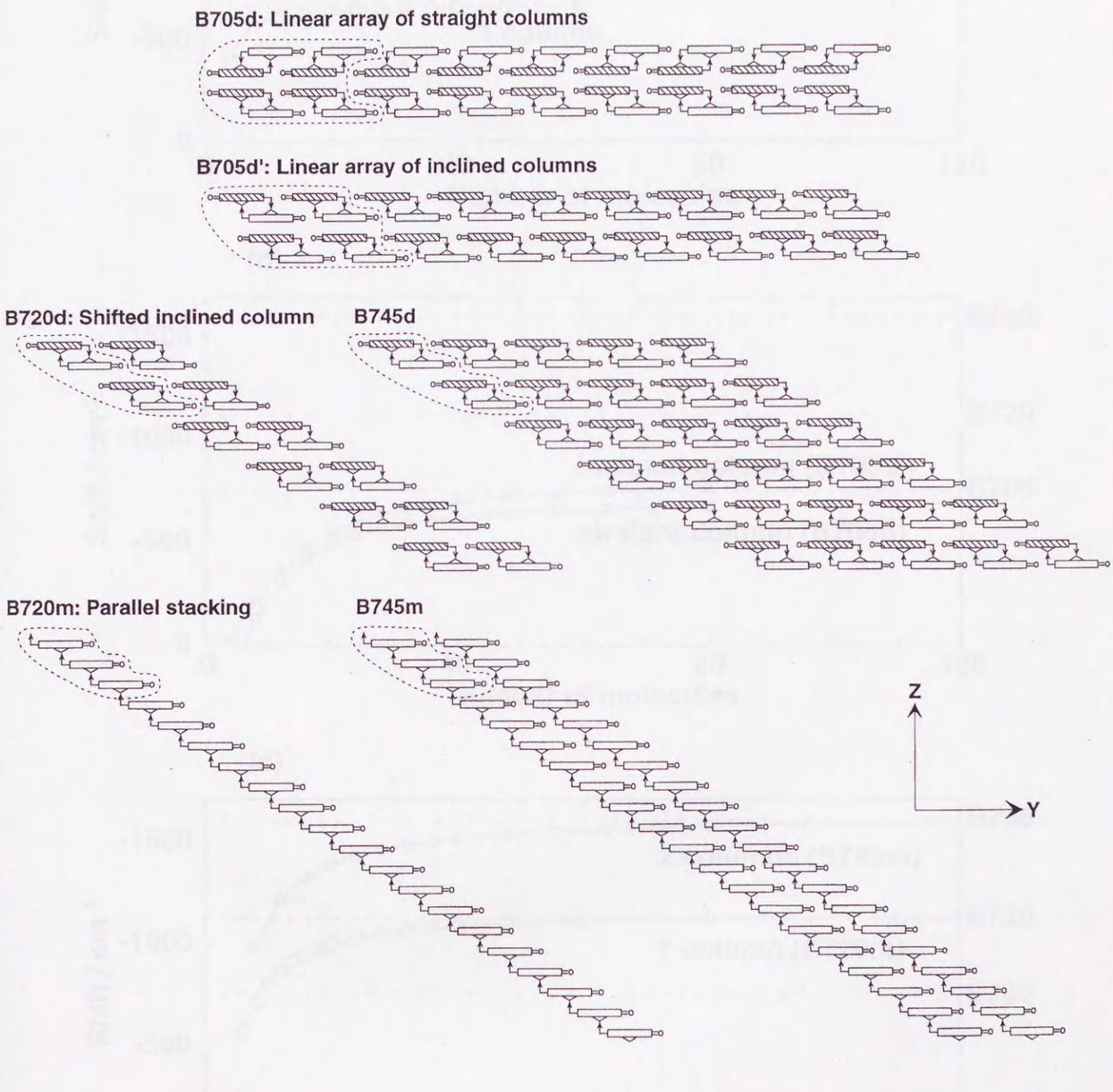
B705d: Linear array of straight columns
B705d': Linear array of inclined columns
B720d: Shifted inclined column
B745d
B720m: Parallel stacking
B745m
Z
Y

Fig. 7

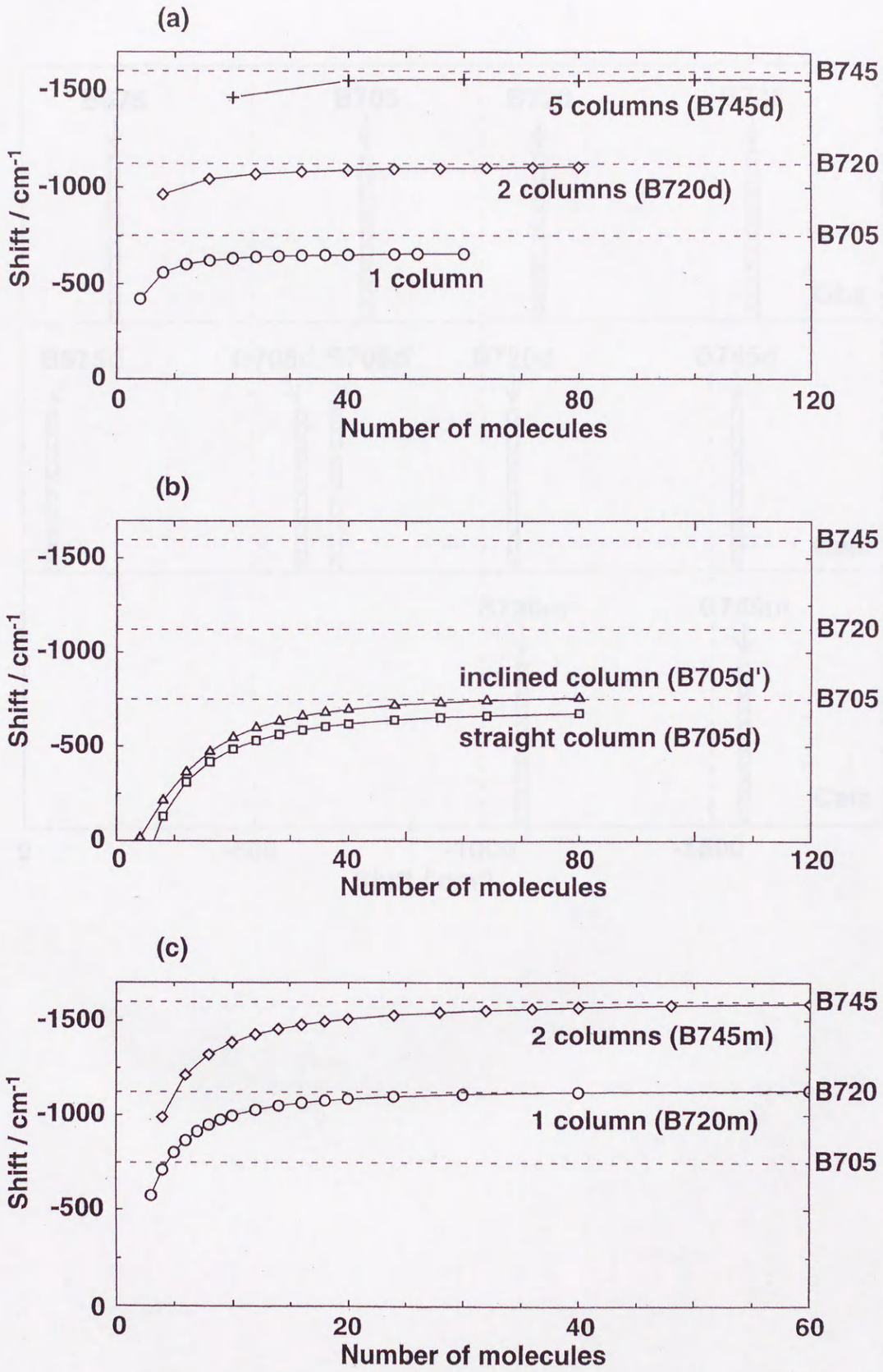
(a)
-1500
-1000
-500
0
Shift / cm-1
B745
B720
B705
5 columns (B745d)
2 columns (B720d)
1 column
0
40
80
120
Number of molecules
(b)
-1500
-1000
-500
0
Shift / cm-1
B745
B720
B705
inclined column (B705d')
straight column (B705d)
0
40
80
120
Number of molecules
(c)
-1500
-1000
-500
0
Shift / cm-1
B745
B720
B705
2 columns (B745m)
1 column (B720m)
0
20
40
60
Number of molecules

Fig. 8

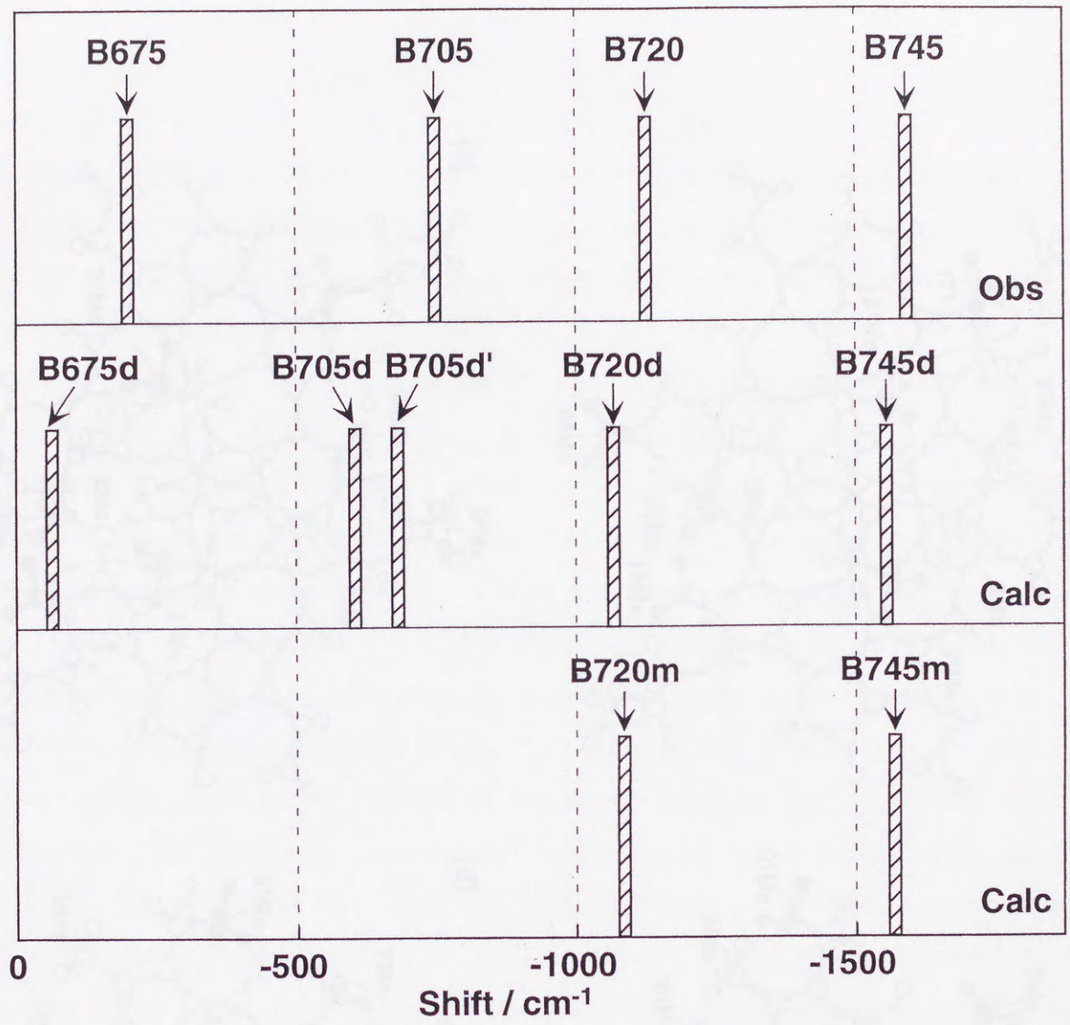
B675
B705
B720
B745
Obs
B675d
B705d
B705d'
B720d
B745d
Calc
B720m
B745m
Calc
0
-500
-1000
-1500
Shift / cm-1

Fig. 9

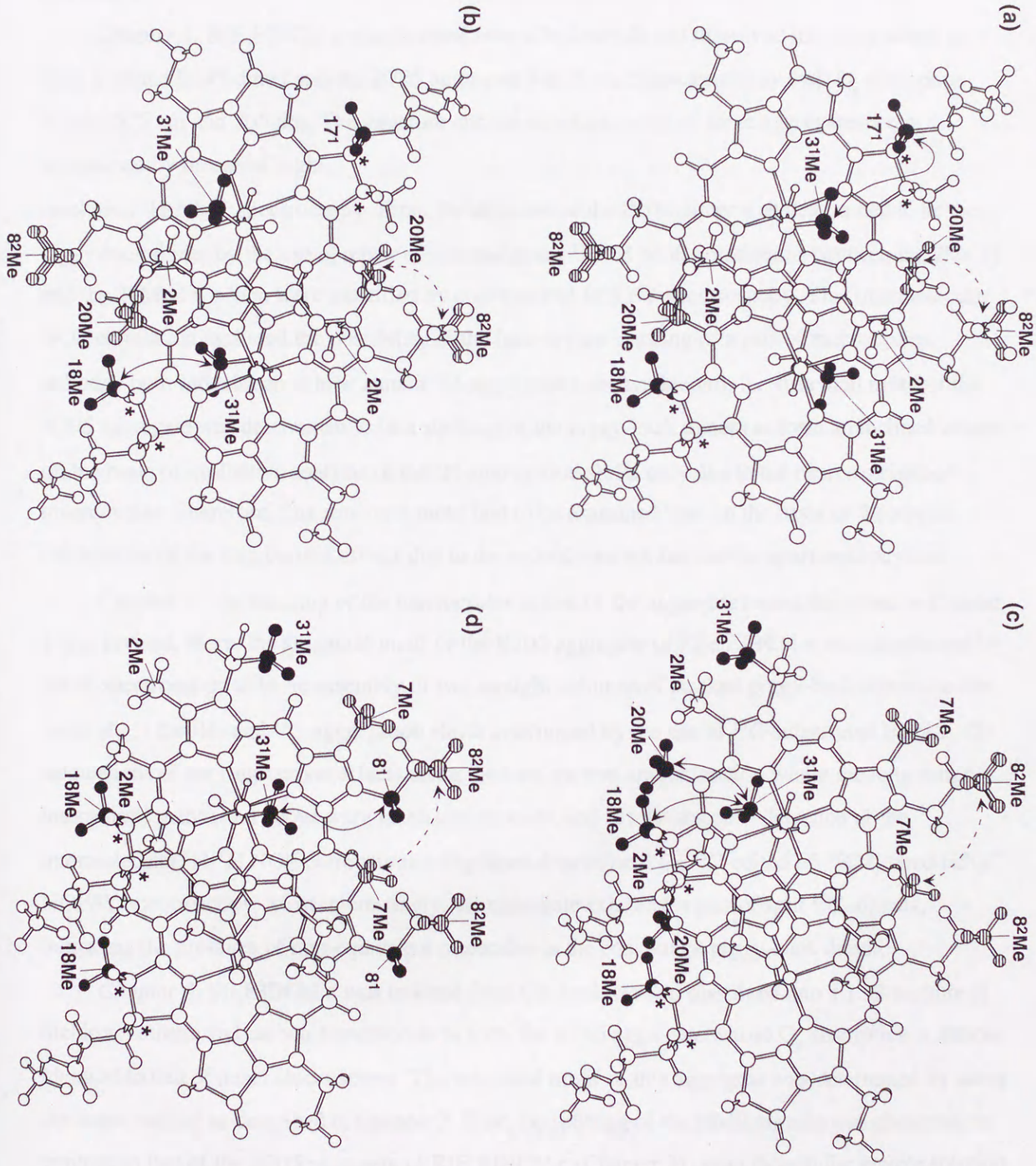
(a)
17¹
31Me
20Me
8²Me
2Me
20Me
18Me
31Me
8²Me
(b)
17¹
31Me
20Me
8²Me
8²Me
2Me
20Me
18Me
2Me
31Me
(c)
31Me
2Me
7Me
20Me
18Me
31Me
8²Me
7Me
2Me
8²Me
20Me
18Me
(d)
31Me
2Me
7Me
8¹
8²Me
31Me
2Me
18Me
7Me
8²Me
8¹
18Me

## SUMMARY


### Section I

*Chapter 1.* R[E,E]BChl **c** was isolated from *Cb. limicola* and dissolved into chloroform to form both the B675 dimer and the B705 aggregate which are characterized by their $Q_y$ absorption around 675 nm and 705 nm. The structure and the structural motif of these aggregates were determined by means of high-resolution $^1$H-NMR spectroscopy. First, the structure of the B675 dimer was determined to be the piggy-back dimer by the use of a pair of intermolecular $^1$H-$^1$H NOE correlations between the 7Me-H and the 20Me-H, which were identified by conventional ROESY spectroscopy. This intermolecular NOE correlation excluded the possibility of the face-to-face stacking of a pair of macrocycles, although both models can exhibit similar $^1$H-aggregation shifts. Second, the structural motif of the B705 aggregate was determined to be a stacking of the piggy-back dimers to form an inclined column on the basis of qualitative analysis of the $^1$H-aggregation shifts only due to the nearest neighbor macrocycles. Therefore, this structural motif had to be examined later on the basis of theoretical calculations of the ring-current effects due to the second-nearest and further apart macrocycles.

*Chapter 2.* The stacking of the macrocycles in one of the aggregate forms described in Chapter 1 was revised. Here, the structural motif of the B705 aggregate of R[E,E]BChl **c** was determined by NMR spectroscopy to be an assembly of two straight columns of stacked piggy-back dimers on the basis of (1) the $^1$H- and $^{13}$C-aggregation shifts determined by the use of $^{13}$C-substituted BChl **c**, (2) calculations of the ring-current effects using the loop-current approximation where the long-range interactions mentioned above were taken into account, and (3) the selective detection of the intermolecular $^1$H-$^1$H NOE correlations using three-dimensional F1 $^{13}$C-edited F3 $^{13}$C-filtered HSQC-NOESY spectroscopy. Most interestingly, the aggregate exhibited a pair of split $^{13}$C-signals, indicating the presence of non-equivalent molecules in the constituent piggy-back dimer.

*Chapter 3.* S[I,E]BChl **c** was isolated from *Cb. limicola* and dissolved into a 1 : 3 mixture of dichloromethane and carbon tetrachloride to form the B745 aggregate whose $Q_y$ absorption is almost identical to that of intact chlorosomes. The structural motif of this aggregate was determined by using the same method as described in Chapter 2: First, no splitting of the NMR signals was observed, in contrast to that of the B705 aggregate of R[E,E]BChl **c** (Chapter 2), even though the sample solution

was cooled down to - 20 C°. This observation strongly suggested that each BChl **c** molecule was located in the same environment in this particular aggregate. Second, the parallel-chain stacking in which the monomeric BChl **c** molecules are stacked together to form an inclined column was proposed on the basis of comparison between the experimentally determine aggregation shifts and the theoretically calculated ring-current effects. Here, both the magnetic-dipole and the loop-current approximations were applied to predict the $^{1}$H- and $^{13}$C-aggregation shifts. Third, the selective detection of $^{1}$H-$^{1}$H intermolecular NOE correlations confirmed the presence of two different types of the parallel-chain stacking, i.e. structure 1 and structure 2. Both structure 1 and structure 2 consisted of a parallel, stepwise stacking of the monomeric BChl **c**, but they were different in the sliding direction of the column.

*Chapter 4.* R[P,E]BChl **c** was isolated from *Cb. limicola* and dissolved into a 1 : 14 mixture of dichloromethane and cyclohexane to form another B745 aggregate, whose $Q_y$ absorption was very similar to that of the B745 aggregate of S[I,E]BChl **c** (Chapter 3). The structural motif of the B745 aggregate of R[P,E]BChl **c** was determined by means of high-resolution NMR spectroscopy using a similar method. First, the splitting of the $^{1}$H-NMR signals was clearly observed even at room temperature, suggesting the presence of non-equivalent molecules in the aggregate most probably as the piggy-back dimer. Second, the structural motif of the B745 aggregate of R[P,E]BChl **c** was proposed to be a shifted inclined column of stacked piggy-back dimers on the basis of the $^{1}$H- and $^{13}$C-aggregation shifts and the calculated ring-current effects using the loop-current approximation.

Thus, two different kinds of stacking of the macrocycles have been identified for the pair of B745 aggregates consisting of different stereoisomers; one, consisting of the (3$^{1}$S)-isomer, is the parallel-chain stacking, in which the monomeric BChl **c** are stacked together to form an inclined column, and the other, consisting of the (3$^{1}$R)-isomer, is the antiparallel-chain stacking, in which the piggy-back dimers are stacked together to form a shifted inclined column. The contradiction of two different models for chlorosomes are most probably ascribable to the presence of two different kinds of stacking in these B745 aggregates, which will be called B745m and B745d.

**Section II**

Changes in the electronic absorption spectra during the process of aggregate formation, by decreasing the amount of dichloromethane in a n-hexane - dichloromethane mixture, were traced for a

complete set of BChl **c** homologues from *Cb. limicola* including R[E,E], R[P,E], R[I,E], S[P,E] and S[I,E]BChl **c**. First, the shift of the $Q_y$ absorption was calculated on the basis of transition dipole - transition dipole interactions among the BChl **c** molecules in various aggregate models. Here, the point-monopole approximation, in which the dipole moment of a BChl molecule is approximated by a sum of the point monopoles on constituent atoms, was used. When a structural motif obtained by NMR spectroscopy was arranged in the y- and/or z-direction(s) to form a higher-order aggregates, the calculated $Q_y$ absorption shifted to the longer wavelength as a function of the number of structural motifs, and converged quickly to a certain value (then, the shift of the $Q_y$ absorption became hardly dependent on the number of the stacked structural units). This is supposed to be the mechanism why each aggregate form can give rise to a discrete $Q_y$ absorption. By comparison between the observed and the calculated shifts of the $Q_y$ absorption (after scaling), the entire structures of the BChl **c** aggregates have been proposed as shown in Figure 3 (the aggregate forms consisting of the piggy-back dimers is labeled 'd', and those consisting of the monomers is labeled 'm'): They include (a) B705d, a linear array of straight columns consisting of a pair of piggy-back dimers; (b) B705d', a liner array of inclined columns consisting of a pair of piggy-back dimers; (c) B720d, an assembly of two shifted inclined columns of more than six piggy-back dimers; (d) B745d, an assembly of five shifted inclined columns of more than six piggy-back dimers; (e) B720m, a parallel, stepwise stacking of ~ 30 monomers; and (f) B745m, an assembly of two columns of the parallel, stepwise stacking of ~ 30 monomers.

Second, changes in the electronic absorption spectra during the transformation from the monomer all the way to the higher aggregate were analyzed by spectral deconvolution, assuming five Gaussian components according to the apparent wavelength of the $Q_y$ absorption. They include the monomer (~ 665 nm), the dimer (B675), and the B705, B720, B745 aggregates. Furthermore, van der Waals energies, within each structural motif and between the structural motifs, were calculated to understand energetically the above transformation which depended on both the stereoisomeric configuration of the $C3^1$ hydroxylethyl group and on the bulkiness of the C8 sidechain. As a result, two different pathways of the transformation have been found; one is the dimer-based transformation for the ($3^1$R)-isomers, i.e., the monomer → B705d (B705d') → B720d → B745d, and the other is the monomer-based transformation for the ($3^1$S)-isomers, i.e., the monomer → B720m → B745m. Further, it has been shown that the bulkiness of sidechain at C8 tends to enhance the formation of the

B745 aggregate (in the order ethyl < propyl < isobutyl) in both cases. Comparison of the changes in electronic absorption spectra between chlorosomes and the B745 aggregate of S[I,E]BChl **c**, during the process of aggregate formation, lead me to the conclusion that the latter pathway of the transformation is most likely in intact chlorosomes. Further, addition of the ($3^1$S)-isomer seems to trigger the B745d → B745m transformation in the aggregate of the ($3^1$R)-isomers. The calculation of van der Waals energies has indicated that the B745d → B745m transformation is energetically advantageous when more than 8 % of the ($3^1$S)-isomer is mixed with the ($3^1$R)-isomers. This value is in excellent agreement with the stereoisomeric composition in the chlorosomes from *Cb. limicola*, i.e. S[I,E] : R[E,E] + R[P,E] ≈ 1: 9. Thus, the structural and energetical bases for the unique role of the ($3^1$S)-isomer to form an aggregate structure like B745m in chlorosomes, have been proposed.

## CONCLUSION

The structural and energetic features of the formation and transformation of the BChl **c** aggregates have been examined by means of high-resolution NMR and electronic-absorption spectroscopies with special emphasis on the stereoisomeric configuration at the $C3^1$ position as well as the bulkiness of the sidechain at the C8 position. As a result, the following answers to the questions addressed in the Introduction section have been obtained: (1) The structural motifs of the following BChl **c** aggregates are determined by NMR spectroscopy as follows: (a) the B675 dimer of R[E,E]BChl **c** forms the piggy-back stacking of a pair of macrocycles; (b) the B705 aggregate of R[E,E]BChl **c** has a straight (or an inclined) column consisting of the piggy-back dimers; (c) both the B720 and B745 aggregates of R[P,E]BChl **c** have a stacking of a pair of piggy-back dimers to form a shifted-inclined column; (d) both the B720 and B745 aggregates of S[I,E]BChl **c** form a parallel stepwise stacking of the monomeric forms (The dotted lines in Figure 3 in the Introduction section depicts these structural motifs). (2) The entire structures of the following BChl **c** aggregates are proposed by comparison of the observed and calculated shifts of the $Q_y$ absorption; here, the aggregate forms consisting of a piggy-back dimer is denoted as 'd', and those consisting of a monomeric form is denoted as "m" in addition to their wavelength of $Q_y$ absorption: (a) the structure of the B705d (B705d') aggregate is a linear array of straight (inclined) columns consisting of a pair of piggy-back dimers; (b) that of the B720d (B745d) aggregate is an assembly of two (five) shifted inclined columns of more than six piggy-back dimers; (c) that of the B720m (B745m) aggregate is an assembly of one (two) parallel stepwise stacking of ~30 monomers. Figure 3 in the Introduction section summarizes the entire structures of the aggregates (Concerning the B720m and B745m aggregates, only 20 monomers is shown in this figure). (3) Two different pathways of the transformation of the B745 aggregate have been identified on the basis of both the deconvolution of each set of electronic absorption spectra during the processes of transformation and the calculation of van der Waals energies for various aggregate forms: One is a transformation among the piggy back dimer-based aggregates of the ($3^1$R)-isomers: the dimer → B705d (B705d') → B720d → B745d. The other is a transformation among the monomer-based aggregates of the ($3^1$S)-isomers, i.e., the monomer → B720m → B745m. Further, it has been shown that addition of the ($3^1$S)-isomer can trigger the B745d → B745m transformation of the aggregates consisting of the ($3^1$R)-isomers. The

structural and energetical bases for a unique feature of BChl **c** molecules, particularly the role of the ($3^1$S)-isomer, have been proposed.

Thus, I propose 'the parallel-chain stacking' of the monomers as the structure of intact chlorosomes on the bases of the structural motifs determined by NMR spectroscopy, the entire structures of the BChl **c** aggregates determined by electronic-absorption spectroscopy, and the calculations of intermolecular van der Waals energies in the aggregates.

## FUTURE OUTLOOK

In this investigation, the structure of chlorosomes is proposed by *extrapolating* the structural and energetical analyses of artificial BChl **c** aggregates, although it needs to be proved by *direct* spectral evidence. From this viewpoint, two-dimensional, CP/MAS, solid-state $^{13}$C-NMR spectroscopy is in progress to determine the intermolecular carbon-carbon contacts in chlorosomes. Since the structures of chlorosomes and various BChl **c** aggregates have been revealed, the application of femto-second, time-resolved absorption and fluorescence spectroscopy is now being planned in order to elucidate the detailed mechanisms of the antenna function, in particular, to reveal the physical implication of the unique aggregate structure.

## ACKNOWLEDGEMENT

The author has been supported by JSPS Fellowships for Japanese Junior Scientists; he thanks also to the Ministry of Education, Science and Culture, Japan, for a grant-in-aid for Encouragement of Young Scientists.

The author especially indebted to Prof. Yasushi Koyama for his heartily guidance and encouragement. His critical reading and correction of the manuscript are also acknowledged. This thesis should have never been accomplished without his patient support.

The author is also indebted to the following collaborators:

(1) The author thanks Prof. Katsumi Matsuura, Prof. Keizo Shimada and Dr. Masamitsu Hirota at Tokyo Metropolitan University for the Gift of the starting material of *Chlorobium limicola* f. sp. *thiosulfatophilum* and the transferring the technique of the preparation of chlorosomes and the hexanol treatment of chlorosomes.

(2) The works concerning the measurements of the intermolecular $^{1}H$-$^{1}H$ NOE correlations described in Chapter 2 and Chapter 3 were carried out as a collaboration with Prof. Fuyuhiko Inagaki and Dr. Kenji Ogura at Tokyo Metropolitan Institute of Medical Science.

(3) The works concerning the theoretical calculation of the ring-current effects described in Chapter 2, Chapter 3 and Chapter 4 were carried out as a collaboration with Prof. Koji Yoshimitsu at Kwansei Gakuin University, and with Mr. Shun Sakamoto and Mr. Kazukimi Hara at our laboratory.

(4) The work concerning the theoretical calculation of the shift of the $Q_y$ absorption described in Chapter 5 was carried out as a collaboration with Prof. Hiroyoshi Nagae at Kobe City University of Foreign Studies.

The author would like to thank his friends, Miss Ritsuko Fujii, Dr. Leenawaty Limantara, Mr. Tokutake Sashima and Dr. Jian-Ping Zhang for their helps, friendship and encouragement. Finally he deeply and sincerely appreciates the encouragement and friendship of all the members in Prof. Koyama's laboratory.

10 January 2000

Tadashi Mizoguchi

## LIST OF PUBLICATIONS

*First author*

(1) Tadashi Mizoguchi, Leenawaty Limantara, Katsumi Matsuura, Keizo Shimada and Yasushi Koyama, Aggregation Forms of 8-Ethyl-12-Ethyl Farnesyl Bacteriochlorophyll *c* in Methanol-Chloroform Mixtures as Revealed by $^1$H-NMR Spectroscopy, *J. Mol. Struct.*, **379** (1996) 249-265.

(2) Tadashi Mizoguchi, Katsumi Matsuura, Keizo Shimada and Yasushi Koyama, The Structure of the Aggregate Form of Bacteriochlorophyll *c* showing the $Q_y$ Absorption above 740 nm: A $^1$H-NMR Study, *Chem. Phys. Lett.*, **260** (1996) 153-158.

(3) Tadashi Mizoguchi, Shun Sakamoto, Yasushi Koyama, Kenji Ogura and Fuyuhiko Inagaki, The Structure of the Aggregate Form of Bacteriochlorophyll *c* Showing the $Q_y$ Absorption above 740 nm as Determined by the Ring-Current Effects on $^1$H and $^{13}$C Nuclei and by $^1$H-$^1$H Intermolecular NOE Correlations, *Photochem. Photobiol.*, **67** (1998) 239-248.

(4) Tadashi Mizoguchi, Kenji Ogura, Fuyuhiko Inagaki and Yasushi Koyama, The Structure of the Aggregate Form of Bacteriochlorophyll *c* Showing the $Q_y$ Absorption at 705 nm as Determined by the Ring-Current Effects on $^1$H and $^{13}$C Nuclei and by $^1$H-$^1$H Intermolecular NOE Correlations, *Biospectroscopy*, **5** (1999) 63-77.

(5) Tadashi Mizoguchi, Kazukimi Hara, Hiroyoshi Nagae and Yasushi Koyama, Structural Transformation among the Aggregate Forms of Bacteriochlorophyll *c* as Determined by Electronic-Absorption and NMR Spectroscopies: Dependence on the Stereoisomeric Configuration and on the Bulkiness of the 8-C Sidechain, submitted to *Photochem. Photobiol.*

*Co-author*

(1) Ying Hu, Tadashi Mizoguchi, Yoshitaka Kurimoto and Yasushi Koyama, Isolation by High-Pressure Liquid Chromatography of Cis-Trans Isomers of β-Apo-12'-Carotenal and Determination of Their Configurations by $^1$H-NMR Spectroscopy, *Spectrochim. Acta Part A*, **51** (1995) 1949-1958.

(2) Ying Hu, Jian-Ping Zhang, Tadashi Mizoguchi, Yasushi Koyama, Yumiko Yamano and Masayoshi Ito, How the Terminal Methyl Group Affects the $S_0$, $S_1$ and $T_1$ Electronic

Structures of a Conjugated Aldehyde Chain: A Comparison between All-Trans-β-Apo-12'-Carotenal and Its Analogue by NMR and Raman Spectroscopy, *Spectrochim. Acta Part A*, **53** (1997) 277-286.

(3) Ritsuko Fujii, Chun-Hai Chen, Tadashi Mizoguchi and Yasushi Koyama, $^1$H-NMR, Electronic-Absorption and Resonance-Raman Spectra of Isomeric Okenone as Compared with those of Isomeric β-Carotene, Canthaxanthin, β-Apo-8'-Carotenal and Spheroidene, *Spectrochim. Acta Part A*, **54** (1998) 727-743.

(4) Mika Komori, Robin Ghosh, Shinichi Takaichi, Ying Hu, Tadashi Mizoguchi, Yasushi Koyama and Michitaka Kuki, A Null Lesion in the Rhodopin 3,4-Desaturase of *Rhodospirillum rubrum* Unmasks a Cryptic Branch of the Carotenoid Biosynthetic Pathway, *Biochemistry*, **37** (1998) 8987-8994.

(5) Grazyna E. Bialek-Bylka, Yoko Sakano, Tadashi Mizoguchi, Toshio Shimamura, Denise Phillip, Yasushi Koyama and Andrew J. Young, Central-*Cis* Isomers of Lutein Found in the Major Light-Harvesting Complex of Photosystem II (LHC IIb) of Higher Plants, *Photosynth. Res.*, **56** (1998) 255-264.

(6) Jian-Ping Zhang, Ritsuko Fujii, Pu Qian, Toru Inaba, Tadashi Mizoguchi, Yasushi Koyama, Kengo Onaka, Yasutaka Watanabe and Hiroyoshi Nagae, Mechanism of the Carotenoid-to-Bacteriochlorophyll Energy Transfer via the $S_1$ State in the LH2 Complexes from Purple Bacteria, submitted to *J. Phys. Chem. B*.

*Proceeding*

(1) Tadashi Mizoguchi and Yasushi Koyama, Stacking of Macrocycles in Bacteriochlorophyll *c* Aggregates and in Chlorosomes, in *Photosynthesis: Mechanisms and Effects*, edited by G. Garab (1998) Vol. I, pp. 113-116, Kluwer Academic Publishers, The Netherlands.

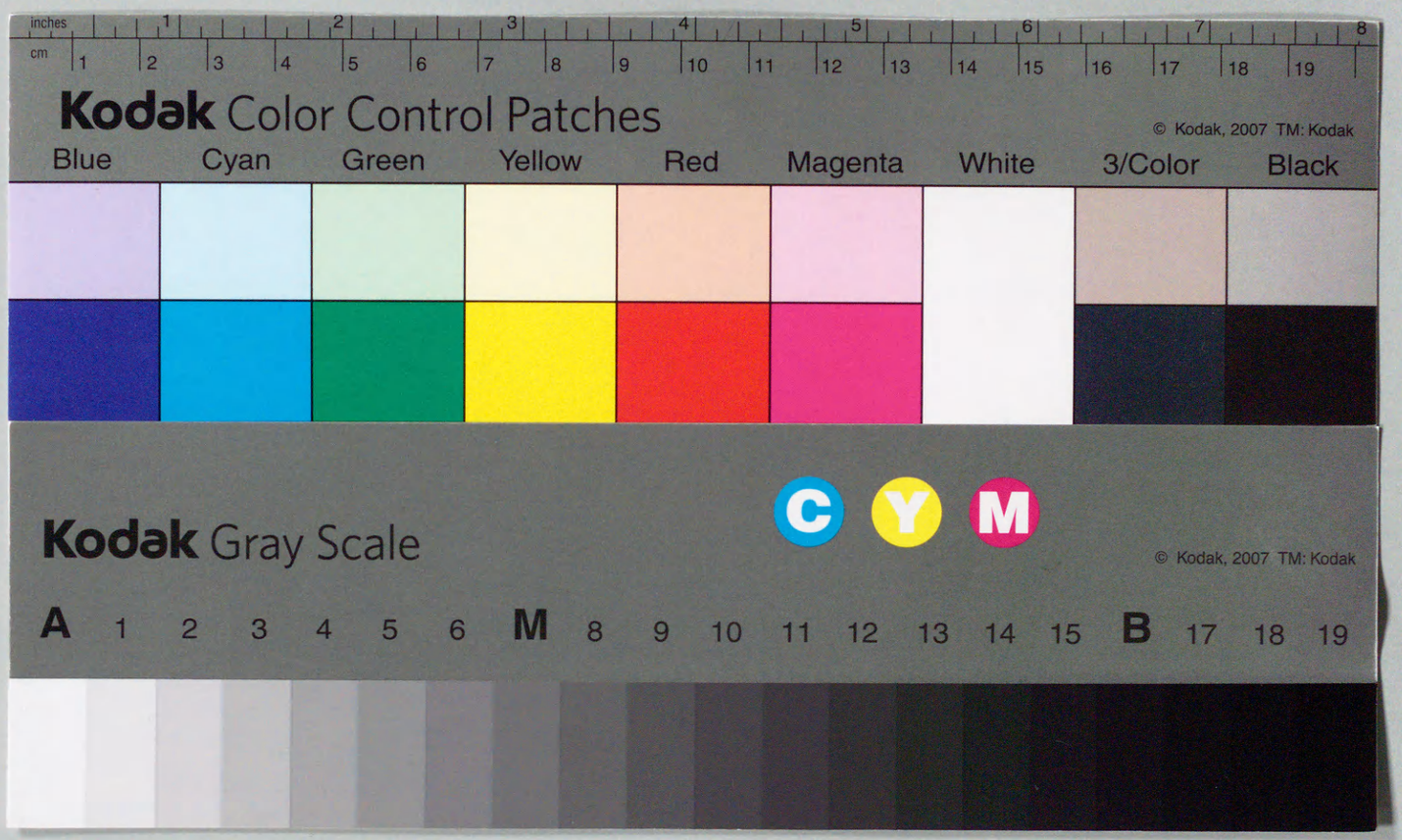
inches
cm
Kodak Color Control Patches
© Kodak, 2007 TM: Kodak
Blue
Cyan
Green
Yellow
Red
Magenta
White
3/Color
Black
Kodak Gray Scale
C
Y
M
© Kodak, 2007 TM: Kodak
A 1 2 3 4 5 6 M 8 9 10 11 12 13 14 15 B 17 18 19